AD_____

Award Number: DAMD17-00-1-0386

TITLE: Molecular Biology of Breast Neoplasia

PRINCIPAL INVESTIGATOR: Virgil C. Jordan, Ph.D.

CONTRACTING ORGANIZATION: Northwestern University
Evanston, Illinois 60208-1110

REPORT DATE: September 2003

TYPE OF REPORT: Annual Summary

PREPARED FOR: U.S. Army Medical Research and Materiel Command
Fort Detrick, Maryland 21702-5012

DISTRIBUTION STATEMENT: Approved for Public Release;
Distribution Unlimited

The views, opinions and/or findings contained in this report are those of the author(s) and should not be construed as an official Department of the Army position, policy or decision unless so designated by other documentation.

REPORT DOCUMENTATION PAGE

Form Approved
OMB No. 074-0188

1. AGENCY USE ONLY (Leave blank)	2. REPORT DATE	3. REPORT TYPE AND DATES COVERED
	September 2003	Annual Summary (1 Sep 2002 - 31 Aug 2003)

4. TITLE AND SUBTITLE
Molecular Biology of Breast Neoplasia

5. FUNDING NUMBERS
DAMD17-00-1-0386

6. AUTHOR(S)
Virgil C. Jordan, Ph.D.

7. PERFORMING ORGANIZATION NAME(S) AND ADDRESS(ES)
Northwestern University
Evanston, Illinois 60208-1110

E-Mail: vcjordan@nwu.edu

8. PERFORMING ORGANIZATION REPORT NUMBER

9. SPONSORING / MONITORING AGENCY NAME(S) AND ADDRESS(ES)
U.S. Army Medical Research and Materiel Command
Fort Detrick, Maryland 21702-5012

10. SPONSORING / MONITORING AGENCY REPORT NUMBER

11. SUPPLEMENTARY NOTES
Original contains color plates: All DTIC reproductions will be in black and white.

12a. DISTRIBUTION / AVAILABILITY STATEMENT
Approved for Public Release; Distribution Unlimited

12b. DISTRIBUTION CODE

13. ABSTRACT (Maximum 200 Words)

The Northwestern University Robert H. Lurie Comprehensive Cancer Center is an NCI-funded comprehensive cancer center. One of the major accomplishments for the Cancer Center has been to establish a nationally recognized program in both laboratory and clinical based breast cancer research. The Cancer Center has received $14.2 million from the Avon Foundation and successfully competed for a SPORE in Breast Cancer from the National Cancer Institute. In September 2000 the Cancer Center received a four year award from the US Army for comprehensive training of graduate students and postdoctoral fellows conducting breast cancer relevant research entitled, "The Molecular Biology of Breast Neoplasia" (DAMD17-00-0386). In year 2003, the Selection Committee reviewed applications and assisted in the selection of 4 graduate students and two postdoctoral fellows for appointment to the Training Program. Trainees and mentors actively participated in the weekly meetings of the Breast Cancer Journal Club, as well as training program course entitled, Advanced Topics in Breast Cancer. Year 2004 appointments have just been completed.

14. SUBJECT TERMS
Training Program, molecular biology, hormones, signal transduction

15. NUMBER OF PAGES
164

16. PRICE CODE

17. SECURITY CLASSIFICATION OF REPORT	18. SECURITY CLASSIFICATION OF THIS PAGE	19. SECURITY CLASSIFICATION OF ABSTRACT	20. LIMITATION OF ABSTRACT
Unclassified	Unclassified	Unclassified	Unlimited

Table of Contents

INTRODUCTION

The Robert H. Lurie Comprehensive Cancer Center has established a premier breast cancer program at Northwestern University, integrating basic laboratory research, clinical research and a program in cancer prevention and control. V. Craig Jordan, OBE, Ph.D., D.Sc. directs the laboratory breast cancer research program and Monica Morrow, M.D., directs the clinical breast cancer research program and the Lynn Sage Comprehensive Breast Center at Northwestern. Dr. Jordan is internationally recognized for his pioneering research on the antiestrogen tamoxifen, an important drug used in the treatment and prevention of breast cancer. In the last five years the Cancer Center has continued to successfully compete for national funding to support the breast cancer program. The Cancer Center received a $4.2 million dollar award from the Avon Foundation in March 2000 to expand the existing breast cancer research programs for medically underserved minority women. The principal investigator is Monica Morrow, M.D. and co-principal investigator is V. Craig Jordan, Ph.D., D.Sc.. The Avon Foundation enhanced their commitment to breast cancer research at the Robert H. Lurie Comprehensive Cancer Center with an additional gift of $10 million to build an Avon Breast Cancer research floor in the new Robert H. Lurie Medical Sciences building that will open in November 2004. In September 2000 the Cancer Center received an award from the National Cancer Institute for a SPORE in Breast Cancer (P50 CA89018). The Program Director of the SPORE is V. Craig Jordan, Ph.D., D.Sc. and the co-director is Monica Morrow, M.D. The five-year award provides $13 million dollars in funding for six translational research projects investigating hormones and breast cancer, four core facilities, and career development and developmental research opportunities in breast cancer. In September 2000 the Cancer Center also received a four year award from the US Army for training of graduate students and postdoctoral fellows, "The Molecular Biology of Breast Neoplasia". This program enables four predoctoral students and two postdoctoral fellows per year to receive in depth training in breast cancer research from laboratory investigators with research relevant to breast cancer and to clinical investigators who provide a translational link. Preceptors are nationally funded basic science faculty with a history of excellence in research with a focus on the cellular and molecular aspects of breast cancer. Ultimately, the goal of the Training Program is to prepare scientists to function as independent investigators in the field of breast cancer research and to integrate their research with therapeutic advances made by clinicians.

BODY

In Year 03 of the grant four graduate students and two postdoctoral fellows were appointed to The Molecular Biology of Breast Neoplasia. The Program's Administrative Director, Dr. Robin Leikin, sent out an email announcement requesting student nominations from faculty in the Breast Cancer Program. The Training Grant Selection Committee reviewed all applications. Committee members include: V. Craig Jordan, Ph.D., D.Sc., Program Director, Steven Rosen, M.D., Director, Cancer Center, Robin Leikin, Ph.D., Administrative Director; Kathleen Rundell, Ph.D., Professor, Microbiology-Immunology and Jonathan Jones, Ph.D., Professor, Cell and Molecular Biology. Students were selected based upon their academic credentials, the relevance of their research projects to breast cancer and their potential as future academicians in breast cancer research. The Training Grant Executive Committee provided final approval for the trainee selections.

All trainees attended the Breast Cancer Journal Club that brings together the members of the Breast Cancer Program on a weekly basis to discuss journal articles relevant to the molecular biology of breast cancer. The Journal Club regularly attracts 15-25 graduate, postdoctoral and faculty participants in addition to the four predoctoral students and two postdoctoral fellows who are required to participate. Trainees were required to present one time per year at this meeting (see Appendix). In addition, trainees were required to attend the course, "Advanced Topics in Breast Cancer" (see Appendix). The monthly lectures given by established

clinical faculty and translational researchers presented an integrated overview of clinical breast cancer for laboratory scientists. At the final meeting trainees presented their research projects for the Advisory Committee responsible for monitoring trainee progress (see Appendix).

The following predoctoral and postdoctoral students were allocated funds in Year 03 of the Grant:

Year 3:

Name	Preceptor	Department
Predocs:		
Joshua Bosman	Richard Morimoto	Biochemistry, Molecular Biology and Cell Biology
Anne Strohecker	Vincent Cryns	Medicine
Danijela Vignjevic	Gary Borisy	Cell and Molecular Biology
Yi Wu	Sharon Stack	Cell and Molecular Biology
Postdocs:		
Joan Lewis	V. Craig Jordan	Cancer Center
Suresh Pillai	Larry Jameson	Medicine

Anne Strohecker
Caspases are the major effectors of apoptosis, functioning to cleave and alter key cellular proteins. Using a novel expression cloning screen, the Cryns Laboratory has recently identified Her-2 as a caspase substrate . They hypothesize that caspase cleavage of Her-2 dramatically alters the function and stability of this protein. Although an orphan receptor itself, Her-2 forms potent signaling heterodimers with other EGFR family members (i.e. Her-3, Her-4, and EGFR) and plays a central role in both the establishment and progression of breast tumors. Overexpression of Her-2 undermines the effectiveness of chemotherapy induced apoptosis through increased signaling via the anti-apoptotic Akt pathway. Ms. Strohecker will perform experiments to map the caspase cleavage site(s) on Her-2 *in vitro* and *in vivo,* and she will examine the functional consequences of caspase cleavage on Her-2 mediated chemoresistance in the breast.

Joshua Bosman
Transcriptional regulation of the heat shock response by heat shock factors (HSF) is a highly controlled process in cells exposed to stress conditions. In fact, many diseases such as cancer, Huntington's, Parkinson's and Alzheimer's, have been associated with altered levels of heat shock proteins Hsp90, Hsp70 or Hsp27, which are under direct control of HSF. Mr. Bosman's research project involves a genome-wide approach to understand at the molecular level how the mammalian family of heat shock factors (HSF) function to regulate gene expression of heat shock proteins (ie Hsp90, Hsp27, Hsp70). His specific aims are:

-Genome-wide analysis of HSF target genes in humans using database searches and microarray data
-Validation of HSF target genes by Chip analysis
- To determine how HSE's and HSF regulate the heat shock response

These studies are critical, as understanding the regulation of molecular chaperones may have application to diseases that correlate with aberrant levels of heat shock proteins and these molecules may be applied in the future as potential novel therapies for cancer.

Danijela Vignjevic

The acquisition of a motile and invasive phenotype is an important step in the development of tumors and tumor metastasis. Electron microscopy analysis indicates that transformed breast cells differ from control cells by development of long filopodia, spike-like extensions of the cell. Actin bundling protein, fascin is present in filopodia and it is implicated with increased cell motility and malignancy. Increased levels of fascin are associated with overexpression of c-erbB2 in breast cancer cells, which correlates with poor prognosis in breast cancer patients. Whether fascin is required for filopodia formation, we addressed using two approaches: (1) expression of constitutively active or inactive fascin mutants tagged with GFP and (2) targeted depletion of fascin by hairpin siRNA expression with a GFP reporter. Both approaches demonstrated that fascin is required for filopodia formation. Expression of active fascin with serine39 mutated to alanine (S39A) dramatically increased number and length of filopodia. In contrast, inactive S39E fascin reduced the number of filopodia. Active fascin was distributed along the length of filopodial shafts similar to wild type fascin, whereas inactive fascin was enriched at the tips of remaining filopodia. Knockdown of fascin by each of two selected targeting sequences also reduced the number of filopodia. The few remaining filopodia were wavy and loosely bundled as determined by electron microscopy. Control transfection with a hairpin construct modified at two nucleotide positions showed wild-type phenotype and no fascin depletion, as evaluated by western blotting and immunostaining. The knockdown phenotype was suppressed by expressing fascin cDNA that was refractory to the siRNA construct through mutation at the third nucleotide of three codons (silent mutations). We conclude that fascin is specifically required to tightly bundle actin filaments in filopodia, which may be important to provide stiffness for filopodial protrusion. Thus, fascin could be a novel target for treatment of tumor metastasis.

Selected by the DOD to receive a travel award to present at the Era of Hope Meeting in Orlando, 2002.

Yi Wu

Yi Wu is studying the function of membrane type 1 matrix metalloproteinase (MT1-MMP) and its regulation in breast cancer cell invasion. The Stack laboratory is interested in membrane type 1-MMP (MT1-MMP) because of studies that correlate enhanced expression with breast cancer disease progression as well as with invasiveness of cultured breast cancer cell lines. This is further supported by in vitro studies showing MT-MMPs are the only subfamily of MMPs that mediates cellular invasion and transgenic mouse studies revealing MT1-MMP also plays a significant role in proliferation at the early stage of tumor development. The overall hypothesis of this research is that post-translational modifications, including proteolysis and glycosylation, regulates MT1-MMP activity, and thereby, controls invasive phenotype in tumor cells. In their studies, they demonstrated that MDA-MB-231 cells invade type I collagen matrix, the most important matrix barrier for tumor, in an MT1-MMP-dependent manner. Interestingly, they detected an inhibitory effect in invasion by overexpressing a truncation 44 kDa mutant, which is a naturally occurring cell surface autolytic product, suggesting MT1-MMP proteinase activity is tightly controlled in vivo. In addition, they identified MT1-MMP as a glycoprotein and found the glycosylation of MT1-MMP is crucial for its efficient activation of MMP-2, which is also extensively implicated in tumor progression. Currently the Stack group is vigorously investigating the significance of MT1-MMP glycosylation in different steps of breast cancer progression.

Suresh Pillai, Ph.D.

Estrogen Receptors (ERs) initiate gene transcription via numerous pathways. In the "classical" pathway, ERs bind to discrete response elements on DNA to activate transcription. In the "tethered" pathway, ERs initiate transcription via interaction with other transcriptional proteins. To examine the effects of selective estrogen receptor modulator (SERM) activation of ER-mediated transcription via the tethered pathway, we used a mutated ERalpha and microarray profiling. Amino acids within the DNA binding region of ERá were mutated

to eliminate classical ER signaling, and an ER-negative breast cancer cell line (MDA-MB-231) was infected with adenoviral vectors containing these mutants. Cells were then treated with vehicle alone, estradiol, ICI 182 780 (a pure anti-estrogen), tamoxifen or raloxifene. RNA from these cells was then extracted, purified, and hybridized to Affymetrix U95A human gene arrays to compare gene expression profiles among the treatment groups. The data between the experiments correlated significantly, and an examination of genes with altered expression differences (2.3-fold) yielded a consensus gene set of 253 targets. While few genes were regulated by estradiol, SERMS activated a much larger number of genes. This suggests that SERMS act, at least in part, through the tethered pathway. The consensus gene set was used in the generation of custom spotted microarrays containing the 253 targets from the high density screen. With standardization and verification of the microarrays now complete, hybridization of RNA from both cell culture and malignant breast tumors is currently underway. We hope to use these slides as a screening tool to generate gene expression profiles for different types of breast tumors.

Joan Lewis, Ph.D.

The Jordan laboratory has developed several long-term estrogen deprived breast cancer cell models to mimic the clinical setting of a post-menopausal woman taking aromatase inhibitors. Wild-type MCF-7 human breast carcinoma cells (MCF-7:WS8) were cultured in estrogen-free media for > 1 year and the following cell lines were derived: MCF-7:ED, MCF-7:2A and MCF-7:5C. Both MCF-7:2A and MCF-7:5C are clones of MCF-7:WS8 cells. One of Dr. Lewis's goals in Dr. Jordan's lab is to determine the long-term effects of estradiol (as well as structurally related estrogens) on the growth of long-term estrogen deprived breast cancer cells. Interestingly, she has found that treating long-term estrogen-deprived breast cancer cells with physiologic concentrations of estradiol (0.1-1 nM) reduces the growth of cancer cells. The growth-inhibitory effect of estradiol appears to be most dramatic in the MCF-7:5C cells and is highly dependent on the media. Further analysis indicates that the reduction in growth of MCF-7:5C cells is due to estradiol-induced cell death. Dr. Lewis is currently trying to elucidate the mechanism(s) for this paradoxical effect of estradiol (i.e. the ability to induce cell death rather than stimulate growth). Dr. Lewis is also interested in characterizing these cell lines in terms of their gene and protein expression profile to determine whether differences exist between MCF-7:WS8 versus MCF-7:5C, MCF-7:ED and MCF-7:2A. The information obtained from these studies using the different cell lines will further our understanding of the regulatory pathways involved in maintaining the critical balance between estrogen-induced cell death and cell proliferation and has important clinical application. Dr. Jordan is currently initiating clinical studies of estrogen therapy in breast cancer patients who have received exhaustive endocrine therapy.

KEY RESEARCH ACCOMPLISHMENTS

- Four predoctoral students and two postdoctoral fellows selected from a pool of candidates by Selection Committee
- Journal Club held on Tuesdays at 11 am throughout the academic year (see attached schedule)
- Students exposed to Advanced Topics in Breast Cancer course (see attached schedule)
- Students exposed to translational relevance of their research through Breast SPORE meetings
- Advisory committee selected 6 trainees for funding in Year 04

REPORTABLE OUTCOMES

The success of the Training Program is exemplified by the publications by the trainees as a direct result of their funding through the Molecular Biology of Breast Neoplasia Training Grant. Publications include:

Wu, Y.I., Munshi, H.G., Maizels, E.T., Hunzicker-Dunn, M., Schnaper, H.W., Green, K.G., and Stack, M.S. (2003). Phosphorylation of membrane type-1 matrix metalloproteinase (MT1-MMP) cytoplasmic tail. (manuscript in preparation)

Wu, Y.I., Munshi, H.G., Sen, R., Snipas, S.J., Salvesen, G.S., Fridman, R., and Stack, M.S. (2003). Glycosylation of membrane type-1 matrix metalloproteinase (MT1-MMP) modulates matrix metalloproteinase-2 (MMP-2) activation. (submitted for publication Sept 30)

Tam, E.M., Morrison, C., **Wu, Y.I.**, Stack, M.S., and Overall, C.M. (2003). Membrane Protease Proteomics: Isotope Coded Affinity Tags/Tandem Mass Spectrometry Identification of Novel MT1-MMP Substrates. (submitted for publication Sept 30)

Munshi, H.G., **Wu, Y.I.**, Mukhopadhyay, S., Platanias, L.C., and Stack, M.S. (2003). Differential regulation of membrane type 1-matrix metalloproteinase (MT1-MMP) activity by ERK 1/2 and p38 mitogen-activated protein kinase in oral squamous cell carcinoma cells. (submitted for publication Sept 30)

Tam, E.M., **Wu, Y.I.**, Butler, G.S., Stack, M.S., and Overall, C.M. (2002). Collagen binding properties of the membrane type-1 matrix metalloproteinase (MT1-MMP) hemopexin C domain. The ectodomain of the 44-kDa autocatalytic product of MT1-MMP inhibits cell invasion by disrupting native type I collagen cleavage. *J Biol Chem.* 277:39005-14.

Munshi, H.G., **Wu, Y.I.**, Ariztia, E.V., and Stack, M.S. (2002). Calcium regulation of matrix metalloproteinase-mediated migration in oral squamous cell carcinoma cells. *J Biol Chem.* 277:41480-8.

Munshi, H.G., Ghosh, S., Mukhopadhyay, S., **Wu, Y.I.**, Sen, R., Green, K.J., and Stack, M.S. (2002). Proteinase suppression by E-cadherin-mediated cell-cell attachment in premalignant oral keratinocytes. *J Biol Chem.* 277:38159-67.

Vignjevic D, Danciu O, Kojima S, Svitkina TM, and Borisy GG. Fascin function in filopodia formation and tumor cell metastais. *J. Cell Biol.* Submitted for publication.

Kojima S, **Vignjevic D** and Borisy GG. An improved silencing vector co-expressing GFP and small hairpin RNA. J. Biotech. Submitted for publication.

Vignjevic D, Yarar D, Welch MD, Peloquin J, Svitkina TM and Borisy GG. Formation of filopodial-like bundles *in vitro* from a dendritic network. *J. Cell Biol.* 2003. 160:951-962

Svitkina TM, Bulanova EA, Chaga OY, **Vignjevic D**, Kojima S, Vasiliev JM and Borisy GG. Mechanism of Filopodia Initiation by Reorganization of a Dendritic Network. 2003. *J. Cell Biol.* 160:409-21.

Joan S. Lewis and V. Craig Jordan. "Chemoprevention of Breast Cancer: Laboratory Principles". Submitted to: Diseases of the Breast, 3rd Edition Lippincott, Williams & Wilkins Editors: Drs. Jay R. Harris (Harvard University), Marc E. Lippman (University of Michigan), Monica Morrow (Northwestern University), C. Kent Osborne (Baylor University).

Joan S. Lewis, Dong Cheng, and V. Craig Jordan "Targeting Oestrogen to Kill the Cancer but not the Patient". Submitted to: British Journal of Cancer (Review Article)

A list of trainee abstracts can be found in the Appendix.

CONCLUSIONS:

The Molecular Biology of Breast Neoplasia continues to provide state of the art laboratory and didactic training to 4 predoctoral students and two postdoctoral fellows in Year 03. Dr. Jordan organized the Breast Cancer Journal Club to bring together the members of the Training Program on a weekly basis to discuss relevant journal articles and areas of research. Trainees on the Molecular Biology of Breast Neoplasia also attended in the Advanced Topics in Breast Cancer course, where the monthly lectures present an integrated overview of clinical and translational breast cancer. Trainees also attended departmental seminars and journal clubs that have direct relevance to breast cancer. The Cancer Center's NCI funded SPORE in Breast Cancer Program provides further educational opportunities. The goal is to enhance the trainees' understanding of clinical breast cancer so that the relevance of their laboratory research can be stimulated.

APPENDIX I
TRAINEE ABSTRACTS

Abstracts:

The Molecular Biology of Breast Neoplasia. Robin Goldman Leikin, Ph.D. and V. Craig Jordan, Ph.D., D.Sc. Presented at the Era of Hope Meeting in Orlando, FL, 2002.

Fascin function in filopodia formation: Reconstruction in vitro and genetic analysis in vivo. **Danijela Vignjevic** and Gary Borisy. Northwestern University Medical School, Chicago, IL. Presented at meeting in Heidelberg, Germany.

In Vitro System for Filopodia Formation. **Danijela Vignjevic**, Tatyana Svitkina and Gary Borisy. Presented at the Era of Hope Meeting in Orlando, FL, 2002

Characterization of the Ovarian Phenotype of the Female ER^{AA} mouse: An in vivo model of the Tethered ERα Signaling Pathway. **Suresh Pillai**, Monika Jakacka, Lisa Hurley , Jeffrey Weiss and J. Larry Jameson. Northwestern University Feinberg School of Medicine, Chicago, IL. Presented at Endocrine Society National Meeting, June 18-22 2003; Philadelphia, PA

Biochemical and Biophysical Studies of Bag-1 and Hsp70 Chaperone Complexes. **Joshua Bosman** and Richard Morimoto. 8th Annual Midwest Stress Response and Chaperone Meeting in January 2003 in Evanston.

17β-Estradiol induces apoptosis in a long-term estrogen deprived variant clone of MCF-7 breast cancer cells. **Joan Lewis**, Vincent Cryns and VC Jordan. Presented at the 5th Annual Lunn Sage Breast Cancer Symposium, Chicago, IL 2003.

Fascin function in filopodia formation: Reconstruction in vitro and genetic analysis in vivo. Danijela Vignjevic and Gary Borisy. Northwestern University Medical School, Chicago, IL. Presented at meeting in Heidelberg, Germany.

Leading edge protrusion is driven by actin polymerization inside two organelles: lamellipodia and filopodia. Filopodia are formed from a preexisting dendritic network by barbed-end elongation of actin filaments and subsequent cross-linking into bundles. Although fascin, an actin bundling protein is localized in filopodia, no functional test has been performed as to whether it is required for filopodia formation. We studied role of fascin in filopodia formation in two systems: in vitro using cytoplasmic extracts, and in vivo using B16F1 melanoma cells. We developed an in vitro system for formation of filopodial-like bundles. Beads coated with Arp2/3 activating proteins in cytoplasmic extracts can induce formation of stars: actin bundles which radiate from the bead. Actin filaments in these bundles are long, unbranched, uniformly polar, grow at the barbed end and have a dendritic network at their roots. Using purified proteins, we showed that only WASP-coated beads, actin, Arp2/3 complex and fascin are sufficient for assembly of filopodia-like bundles. Although, a-actinin was able to drive star assembly, the star bundles had wavy rays and lacked a tight, parallel bundle organization. Consistent with our in vitro data, we found by double labeling of living cells with YFP/CFP fascin/a-actinin, that fascin is the major bundling protein present in filopodia. Molecular genetic experiments of two types were carried out to determine whether fascin was necessary for filopodia formation: expression of GFP-mutant forms of fascin and knock-down of fascin gene product using siRNA hairpin constructs. Constitutively active fascin mutants dramatically increased filopodia number while an inactive form decreased their number. Knock down of fascin resulted in reduction of filopodia number and the few remaining filopodia mostly consisted of microspikes. We conclude that fascin is required to form the tightly bundled actin filaments necessary to generate extension of filopodia.

In Vitro System for Filopodia Formation. Danijela Vignjevic, Tatyana Svitkina and Gary Borisy. Presented at the Era of Hope Meeting in Orlando, FL, 2002

The acquisition of a motile phenotype is an important step in the development of tumors and ultimately metastasis. Ultrastructural analysis indicates that transformed breast cells differ from control cells by the development of long filopodia, spike-like extensions of the cell containing a bundle of actin filaments. The actin bundling protein, fascin has a role in construction of filopodia which leads to increased cell motility.

We report here the initial development of an in vitro system for filopodia formation. The brain extract when highly diluted gave rise to star-like actin assemblies which consisted of radial actin bundles emerging from an actin cloud proximal to the bead. Coating of the beads with Arp2/3-activating proteins was required for star formation. Time-lapse microscopy showed that thin actin bundles arose from the actin cloud followed by elongation and coalescence into thicker bundles. The efficient bundling of actin filaments by fascin into parallel bundles within filopodia may promote linear extension and stiffening of filopodia. Immunofluorescence of stars showed that fascin is present along the whole length of actin bundles. Addition of capping protein to extracts blocked bundle formation, but allowed for continuous growth of actin clouds. This suggests that star formation results from low levels of barbed end capping. Pulse-labeling showed that actin incorporation was at the bead surface and at the tips of actin bundles. EM demonstrated that clouds consisted of a dendritic actin network whereas bundles consisted of long unbranched filaments of uniform polarity with barbed ends pointing away from the bead as determined by myosin S1 fragment decoration. The actin filaments of star-bundles share with filopodia in living cells the properties of being long, unbranched, parallel and of uniform polarity. Both structures grow at their barbed ends and require fascin for their formation. As the presence of filopodia can serve as a hallmark of breast cancer cells and the beginning of metastasis, it is important to understand the mechanism of filopodia formation. Therefore, we propose that actin stars may serve as a model for filopodia formation in vitro. Molecular players in this process could serve as novel targets for the treatment of cancer.

Characterization of the Ovarian Phenotype of the Female ER^{AA} mouse: An *in vivo* model of the Tethered ERα Signaling Pathway.

Suresh B. Pillai, Monika H. Jakacka, Lisa A. Hurley, Jeffrey Weiss, and J. Larry Jameson. Northwestern University Feinberg School of Medicine, Chicago, IL 60611.

In addition to the classical pathway, ERα also signals through a tethered pathway. The tethered pathway is initiated by antagonist binding to ERα that subsequently binds to transcription factors such as AP1, Sp1, and NFκB. The tethering of ERα to these factors is thought to regulate genes distinct from those regulated by other ERα signaling pathways. To examine the role of tethered ERα signaling *in vivo*, we mutated residues 207 and 208 of ERα (within the first zinc finger of the DNA binding domain) to alanines. This mutant ERα (ERαAA) abolishes classical ERα signaling while preserving the tethered pathway. We used this mutant to generate an *in vivo* model for tethered ERα signaling, the ER^{AA} (NERKI) mouse. $ER^{WT/AA}$ females are anovulatory, and they are infertile even when superovulated. To generate animals that signal only via the tethered pathway, we crossbred $ER^{WT/AA}$ animals to ERαKO animals (Dr. Ken Korach). This breeding strategy generated $ER^{AA/-}$ mice, animals that exclusively expressed our ERαAA mutant receptor. We then compared the ovarian phenotypes of $ER^{WT/AA}$, $ER^{AA/-}$, and $ER^{-/-}$ females with $ER^{WT/WT}$ females. Females from all of these genotypes are infertile versus controls. Ovaries from $ER^{-/-}$ and $ER^{AA/-}$ were similar; both contained follicles at various stages of development, but with a greater percentage of atretic follicles versus developing follicles when compared to $ER^{WT/WT}$ controls. Both also lacked corpora lutea (evidence of ovulation), but only the $ER^{-/-}$ ovaries contained hemorrhagic cysts. This suggests that the presence of a single ER^{AA} allele exerts some type of protective effect against the emergence of these cysts. We also compared the $ER^{WT/AA}$ female to the $ER^{WT/-}$ female. In this case, the presence of a single ERαAA allele results in an anovulatory phenotype with steroidogenic abnormalities. This differs from the $ER^{WT/-}$ female, which are normal. Differences are also apparent in patterns of ovarian apoptosis. While TUNEL staining of $ER^{-/-}$ ovaries had evidence of apoptosis only within granulosa cells, all ER^{AA} genotypes exhibited DNA fragmentation in both granulosa and stromal cells. These findings suggest that the tethered pathway plays a critical role in ovarian growth and development. Furthermore, a gene dosage effect appears to accompany expression of the ERαAA mutant *in vivo*, contributing to the differing phenotypes of the $ER^{WT/AA}$, $ER^{AA/-}$, and $ER^{-/-}$ ovaries.

5th Annual Lynn Sage Breast Cancer Symposium

Poster Abstract Form

Friday, September 19, 2003

Type inside box at right, using an 11-point typeface or larger. Do not fold abstract.

Abstract must be received in the symposium office no later than ***July 28, 2003***, to be considered. Original or Internet form accepted.

Poster Abstract-form available at www.cancer.northwestern.edu

Mail completed form to:
Denise Marshall
Office of Public Affairs and Communications
Robert H. Lurie Comprehensive Cancer Center
of Northwestern University
676 North St. Clair, Suite 1200
Chicago IL 60611

Faxes will not be accepted.
For additional information, e-mail:
d-marshall4@northwestern.edu

Poster Author's Information

LEWIS
Last Name

JOAN S
First Name MI

Academic Degree ☐ MD ☑ PhD

☐ Mr. ☐ Mrs. ☐ Ms.

NORTHWESTERN UNIVERSITY
Institution

710 N FAIRBANKS
Mailing Address

CHICAGO IL 60611 U.S.A
City State/ZIP Code COUNTRY

J-lewis4@northwestern.edu
E-Mail Address

312-503-1945
Telephone Office Fax

Poster Presenter *(if different than author)*

Last Name First Name

E-Mail Address

Telephone Office Fax

Detach Along Perforated Line

17β-Estradiol induces apoptosis in a long-term estrogen deprived variant clone of MCF-7 breast cancer cells.

Lewis, J.S., Cryns V., and Jordan, V.C.
Robert H. Lurie Comprehensive Cancer Center of the Feinberg School of Medicine, Northwestern University, Chicago, IL

Depriving breast cancer cells of estrogenic stimulation, through the use of aromatase inhibitors, represents a potential treatment strategy for controlling tumor growth. Indeed, aromatase inhibitors have been shown to cause tumor regression by lowering estrogen concentration in the blood and in tumor tissue. At present, however, the consequences of long-term estrogen deprivation on the growth of breast cancer cells are not completely known. We have developed an estrogen-independent breast cancer cell line that is a clone of parental MCF-7:WS8 cells (clone MCF-7:5C). The MCF-7:5C clone was derived after long-term culture (>1 year) of MCF-7:WS8 cells in phenol red-free MEM media containing 5% stripped fetal calf serum, followed by two rounds of limiting dilution cloning. For our experiments, we treated MCF-7:5C cells with various concentrations of estradiol-17 beta (0.1-10 nM) and assayed their growth by DNA quantitation and cell counting. Our results showed that the growth of MCF-7:5C cells (in MEM) was not significantly altered by either estradiol or the antiestrogens 4-hydroxytamoxifen and ICI 182,780. Interestingly, when MCF-7:5C cells were cultured in phenol red-free RPMI medium containing 10% stripped fetal bovine serum, a completely different phenomenon was observed. Estradiol treatment of MCF-7:5C cells (in RPMI) resulted in a dramatic reduction (60-80%) in the growth of these cells compared to vehicle control. The antiestrogens, 4-OHT and ICI 182,780 also reduced the growth of MCF-7/5C cells in RPMI medium, however, their effect was less pronounced compared to E_2. To investigate whether the estradiol-induced growth inhibition of MCF-7:5C cells (in RPMI) was due to induction of apoptosis, analysis was performed by flow cytometry after staining with FITC-Annexin V/PI. Flow cytometry analysis revealed that apoptotic cell population increased gradually from < 5% in vehicle control to ~55% with 1 nM estradiol. Further analysis showed that ICI 182,780 was able to partially block the estradiol-induced apoptosis in MCF-7:5C cells, thus suggesting the involvement of the ER in this process. Western blot analyses of known mediators of apoptosis reveal that FasR, p53, p21, and Bax proteins were constitutively overexpressed in MCF-7:5C cells compared to parental MCF-7:WS8, estradiol treatment, however, did not cause any further increase in their protein levels. Overall, these results show that estradiol is capable of inducing apoptosis in a variant clone of MCF-7:WS8 breast cancer cells and that this effect is highly influenced by the medium in which the cells are grown.

THE MOLECULAR BIOLOGY OF BREAST NEOPLASIA

Robin Goldman Leikin, Ph.D. and V. Craig Jordan, Ph.D., D.Sc.

Robert H. Lurie Comprehensive Cancer Center
Northwestern University
Chicago, IL 60611

E-mail: rleikin@northwestern.edu

The Robert H. Lurie Comprehensive Cancer Center has established a premier breast cancer program at Northwestern University, integrating basic laboratory research, clinical research and a program in cancer prevention and control. The Department of Defense funded training program, The Molecular Biology of Breast Neoplasia, enables the Cancer Center to provide state of the art laboratory and didactic training to 4 predoctoral students and two postdoctoral fellows per year. Preceptors are nationally funded faculty with a history of excellence in research with a focus on the cellular and molecular aspects of breast cancer. Predoctoral trainees enroll in the core curriculum of biochemistry, cell biology, molecular biology and biostatistics. In addition, all trainees present once per year at the Breast Cancer Journal Club that brings together the members of the Breast Cancer Program on a weekly basis to discuss journal articles relevant to the molecular biology of breast cancer. In January 2002 we implemented a course in breast cancer biology and treatment, "Advanced Topics in Breast Cancer". The monthly lectures present an integrated overview of clinical breast cancer for laboratory scientists. Trainees are also encouraged to participate in Cancer Center sponsored seminars, symposia and Breast SPORE meetings. The Selection Committee is responsible for selecting applicants and recommending admission to the Program. An Advisory Committee monitors trainee progress. Ultimately, the goal of the Training Program is to prepare scientists to function as independent investigators in the field of breast cancer research and to integrate their research with therapeutic advances made by clinicians.

Supported by the U.S. Army Medical Research and Materiel Command under DAMD17-00-1-0386

BIOCHEMICAL AND BIOPHYSICAL STUDIES OF BAG-1 AND HSP70 CHAPERONE COMPLEXES.

Joshua Bosman and Richard Morimoto. Department of Biology, Molecular Biology, and Cellular Biology; Northwestern University, Evanston, IL.

Chaperone networks guide the folded states of polypeptides as they cycle between ATP and ADP states, thus influencing their activities, sub-cellular localization, and stability. Co-chaperones that enhance or inhibit the ATPase and folding activities of Hsp70 or Hsp90 chaperones confer important regulatory features. The co-chaperone Hdj-1 stimulates the ATPase of Hsp70 quickening the cycle as well as the refolding rate of Hsp70. An additional co-chaperone, Hip, further positively regulates refolding capacity, but without affecting the ATPase. On the other hand, Bag-1 negatively regulates refolding activity while stimulating ATPase activity. My research is to characterize, at the biochemical and biophysical levels, the molecular interactions between Bag-1, Hsp70, and other proteins that may interact to form a complex. How Bag-1 regulates Hsp70 is still somewhat controversial and the biochemical mechanism by which this occurs remains unresolved. It remains unclear whether Bag-1 inhibits chaperone activity by preventing the association of a substrate with the carboxyl-terminal substrate-binding domain of Hsp70 or by preventing the release of a bound substrate by altering the ATPase cycle. In order to elucidate a mechanism, we will generate and characterize a collection of site-directed mutations in Hsp70 using biochemical approaches to assess nucleotide binding and hydrolysis, substrate interactions using fluorescence methodologies, and complex formation to Bag-1 interaction with Hsp70. The outcome of these experiments should provide a detailed understanding of the biochemical interactions between Bag-1 and Hsp70. In other studies, we will examine how these chaperone complexes are assembled and employ analytical ultracentrifugation as well as high-resolution cryoelectron microscopy to establish stoichiometry and a three-dimensional structure.

APPENDIX II

BREAST CANCER JOURNAL CLUB

Breast Cancer Journal Club Schedule for 2002/2003

November 12:	Eric Ariazi	e-ariazi@northwestern.edu
November 19:	Noman Kidwai	n-kidwai@northwestern.edu
November 26:	Joan Lewis	j-lewis4@northwestern.edu
December 3:	Vince Cryns	v-cryns@northwestern.edu
January 14:	Ruth O'Regan	rmo@461merle.it.northwestern.edu
January 21:	Jennifer Fox	jenfox@northwestern.edu
January 28:	Anne Strohecker	a-strohecker@northwestern.edu
February 4:	Carla Jorgensen	c-walker3@md.northwestern.edu
February 11:	Clodia Osipo	c-osipo@northwestern.edu
February 18:	Yi Wu	ywu@northwestern.edu
February 25:	Jennifer Schafer	jim595@northwestern.edu
March 4:	Ana Levenson	a-levenson@northwestern.edu
March 11:	Sandra Pearce	s-pearce2@northwestern.edu
March 18:	Suresh Pillai	suresh@northwestern.edu
March 25:		
April 1:		
April 15:	Josh Bosman	j-bosman@northwestern.edu
May 6:	Susan Gapstur	sgapstur@northwestern.edu
May 13:	Hong Liu	h-liu4@northwestern.edu
May 20:	Bin Chen	bch075@northwestern.edu
May 27:	Danijela Vignjevic	nele@northwestern.edu

APPENDIX III

ADVANCED TOPICS IN BREAST CANCER

ROBERT H. LURIE
COMPREHENSIVE CANCER CENTER
OF NORTHWESTERN UNIVERSITY

Advanced Topics in Breast Cancer Course

V. Craig Jordan, Ph.D., D.Sc.
Course Director

Advanced Topics in Breast Cancer will consist of eight classes taught be members of the Robert H. Lurie Comprehensive Cancer Center Breast Cancer Program. All sessions will be held on Wednesdays in the Vanderwicken Library, Olson 8260, from 9 am to 10:30 am. The final class will present current controversies in breast cancer.

DATE	FACULTY	TOPIC
January 8, 2003	Susan Gapstur , Ph.D.	Epidemiology of Breast Cancer
February 12, 2003	Monica Morrow, M.D.	Surgical Management of Breast Cancer
March 12, 2003	Elizabeth Wiley, M.D.	Pathology of Breast Cancer
April 16, 2003	V. Craig Jordan, Ph.D.	Endocrine Therapy of Breast Cancer
May 14, 2002	Gerald Soff, M.D.	Angiogenesis and Breast Cancer
June 11, 2003	William Gradishar, M.D.	Medical Oncology of Breast Cancer
July 9, 2003	Boris Pasche, M.D., Ph.D.	Genetics of Breast Cancer
August 13, 2003	V. Craig Jordan, Ph.D.	Student Presentations

Advanced Topics in Breast Cancer
Final Presentations by Trainees

Vanderwicken Library
Olson 8260
9:00 am

Danijela Vignivec
Gary Borisy Laboratory
Fascin function in filopodia formation

Yi Wu
Stack Laboratory
Regulation of MT1-MMP activity by proteolysis and glycosylation in breast cancer cells.

Anne Strohecker
Cryns Laboratory
Caspase cleavage of Her-2/Neu

Josh Bosman
Morimoto Lab

Suresh Pillai, Ph.D.
Jameson Lab
Microarray analysis of tethered ER-alpha signaling in breast cancer cells.

Joan Lewis, Ph.D.
Jordan Lab

APPENDIX IV

PUBLICATIONS

THE JOURNAL OF BIOLOGICAL CHEMISTRY
Vol. 277, No. 41, Issue of October 11, pp. 39005–39014, 2002
Printed in U.S.A.

Collagen Binding Properties of the Membrane Type-1 Matrix Metalloproteinase (MT1-MMP) Hemopexin C Domain

THE ECTODOMAIN OF THE 44-kDa AUTOCATALYTIC PRODUCT OF MT1-MMP INHIBITS CELL INVASION BY DISRUPTING NATIVE TYPE I COLLAGEN CLEAVAGE*

Received for publication, July 10, 2002
Published, JBC Papers in Press, July 26, 2002, DOI 10.1074/jbc.M206874200

Eric M. Tam‡§, Yi I. Wu¶‖, Georgina S. Butler, M. Sharon Stack¶, and Christopher M. Overall‡**‡‡**

*From the C.I.H.R. Group in Matrix Dynamics, Departments of ‡Biochemistry and Molecular Biology, **Oral Biological and Medical Sciences, University of British Columbia, Vancouver, British Columbia V6T 1Z3, Canada and the ¶Department of Cell and Molecular Biology, Northwestern University Medical School, Chicago, Illinois 60611*

Up-regulation of the collagenolytic membrane type-1 matrix metalloproteinase (MT1-MMP) leads to increased MMP2 (gelatinase A) activation and MT1-MMP autolysis. The autocatalytic degradation product is a cell surface 44-kDa fragment of MT1-MMP (Gly^{285}–Val^{582}) in which the ectodomain consists of only the linker, hemopexin C domain and the stalk segment found before the transmembrane sequence. In the collagenases, hemopexin C domain exosites bind native collagen, which is required for triple helicase activity during collagen cleavage. Here we investigated the collagen binding properties and the role of the hemopexin C domain of MT1-MMP and of the 44-kDa MT1-MMP ectodomain in collagenolysis. Recombinant proteins, MT1-LCD (Gly^{285}–Cys^{508}), consisting of the linker and the hemopexin C domain, and MT1-CD (Gly^{315}–Cys^{508}), which consists of the hemopexin C domain only, were found to bind native type I collagen but not gelatin. Functionally, MT1-LCD inhibited collagen-induced MMP2 activation in fibroblasts, suggesting that interactions between collagen and endogenous MT1-MMP directly stimulate the cellular activation of pro-MMP2. MT1-LCD, but not MT1-CD, also blocked the cleavage of native type I collagen by MT1-MMP *in vitro*, indicating an important role for the MT1-MMP linker region in triple helicase activity. Similarly, soluble MT1-LCD, but not MT1-CD or peptide analogs of the MT1-MMP linker, reduced the invasion of type I collagen matrices by MDA-MB-231 cells as did the expression of recombinant 44-kDa MT1-MMP on the cell surface. Together, these studies demonstrate that generation of the 44-kDa MT1-MMP autolysis product regulates collagenolytic activity and subsequent invasive potential, suggesting a novel feedback mechanism for the control of pericellular proteolysis.

Type I collagen is the most abundant protein of the extracellular matrix and is an important structural component in blood vessels, skin, tendons, ligaments, and bone (1). Accordingly, the synthesis and degradation of type I collagen is tightly regulated. Disruptions in this homeostasis can lead to diseases such as pulmonary fibrosis, scleroderma, arthritis, and osteoporosis, which, if untreated, can result in loss of tissue function and integrity. In a number of cancer cells, the capacity to degrade type I collagen and invade through type I collagen matrices often correlates with metastatic potential (2), a characteristic that is as important for the local dissemination of tumor cells as type IV collagen degradation and basement membrane penetration is for metastasis (3). Despite the importance of maintaining correct collagen homeostasis in tissues, the proteases responsible for type I collagen degradation *in vivo* remain unclear. An intracellular pathway may play an important role in collagen degradation (4) that, in bone, utilizes the cysteine protease cathepsin K at low pH (5). Extracellularly, fibrillar type I collagen may be degraded at neutral pH by several matrix metalloproteinases (MMPs),[1] a 24-member family of zinc-dependent endopeptidases in humans (2). The major collagenolytic MMPs are the secreted collagenases, MMP1, MMP8, and MMP13 (6), and the cell surface membrane type 1 (MT1)-MMP (7, 8). MT1-MMP also activates collagenase-2 (MMP13) (9) and is the primary activator of MMP2 (10), a gelatinase that exhibits weak native type I collagenolytic activity (11–13).

MMPs share a common overall structure consisting of a propeptide, catalytic domain, linker (also called a hinge), and a hemopexin C domain (14). Whereas the majority of MMPs are secreted as latent zymogens, MT-MMPs, the largest subgroup of MMPs, are membrane-anchored by the presence of a type I transmembrane sequence and cytoplasmic tail (MT1-, MT2-, MT3-, and MT5-MMP) or by glycosylphosphatidylinositol linkage (MT4- and MT6-MMP) (14). MT1-MMP is activated intracellularly by proprotein convertase-dependent and -independent pathways (15, 16) and is expressed as an active protease on the surface of many normal and pathological cell types (10, 17). The importance of MT1-MMP is indicated by its requirement for the invasion of endothelial and cancer cells through type I collagen matrices (18–20). Moreover, mice deficient in MT1-

* This work was supported by grants from the National Cancer Institute of Canada, Canadian Institutes for Health Research, and the National Institutes of Health Research. The costs of publication of this article were defrayed in part by the payment of page charges. This article must therefore be hereby marked "*advertisement*" in accordance with 18 U.S.C. Section 1734 solely to indicate this fact.

§ Supported by a Roman Babicki Scholarship and Canadian Arthritis Network Trainee Award.

‖ Supported by a United States Army MRMC Training Grant.

‡‡ Supported by a Canada Research Chair in Metalloproteinase Biology. To whom correspondence should be addressed: University of British Columbia, 2199 Wesbrook Mall, J.B. Macdonald Bldg., Vancouver, British Columbia V6T 1Z3, Canada. Tel.: 604-822-2958; Fax: 604-822-3562; E-mail: chris.overall@ubc.ca; Website: www.clip.ubc.co.

[1] The abbreviations used are: MMP, matrix metalloproteinase; MT, membrane type; CD, C domain; LCD, C domain with linker; sMT1-MMP, soluble MT1-MMP; TIMP, tissue inhibitor of metalloproteinases; DMEM, Dulbecco's modified Eagle's medium; BSA, bovine serum albumin; ConA, concanavalin A; PBS, phosphate-buffered saline; HRP, horseradish peroxidase; Mca, 7-methoxycoumarin-4-yl)acetyl.

MMP developed severe aberrations in type I collagen-abundant tissues, such as bone and skin, and the mice exhibited arthritis and scleroderma (21, 22). In humans, homoallelic loss-of-function mutations in the *MMP2* gene result in excessive bone resorption and arthritis (23). This condition resembles the phenotype of the MT1-MMP knockout mouse, supporting the close functional connection of MMP2 and MT1-MMP in regulating pericellular collagen homeostasis in mice and humans.

Native type I collagen consists of two α1(I) chains and one α2(I) chain interwound in a right-handed triple helix that is resistant to cleavage by most proteinases at neutral pH with the exception of the MMP collagenases (14). Because the active site of collagenolytic MMPs can only accommodate a single α-chain, cleavage of the three α-chains occurs sequentially at the single collagenase-susceptible site, Gly^{775}-Ile/Leu^{776}, to generate ¾ and ¼ collagen fragments. To achieve this, the collagen helix must be initially unwound by a triple helicase mechanism in order to expose the scissile bonds. This critical step requires the presence of collagen-binding exosites (14), in addition to elements within the active site (24–26). In MMP1, MMP8, and MMP13, the hemopexin C domain supports binding to collagen and is required for native collagen cleavage (27–32). Deletion or mutation of the MMP8 linker also reduces collagenolysis (33, 34). Furthermore, synthetic peptide analogs of the MMP1 linker bound collagen and inhibited collagen cleavage (35). Interestingly, the 35-amino acid residue linker of MT1-MMP is twice the length of other collagenase linkers (18 residues); however, the significance of this and its role in collagen cleavage have yet to be examined.

The regulation of MT1-MMP activity, MMP2 activation and pericellular type I collagen levels is complex. In a variety of cells, stimulation by fibrillar type I collagen has been shown to increase the cell surface expression of MT1-MMP and induce the cellular activation of pro-MMP2 (36–42). This response is in part dependent on β_1 integrin clustering and signaling (40, 42, 43) and is potentially self-regulating, since type I collagen is susceptible to MT1-MMP and MMP2 proteolysis (14, 44). Concentration of MT1-MMP by overexpression (45, 46) or clustering interactions (47–50) favors MMP2 activation and collagenolysis (50). Concomitant with increased MT1-MMP expression and MMP2 activation is the autocatalytic processing of MT1-MMP at Gly^{284}–Gly^{285} to shed the catalytic domain from the hemopexin C domain, which is retained on the cell membrane (40, 46, 51). Hence, the ectodomain of the residual 44-kDa MT1-MMP fragment (Gly^{285}–Val^{582}) on the cell surface consists of the linker, hemopexin C domain, and stalk segment only (see Fig. 1*A*, *ii*) and thus is catalytically inactive. The significance of the 44-kDa MT1-MMP *in vivo* is not clear. In addition to being present following cell binding to type I collagen, the 44-kDa MT1-MMP has also been detected on the surface of tumor cells (40, 51). During MMP2 activation, TIMP-2-free MT1-MMP must be in close proximity to a trimeric complex of MT1-MMP·TIMP-2·pro-MMP2 in order to activate the bound pro-MMP2 (52). The mechanisms of MT1-MMP oligomerization are not clear. The recombinant hemopexin C domain of MT1-MMP did not form oligomers in solution or modulate MMP2 activation when added to cells (47). Recent reports using transmembrane MT1-MMP chimera and deletion mutants have suggested that the hemopexin C domain can mediate homophilic complex formation of cellular MT1-MMP for efficient MMP2 activation (48, 49). Expression of a transmembrane-tethered MT1-MMP hemopexin C domain lacking the linker, termed PEX (Thr^{313}–Val^{582}), in HT1080 cells inhibited MT1-MMP oligomerization, the cellular activation of pro-MMP2, and Matrigel invasion (48), a function previously attributed to MMP2 proteolytic activity against type IV collagen (53).

Considering that MT1-MMP is a collagenase, we hypothesized that exosites on the hemopexin C domain would bind to type I collagen and be essential for collagenolytic activity. Thus, the autolytically generated 44-kDa MT1-MMP ectodomain would be predicted to modulate pericellular collagenolysis on the membrane through dominant-negative interactions. Since native type I collagen stimulates MMP2 activation, we also hypothesized that collagen binding by the hemopexin C domain of MT1-MMP would modulate MMP2 activation with 44-kDa MT1-MMP opposing these effects *in vivo*. Experiments reported here demonstrate that collagen binding by the MT1-MMP hemopexin C domain is essential for collagenolytic activity and enhancement of MMP2 activation by MT1-MMP. Inhibition of this interaction either *in vitro* or on the cell surface inhibits collagen degradation. Together, these studies suggest a novel feedback mechanism through which generation of the 44-kDa MT1-MMP autolysis product regulates pericellular collagenolytic activity and subsequent invasive potential.

EXPERIMENTAL PROCEDURES

Materials—Rat tail type I collagen was prepared as previously described (54). Vitrogen® was purchased from Cohesion (Palo Alto, CA). Biotin-labeled type I collagen was prepared as previously described (55). Human placental type I collagen was purchased from Sigma. The triple helical nature of collagen was confirmed by the absence of trypsin sensitivity at an enzyme/substrate ratio of 1:10 over 3 h, 28 °C. The general hydroxamate inhibitor BB2116 was provided by British Biotech Pharmaceuticals (Oxford, UK). Hydroxamate inhibitor GM6001 and AB8102 (blocking antibody raised against the human MT1-MMP catalytic domain) were purchased from Chemicon (Temecula, CA). The polyclonal antibody RP1MMP-14 (raised against the MT1-MMP linker) was purchased from Triple Point Biologics (Portland, OR). The affinity-purified polyclonal antibodies αMT1-CD and αHis_6 were described previously (47).

Synthetic Peptides and Recombinant Proteins—The MT1-MMP linker peptide analogs MT1-L18 (^{302}RPSVPDKPKNPTYGPNIC^{319}) (University of Victoria, Victoria, Canada) and MT1-L35 (^{285}GESGF-PTKMPPQPRTTSRPSVPDKPKNPTYGPNIC^{319}) (Tufts University, Medford, MA) (Fig. 1*A*, *iii*) were synthesized and verified by mass spectrometry. Recombinant domains of human MT1-MMP and MMP2 were expressed in *Escherichia coli* as N-terminal His-tagged proteins. The MT1-MMP hemopexin C domain (CD) with or without the linker (L) (MT1-LCD, Gly^{285}–Cys^{508}; MT1-CD, Gly^{315}–Cys^{508}) (*see* Fig. 1*A*) and the MMP2 hemopexin C domain with the linker (MMP2-LCD, Gly^{446}–Cys^{660}) were prepared as previously described (47). Recombinant human MMP2-CBD (Val^{220}–Gln^{393}) (collagen binding domain consisting of three fibronectin type II modules) was prepared previously (54). Any bacterial endotoxins in purified recombinant protein preparations were removed by polymyxin B-agarose columns (Sigma). The fidelity of purified recombinant proteins was confirmed by electrospray ionization mass spectrometry (47) and N-terminal Edman sequencing of protein bands cut from the membrane of Western blots. Human soluble MT1-MMP, truncated C-terminal to the hemopexin C domain (sMT1-MMP), was kindly provided by British Biotech Pharmaceuticals. Recombinant human MMP2, TIMP-1, and TIMP-2 were expressed in a mammalian cell system and purified as previously described (56) or kindly provided by Dr. H. Nagase (Imperial College School of Medicine, London, UK).

Electrophoretic Techniques—Samples in reducing (65 mM dithiothreitol) or nonreducing sample buffer (125 mM Tris-HCl, pH 6.8, 2.0% SDS, 2.0 M urea, 0.05% bromphenol blue) were separated on 15% SDS-PAGE gels and analyzed by either silver nitrate staining or by Western blotting using αMT1-CD and αHis_6 antibodies. ECL detection was performed according to the manufacturer's instructions (Amersham Biosciences). For zymographic analysis, samples were separated under nonreducing conditions on 10% SDS-PAGE gels co-polymerized with 0.5 mg/ml gelatin. Gels were washed for 30 min with 2.5% Triton X-100, rinsed with deionized water, and incubated with assay buffer (100 mM Tris, pH 8.0, 30 mM $CaCl_2$, 0.05% Brij, 0.025% NaN_3) at 37 °C for 4 h before staining with Coomassie Brilliant Blue G250.

Gel Filtration Chromatography—Purified MT1-LCD (0.5 mg) was subjected to gel filtration chromatography on a Superdex 75 column equilibrated with PBS (10 mM Na_2HPO_4, 1.8 mM NaH_2PO_4, 2.7 mM KCl,

140 mM NaCl, pH 7.4) and run on an AKTA purifier (Amersham Biosciences). Protein elution was monitored at 215 nm. Molecular mass standards used were BSA (67 kDa), ovalbumin (43 kDa), chymotrypsin A (25 kDa), and ribonuclease A (13.7 kDa).

Solid Phase Binding Assays—Native and heat-denatured type I collagen (rat tail) (5 μg/ml) were diluted in 15 mM Na_2CO_3, 35 mM $NaHCO_3$, 0.02% NaN_3, pH 9.6 (100 μl), and coated onto 96-microwell plates (Falcon) overnight at 4 °C as described previously (54, 57). Wells coated with myoglobin served as a control for nonspecific binding. The coated wells were blocked with 1% BSA to which serially diluted recombinant proteins in PBS (100 μl total volume) were added and incubated for 1 h at room temperature. After extensive washes, bound proteins were quantitated using affinity-purified polyclonal antibodies followed by incubation with goat anti-rabbit alkaline phosphatase-conjugated secondary antibody. Substrate, *p*-nitrophenyl phosphate disodium (Sigma), was added to the wells, and color development was monitored at 405 nm in a Thermomax plate reader (Molecular Devices).

Ligand Blot Assays—Proteins (5 μg) in 50 mM Tris-HCl, pH 8.0, 150 mM NaCl were filtered onto an Immobilon-P® membrane (Millipore Corp.) by vacuum. Membranes were blocked with 1% BSA in PBS and incubated with biotin-labeled native type I collagen in PBS/Tween 20 for 1 h. Bound collagen was visualized using horseradish peroxidase (HRP)-conjugated streptavidin and ECL detection.

Enzyme Assays—Biotin-labeled type I collagen (0.025 pmol) was incubated with either sMT1-MMP or MMP2 in assay buffer (50 mM Tris-HCl, pH 7.4, 200 mM NaCl, 5 mM $CaCl_2$, 3.8 mM NaN_3, 0.05% Brij) for 18 h at 28 °C. MMPs were activated with 2 mM 4-aminophenylmercuric acetate. Recombinant proteins and BB2116 in assay buffer were added to the reactions where indicated. Following digestion, samples were separated by 7.5% SDS-PAGE and analyzed by Western blotting using streptavidin-HRP and ECL detection. α1(I) and α2(I) chains were quantitated by scanning densitometry, and the percentage of native collagen cleavage was calculated as previously described (58). Cleavage of the quenched fluorescent substrate, Mca-Pro-Leu-Gly-Dpa-Ala-Arg-NH_2, was performed as described previously (56). MT1-LCD and MT1-CD in assay buffer (100 mM Tris-HCl, pH 7.4, 100 mM NaCl, 10 mM $CaCl_2$, 0.05% Brij) were added to the reaction where indicated.

Transmembrane MT1-MMP and MT1-MMP Hemopexin C Domain Constructs—The mammalian expression vector pCR3.1-Uni (Invitrogen) carrying human MT1-MMP cDNA was the generous gift of Dr. D. Pei (University of Minnesota). To express cell surface (c) transmembrane MT1-MMP hemoperin C domain, cMT1-CD (Δ112–315) and cMT1-LCD (Δ112–284), two-step overlapping PCR was used with T7 and reverse primer as external primers and either 5′-CGAAGGAAGCGCCCCAACATCTGTGACGGGAAC-3′ and 5′-ACAGATGTTGGGGCGCTTCCTTCGAACATTGGC-3′ (cMT1-CD, Δ112–315) or 5′-CGAAGGAAGCGCGGTGAGTCAGGGTTCCCCACC-3′ and 5′-CCCTGACTCACCGCGCTTCCTTCGAACATTGGCC-3′ (cMT1-LCD, Δ112–284) as internal primer pairs. The catalytically inactive MT1-MMP (E240A) mutant construct was generated using 5′-GGTGGCTGTGCACGCGCTGGGCCATGCC-3′ and 5′-GGCATGGCCCAGCGCGTGCACAGCCACC-3′ (E240A) primers. Full-length constructs were synthesized by PCR with T7 and reverse primers, digested with *Hin*dIII and *Eco*RI, ligated back to pCR3.1-Uni vector, and fully sequenced.

Cell Culture and Stable Transfection—Early passage human gingival fibroblasts were kindly provided by Dr. D. Brunette (University of British Columbia, Vancouver, Canada) and maintained in Dulbecco's modified Eagle's medium (DMEM) containing 10% newborn calf serum (Invitrogen). MDA-MB-231 breast carcinoma cells were kindly provided by Dr. V. G. Jordan (Northwestern University, Chicago, IL) and cultured in DMEM (Cellgro) supplemented with 10% fetal bovine serum (U.S. Bio-Technologies Inc.). MDA-MB-231 cells were transfected with MT1-MMP cDNA constructs using FuGENE 6 (Roche Molecular Biochemicals) according to the manufacturer's instructions. Stable cell lines were clone-selected and maintained in medium containing 1 mg/ml G418 (Mediatech Inc.). For each line, five clones were pooled and used in the experiments.

Transwell Invasion and Migration Assay—MDA-MB-231 cell invasion and migration assays through type I collagen (human placental) were performed as described previously (42). Endotoxin-free recombinant proteins, linker peptide analogs and antibodies in PBS were added to the cell media with BSA or IgG as controls. GM6001 was added to the cells in Me_2SO.

Collagen Gels—To prepare collagen gels, 8 volumes of Vitrogen was neutralized with 1 volume of 10× concentrated PBS and 1 volume of 0.1 M NaOH. Fibroblasts were detached with PBS containing 0.54 mM EDTA and 1.1 mM glucose and resuspended in a neutralized Vitrogen solution (2.0 mg/ml) containing 11.3% DMEM and 2.5% new born calf serum. The cell/collagen solution (75 μl) was then transferred into 96-well tissue culture plates and incubated at 37 °C for 1 h to allow for collagen polymerization. Cells were supplemented with DMEM containing 2.5% newborn calf serum for 18 h. Collagen gels were then rinsed with DMEM, and cells were cultured under serum-free conditions with or without MT1-LCD (endotoxin-free, in PBS) for the duration of the experiment. Cell conditioned medium was replaced every 24 h and analyzed by gelatin zymography after 72 h.

Latex Beads—Native and denatured type I collagen (100 μg/ml) were incubated with latex beads (1%) (Sigma) for 1 h at room temperature to allow for adsorption. The beads were then washed with PBS and blocked with 1% BSA for 1 h. Beads not absorbed with collagen served as a control. Blocked beads were rinsed with PBS and resuspended in DMEM at a concentration of 0.2% (v/v). Fibroblasts cultured in 96-well tissue culture plates were rinsed and incubated in serum-free medium for 1 h prior to incubation with the latex beads in DMEM (100 μl). Endotoxin-free MT1-LCD in PBS was added to the latex bead preparations where indicated. Cells were cultured for 24 h, after which the conditioned cell medium was analyzed by gelatin zymography.

RESULTS

Recombinant Protein Expression—To characterize the hemopexin C domain of MT1-MMP and the ectodomain of 44-kDa MT1-MMP, two forms of the MT1-MMP hemopexin C domain were cloned and expressed in *E. coli*. MT1-LCD (Gly^{285}–Cys^{508}) corresponds to the N terminus of 44-kDa MT1-MMP and includes both the linker and the hemopexin C domain (Fig. 1*A*, *iv*). MT1-CD (Gly^{315}–Cys^{508}) consists of the hemopexin C domain only (Fig. 1*A*, *iv*). Yields of purified protein were typically ~20 mg from 3 liters of liquid culture. The identities of the purified proteins were confirmed by Western blotting with αMT1-CD antibody (Fig. 1*B*) and αHis_6 (data not shown). Nonreducing SDS-PAGE analysis demonstrated the absence of dimeric intermolecular disulfide cross-linked aggregates (Fig. 1*B*). Reducing SDS-PAGE and electrospray ionization mass spectrometry determination of the purified protein masses were consistent with the predicted masses. As shown in Fig. 1*B*, both MT1-LCD (27,894 Da) and MT1-CD (24,612 Da) were within 1–2 Da of the predicted mass after accounting for the removal of the N-terminal methionine and hydrogen atoms after disulfide bond formation. Edman sequencing also confirmed N-terminal methionine processing and the presence of the N-terminal His_6 tag (Fig. 1*B*). MT1-LCD did not form noncovalent multimeric complexes under native conditions in solution as shown by the elution of a single peak at 28 kDa corresponding to the monomeric form of MT1-LCD upon gel filtration chromatography (Fig 1*C*).

Collagen Binding Properties of the MT1-MMP Hemopexin C Domain—We first assessed the collagen binding properties of the MT1-MMP hemopexin C domain by performing solid phase binding assays with type I collagen, the preferred collagen substrate of MT1-MMP. As shown in Fig. 2*A*, binding of MT1-CD and MT1-LCD to native collagen films was similar, indicating that the linker had little apparent affect on collagen binding affinity. Unlike MMP2-CBD, both MT1-CD and MT1-LCD did not bind denatured collagen (Fig. 2*B*), confirming specificity. As a control, MMP2-LCD did not bind native or denatured type I collagen as shown previously (57). Binding of soluble native type I collagen to MT1-CD and MT1-LCD was confirmed by ligand blot analysis with MMP2-LCD and BSA serving as negative controls (Fig. 2*C*).

Collagen/MT1-MMP Hemopexin C Domain Interactions during Collagen-induced MMP2 Activation—Physical clustering of MT1-MMP was previously shown to facilitate the pro-MMP2 activation reaction by increasing the proximity of catalytically active MT1-MMP to the trimeric activation complex (52). Due to the collagen binding properties of the MT1-MMP hemopexin C domain, we postulated that type I collagen may function as an *in vivo* mechanism to directly bind and concentrate cell surface MT1-MMP to facilitate the cellular activation of pro-

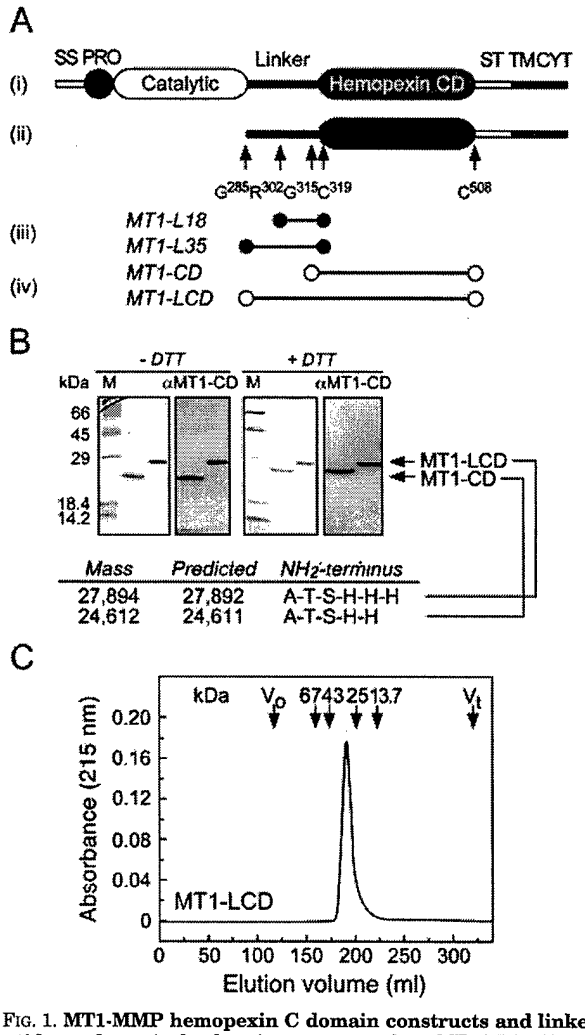

FIG. 1. **MT1-MMP hemopexin C domain constructs and linker peptide analogs.** *A*, the domain structures of pro-MT1-MMP (*i*) and 44-kDa MT1-MMP (*ii*) are shown in a linear diagram. The signal sequence (*SS*), propeptide domain (*PRO*), stalk segment (*ST*), transmembrane sequence (*TM*), and cytoplasmic tail (*CYT*) of MT1-MMP are indicated. Schematic representations of MT1-MMP linker peptide analogs MT1-L18 and MT1-L35 (*iii*) and hemopexin C domain constructs MT1-CD and MT1-LCD (*iv*) are shown with N- and C-terminal residues indicated. *B*, purified MT1-CD and MT1-LCD (0.1 μg) were electrophoresed on SDS-PAGE (15%) gels under reducing (+*DTT*) and nonreducing (−*DTT*) conditions. Gels were analyzed by either silver staining or by Western blotting using αMT1-CD antibody. Protein masses measured by electrospray ionization mass spectrometry (*Mass*), predicted masses, and N-terminal Edman sequence analysis are indicated. *C*, MT1-LCD was subjected to FPLC gel filtration chromatography on a Superdex 75 column, and elution was monitored at 215 nm. The elution volumes of the void volume (V_o) and column volume (V_t) and molecular weight standards are indicated.

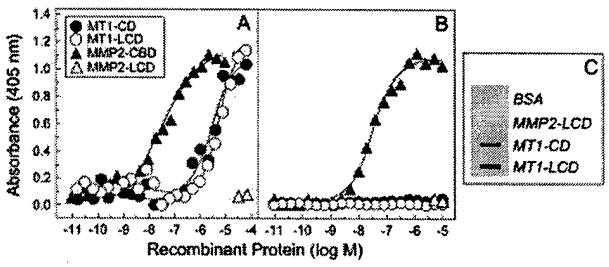

FIG. 2. **Type I collagen binding properties of MT1-MMP hemopexin C domain constructs.** Serial dilutions of MT1-CD and MT1-LCD were incubated in the same 96-microwell plates coated with native (*A*) or heat-denatured (65 °C for 1 h) (*B*) type I collagen (0.5 μg/well) as described under "Experimental Procedures." MMP2-CBD and MMP2-LCD were included as positive (54) and negative controls (57), respectively. Bound recombinant domains were detected using α-His_6 antibody. *C*, ligand blot assay. Immobilized MT1-CD and MT1-LCD and control proteins, BSA and MMP2-LCD (5 μg each), were incubated with biotin-labeled type I collagen (0.1 μg/ml) in PBS as described under "Experimental Procedures." Bound collagen was detected using streptavidin-HRP and ECL detection.

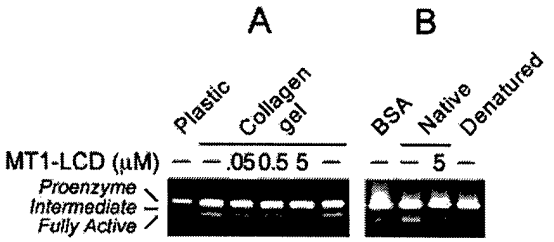

FIG. 3. **Recombinant MT1-MMP hemopexin C domain reduces collagen-induced activation of MMP2.** *A*, fibroblasts (1×10^4) grown on tissue culture plastic or within type I collagen gels (2.0 mg/ml) were incubated with MT1-LCD (0, 0.05–5 μM) in DMEM for 72 h. MMP2 in the conditioned cell media was visualized by gelatin zymography. *B*, fibroblasts (1×10^4) grown on plastic were incubated with latex beads adsorbed with type I collagen (native or denatured) or BSA in DMEM for 24 h. Exogenous MT1-LCD (5 μM) was added to the cultures where indicated. Conditioned cell media were analyzed by gelatin zymography. Lanes presented in both *A* and *B* are from the same zymogram.

MMP2. To test this, human gingival fibroblasts were cultured in three-dimensional type I collagen gels for 72 h to stimulate the activation of pro-MMP2. Soluble MT1-LCD was added to the cultures to compete with endogenous MT1-MMP for collagen binding. As shown in Fig. 3*A*, activation of pro-MMP2 in the cell cultures was reduced with increasing concentrations of MT1-LCD. Control cells cultured on plastic did not activate pro-MMP2. To confirm this response, latex beads coated with type I collagen were found to stimulate pro-MMP2 activation in fibroblasts cultured on plastic (Fig. 3*B*). Consistent with our observations of cells in collagen gels, induction of pro-MMP2 activation by native collagen-adsorbed beads was reduced by the presence of MT1-LCD to the levels seen with BSA-adsorbed beads (Fig. 3*B*). The requirement for fibrillar collagen was confirmed, since gelatin-adsorbed beads did not stimulate pro-MMP2 activation. In the absence of latex beads, the addition of soluble native collagen to fibroblasts cultured on plastic produced inconsistent and variable levels of activation (data not shown). Together, these results demonstrate that native type I fibrillar collagen interactions with the MT1-MMP hemopexin C domain in fibroblasts may concentrate cell surface MT1-MMP to stimulate the cellular activation of pro-MMP2.

Effect of Exogenous MT1-MMP Hemopexin C Domain on Collagenolysis by sMT1-MMP and MMP2—Studies of collagenases have shown that the hemopexin C domain is required to support binding to and cleavage of collagen (27–29, 31, 32, 59). To examine the role of the hemopexin C domain in MT1-MMP collagenolysis, recombinant hemopexin C domain constructs were incubated with sMT1-MMP and biotin-labeled type I collagen. Reactions were performed at 28 °C to maintain collagen triple helicity, as confirmed by the lack of collagen cleavage in the presence of trypsin even at a 1:10 enzyme/substrate molar ratio (data not shown). sMT1-MMP cleaved native type I collagen (Fig. 4*A*) and was inhibited by TIMP-2 and BB2116 (data not shown). As seen in Fig. 4*A* (*left panel*), the sMT1-MMP cleavage of native type I collagen was inhibited by the presence of MT1-LCD in a concentration-dependent manner. In contrast, neither MT1-CD (Fig. 4*A*, *right panel*) nor the control protein, MMP2-LCD, had any effect on cleavage. The percent-

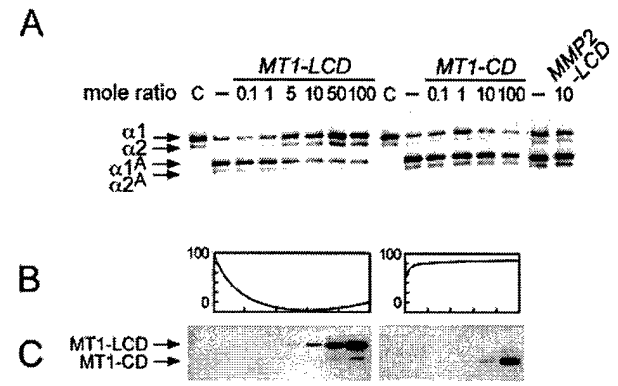

FIG. 4. **Recombinant MT1-MMP hemopexin C domain reduces MT1-MMP collagenolysis.** *A*, biotin-labeled type I collagen was incubated in the absence (*C*) or presence of sMT1-MMP (1 pmol) for 18 h at 28 °C. Recombinant proteins, MT1-LCD, MT1-CD, and MMP2-LCD were added at the indicated molar equivalents relative to sMT1-MMP. Reactions were separated by SDS-PAGE (7.5%), followed by Western blotting using streptavidin-HRP. *B*, percentage of α-chain cleavage was determined by densitometric analysis as described under "Experimental Procedures" and plotted against the amount of recombinant hemopexin C domain added. *C*, MT1-LCD and MT1-CD were detected in reaction samples by SDS-PAGE (15%) and Western blotting using the αMT1-CD antibody.

age of α-chain cleavage for each reaction was quantitated by scanning densitometry and graphically plotted against the amount of MT1-LCD or MT1-CD added (Fig. 4*B*). The presence of hemopexin C domain proteins at the end of each reaction was confirmed by Western blot analysis (Fig. 4*C*). As a control, MT1-CD and MT1-LCD did not affect sMT1-MMP activity against the quenched fluorescent peptide, Mca-Pro-Leu-Gly-Dpa-Ala-Arg-NH_2 (Table I), demonstrating that inhibition by MT1-LCD is specific for triple helical substrates and that peptide bond cleavage by MT1-MMP does not require the hemopexin C domain. Due to the unique association between MT1-MMP and MMP2 *in vivo*, we assessed whether the MT1-MMP hemopexin C domain may affect MMP2 collagenolysis. Similar to that observed for MT1-MMP, MT1-LCD, but not MT1-CD, disrupted MMP2 cleavage of native type I collagen (Fig. 5).

Collagen Binding Properties of MT1-MMP Linker Peptide Analogs and the Effect on Collagenolysis—Although both MT1-MMP hemopexin C domain constructs share similar collagen binding properties, only MT1-LCD disrupted collagenolysis. Since this result indicated an important role for the linker in native collagen cleavage, we generated two synthetic peptide linker analogs to further study the effect of the MT1-MMP linker on MT1-MMP collagenolysis. From clustal alignments, we synthesized the peptide analog MT1-L18 (Arg^{302}–Cys^{319}), which corresponds to an 18-amino acid residue region of similarity possessed by the collagenolytic MMPs, MMP1, MMP2, MMP8, and MMP13 (Fig. 6*A*). MT1-L35 (Gly^{285}–Cys^{319}) encompasses the entire MT1-MMP linker and includes the unique 17-amino acid residue region that is N-terminal to the homologous 18-amino acid residue region (Fig. 6*A*). As shown in Fig. 6*B*, neither MT1-L18 nor MT1-L35 showed affinity for native (Fig. 6*B*, *i*) or denatured type I collagen (Fig. 6*B*, *ii*), indicating that the MT1-MMP linker alone does not contribute to collagen binding or that the collagen binding site spans the junction of the linker and hemopexin C domain. Similarly, both peptide analogs did not disrupt native type I collagen cleavage by sMT1-MMP, even at a 1000-fold molar excess (Fig. 6*C*). To determine whether either linker peptide sequence could confer regulatory activity on the MT1-CD polypeptide, MT1-L18 or MT1-L35 was added to the reaction mixture containing MT1-CD. As shown in Fig. 6*C*, no inhibition of collagenolysis was observed. In a second set of experiments, MT1-LCD inhibited collagen cleavage as previously observed (Fig. 4), regardless of whether MT1-L18 or MT1-L35 was added. Since the presence of the linker sequence and the hemopexin C domain together as separate polypeptides is not sufficient for disrupting cleavage, these data suggest that the ability of the MT1-LCD to inhibit collagenolysis is context- and/or conformation-specific.

TABLE I
Quenched fluorescent peptide cleavage by sMT1-MMP

Mca-Pro-Leu-Gly-Dpa-Ala-Arg-NH_2 (0.1 nmol) was incubated with (control) or without (buffer) sMT1-MMP (0.035 pmol) for 1 h at 37 °C. MT1-LCD and MT1-CD were added to the reaction at a 100-fold molar excess to sMT1-MMP. RFU, relative fluorescence units.

	Buffer	Control	MT1-LCD	MT1-CD
Rate of cleavage (RFU × $10^{-3} \cdot s^{-1}$)	0.05	6.7	7.0	7.0

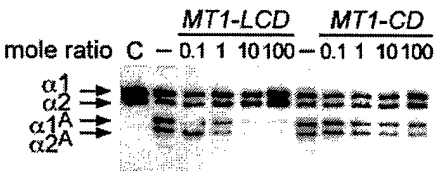

FIG. 5. **Recombinant MT1-MMP hemopexin C domain blocks MMP2 cleavage of native collagen.** *A*, biotin-labeled type I collagen was incubated in the absence (*C*) or presence of MMP2 (0.84 pmol) for 18 h at 28 °C. MT1-LCD and MT1-CD (0.1–100-fold molar equivalents) were added to the reactions where indicated. Following digestion, samples were separated by SDS-PAGE (7.5%), followed by Western blotting using streptavidin-HRP.

Cellular Invasion of Type I Collagen is Inhibited by a 44-kDa MT1-MMP Ectodomain Fragment—Active MT1-MMP is efficiently processed to a 44-kDa ectodomain fragment containing the MT1-LCD sequence (Gly^{285}–Cys^{508}) that is retained on the cell membrane (40, 46, 51). Since the soluble MT1-LCD inhibits native collagen cleavage by sMT1-MMP, we hypothesized that 44-kDa MT1-MMP may also function in a similar manner at the cell surface to modulate the collagenolytic activity of transmembrane MT1-MMP. To test this hypothesis, we used MDA-MB-231 breast carcinoma cells, which express endogenous MT1-MMP in the absence of detectable levels of MMP2. Invasion of three-dimensional collagen gels overlaid onto a porous polycarbonate filter requires collagenolytic activity (42). In control experiments, MDA-MB-231 cellular invasive activity was inhibited by the hydroxamate inhibitor GM6001, indicating a requirement for metalloproteinase activity (Fig. 7*A*). TIMP-2 significantly reduced invasion ($p < 0.05$), whereas TIMP-1 or the BSA control had no effect, confirming the dependence for MT-MMPs (60) in MDA-MB-231 cell invasion. A blocking antibody against the MT1-MMP active site (Fig. 7*A*, *anti-MT1*) also reduced invasion compared with IgG controls ($p < 0.05$), identifying MT1-MMP as the critical protease in this process. Indeed, overexpression of MT1-MMP on MDA-MB-231 cells increased collagen invasion ~2.5-fold compared with vector transfectants ($p < 0.05$, Fig. 7*A*, *black bars*). Furthermore, expression of the inactive mutant, MT1-MMP (E240A), on MDA-MB-231 cells resulted in inhibition of invasion to below control values, suggesting that this species may function in a dominant negative manner.

To determine whether the MT1-LCD could inhibit cell-associated collagenolytic activity, cells were incubated with MT1-LCD, MT1-L35, or BSA. At low concentrations (4 μM), the invasion of MT1-MMP transfected (Fig. 7*B*) or parental (data not shown) MDA-MB-231 cells was unaffected. MT1-L35 did not affect invasion at any concentration tested (data not

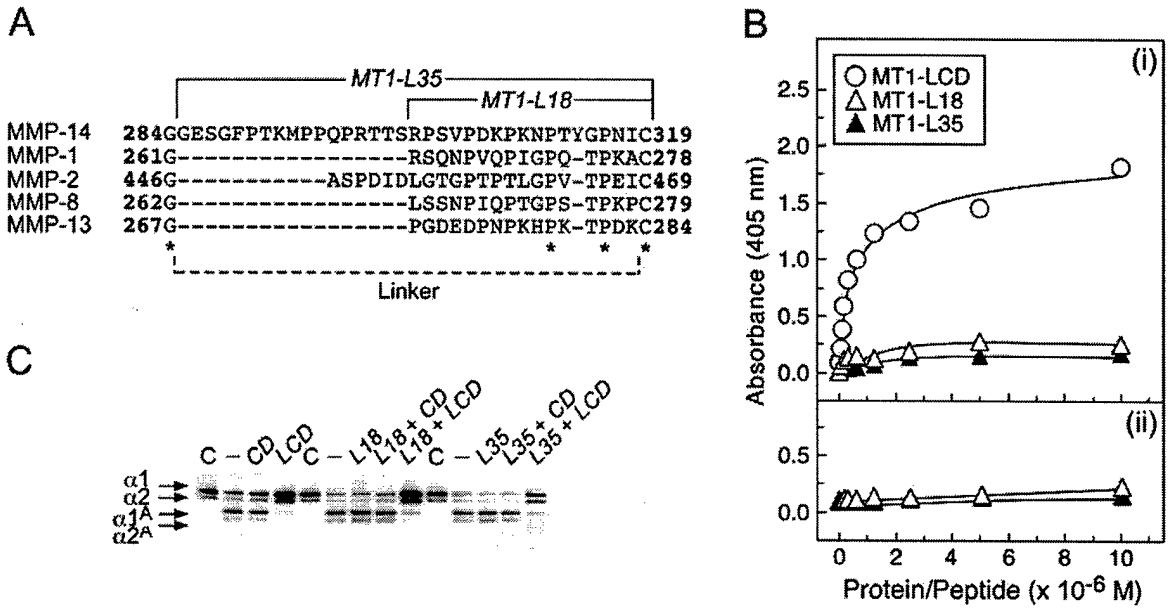

FIG. 6. **Characterization of MT1-MMP peptide linker analogs.** *A*, sequence alignment of collagenolytic MMP linkers using Megalign (DNASTAR Inc.) (Clustal method). Conserved residues are denoted with *asterisks*. Sequences of the peptide analogs of MT1-MMP are indicated. *B*, a 96-well plate was coated with either native (*i*) or denatured (*ii*) type I collagen (rat tail) (0.5 μg/well). Serial dilutions of MT1-LCD, MT1-L18, and MT1-L35 were added, and bound protein/peptide was detected using RP1MMP-14 antibody, which recognizes the linker. *C*, biotin-labeled type I collagen was incubated in the absence (*C*) or presence of sMT1-MMP (1 pmol) for 18 h at 28 °C. Molar excesses of MT1-MMP hemopexin C domain constructs (*CD* and *LCD*) (100-fold) and linker peptide analogs (*L18* and *L35*) (1000-fold) were added to the reaction where indicated. Reactions were separated by SDS-PAGE (7.5%), followed by Western blotting using streptavidin-HRP.

shown). However, since MT1-LCD binds native collagen, the effective concentration of free protein available to the cells may be reduced by binding to the collagen filters. Therefore, the highest concentration possible with these protein preparations (30 μM) was used to ensure saturation of binding sites within the collagen-coated filters and availability of free protein at the cell surface to interact with MT1-MMP. Under these conditions, collagen invasion was significantly reduced ($p < 0.05$; Fig. 7*B*), demonstrating inhibition of cell-associated MT1-MMP collagenolytic activity and confirming the *in vitro* analysis of MT1-LCD inhibiting collagen cleavage.

Because autolysis of transmembrane MT1-MMP leads to the accumulation of a cell surface 44-kDa MT1-MMP ectodomain fragment containing the linker and hemopexin C domain but lacking the active site, the effect of this cell-associated product on cellular MT1-MMP-mediated collagenolysis was assessed. For this experiment, transmembrane constructs of MT1-LCD (Gly^{285}–Val^{582}, designated cMT1-LCD) and MT1-CD (Pro^{316}–Val^{582}, designated cMT1-CD) (Fig. 8*A*) were expressed in MDA-MB-231 cells, and type I collagen invasion was assessed relative to vector-transfected controls. Intracellular furin processing of these constructs at Arg^{111} generates the 44-kDa MT1-MMP and the linker-deleted form thereof. Expression of cMT1-LCD significantly reduced invasion by 50% to levels similar to those seen with soluble MT1-LCD when compared with cells expressing cMT1-CD ($p < 0.05$; Fig. 8*B*). This confirms the above results and the *in vitro* biochemical analyses and demonstrates the importance of the MT1-MMP linker-hemopexin C domain in native collagen cleavage by cellular MT1-MMP. In control experiments, migration of MDA-MB-231 cells toward type I collagen, a process independent of collagenase activity (42, 61), was unaffected by expression of cMT1-LCD or cMT1-CD (Fig. 8*C*). Since these data clearly demonstrate the ability of cMT1-LCD to modulate type I collagen cleavage by transmembrane MT1-MMP, our results suggest that a function of the endogenous MT1-MMP autolysis product, 44-kDa MT1-MMP, is to regulate pericellular collagenolytic activity.

DISCUSSION

As an integral membrane protein, MT1-MMP appears suited for coordinating the homeostatic catabolism of pericellular type I collagen under the guide of the cell (62–65). MT1-MMP mediates collagen degradation directly by cleaving native collagen and, indirectly, by activating MMP13 (9) and the gelatinase and weak collagenase, MMP2 (11–13). Spatially and temporally, these two distinct activities of MT1-MMP regulate collagenolytic and gelatinolytic activities on the cell surface. Since MT1-MMP is a critical initiator and effector in the pericellular collagenolytic cascade, the regulation of its biological activity is very important in physiological and pathological collagen remodeling. The studies reported here have revealed the importance of the MT1-MMP hemopexin C domain and linker in the mechanism of collagen cleavage and demonstrated the role of collagen binding to MT1-MMP in stimulating MMP2 activation by cells. Moreover, these actions may be modulated in a dominant negative manner by the 44-kDa remnant form of MT1-MMP on the cell surface, revealing a novel regulatory function in proteolysis for an autolytic fragment of a protease.

The structure of collagen presents a challenge for proteolytic cleavage, as indicated by the low k_{cat}/K_m values for collagenases (66). Despite several studies from a number of laboratories, the triple helicase mechanism remains enigmatic (14). Our use of recombinant domains and polypeptides to probe the exosite requirements of MT1-MMP for collagenolysis revealed similar domain requirements for triple helicase activity as the secreted collagenases. The binding of the MT1-MMP hemopexin C domain, with or without the linker, to native collagen is consistent with previous reports for the collagenolytic MMPs (27, 30–32). The hemopexin C domain of MMP2, in contrast, does bind native collagen stably (57). Interestingly, the MT1-MMP hemopexin C domain does not bind denatured collagen. This suggests that, following cleavage, subsequent denaturation of the collagen would result in the release of MT1-MMP from the cleaved substrate facilitating turnover.

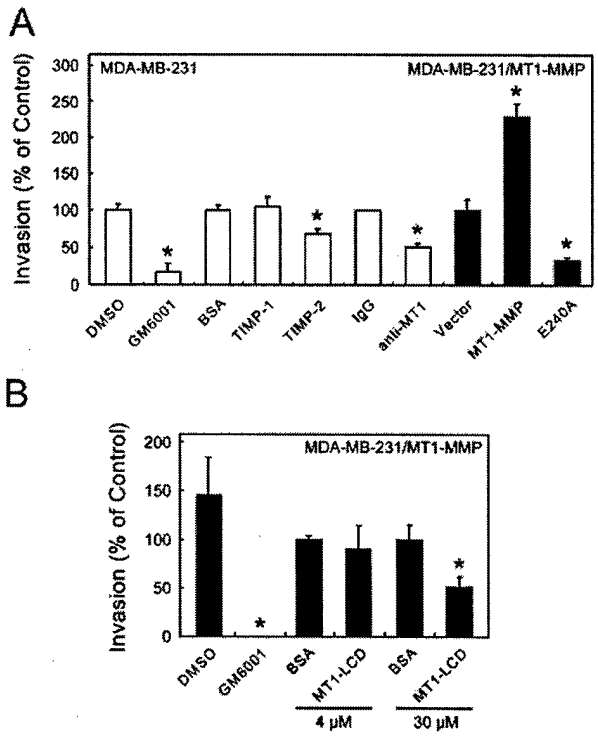

FIG. 7. **Invasion of MDA-MB-231 cells is MT1-MMP-dependent and is inhibited by recombinant MT1-MMP hemopexin C domain.** *A* and *B*, invasion of type I collagen. Cells (2.5×10^5) were seeded onto Transwell filters (8-μm pore) coated with a type I collagen gel (20 μg) and allowed to invade for 24 h as described under "Experimental Procedures." Noninvading cells were removed from the upper chamber with a cotton swab. Filters were then stained, and cells, adherent to the underside of the filter, were enumerated using an ocular micrometer. The average of triplicate experiments were normalized to corresponding controls (designated 100%) and are presented with S.D. value shown (*, $p < 0.05$). *A*, parental MDA-MB-231 cells (*white*) were allowed to invade in the presence of Me_2SO (*DMSO*), GM6001 (10 μM), BSA (10 nM), TIMP-1 (10 nM), TIMP-2 (10 nM), purified rabbit IgG (*IgG*; 10 μg/ml), or AB8102 antibody (*anti-MT1*; 10 μg/ml). MDA-MB-231 cells expressing MT1-MMP or MT1-MMP(E240A) (*black*) were also analyzed. Results are expressed as percentage of control invasion (*versus BSA* and *Vector*, as appropriate). *B*, MDA-MB-231 cells expressing MT1-MMP (2.5×10^5) were incubated with Me_2SO, GM6001 (10 μM), MT1-LCD, and BSA (4 and 30 μM) and allowed to invade for 24 h. Results are expressed as percentage of control invasion (*versus* BSA).

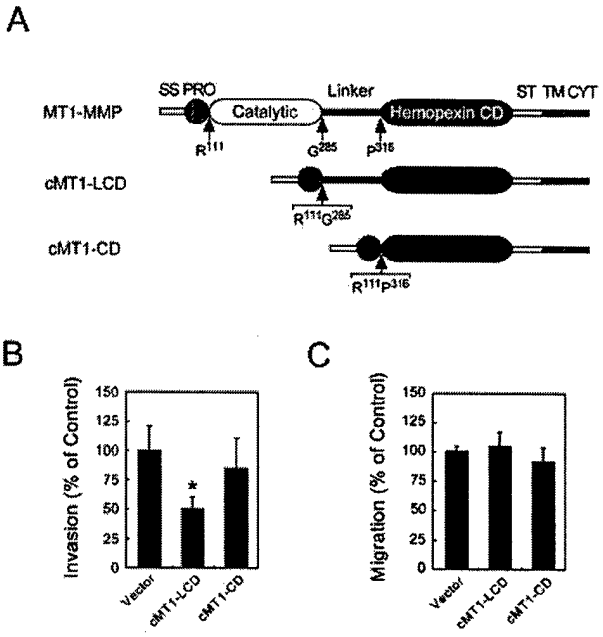

FIG. 8. **Recombinant 44-kDa MT1-MMP inhibits MDA-MB-231 cell invasion.** *A*, linear diagram of MT1-MMP and deletion mutants, cMT1-LCD (Δ112–284) and cMT1-CD (Δ112–315). The signal sequence (*SS*), propeptide domain (*PRO*), stalk segment (*ST*), transmembrane sequence (*TM*), and cytoplasmic tail (*CYT*) are indicated. Invasion of type I collagen (*B*) and migration (*C*) of MDA-MB-231 cells expressing MT1-MMP deletion mutants, cMT1-LCD and cMT1-CD, were assessed. *B*, cells (2.5×10^5) were seeded onto Transwell filters (8-μm pore) coated with a type I collagen gel (20 μg) and allowed to invade for 24 h as described under "Experimental Procedures." *C*, cells (2.5×10^5) were seeded onto Transwell filters coated with a thin layer of collagen on the underside and incubated for 1.5 h to permit migration. In both assays, noninvading or nonmigrating cells were removed from the upper chamber with a cotton swab. Filters were then stained, and cells, adherent to the underside of the filter, were enumerated using an ocular micrometer. The averages of triplicate experiments were normalized to the vector control (designated 100%) and are presented with S.D. value as shown (*, $p < 0.05$).

Inhibition of sMT1-MMP collagen cleavage using MT1-MMP hemopexin C domain constructs required the presence of the linker, indicating that collagen binding, by the hemopexin C domain alone, is not sufficient to disrupt collagenolysis. This requirement was also observed in MMP2 collagenolysis, since MT1-LCD, but not MT1-CD, blocked MMP2 cleavage of native collagen. Protein engineering studies of MMP1 and MMP8 have previously shown a role for the linker in triple helicase activity (33–35); however, our studies have revealed some unique features of the MT1-MMP linker. De Souza *et al.* (67) proposed that the MMP1 collagenase linker, due to its proline content, intercalates with the collagen triple helix, thereby displacing individual α-chains for cleavage. We found that MT1-MMP linker peptide analogs of either the full-length 35-amino acid residue linker or the 18-amino acid residue region, corresponding to that found in the secreted collagenases, did not bind native or denatured type I collagen. These results indicate that the MT1-MMP linker may not bind or intercalate with the collagen triple helix as proposed for the MMP1 linker. Indeed, the low glycine content renders triple helix formation by these linkers impossible. Potentially, the full collagen binding exosite of the MT1-MMP hemopexin C domain that recognizes the ¾-¼ collagen site may span the linker/hemopexin C domain junction, thereby accounting for the lack of collagen binding by the linker analogs alone and the ineffectiveness of MTI-CD in blocking collagenolysis. The MT1-MMP linker, when connected to the hemopexin C domain, may act as a specificity determinant directing binding of the protease to the ¾-¼ collagen cleavage site. Thus, competition from MT1-LCD, but not MT1-CD, may block MT1-MMP from binding collagen here and so inhibit cleavage. Topographically, the MT1-MMP, and other collagenase linkers, may also correctly configure the catalytic domain relative to the hemopexin C domain for collagenolytic competence. Indeed, the MT1-MMP linker has predicted rigidity due to the presence of 9 proline residues, and we interpret the x-ray crystallographic structure of the MMP1 linker (68) to also indicate that the linker is not as flexible as generally thought. Hence, MT1-LCD binding of collagen may sterically disrupt the collagenolytic configuration of sMT1-MMP at the ¾-¼ collagen cleavage site, thereby inhibiting cleavage.

The importance of MT1-MMP in collagen homeostasis is supported by the finding that fibrillar type I collagen induces cell surface expression of MT1-MMP and subsequent MMP2 activation through transcriptional and nontranscriptional pathways (36–41, 69). Induction of MT1-MMP transcription is dependent on β_1 integrin receptors and actin cytoskeleton rearrangement (38, 43). Clustering of β_1 integrins by collagen

ligation or antibody cross-linking induces *de novo* expression of MT1-MMP and subsequent MMP2 activation (40, 42). Interestingly, our data reveal that collagen may also assemble MT1-MMP on the cell surface via binding to the hemopexin C domain, thereby increasing the local concentration of MT1-MMP for collagenolysis and efficient MMP2 activation. In view of the demonstrated absence of oligomer formation by the MT1-LCD used here and previously reported (47), we interpret the reduction in collagen-induced MMP2 activation by MT1-LCD to be the result of competitive binding for collagen between the exogenous MT1-LCD and cell surface MT1-MMP, rather than competitively disrupting any MT1-MMP·MT1-MMP binding interactions. Indeed, this interaction between MT1-MMP and collagen may represent a biological mechanism similar to that observed with ConA, which clusters MT1-MMP on the cell surface during MMP2 activation (47). As originally shown, ConA increases the matrix-degradative phenotype of the cell through transcriptional and post-transcriptional regulation of MMP and TIMP genes that was reflected by extensive endogenous collagen degradation in the conditioned media and in biochemical assays (50). Cleavage of β_1 integrin-ligated collagen also releases bound pro-MMP2, which can now enter the activation pathway, which otherwise is recalcitrant to activation (70). Hence, pericellular collagen has multiple effects in binding and regulating the activities of collagenolytic MMPs, representing an unusual relationship between a protease and cognate substrate that appears to contribute to the homeostatic maintenance of collagen levels.

MT1-MMP activity on the cell surface is further regulated by endocytosis (71, 72), TIMP binding (45, 56, 73), and trimolecular complex formation (56, 74) as well as the autolytic shedding of the catalytic domain to yield 44-kDa MT1-MMP (46, 51, 75, 76). Currently, the role of 44-kDa MT1-MMP *in vivo* is not clear. It has been reported recently that the hemopexin C domain and the cytoplasmic tail of MT1-MMP mediate homophilic interactions that increase MMP2 activation (48, 49). Using HT1080 cells, Itoh *et al.* (48) found that expression of MT1-MMP PEX (Thr^{313}–Val^{582}), a truncated form of 44-kDa MT1-MMP that lacks most of the linker and hence is similar to cMT1-CD used here, reduced MMP2 activation and subsequent Matrigel invasion, presumed to be by disrupting the formation of oligomeric MT1-MMP complexes. PEX is unfortunately a confusing designation for the MT1-MMP hemopexin C domain, since PEX was already the name of a cell surface zinc metallopeptidase belonging to the neprilysin family (77, 78). As reported here and previously (47), we have found no evidence for oligomerization using MT1-LCD or MT1-CD, emphasizing the importance of cell membrane context or the stalk segment, transmembrane sequence, and cytoplasmic tail in these proposed complexes. Our recent data[2] indicate that the stalk segment also does not dimerize or drive oligomerization of 44-kDa MT1-MMP. Unlike the effects of MT1-LCD in disrupting the collagen-induced activation of MMP2 shown here, the inability of soluble MT1-LCD or MT1-CD to competitively block ConA-induced MMP2 activation in cells cultured on plastic reported previously (47) indicates the importance of cellular context for these effects and highlights the difference in collagen-mediated activation of MMP2, which is blocked by MT1-LCD, from activation induced by MT1-MMP overexpression or ConA, which is not.

In our previous studies of chemokine cleavage by MMP2, we found that MCP-3 and SDF-1α binding to the hemopexin C domain markedly improved the catalytic efficiency of cleavage (79, 80). Notably, the addition of recombinant MMP2 hemopexin C domain to mixtures of chemokine and active MMP2 in enzyme assays could entirely block substrate cleavage (80). Therefore, the presence of the entire 35-amino acid residue linker and hemopexin C domain in the 44-kDa MT1-MMP ectodomain suggested to us that this autolytic product has the potential to antagonize the proteolytic activity of MT1-MMP in a dominant-negative manner by interacting with native collagen. Our data demonstrate that expression of cMT1-LCD (Gly^{285}–Val^{582}), representing the 44-kDa MT1-MMP in its entirety (46, 76), on MDA-MB-231 cells inhibits MT1-MMP-mediated type I collagen cleavage and cell invasion. The inhibitory effect of cMT1-LCD expression on cell invasion was confirmed by the addition of soluble MT1-LCD to MT1-MMP-transfected cells. Since MDA-MB-231 cells do not express MMP2, the effect of cMT1-LCD expression and MT1-LCD on collagenolysis and cell invasion is distinct from that reported previously (48) and discussed above. Nonetheless, the capacity of MT1-LCD to also block MMP2 native collagen cleavage may amplify the down-regulation of collagenolysis *in vivo* by blocking MMP2 in addition to MT1-MMP but sparing MMP2 gelatinolysis. Invasion was also inhibited with the expression of MT1-MMP (E240A), a dominant-negative mutant mimicking TIMP-2-inhibited MT1-MMP, further supporting the role of MT1-MMP in collagen invasion and of inactive MT1-MMP forms in competing for collagen binding and down-regulating collagen cleavage. Consistent with our biochemical analysis, neither the expression of cMT1-CD nor the addition of soluble MT1-CD (data not shown) affected cell invasion to a significant degree, confirming the importance of the MT1-MMP linker in context with the hemopexin C domain in collagenolysis. In view of these effects, we propose that 44-kDa MT1-MMP may reduce MMP2 activation by reducing MT1-MMP clustering mediated by pericellular collagen. Together, these results clearly reveal the 44-kDa MT1-MMP as a novel inhibitor of pericellular type I collagen cleavage by MT1-MMP and MMP2 activities. Our studies also demonstrate the feasibility of designing new MMP inhibitors that target the substrate rather than the protease (81). This new class of inhibitors may exert highly selective substrate-specific protease inhibition while sparing the cleavage of other substrates in the protease degradome. Similarly, targeting the protease exosite rather than the active site may also represent new avenues of substrate-specific inhibition to achieve levels of specificity not possible with active site inhibitors (81).

The degradation of pericellular type I collagen is revealed to be a dynamic self-regulated process. We have previously proposed models regarding the regulation of pericellular type I collagen levels upon β_1 integrin stimulation of MT1-MMP and MMP2 activity (14, 40, 70). Our investigation into the role of the 44-kDa MT1-MMP ectodomain adds a new dimension to this homeostatic process. As modeled in Fig. 9, fibrillar type I collagen induces a β_1 integrin-dependent increase in MT1-MMP expression on the cell surface, thus favoring an initial collagenolytic phase. Our data show that the collagen binding properties of the MT1-MMP hemopexin C domain are necessary for native collagen cleavage (Fig. 9*A*). As suggested previously (70), the release of collagen-bound pro-MMP2 from the cell surface following collagen cleavage by MT1-MMP allows pro-MMP2 reservoirs to be optimally activated temporally and spatially in relation to its substrate. Collagen binding by the MT1-MMP hemopexin C domain also potentiates MMP2 activation, most likely by concentrating MT1-MMP·TIMP-2·pro-MMP2 complexes with TIMP-free MT1-MMP (Fig. 9*A*). Furthermore, in the MMP2 activation process, MT1-MMP collagenolytic activities are suppressed by TIMP-2 binding to form the trimolecular pro-MMP2 complex and by MT1-MMP autolysis, converting the proteolytic signature of the cell from

[2] E. M. Tam and C. M. Overall, unpublished data.

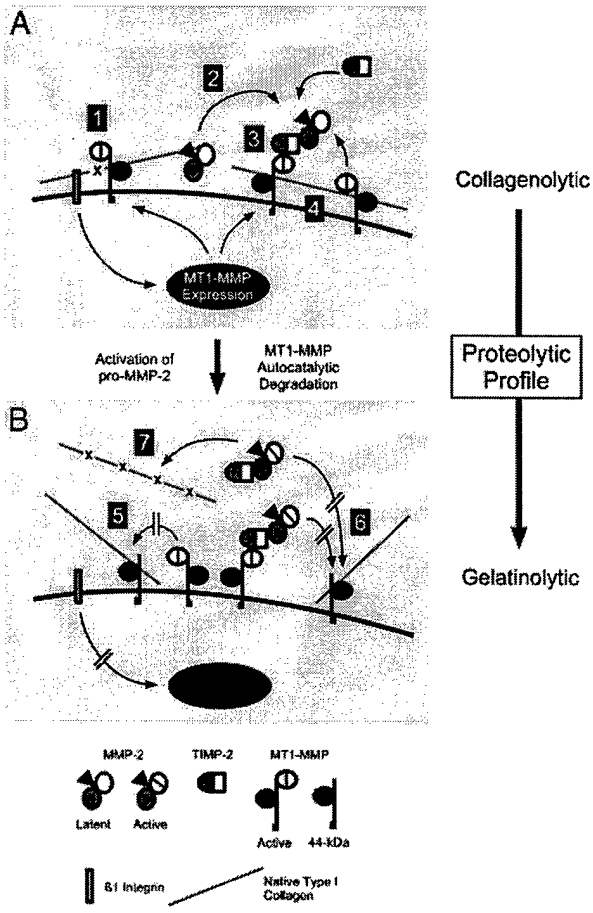

FIG. 9. **Potential role of the 44-kDa MT1-MMP in pericellular collagen degradation.** *A*, collagenolytic cell profile. Upon collagen-induced engagement of β_1 integrins and intracellular signaling, expression of MT1-MMP is up-regulated on the cell surface. Increased MT1-MMP expression promotes the cleavage of native collagen (*1*) and the release of collagen-bound pro-MMP2, which now enters into the activation pathway (*2*). The conversion from collagenolysis to gelatinolysis commences with the formation of the trimolecular complex (*3*), which reduces MT1-MMP collagenolytic activity, and the activation of pro-MMP2, which is enhanced by the collagen-mediated assembly of MT1-MMP (*4*). Collagen binding by TIMP-2-inhibited MT1-MMP in the trimolecular complex may also block collagen cleavage by uninhibited MT1-MMP. *B*, gelatinolytic cell profile. Following pro-MMP2 activation and MT1-MMP autolysis, the 44-kDa MT1-MMP accumulates on the cell surface, binds native collagen, and suppresses collagen degradation by inhibiting MT1-MMP (*5*) and MMP2 (*6*) collagenolysis but not MMP2 gelatinolysis (*7*). Stimulation of cell surface MT1-MMP expression is reduced due to the absence of native collagen and β_1 integrin engagement which together allow collagen levels to increase.

collagenolytic to gelatinolytic. Following MT1-MMP autolytic shedding, our data show that the 44-kDa MT1-MMP continues to bind collagen, further reducing pericellular collagenolysis by MT1-MMP and MMP-2 (Fig. 9*B*). Overall, these intimately related and complex events allow for a conversion of proteolytic activity to take place on the cell surface. This shift from a collagenolytic to a gelatinolytic profile may be important for maintaining pericellular collagen levels. Thus, collagen is a unique substrate; by binding the proteases responsible for its cleavage, these interactions recruit and regulate collagenolytic and gelatinolytic activities in a homeostatic manner. Hence, the studies reported here reveal several new aspects in the biology of MT1-MMP as a consequence of native type I collagen binding by the hemopexin C domain. This also provides a novel explanation for the generation of MT1-MMP clusters on the cell surface and adds a new layer of control to the complex regulation of focal proteolysis by MT1-MMP and MMP2.

REFERENCES

1. Vuorio, E., and de Crombrugghe, B. (1990) *Annu. Rev. Biochem.* **59,** 837–872
2. Egeblad, M., and Werb, Z. (2002) *Nat. Rev. Cancer* **2,** 161–174
3. Stetler-Stevenson, W. G., and Yu, A. E. (2001) *Semin. Cancer Biol.* **11,** 143–152
4. Overall, C. M., and Sodek, J. (1988) in *Biological Mechanisms of Tooth Eruption and Root Resorption* (Davidovitch, Z., ed) pp. 303–312, EBSCO Media, Birmingham, Alabama
5. Saftig, P., Hunziker, E., Wehmeyer, O., Jones, S., Boyde, A., Rommerskirch, W., Moritz, J. D., Schu, P., and von Figura, K. (1998) *Proc. Natl. Acad. Sci. U. S. A.* **95,** 13453–13458
6. Nagase, H., and Woessner, J. F., Jr. (1999) *J. Biol. Chem.* **274,** 21491–21494
7. Pei, D., and Weiss, S. J. (1996) *J. Biol. Chem.* **271,** 9135–9140
8. Ohuchi, E., Imai, K., Fujii, Y., Sato, H., Seiki, M., and Okada, Y. (1997) *J. Biol. Chem.* **272,** 2446–2451
9. Cowell, S., Knauper, V., Stewart, M. L., D'Ortho, M. P., Stanton, H., Hembry, R. M., Lopez-Otin, C., Reynolds, J. J., and Murphy, G. (1998) *Biochem. J.* **331,** 453–458
10. Sato, H., Takino, T., Okada, Y., Cao, J., Shinagawa, A., Yamamoto, E., and Seiki, M. (1994) *Nature* **370,** 61–65
11. Sodek, J., and Overall, C. M. (1992) *Matrix Suppl.* **1,** 352–362
12. Aimes, R. T., and Quigley, J. P. (1995) *J. Biol. Chem.* **270,** 5872–5876
13. Patterson, M. L., Atkinson, S. J., Knauper, V., and Murphy, G. (2001) *FEBS Lett.* **503,** 158–162
14. Overall, C. M. (2001) *Methods Mol. Biol.* **151,** 79–120
15. Yana, I., and Weiss, S. J. (2000) *Mol. Biol. Cell* **11,** 2387–2401
16. Rozanov, D. V., Deryugina, E. I., Ratnikov, B. I., Monosov, E. Z., Marchenko, G. N., Quigley, J. P., and Strongin, A. Y. (2001) *J. Biol. Chem.* **276,** 25705–25714
17. Takino, T., Sato, H., Yamamoto, E., and Seiki, M. (1995) *Gene (Amst.)* **155,** 293–298
18. Galvez, B. G., Matias-Roman, S., Albar, J. P., Sanchez-Madrid, F., and Arroyo, A. G. (2001) *J. Biol. Chem.* **276,** 37491–37500
19. Belien, A. T., Paganetti, P. A., and Schwab, M. E. (1999) *J. Cell Biol.* **144,** 373–384
20. Aznavoorian, S., Moore, B. A., Alexander-Lister, L. D., Hallit, S. L., Windsor, L. J., and Engler, J. A. (2001) *Cancer Res.* **61,** 6264–6275
21. Holmbeck, K., Bianco, P., Caterina, J., Yamada, S., Kromer, M., Kuznetsov, S. A., Mankani, M., Robey, P. G., Poole, A. R., Pidoux, I., Ward, J. M., and Birkedal-Hansen, H. (1999) *Cell* **99,** 81–92
22. Zhou, Z., Apte, S. S., Soininen, R., Cao, R., Baaklini, G. Y., Rauser, R. W., Wang, J., Cao, Y., and Tryggvason, K. (2000) *Proc. Natl. Acad. Sci. U. S. A.* **97,** 4052–4057
23. Martignetti, J. A., Aqeel, A. A., Sewairi, W. A., Boumah, C. E., Kambouris, M., Mayouf, S. A., Sheth, K. V., Eid, W. A., Dowling, O., Harris, J., Glucksman, M. J., Bahabri, S., Meyer, B. F., and Desnick, R. J. (2001) *Nat. Genet.* **28,** 261–265
24. Knauper, V., Patterson, M. L., Gomis-Ruth, F. X., Smith, B., Lyons, A., Docherty, A. J., and Murphy, G. (2001) *Eur. J. Biochem.* **268,** 1888–1896
25. Chung, L., Shimokawa, K., Dinakarpandian, D., Grams, F., Fields, G. B., and Nagase, H. (2000) *J. Biol. Chem.* **275,** 29610–29617
26. Brandstetter, H., Grams, F., Glitz, D., Lang, A., Huber, R., Bode, W., Krell, H. W., and Engh, R. A. (2001) *J. Biol. Chem.* **276,** 17405–17412
27. Allan, J. A., Hembry, R. M., Angal, S., Reynolds, J. J., and Murphy, G. (1991) *J. Cell Sci.* **99,** 789–795
28. Clark, I. M., and Cawston, T. E. (1989) *Biochem. J.* **263,** 201–206
29. Windsor, L. J., Birkedal-Hansen, H., Birkedal-Hansen, B., and Engler, J. A. (1991) *Biochemistry* **30,** 641–647
30. Murphy, G., Allan, J. A., Willenbrock, F., Cockett, M. I., O'Connell, J. P., and Docherty, A. J. (1992) *J. Biol. Chem.* **267,** 9612–9618
31. Knauper, V., Osthues, A., DeClerck, Y. A., Langley, K. E., Blaser, J., and Tschesche, H. (1993) *Biochem. J.* **291,** 847–854
32. Knauper, V., Cowell, S., Smith, B., Lopez-Otin, C., O'Shea, M., Morris, H., Zardi, L., and Murphy, G. (1997) *J. Biol. Chem.* **272,** 7608–7616
33. Hirose, T., Patterson, C., Pourmotabbed, T., Mainardi, C. L., and Hasty, K. A. (1993) *Proc. Natl. Acad. Sci. U. S. A.* **90,** 2569–2573
34. Knauper, V., Docherty, A. J., Smith, B., Tschesche, H., and Murphy, G. (1997) *FEBS Lett.* **405,** 60–64
35. de Souza, S. J., and Brentani, R. (1992) *J. Biol. Chem.* **267,** 13763–13767
36. Azzam, H. S., and Thompson, E. W. (1992) *Cancer Res.* **52,** 4540–4544
37. Gilles, C., Polette, M., Seiki, M., Birembaut, P., and Thompson, E. W. (1997) *Lab. Invest.* **76,** 651–660
38. Tomasek, J. J., Halliday, N. L., Updike, D. L., Ahern-Moore, J. S., Vu, T. K., Liu, R. W., and Howard, E. W. (1997) *J. Biol. Chem.* **272,** 7482–7487
39. Haas, T. L., Davis, S. J., and Madri, J. A. (1998) *J. Biol. Chem.* **273,** 3604–3610
40. Ellerbroek, S. M., Fishman, D. A., Kearns, A. S., Bafetti, L. M., and Stack, M. S. (1999) *Cancer Res.* **59,** 1635–1641
41. Ruangpanit, N., Chan, D., Holmbeck, K., Birkedal-Hansen, H., Polarek, J., Yang, C., Bateman, J. F., and Thompson, E. W. (2001) *Matrix Biol.* **20,** 193–203
42. Ellerbroek, S. M., Wu, Y. I., Overall, C. M., and Stack, M. S. (2001) *J. Biol. Chem.* **276,** 24833–24842
43. Seltzer, J. L., Lee, A. Y., Akers, K. T., Sudbeck, B., Southon, E. A., Wayner, E. A., and Eisen, A. Z. (1994) *Exp. Cell Res.* **213,** 365–374
44. Ellerbroek, S. M., and Stack, M. S. (1999) *Bioessays* **21,** 940–949
45. Butler, G. S., Butler, M. J., Atkinson, S. J., Will, H., Tamura, T., van Westrum, S. S., Crabbe, T., Clements, J., d'Ortho, M. P., and Murphy, G. (1998) *J. Biol. Chem.* **273,** 871–880
46. Hernandez-Barrantes, S., Toth, M., Bernardo, M. M., Yurkova, M., Gervasi, D. C., Raz, Y., Sang, Q. A., and Fridman, R. (2000) *J. Biol. Chem.* **275,**

12080–12089
47. Overall, C. M., Tam, E., McQuibban, G. A., Morrison, C., Wallon, U. M., Bigg, H. F., King, A. E., and Roberts, C. R. (2000) *J. Biol. Chem.* **275,** 39497–39506
48. Itoh, Y., Takamura, A., Ito, N., Maru, Y., Sato, H., Suenaga, N., Aoki, T., and Seiki, M. (2001) *EMBO J.* **20,** 4782–4793
49. Lehti, K., Lohi, J., Juntunen, M. M., Pei, D., and Keski-Oja, J. (2002) *J. Biol. Chem.* **277,** 8440–8448
50. Overall, C. M., and Sodek, J. (1990) *J. Biol. Chem.* **265,** 21141–21151
51. Lehti, K., Lohi, J., Valtanen, H., and Keski-Oja, J. (1998) *Biochem. J.* **334,** 345–353
52. Kinoshita, T., Sato, H., Okada, A., Ohuchi, E., Imai, K., Okada, Y., and Seiki, M. (1998) *J. Biol. Chem.* **273,** 16098–16103
53. Albini, A., Melchiori, A., Santi, L., Liotta, L. A., Brown, P. D., and Stetler-Stevenson, W. G. (1991) *J. Natl. Cancer Inst.* **83,** 775–779
54. Steffensen, B., Wallon, U. M., and Overall, C. M. (1995) *J. Biol. Chem.* **270,** 11555–11566
55. Mancini, S., Romanelli, R., Laschinger, C. A., Overall, C. M., Sodek, J., and McCulloch, C. A. (1999) *J. Periodontol.* **70,** 1292–1302
56. Bigg, H. F., Morrison, C. J., Butler, G. S., Bogoyevitch, M. A., Wang, Z., Soloway, P. D., and Overall, C. M. (2001) *Cancer Res.* **61,** 3610–3618
57. Wallon, U. M., and Overall, C. M. (1997) *J. Biol. Chem.* **272,** 7473–7481
58. Overall, C. M., and Sodek, J. (1987) *J. Dent. Res.* **66,** 1271–1282
59. d'Ortho, M. P., Will, H., Atkinson, S., Butler, G., Messent, A., Gavrilovic, J., Smith, B., Timpl, R., Zardi, L., and Murphy, G. (1997) *Eur. J. Biochem.* **250,** 751–757
60. Strongin, A. Y., Marmer, B. L., Grant, G. A., and Goldberg, G. I. (1993) *J. Biol. Chem.* **268,** 14033–14039
61. Fishman, D. A., Liu, Y., Ellerbroek, S. M., and Stack, M. S. (2001) *Cancer Res.* **61,** 3194–3199
62. Nakahara, H., Howard, L., Thompson, E. W., Sato, H., Seiki, M., Yeh, Y., and Chen, W. T. (1997) *Proc. Natl. Acad. Sci. U. S. A.* **94,** 7959–7964
63. Nabeshima, K., Inoue, T., Shimao, Y., Okada, Y., Itoh, Y., Seiki, M., and Koono, M. (2000) *Cancer Res.* **60,** 3364–3369
64. Lehti, K., Valtanen, H., Wickstrom, S., Lohi, J., and Keski-Oja, J. (2000) *J. Biol. Chem.* **275,** 15006–15013
65. Hotary, K., Allen, E., Punturieri, A., Yana, I., and Weiss, S. J. (2000) *J. Cell Biol.* **149,** 1309–1323
66. Welgus, H. G., Jeffrey, J. J., Stricklin, G. P., Roswit, W. T., and Eisen, A. Z. (1980) *J. Biol. Chem.* **255,** 6806–6813
67. De Souza, S. J., Pereira, H. M., Jacchieri, S., and Brentani, R. R. (1996) *FASEB J.* **10,** 927–930
68. Li, J., Brick, P., O'Hare, M. C., Skarzynski, T., Lloyd, L. F., Curry, V. A., Clark, I. M., Bigg, H. F., Hazleman, B. L., and Cawston, T. E. (1995) *Structure* **3,** 541–549
69. Gilles, C., Bassuk, J. A., Pulyaeva, H., Sage, E. H., Foidart, J. M., and Thompson, E. W. (1998) *Cancer Res.* **58,** 5529–5536
70. Steffensen, B., Bigg, H. F., and Overall, C. M. (1998) *J. Biol. Chem.* **273,** 20622–20628
71. Jiang, A., Lehti, K., Wang, X., Weiss, S. J., Keski-Oja, J., and Pei, D. (2001) *Proc. Natl. Acad. Sci. U. S. A.* **98,** 13693–13698
72. Uekita, T., Itoh, Y., Yana, I., Ohno, H., and Seiki, M. (2001) *J. Cell Biol.* **155,** 1345–1356
73. Will, H., Atkinson, S. J., Butler, G. S., Smith, B., and Murphy, G. (1996) *J. Biol. Chem.* **271,** 17119–17123
74. Strongin, A. Y., Collier, I., Bannikov, G., Marmer, B. L., Grant, G. A., and Goldberg, G. I. (1995) *J. Biol. Chem.* **270,** 5331–5338
75. Stanton, H., Gavrilovic, J., Atkinson, S. J., d'Ortho, M. P., Yamada, K. M., Zardi, L., and Murphy, G. (1998) *J. Cell Sci.* **111,** 2789–2798
76. Toth, M., Hernandez-Barrantes, S., Osenkowski, P., Bernardo, M. M., Gervasi, D. C., Shimura, Y., Meroueh, O., Kotra, L. P., Gatvez, B. G., Arroyo, A. G., Mobashery, S., and Fridman, R. (2002) *J. Biol. Chem.* **277,** 26340–26350
77. Consortium, T. H. (1995) *Nat. Genet.* **11,** 130–136
78. Turner, A. J., Isaac, R. E., and Coates, D. (2001) *Bioessays* **23,** 261–269
79. McQuibban, G. A., Gong, J. H., Tam, E. M., McCulloch, C. A., Clark-Lewis, I., and Overall, C. M. (2000) *Science* **289,** 1202–1206
80. McQuibban, G. A., Butler, G. S., Gong, J. H., Bendall, L., Power, C., Clark-Lewis, I., and Overall, C. M. (2001) *J. Biol. Chem.* **276,** 43503–43508
81. Overall, C. M., and Lopéz-Otín, C. (2002) *Nat. Rev. Cancer* **2,** 657–672

THE JOURNAL OF BIOLOGICAL CHEMISTRY
Vol. 277, No. 44, Issue of November 1, pp. 41480–41488, 2002
Printed in U.S.A.

Calcium Regulation of Matrix Metalloproteinase-mediated Migration in Oral Squamous Cell Carcinoma Cells*

Received for publication, July 30, 2002
Published, JBC Papers in Press, August 22, 2002, DOI 10.1074/jbc.M207695200

Hidayatullah G. Munshi‡§¶, Yi I. Wu‖, Edgardo V. Ariztia‖, and M. Sharon Stack§‖**

From the ‡Division of Hematology/Oncology, Department of Medicine and ‖Department of Cell and Molecular Biology, Feinberg School of Medicine, Northwestern University, and the §Robert H. Lurie Comprehensive Cancer Center of Northwestern University, Chicago, Illinois 60611

Activation of matrix metalloproteinase 2 (MMP-2) has been shown to play a significant role in the behavior of cancer cells, affecting both migration and invasion. The activation process requires multimolecular complex formation involving pro-MMP-2, membrane type 1-MMP (MT1-MMP), and tissue inhibitor of metalloproteinases-2 (TIMP-2). Because calcium is an important regulator of keratinocyte function, we evaluated the effect of calcium on MMP regulation in an oral squamous cell carcinoma line (SCC25). Increasing extracellular calcium (0.09–1.2 mM) resulted in a dose-dependent increase in MT1-MMP-dependent pro-MMP-2 activation. Despite the requirement for MT1-MMP in the activation process, no changes in MT1-MMP expression, cell surface localization, or endocytosis were apparent. However, increased generation of the catalytically inactive 43-kDa MT1-MMP autolysis product and decline in the TIMP-2 levels in conditioned media were observed. The decrease in TIMP-2 levels in the conditioned media was prevented by a broad spectrum MMP inhibitor, suggesting that calcium promotes recruitment of TIMP-2 to MT1-MMP on the cell surface. Despite the decline in soluble TIMP-2, no accumulation of TIMP-2 in cell lysates was seen. Blocking TIMP-2 degradation with bafilomycin A1 significantly increased cell-associated TIMP-2 levels in the presence of high calcium. These data suggest that the decline in TIMP-2 is because of increased calcium-mediated MT1-MMP-dependent degradation of TIMP-2. In functional studies, increasing calcium enhanced MMP-dependent cellular migration on laminin-5-rich matrix using an *in vitro* colony dispersion assay. Taken together, these results suggest that changes in extracellular calcium can regulate post-translational MMP dynamics and thus affect the cellular behavior of oral squamous cell carcinoma.

Oral squamous cell carcinoma (OSCC)[1] is characterized by local, regional, and distant spread of the disease; however, the cellular and molecular events that control the invasive behavior are poorly understood (1, 2). Immunohistochemical studies have implicated enzymes belonging to the matrix metalloproteinase (MMP) family in basement membrane proteolysis and tissue invasion in OSCC (3). MMPs are a large family of metallo-endopeptidases with activity directed against a variety of extracellular matrix substrates (4–7). Expression of MMP-2 (gelatinase A, a 72-kDa type IV collagenase) is observed in invasive and metastatic cases of OSCC (3, 8). Furthermore, increased expression of MMP-2 is associated with decreased staining of extracellular matrix in OSCC, suggesting that MMP-2 promotes matrix breakdown (3, 8). MMP-2 is secreted from cells as a zymogen (pro-MMP-2) and is activated post-translationally by a trans-membrane MMP designated as membrane type 1-MMP (MT1-MMP) (9–11). MT1-MMP is also up-regulated in OSCC, and increased expression is observed in highly invasive and metastatic cases (3, 8). Pro-MT1-MMP is synthesized as a 63–66-kDa zymogen and is activated intracellularly to a 55-kDa species by the serine proteinase furin, a member of the proprotein convertase family (12–14).

The activation of pro-MMP-2 is regulated by a complex mechanism involving formation of a trimolecular complex with MT1-MMP and tissue inhibitor of metalloproteinase-2 (TIMP-2) (10, 15–17). In this model, TIMP-2 plays a dual role in the regulation of MMP-2 activation, functioning both to promote and to inhibit the activation process in a concentration-dependent manner (16, 18). TIMP-2 bridges the interaction between the MMP-2 zymogen and MT1-MMP via N-terminal binding to the active site of MT1-MMP with the concomitant C-terminal binding to the pro-MMP-2 hemopexin domain (10, 15–20). Thus, at low TIMP-2 concentration, an adjacent TIMP-2-free MT1-MMP can effectively process the cell surface-bound pro-MMP-2 to a 68-kDa intermediate species, which undergoes autolytic processing to the mature 62-kDa active species. However at high TIMP-2 concentration, all of the cell surface MT1-MMPs undergo complex formation with TIMP-2, thereby inhibiting pro-MMP-2 activation (10, 15–20).

As stringent control of MMP activity plays an important role in keratinocyte behavior (21–23) and dysregulation of MMP activity has been correlated with metastatic progression, factors that control acquisition of net MMP activity in OSCC were evaluated. Of the many agents that are known to affect keratinocyte behavior, calcium is one of the key factors (24–27). There is a steep calcium gradient within the epidermis, with

* This work was supported in part by NIDCR Grant PO1 DE12328 (to M. S. S.) from the National Institutes of Health. The costs of publication of this article were defrayed in part by the payment of page charges. This article must therefore be hereby marked "*advertisement*" in accordance with 18 U.S.C. Section 1734 solely to indicate this fact.

¶ Supported in part by Grant 5T32 CA70085 from the National Institutes of Health to the RHL Comprehensive Cancer Center's Training Program in Signal Transduction and Cancer and is the recipient of the 2002 American Society of Clinical Oncology Young Investigator Award.

** To whom correspondence should be addressed: Dept. of Cell and Molecular Biology, Northwestern University Medical School, 303 E. Chicago Ave., Tarry 8-715, Chicago IL 60611. Tel.: 312-908-8216; Fax: 312-503-7912; E-mail: mss130@northwestern.edu.

[1] The abbreviations used are: OSCC, oral squamous cell carcinoma; MMP, matrix metalloproteinase; MT1-MMP, membrane type 1-MMP; TIMP, tissue of inhibitor of metalloproteinases; RVKR, decanoyl-Arg-Val-Lys-Arg-chloromethyl ketone; DMEM, Dulbecco's modified Eagle's media; PBS, phosphate-buffered saline; PMA, phorbol 12-myristate 13-acetate; MESNA, mercaptoethanesulfonic acid; EGF, epidermal growth factor; ELISA, enzyme-linked immunosorbent assay; RT, reverse transcriptase; GAPDH, glyceraldehyde-3-phosphate dehydrogenase.

higher calcium present in the uppermost layers (28–30). Moreover, altering extracellular calcium has been used to effectively model *in vitro* physiologic changes in keratinocytes that occur within the epidermis as cells migrate from the basal to the uppermost layers. Interestingly, recent studies (31–33) have demonstrated a relationship between extracellular calcium and enhanced matrix metalloproteinase gene expression in primary human keratinocytes.

Because calcium is an important regulator of keratinocyte function, we evaluated the effect of calcium on MMP regulation in an oral squamous cell carcinoma line (SCC25). Increasing extracellular calcium resulted in a dose-dependent increase in pro-MMP-2 activation, accompanied by enhanced MT1-MMP autolytic processing and a decline in the levels of soluble TIMP-2. The decrease in TIMP-2 levels in the conditioned media was prevented by a broad spectrum MMP inhibitor, suggesting that calcium promotes recruitment of TIMP-2 to MT1-MMP on the cell surface. Despite the decline in soluble TIMP-2, no accumulation of TIMP-2 in cell lysates was seen. However, blocking TIMP-2 degradation with bafilomycin A1 significantly increased cell-associated TIMP-2 levels in the presence of high calcium. These data suggest that the decline in TIMP-2 is due to increased calcium-mediated MT1-MMP-dependent degradation of TIMP-2. Moreover, calcium enhanced MMP-dependent cellular migration on laminin-5-rich matrix. These results suggest that changes in extracellular calcium can regulate post-translational MMP dynamics and thus affect the cellular behavior of OSCC.

EXPERIMENTAL PROCEDURES

Materials—Gelatin, type I collagen, cell culture reagents, Chelex 100, MESNA, peroxidase-conjugated secondary antibodies, and the MT1-MMP antibody directed against the hinge region were purchased from Sigma. Phorbol 12-myristate 13-acetate (PMA), epidermal growth factor (EGF), and bafilomycin A1 were from Calbiochem. Dulbecco's modified Eagle's media (DMEM), DMEM without calcium, Ham's F-12, G418, Trizol, and One-step RT-PCR kits were purchased from Invitrogen. Purified TIMP-1 and TIMP-2 proteins, rabbit polyclonal TIMP-2 antibody, and the broad spectrum MMP inhibitor GM6001 were purchased from Chemicon (Temecula, CA). TIMP-2 ELISA kit was from Oncogene Research Products (Boston, MA). SuperSignal enhanced chemiluminescence (ECL) reagent, EZ-Link Sulfo-NHS-LC-Biotin, EZ-Link Sulfo-NHS-SS-Biotin, and UltraLink immobilized streptavidin gel were obtained from Pierce. The furin inhibitor decanoyl-Arg-Val-Lys-Arg-chloromethyl ketone (RVKR) was from Alexis Biochemicals (San Diego, CA). Microcon 10 microconcentrators and polyvinylidene difluoride membranes were purchased from Millipore (Bedford, MA). FuGENE 6 was obtained from Roche Molecular Biochemicals. RQ1 DNase was from Promega (Madison, WI).

Cell Cultures—SCC25 cells were obtained from American Type Culture Collection (ATCC). SCC25 cells were routinely maintained in DMEM/Ham's F-12 = 1:1 media containing 10% fetal calf serum and supplemented with 100 units/ml penicillin. SCC25 and SCC25-MT (defined below) cells were plated in DMEM containing 0.09 mM calcium and supplemented with Chelex-treated 10% fetal calf serum. After overnight serum starvation, the cells were switched to serum-free DMEM containing the indicated calcium concentration. In additional experiments, inhibitors or other chemical reagents were added 30 min prior to the medium change.

In some experiments, cells were cultured on thin layer or three-dimensional collagen surfaces (34). Briefly, acid-solubilized rat tail type I collagen was diluted to 50 μg/ml in 0.02 N acetic acid and added to the tissue culture plate for 1 h at 18 °C. The solution was aspirated, and the plate was rinsed three times with PBS. Three-dimensional collagen gels were prepared by diluting acid-solubilized type I collagen to a concentration of 1 mg/ml in cold DMEM (calcium-free), neutralizing with sodium hydroxide, and then allowing to gel (700 μl in 12-well plates) for 30 min at 37 °C prior to plating cells.

Generation of SCC25-MT Cells—Human MT1-MMP cDNA (a kind gift from Duanqing Pei, University of Minnesota) was cloned into pCR3.1-Uni (Invitrogen) mammalian expression vector. SCC25 cells were stably transfected using FuGENE 6 according to the manufacturer's instructions. Cell clones resistant to 0.8 mg/ml G418 were chosen and screened for MMP-2 activation by zymography as described below and for MT1-MMP expression by Western blotting using antibody directed against the hinge region. Six different clones with high levels of MT1-MMP expression were selected for subsequent experiments. The cells were then maintained in DMEM/Ham's F12 media = 1:1 supplemented with 10% fetal calf serum, 100 units/ml penicillin, and 0.65 mg/ml G418.

Analysis of MMP-2 and TIMP-2 Expression—Gelatinase activities in 24-h serum-free conditioned media were determined using SDS-PAGE gelatin zymography as described previously (34). Briefly, SDS-PAGE gels (9% acrylamide) were co-polymerized with 0.1% gelatin, and samples were electrophoresed without reduction or boiling using 5× Laemmli sample buffer (35). SDS was removed through a 30-min incubation in 2.5% Triton X-100, and gels were incubated in 20 mM glycine, pH 8.3, 10 mM $CaCl_2$, 1 μM $ZnCl_2$ at 37 °C for 24–36 h. The gels were stained with Coomassie Blue to visualize zones of gelatinolytic activity. The conditioned media were concentrated 15–20-fold using Microcon 10 microconcentrators, boiled in Laemmli sample dilution buffer (35), analyzed for TIMP-2 by SDS-PAGE (15% gels), and immunoblotted with rabbit polyclonal antibody (Chemicon). Levels of TIMP-2 protein in the cell lysates were quantified by ELISA (Oncogene Research Products) according to the manufacturer's specifications.

MT1-MMP and TIMP-2 RNA Levels—Total RNA was isolated from SCC25 and SCC25-MT cells using Trizol reagent according to the manufacturer's instructions. Following digestion with RQ1 DNase for 30 min at 37 °C, the total RNA concentration was determined by spectrophotometric measurement. Primer pairs for human MT1-MMP, human TIMP-2, and human GAPDH were as follows: forward primer 5′-GCCCATTGGCCAGTTCTGGCGGG-3′ and reverse primer 5′-CCTCGTCCACCTCAATGATGATC-3′ for MT1-MMP; forward primer 5′-GGCGTTTTGCAATGCAGATGTAG-3′ and reverse primer 5′-CACAGGAGCCGTCACTTCTCTTG-3′ for TIMP-2; and forward primer 5′-CGGAGTCAACGGATTTGGTCGTAT-3′ and reverse primer 5′-AGCCTTCTCCATGGTGGTGAAGAC-3′ for GAPDH (36). The length of the MT1-MMP, TIMP-2, and GAPDH amplicons were 530, 497, and 307 bp, respectively. RT-PCR was performed using the One-step RT-PCR kit where reverse transcription and DNA amplification occur in the same reaction. Briefly, 1 μg of total RNA was used as template in a reaction that included the appropriate primers in the presence of both reverse transcriptase and *Taq* polymerase. The mixture was incubated at 45 °C for 30 min and cycled 30 times at 94 °C for 30 s, 55 °C for 30 s, and 72 °C for 2 min. Appropriate negative controls of amplification included reactions without reverse transcriptase. PCR products were visualized by UV transillumination of 1.5% agarose gels stained with ethidium bromide.

Cell Surface Biotinylation—To label cell surface proteins, SCC25-MT cells were grown to confluence in a 6-well plate, washed with ice-cold PBS, and incubated at 4 °C with gentle shaking for 30 min with 0.5 mg/ml cell-impermeable Sulfo-NHS-LC-Biotin in ice-cold PBS, followed by washing with 100 mM glycine to quench free biotin. Cells were detached by scraping, lysed in modified RIPA buffer (50 mM Tris, pH 7.4, 150 mM NaCl, 5 mM EDTA, 1% Triton X-100 and 0.1% SDS) with proteinase inhibitors (1 μg/ml aprotinin, 1 μM pepstatin, and 10 μM leupeptin), and clarified by centrifugation. To isolate biotinylated cell surface proteins, equal amounts of protein from each sample were incubated with streptavidin beads at 4 °C for 14 h, followed by centrifugation. After boiling in Laemmli sample dilution buffer (35) to dissociate streptavidin bead-biotin complexes, the biotin-labeled samples were analyzed by SDS-PAGE (9% gels) and immunoblotted for MT1-MMP.

MT1-MMP Endocytosis—To determine whether calcium affects MT1-MMP endocytosis, SCC25-MT cells grown to confluence in a 6-cm dish were washed with ice-cold PBS and then incubated with cleavable cell-impermeable sulfo-NHS-SS-biotin (1 mg/ml) for 20 min in an ice bath. Biotinylation was stopped by washing with ice-cold PBS followed by 100 mM glycine in PBS to quench free biotin. Cells were then incubated with DMEM containing either 0.09 mM or 1.2 mM calcium at 37 °C for 40 min to initiate endocytosis. Endocytosis of cell surface proteins was then stopped by placing the cells on ice and washing them with ice-cold PBS. Biotin was then cleaved off the exposed cell surface by incubating the cells with membrane-impermeable reducing agent MESNA (100 mM) for 30 min at 4 °C (37). The cells were lysed in modified RIPA buffer with proteinase inhibitors (1 μg/ml aprotinin, 1 μM pepstatin, and 10 μM leupeptin) and clarified by centrifugation. To isolate biotinylated proteins (representing endocytosed surface-labeled species), equal amounts of protein from each of the samples were incubated with streptavidin beads at 4 °C for 14 h, followed by centrifugation. After boiling in Laemmli sample dilution buffer (35) to disso-

ciate streptavidin bead-biotin complexes, the samples were analyzed by SDS-PAGE (9% gels) and immunoblotted for MT1-MMP. In control experiments to determine the efficiency of surface stripping with MESNA, cells were maintained on ice for the duration of the experiment and were not induced to undergo endocytosis via a temperature shift. In additional control experiments, the MESNA stripping step was omitted such that total labeled protein (endocytosed and the cell surface pool) was analyzed.

Generation of Laminin-5-enriched Matrix and Cell Dispersion Assays—The extracellular matrix deposited by SCC25 cells was generated as described previously (34, 38). Briefly, SCC25 cells were grown in 12-well plates to 48–72 h post-confluence prior to treatment for 7 min with 20 mM ammonium hydroxide to remove cells. After 3 rapid washes each in sterile distilled water and PBS, the laminin-5-enriched matrix was then used for *in vitro* migration assays. The effect of calcium on laminin-5-induced migration was assessed using a cell dispersion assay as described previously (39). Briefly, SCC25 and SCC25-MT cells (3×10^4) were plated in DMEM (0.09 mM calcium) inside a cloning cylinder placed in the middle of a 12-well plate coated with laminin-5-enriched matrix. After the cells have attached and spread, the cloning cylinder was removed, and the cells were washed twice with DMEM containing 0.09 mM calcium and serum-starved for an additional 3 h. The media were then switched to DMEM containing either 0.09 or 1.2 mM calcium supplemented with 20 ng/ml EGF. In selected experiments, the proteinase dependence of migration was determined by adding the MMP inhibitor GM6001 (10 μM). To quantify the relative motility, the migratory front was photographed every 12 h for 48 h, and the percentage of cells crossing a line designated "migratory max" was enumerated.

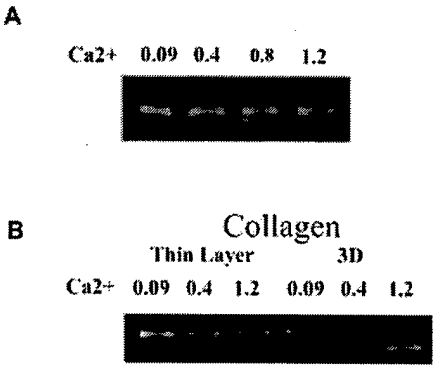

FIG. 1. **Extracellular calcium regulates pro-MMP-2 activation.** *A*, SCC25 cells were plated on plastic in medium containing 0.09 mM calcium. Following overnight serum starvation, cells were transferred to medium containing the indicated calcium concentration (0.09–1.2 mM). The conditioned media were collected at 24 h and analyzed for MMP activity by gelatin zymography. *B*, SCC25 cells were plated in medium containing 0.09 mM calcium on thin layer or three-dimensional (*3-D*) collagen as described under "Experimental Procedures." Following serum starvation, media were replaced with serum-free medium at the indicated calcium concentration. The conditioned media were collected at 24 h and analyzed for MMP activity by gelatin zymography. The results are representative of at least four independent experiments.

RESULTS

Extracellular Calcium Regulates Pro-MMP-2 Activation—MMP activity is subject to complex post-translational regulation by a number of processes including zymogen activation, enzyme-inhibitor binding, endocytosis, and shedding (4–7, 40, 41); however, the biologic factors that control and coordinate these processes are poorly understood. As keratinocytes are subjected to fluctuations in extracellular calcium in the epidermal milieu, the effect of calcium on MMP activation was evaluated in SCC25 cells. The predominant soluble MMP expressed by SCC25 cells is MMP-2, with low level expression of MMP-9. SCC25 cells were plated in low calcium media (0.09 mM), serum-starved, and incubated with fresh serum-free media containing increasing calcium. Conditioned media were collected at 24 h and analyzed for MMP activity by gelatin zymography. Whereas cells cultured in 0.09 mM calcium concentration expressed pro-MMP-2 (Fig. 1*A*, *1st lane*), increasing calcium concentration resulted in a dose-dependent MMP-2 activation (Fig. 1*A*, *2nd* to *4th lanes*). There was no change in MMP-9 expression with increasing calcium concentration in these cells (data not shown). Because collagen has been shown to affect MMP-2 expression and/or processing (42–48), the effect of calcium on collagen-induced MMP-2 activation was examined. Similar to the results obtained with SCC25 cells on plastic (Fig. 1*A*), cells plated on thin layer collagen demonstrated MMP-2 activation with increasing calcium concentration (Fig. 1*B*, *1st* to *3rd lanes*). Although cells cultured on three-dimensional collagen gels had a more pronounced base-line MMP-2 activation (Fig. 1*B*, *4th lane*), a calcium-dependent increase in MMP-2 activation was observed (Fig. 1*B*, *5th* and *6th lanes*). These data indicate that extracellular calcium-mediated regulation of MMP-2 activation in SCC25 cells may act in synergy with collagen-induced pro-MMP-2 processing.

To investigate the proteolytic process leading to MMP-2 activation, SCC25 cells were treated with a broad spectrum MMP inhibitor, GM6001, or vehicle (Me_2SO) control. GM6001 inhibited calcium-induced pro-MMP-2 activation, demonstrating the involvement of an MMP in the activation process (Fig. 2*A*, *lanes 3* and *4*). To investigate MMP dependence further, SCC25 cells were treated with TIMP-1 and TIMP-2. TIMP-2 blocks both MMP-2 and MT1-MMP activities, whereas MT1-MMP activity is not inhibited by TIMP-1 (49, 50). TIMP-1 had no effect on calcium-induced MMP-2 activation (Fig. 2*A*, *lanes 5* and *6*), whereas TIMP-2 completely abrogated the response (Fig. 2*A*, *lanes 7* and *8*), implicating MT1-MMP-in the calcium-induced pro-MMP-2 activation reaction.

To investigate further the involvement of MT1-MMP in calcium-dependent pro-MMP-2 activation, SCC25 cells were treated with a furin inhibitor decanoyl-Arg-Val-Lys-Arg-chloromethyl ketone (RVKR), which has been shown to block activation of pro-MT1-MMP (51). Treatment of SCC25 cells with RVKR inhibited calcium-mediated MMP-2 activation, further implicating MT1-MMP in the calcium-induced pro-MMP-2 activation (compare Fig. 2*B*, *lanes 1* and *3*, with Fig. 2*B*, *lanes 5* and *7*). To determine whether calcium can act in synergy with PMA, another agent that has been shown to induce MMP-2 activation via MT1-MMP (11, 52), cells were cultured in low *versus* high calcium concentration in the presence of PMA and various proteinase inhibitors. As reported previously (52, 53), PMA induced pro-MMP-9 expression, irrespective of calcium concentration (Fig. 2*C*, compare *lanes 1* and *2* with *lanes 5* and *6*). In contrast, expression of pro-MMP-2 was not affected; however, activation was stimulated (Fig. 2*C*, *lanes 1* and *2* and *lanes 5* and *6*). Addition of calcium further increased PMA-induced pro-MMP-2 activation (compare Fig. 2*C*, *lanes 2* and *6*), indicative of synergistic stimulation of MMP processing. In control experiments, activation was blocked by both RVKR and GM6001 (Fig. 2*C*, *lanes 3* and *7* and *4* and *8*, respectively).

Overexpression of MT1-MMP in SCC25 Cells—To investigate further the involvement of MT1-MMP in calcium-dependent pro-MMP-2 activation, SCC25 cells overexpressing MT1-MMP (designated SCC25-MT) were generated (Fig. 3*A*). Overexpression of MT1-MMP in SCC25-MT cells was verified by Western blotting of whole cell lysates, indicating the presence of the 55-kDa active species and the 43-kDa catalytically inactive autolysis product (Fig. 3*A*). As reported previously (54, 55), GM6001 prevents autolysis of MT1-MMP and thus increases the accumulation of the 55-kDa species (Fig. 3*A*, *2nd lane*). Correlating with the enhanced MT1-MMP expression in SCC25-MT cells (Fig. 3*A*, *4th lane*), a significantly increased MMP-2 activation is observed (Fig. 3*A*, *lower panel*, *4th lane*). Similar to wild-type SCC25 cells, calcium increased pro-MMP-2 activation by SCC25-MT cells in a dose-dependent manner (Fig.

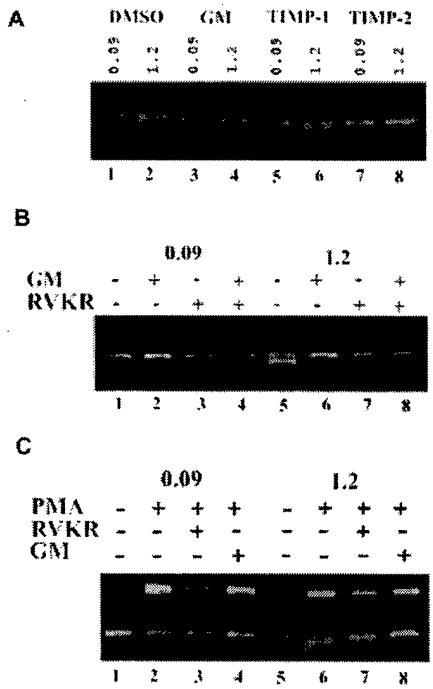

FIG. 2. **Calcium-induced pro-MMP-2 activation involves MT1-MMP.** *A*, SCC25 cells were plated on plastic in medium containing 0.09 mM calcium, subjected to overnight serum starvation, and transferred to fresh medium at the indicated calcium concentration. At the time of calcium switch, the cells were treated with Me_2SO (*DMSO*, vehicle control), MMP inhibitor GM6001 (*GM*, 10 μM), TIMP-1 (20 ng/ml), or TIMP-2 (20 ng/ml). The conditioned media were collected at 24 h and analyzed for MMP activity by gelatin zymography. *B* and *C*, SCC25 cells were plated on plastic in medium containing 0.09 mM calcium, subjected to overnight serum starvation, and transferred to fresh medium at the indicated calcium concentration. At the time of calcium switch, the cells were treated with PMA (20 nM), MMP inhibitor GM6001 (10 μM), and/or furin inhibitor decanoyl-Arg-Val-Lys-Arg-chloromethyl ketone (RVKR, 20 μM). The conditioned media were collected at 24 h and analyzed for MMP activity by gelatin zymography. The results are representative of three independent experiments.

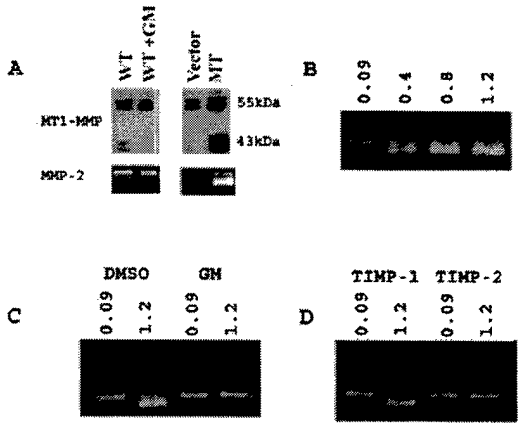

FIG. 3. **Overexpression of MT1-MMP in SCC25 cells.** *A*, SCC25 cells overexpressing MT1-MMP (SCC25-MT) were generated as described under "Experimental Procedures." At 24 h the cell lysates from wild-type (*WT*) SCC25 and SCC25-MT cells were analyzed for MT1-MMP expression by Western blotting and the conditioned media for MMP-2 activity by gelatin zymography. The membranes were immunoblotted with anti-MT1-MMP antibody followed by peroxidase-conjugated secondary antibody and enhanced chemiluminescence detection. *B*, SCC25-MT cells were plated on plastic in medium containing 0.09 mM calcium. Following overnight serum starvation, cells were transferred to medium containing the indicated calcium concentration (0.09–1.2 mM). Conditioned media were collected at 24 h and analyzed for MMP activity by gelatin zymography. *C* and *D*, SCC25-MT cells were plated on plastic in medium containing 0.09 mM calcium, and following overnight serum starvation, the media were changed to either 0.09 or 1.2 mM calcium concentration. At the time of calcium switch, the cells were treated with Me_2SO (*DMSO*, vehicle control), MMP inhibitor GM6001 (*GM*, 10 μM), TIMP-1 (20 ng/ml) or TIMP-2 (20 ng/ml). The conditioned media were collected at 24 h and analyzed for MMP activity by gelatin zymography. The results are representative of two independent experiments.

3*B*). Activation was inhibited by the broad spectrum MMP inhibitor GM6001 (Fig. 3*C*) and by TIMP-2 (Fig. 3*D*).

Effect of Extracellular Calcium on MT1-MMP—To determine whether the calcium-induced increases in pro-MMP-2 activation are the result of enhanced MT1-MMP expression, the MT1-MMP mRNA levels from SCC25 and SCC25-MT cells were analyzed by RT-PCR. Changes in the message levels for GAPDH were used as internal control. SCC25-MT cells expressed higher levels of MT1-MMP message compared with SCC25 cells; however, calcium did not alter the steady state levels of MT1-MMP mRNA (Fig. 4*A*).

As the RT-PCR data indicated that MT1-MMP expression levels were unaffected by calcium, post-translational mechanisms of MT1-MMP regulation were investigated. To evaluate the effect of calcium on MT1-MMP processing, SCC25-MT cells were plated in low calcium, serum-starved, and incubated in fresh medium containing low (0.09 mM) or high (1.2 mM) calcium concentration in the presence or absence of GM6001 to prevent autocatalytic processing of MT1-MMP to the 43-kDa species. After 24 h, the cell lysates were probed for MT1-MMP by Western blotting. In agreement with the RT-PCR data, no significant change in overall MT1-MMP protein expression was observed (Fig. 4*B*, *upper panel*). However, increased processing of MT1-MMP to the 43-kDa autolysis product was observed in high calcium, indicative of enhanced MT1-MMP activity, as further supported by zymogram data showing increased pro-MMP-2 activation (Fig. 4*B*, *lower panel, 3rd lane*).

To determine whether MT1-MMP activity is enhanced via increased cell surface association, surface biotinylation was used to probe calcium-induced changes in the cell surface MT1-MMP species. Serum-starved SCC25-MT cells were maintained in low or high calcium for 24 h as indicated and then incubated with cell-impermeable NHS-biotin to label cell surface proteins and lysed in modified RIPA buffer. Following precipitation of surface-labeled proteins with streptavidin beads, samples were electrophoresed and probed for MT1-MMP by immunoblotting. Similar to the results obtained with whole cell lysates, calcium had no effect on the surface expression of MT1-MMP (Fig. 4*C*). Enhanced surface levels of 43-kDa autolysis product were also observed, providing additional evidence for increased cell surface MT1-MMP activity.

Rapid Kinetics of Calcium-induced Pro-MMP-2 Activation—To evaluate the kinetics of pro-MMP-2 activation, serum-starved SCC25 and SCC25-MT cells were first incubated in low calcium medium (0.09 mM) to accumulate pro-MMP-2 and TIMP-2 in the conditioned media. After 24 h, activation was initiated by the addition of calcium from a concentrated stock solution to a final concentration of 1.2 mM. At various time points, conditioned media and cell lysates were collected, and the relative kinetics of pro-MMP-2 activation were analyzed by gelatin zymography. Rapid MMP-2 activation was detected at the cell surface within 30 min following calcium restoration in both wild-type and MT1-MMP-overexpressing SCC25 cells (Fig. 5, *A* and *B*). Surface activation was followed by a more gradual release of MMP-2 as evidenced by accumulation of activated MMP-2 in the conditioned media (Fig. 5, *C* and *D*). The rapid calcium-induced activation of pro-MMP-2 was blocked by GM6001 (data not shown).

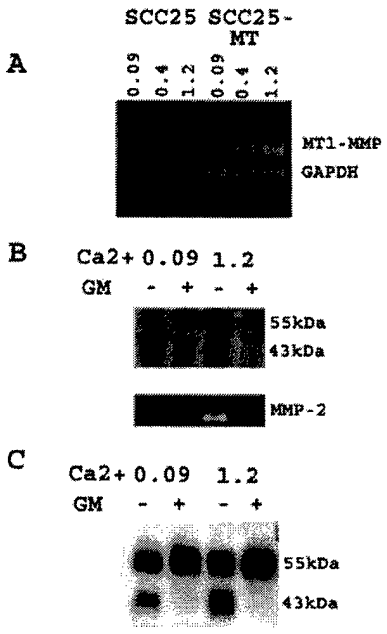

FIG. 4. **Effect of extracellular calcium on MT1-MMP.** *A*, SCC25 (*1st to 3rd lanes*) and SCC25-MT (*4th to 6th lanes*) cells were cultured for 24 h in medium at the indicated calcium concentration. Total RNA was isolated using Trizol reagent and quantified, and RT-PCR for MT1-MMP message was performed using primers as detailed under "Experimental Procedures." As loading control, amplification primers for GAPDH were used. PCR products were visualized by UV transillumination of 1.5% agarose gels stained with ethidium bromide. *B*, SCC25-MT cells were cultured in calcium-containing medium as indicated in the presence or absence of GM6001 (*GM*, 10 μM). Cells were lysed at 24 h in modified RIPA buffer containing proteinase inhibitors. Equal amounts of cell lysates were separated by SDS-PAGE, and the membranes were immunoblotted with anti-MT1-MMP antibody followed by peroxidase-conjugated secondary antibody and enhanced chemiluminescence detection (*upper panel*). The conditioned media were analyzed for MMP-2 activation using gelatin zymography (*lower panel*). *C*, SCC25-MT cells were cultured in calcium-containing medium as indicated in the presence or absence of GM6001 (10 μM). After 24 h the cells were surface-biotinylated and lysed. Samples were immunoprecipitated with streptavidin beads at 4 °C for 14 h to isolate cell surface (biotinylated) proteins and electrophoresed on a 9% SDS-polyacrylamide gel. The membranes were immunoblotted with anti-MT1-MMP antibody followed by peroxidase-conjugated secondary antibody and enhanced chemiluminescence detection. The results are representative of at least two independent experiments.

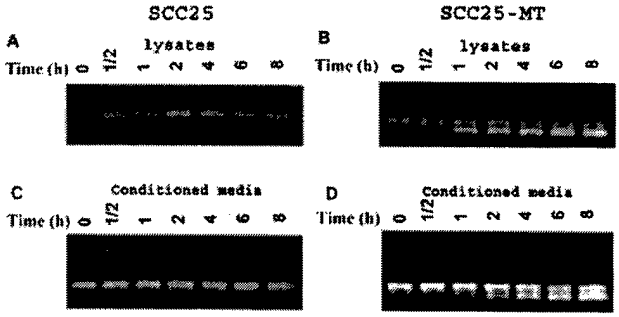

FIG. 5. **Calcium induces rapid surface activation of pro-MMP-2.** SCC25 and SCC25-MT cells were serum-starved overnight and incubated for an additional 24 h in medium containing 0.09 mM calcium. Calcium from a concentrated solution was added to the conditioned media to a final concentration of 1.2 mM, and at the indicated times (in hours) the cell lysates and conditioned media (*CM*) from SCC25 (*A* and *C*) and SCC25-MT (*B* and *D*) cells were analyzed for MMP-2 activation by gelatin zymography. The results are representative of four independent experiments.

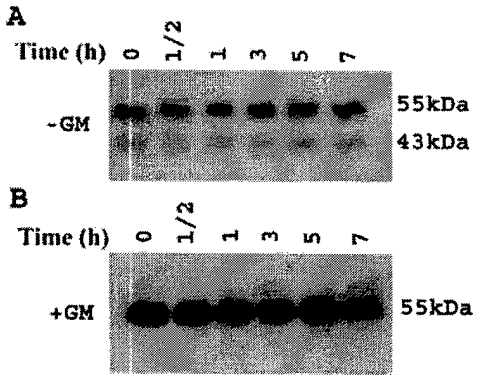

FIG. 6. **Calcium does not affect cell surface MT1-MMP levels.** SCC25-MT cells were serum-starved overnight and then incubated for an additional 24 h with Me_2SO or GM6001 (*GM*, 10 μM) in medium containing 0.09 mM calcium. Calcium from a concentrated solution was added to the conditioned media to a final concentration of 1.2 mM, and at the indicated times the samples were surface-labeled with biotin, immunoprecipitated with streptavidin, and electrophoresed on a 9% SDS-polyacrylamide gel as described under "Experimental Procedures." The membranes were immunoblotted with anti-MT1-MMP antibody, followed by peroxidase-conjugated secondary antibody and enhanced chemiluminescence detection. The results are representative of three independent experiments.

Because MMP-2 activation occurs rapidly following calcium addition, two distinct approaches were utilized to address the potential for rapid calcium-induced changes in the surface localization of MT1-MMP. In initial experiments, cells were cultured in low calcium medium (0.09 mM), switched to high calcium (1.2 mM), and at the indicated times cell surface proteins were labeled with NHS-biotin followed by lysis in modified RIPA buffer. The surface-labeled proteins were immunoprecipitated with streptavidin beads and probed for MT1-MMP by immunoblotting. No significant changes in the surface levels of the 55-kDa MT1-MMP species were induced by calcium supplementation (Fig. 6*A*), although GM6001 stabilized cell surface MT1-MMP against autolysis (Fig. 6*B*).

Recent data demonstrate that MT1-MMP can be regulated post-translationally via internalization from the cell surface (56, 57). To determine whether calcium induces dynamic turnover of MT1-MMP and thereby regulates MMP-2 activation, we evaluated MT1-MMP endocytosis in SCC25-MT cells. SCC25-MT cells were surface-biotinylated with cleavable cell-impermeable NHS-SS-biotin at 4 °C to block endocytosis and then transferred to 37 °C in 0.09 or 1.2 mM calcium-containing medium to allow for internalization (Fig. 7*A*, [*1*]). Control cells were maintained at 4 °C to prevent internalization (Fig. 7*A*, [*2*]). After a 40-min incubation at 37 °C, the cells were returned to 4 °C to stabilize surface protein profiles and block further internalization (Fig. 7*A*, [*3*]). Biotin on the remaining cell surface proteins was then removed using the reducing agent MESNA (Fig. 7*A*, [*4*]). In control experiments, MESNA was omitted to enable evaluation of total labeled proteins (*i.e.* surface and internalized) (Fig. 7*A*, [*5*]). Cells were washed with ice-cold PBS and lysed, and labeled proteins were precipitated with streptavidin beads (Fig. 7*A*, [*6–8*]), electrophoresed, and probed for MT1-MMP by immunoblotting. In cells not subject to the temperature shift prior to reduction (Fig. 7*A*, (*a*)), no MT1-MMP was detected, demonstrating the efficacy of MESNA in removing the biotin from surface-labeled MT1-MMP (Fig. 7*B*, *lanes 1* and *4*). In contrast, cells incubated at 37 °C contained a protected, MESNA-resistant pool of MT1-MMP (Fig. 7*A*, (*b*)), demonstrating internalization of MT1-MMP in SCC25-MT cells (Fig. 7*B*, *lanes 2* and *5*). Treatment of cells with GM6001 for 40 min did not affect internalization of the

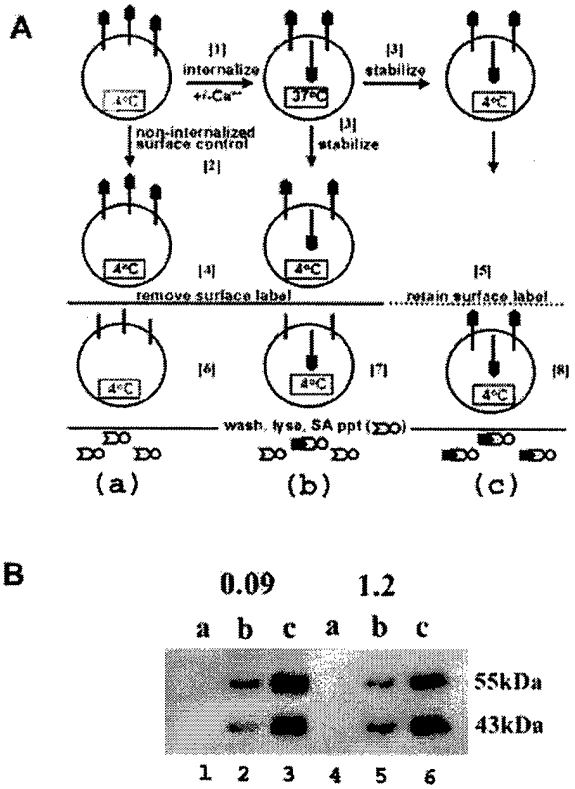

FIG. 7. **Calcium does not affect MT1-MMP endocytosis.** *A*, schematic of endocytosis protocol. *[1]*, SCC25-MT cells were surface-biotinylated on ice to block endocytosis with cleavable sulfo-NHS-SS-biotin and transferred to 37 °C in medium containing 0.09 or 1.2 mM calcium. *[2]*, control cells were maintained at 4 °C. *[3]*, after a 40-min incubation, cells were returned to 4 °C to block further internalization. *[4]*, surface biotin was removed with 100 mM MESNA. *[5]*, in control experiments, MESNA was omitted to assess total labeled protein (surface and internalized). *[6–8]*, cells were washed with ice-cold PBS, lysed, and labeled proteins precipitated at 4 °C for 14 h with streptavidin beads to isolate labeled proteins. *B*, samples prepared as described above were boiled, electrophoresed on a 9% SDS-polyacrylamide gel, and immunoblotted with anti-MT1-MMP antibody, followed by peroxidase-conjugated secondary antibody and enhanced chemiluminescence detection. The results are representative of three independent experiments.

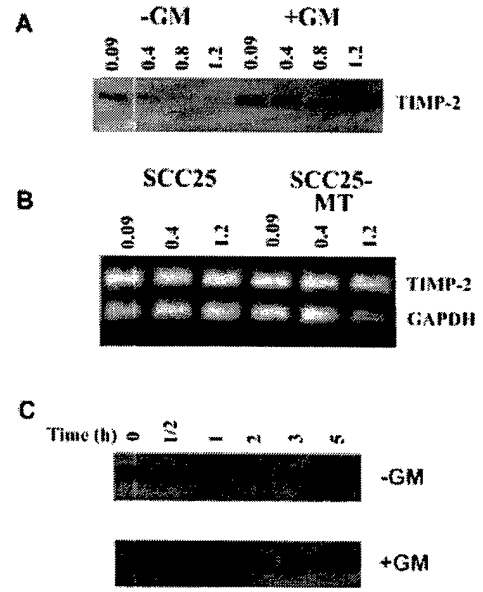

FIG. 8. **Calcium decreases soluble TIMP-2.** *A*, SCC25-MT cells were cultured for 24 h in medium at the indicated calcium concentration in the presence or absence of GM6001 (*GM*, 10 μM). The conditioned media were collected at 24 h, concentrated 15–20-fold using Micron 10 microconcentrators, electrophoresed on a 15% SDS-polyacrylamide gel, and immunoblotted with anti-TIMP-2 antibody followed by peroxidase-conjugated secondary antibody and enhanced chemiluminescence detection. *B*, SCC25 (*1st* to *3rd lanes*) and SCC25-MT (*4th* to *6th lanes*) cells were cultured for 24 h in medium at the indicated calcium concentrations. Total RNA was isolated using Trizol reagent and quantified, and RT-PCR for TIMP-2 message was performed using primers described under "Experimental Procedures." As loading control, amplification primers for GAPDH were used. The samples were electrophoresed on a 1.5% agarose gel, stained with ethidium bromide, and visualized by UV transillumination. *C*, SCC25-MT cells were serum-starved overnight and incubated for an additional 24 h in medium containing 0.09 mM calcium in the presence or absence of GM6001 (10 μM). Calcium from a concentrated solution was added to the conditioned media to a final concentration of 1.2 mM, and at the indicated times the conditioned medium was harvested, concentrated 15–20-fold, electrophoresed on a 15% SDS-polyacrylamide gel, and immunoblotted with anti-TIMP-2 antibody followed by peroxidase-conjugated secondary antibody and enhanced chemiluminescence detection. The results are representative of at least three independent experiments.

55-kDa MT1-MMP species (data not shown). To evaluate the effect of calcium on MT1-MMP endocytosis, calcium levels in the medium were modulated at the time of temperature shift. MT1-MMP was effectively internalized in both low (0.09) and high (1.2 mM) calcium conditions (Fig. 7*B*, *lanes 2* and *5*). Analysis of total cellular MT1-MMP (Fig. 7*A*, *(c)*; surface and internalized) confirmed previous results and indicated no change in the overall expression levels (Fig. 7*B*, *lanes 3* and *6*). Together, these data demonstrate that MT1-MMP is regulated by endocytosis under both low and high calcium conditions. However, the rapid calcium-induced changes in pro-MMP-2 activation kinetics are not mirrored by corresponding changes in surface MT1-MMP expression or endocytosis.

Calcium Regulates TIMP-2 Levels—TIMP-2 plays an important role in pro-MMP-2 activation (10, 15–20); at low concentrations it facilitates activation by bridging trimolecular-activation complex formation, whereas at higher concentrations the activation is inhibited via interaction of TIMP-2 with the catalytically competent MT1-MMP active site. Because the calcium-induced pro-MMP-2 activation could not be attributed to changes in either MT1-MMP expression or to surface localization, the remaining component of the trimolecular complex, TIMP-2, was evaluated. Following serum starvation in low calcium, SCC25-MT cells were maintained in medium containing the indicated calcium concentration in the presence or absence of GM6001. Conditioned media were collected at 24 h, concentrated 15–20-fold, and TIMP-2 analyzed by Western blotting. A dose-dependent decrease in soluble TIMP-2 was observed (Fig. 8*A*, *1st* to *4th lanes*). To determine whether the calcium-induced decrease in soluble TIMP-2 results from decreased expression, the TIMP-2 message levels from SCC25 and SCC25-MT cells were analyzed by RT-PCR. No calcium-induced changes in TIMP-2 message levels were observed either in SCC25 or SCC25-MT cells (Fig. 8*B*). However, analysis of soluble TIMP-2 protein levels in cells cultured with GM6001 indicated that GM6001 blocked the calcium-mediated decline in soluble TIMP-2 (Fig. 8*A*, *5th* to *8th lanes*). Together, these data suggest that blocking the MT1-MMP active site with GM6001 may prevent the loss of soluble TIMP-2 by affecting recruitment of TIMP-2 to the cell surface-activation complex, providing evidence that calcium regulates TIMP-2 at the post-translational level.

To determine whether the rapid calcium-mediated induction of pro-MMP-2 activation reflects changes in surface-associated TIMP-2 levels, the effect of calcium on the kinetics of TIMP-2 loss from the conditioned media was examined. SCC25-MT cells were incubated in low calcium (0.09 mM) medium to accu-

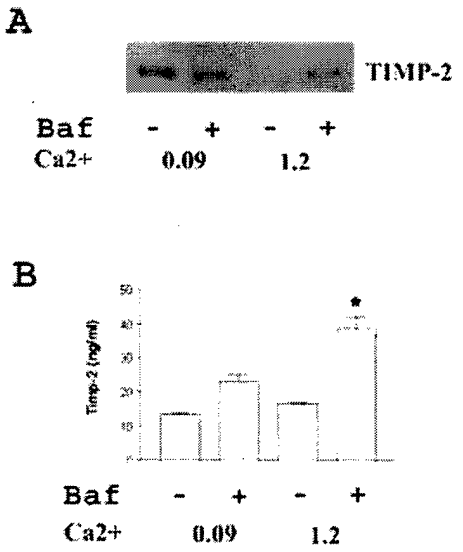

FIG. 9. **Calcium promotes degradation of TIMP-2.** SCC25-MT cells were serum-starved overnight and incubated for an additional 24 h at the indicated calcium concentration in the presence or absence of bafilomycin A1 (75 nM). *A*, conditioned media were concentrated 15–20-fold using Micron 10 microconcentrators and electrophoresed on a 15% SDS-polyacrylamide gel. The membranes were immunoblotted with anti-TIMP-2 antibody followed by peroxidase-conjugated secondary antibody and enhanced chemiluminescence detection. *B*, TIMP-2 levels in the cell lysates were quantified using ELISA according to the manufacturer's specifications. The results are representative of at least two independent experiments. *, significantly different from control (Ca^{2+} 0.09, *Baf*−) with $p < 0.05$.

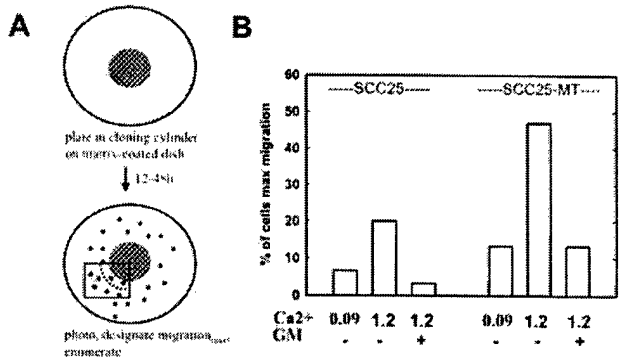

FIG. 10. **Calcium promotes cell migration.** *A*, schematic of migration protocol. Cells were plated in medium containing 0.09 mM calcium on laminin-5-enriched matrix inside a glass ring. After removal of the ring, the cells were serum-starved for 3 h, and then fresh serum-free medium containing either 0.09 or 1.2 mM calcium supplemented with 20 ng/ml EGF was added. Cells were allowed to migrate for 12–48 h. To quantify the relative motility, the migratory front was photographed every 12 h for 48 h, and the percentage of cells crossing a line designated "migratory max" was enumerated. *B*, SCC25 and SCC25-MT cells were allowed to migrate as described above in the presence or absence of GM6001 (*GM*, 10 μM). In a representative experiment, the relative motility at 24 h was quantified by determining the percentage of the SCC25 and SCC25-MT cells crossing the migratory max line. The results are representative of three independent experiments.

mulate pro-MMP-2 and TIMP-2 in the conditioned media. After 24 h, calcium from a concentrated stock solution was added to a final concentration of 1.2 mM. At the indicated times, the conditioned media were collected, concentrated, and TIMP-2 analyzed by Western blotting. TIMP-2 levels in the conditioned media changed with time, with the decrease apparent at 2 h following calcium restoration (Fig. 8*C*, *upper panel*). The presence of GM6001 blocked the decline (Fig. 8*C*, *lower panel*), further supporting the hypothesis that calcium promotes MT1-MMP dependent recruitment of TIMP-2 to the cell surface trimolecular activation complex.

To differentiate whether the calcium-induced decrease in soluble TIMP-2 levels reflected enhanced surface accumulation *versus* increased degradation of TIMP-2, the vacuolar ATPase inhibitor bafilomycin A1 was utilized. The rationale for this experiment was based on previous studies (58) showing that PMA-induced stimulation of pro-MMP-2 activation and corresponding loss of soluble TIMP-2 resulted from MT1-MMP-mediated TIMP-2 internalization and subsequent intracellular degradation in endosomal and/or lysosomal compartments. Increasing the pH of these compartments with bafilomycin A1 blocked TIMP-2 degradation, leading to a build-up of cellular TIMP-2 levels (58). Thus, SCC25-MT cells were cultured in 0.09 or 1.2 mM calcium for 24 h in the presence or absence of bafilomycin A1 (75 nM), and conditioned media were collected, concentrated 15–20-fold, and evaluated for TIMP-2 by Western blotting. In addition, the cell lysates at 24 h were collected and analyzed for TIMP-2 by ELISA. As shown above (Fig. 8*A*), calcium decreased the TIMP-2 levels in the conditioned media (Fig. 9*A*, *1st* and *3rd lanes*) but did not affect the levels of TIMP-2 in the cell lysates (Fig. 9*B*). Together, these data indicate that the calcium-mediated decline in soluble TIMP-2 is not due to cell surface accumulation of the inhibitor and suggest that TIMP-2 degradation is increased in high calcium. This is supported by experiments using bafilomycin A1, which partially blocked the calcium-mediated decline in soluble TIMP-2 (Fig. 9*A*, *4th lane*). Because bafilomycin A1 blocks TIMP-2 degradation (58), these data support the hypothesis that the decline in soluble TIMP-2 observed under high calcium conditions reflects increased degradation of TIMP-2.

Calcium Promotes SCC25 Cell Migration—To evaluate the functional consequences of calcium-induced MMP-2 activation, the effect of calcium on SCC25 and SCC25-MT cell migration on laminin-5-rich matrix was examined. Migration was quantified using an *in vitro* cell dispersion assay (39), in which cells are plated at high density in a glass ring and allowed to migrate after removal of the ring (Fig. 10*A*). After the cells have attached and spread, the ring is removed, serum-starved for 3 h, and the media switched to either low (0.09 mM) or high (1.2 mM) calcium supplemented with 20 ng/ml EGF, and migration is quantified at 12–48 h. In a representative experiment quantified at 24 h, SCC25 cells migrated on laminin 5-rich matrix, with SCC25-MT cells displaying increased migration relative to wild-type cells (Fig. 10*B*). Calcium enhanced the motility of both wild-type and MT1-MMP-overexpressing SCC25 cells. Calcium-induced migration was blocked by GM6001, indicating that the enhanced migration observed can be attributed to increased MMP activity.

DISCUSSION

Studies using multiple cancer models have shown that MMP-2 activation is important in cellular behavior (59–62). The activation of MMP-2 *in vitro* is associated with increased migration and invasiveness of cancer cells (63–65). Furthermore, there is increased MMP-2 activation with lymph node metastasis in a number of different cancers, including OSCC (3, 8, 66). Hence, the regulation of MMP-2 activation has been studied extensively. Previously, it was shown that MMP-2 activation could be promoted with non-physiological agents like PMA (11, 52) and concanavalin A (67, 68) and also by proteins of the extracellular matrix such as collagen and fibronectin (42–48, 69, 70). In this study, we show that calcium also regulates pro-MMP-2 activation without altering expression of the zymogen. Increasing extracellular calcium resulted in a dose-dependent activation of pro-MMP-2, accompanied by enhanced

generation of 43-kDa catalytically inactive MT1-MMP species and a decline in the levels of soluble TIMP-2. Calcium did not affect the steady state levels of TIMP-2 in the cell lysates, suggesting that calcium induces TIMP-2 degradation. As a functional consequence, calcium promoted cellular migration, suggesting that calcium may control keratinocyte migration via regulation of MMP-2 activation.

Calcium-mediated MMP-2 activation was MT1-MMP-dependent; however, calcium did not affect MT1-MMP message or cell surface protein levels, consistent with the observation that calcium-mediated activation of MMP-2 occurs rapidly at the cell surface. Increased generation of the catalytically inactive 43-kDa MT1-MMP species autolysis product was also observed. These data are in agreement with the recent reports (58, 69, 70) showing that MMP-2 activation induced by fibronectin and PMA increased accumulation of the 43-kDa MT1-MMP species without affecting the levels of the 55-kDa MT1-MMP species. Despite the rapid activation of MMP-2 at the cell surface, calcium did not affect MT1-MMP endocytosis.

Calcium-induced MMP-2 activation was associated with an MT1-MMP-dependent decline in soluble TIMP-2. A similar phenomenon has been reported recently (58, 69, 71) in other model systems. For example, PMA and type IV collagen-induced MMP-2 activation in HT1080 cells is coupled with TIMP-2 degradation (58, 69). In SCC25 cells, the calcium-induced decline in TIMP-2 also likely results from degradation as treatment with bafilomycin A1, a highly specific inhibitor of vacuolar ATPase that was previously shown to block MT1-MMP-mediated degradation of TIMP-2 (58), restored soluble TIMP-2 levels. This is in contrast to the loss of soluble TIMP-2 that accompanies concanavalin A-induced pro-MMP-2 activation, which results from enhanced cell surface binding rather than degradation (58, 69, 72). The mechanism by which changes in extracellular calcium promote TIMP-2 internalization and degradation is currently under investigation. Nevertheless, it is interesting to note that an inverse relationship between MMP-2 activation and soluble TIMP-2 has been observed in many human cancer cell lines (22, 51, 72).

The calcium-induced changes in post-translational MMP regulation correlated with increased migration over laminin-5-enriched matrix. Several reports (63, 64, 74, 75) have demonstrated involvement of active MMP-2 in cellular migration, including laminin-5-driven motility (73, 76). MT1-MMP has also been implicated in epithelial cell migration over laminin-5 matrix (39, 73). Our data demonstrate that migration on laminin-5 is enhanced both in MT1-MMP-overexpressing cells and under conditions that promote MMP-2 activation. Because calcium is a key regulator of keratinocyte function, these data suggest that localized changes in calcium in the extracellular milieu may function as a fine regulatory mechanism for post-translational control of MMP activity and MMP-influenced cellular behaviors such as migration and invasion.

REFERENCES

1. Liotta, L. A., Tryggvason, K., Garbisa, S., Hart, I., Foltz, C. M., and Shafie, S. (1980) *Nature* **284,** 67–68
2. Forastiere, A., Koch, W., Trotti, A., and Sidransky, D. (2001) *N. Engl. J. Med.* **345,** 1890–1900
3. Kurahara, S., Shinohara, M., Ikebe, T., Nakamura, S., Beppu, M., Hiraki, A., Takeuchi, H., and Shirasuna, K. (1999) *Head Neck* **21,** 627–638
4. Werb, Z. (1997) *Cell* **91,** 439–442
5. Nagase, H., and Woessner, J. F., Jr. (1999) *J. Biol. Chem.* **274,** 21491–21494
6. Sternlicht, M. D., and Werb, Z. (2001) *Annu. Rev. Cell Dev. Biol.* **17,** 463–516
7. Egeblad, M., and Werb, Z. (2002) *Nat. Rev. Cancer* **2,** 161–174
8. Shimada, T., Nakamura, H., Yamashita, K., Kawata, R., Murakami, Y., Fujimoto, N., Sato, H., Seiki, M., and Okada, Y. (2000) *Clin. Exp. Metastasis* **18,** 179–188
9. Sato, H., Takino, T., Okada, Y., Cao, J., Shinagawa, A., Yamamoto, E., and Seiki, M. (1994) *Nature* **370,** 61–65
10. Butler, G. S., Butler, M. J., Atkinson, S. J., Will, H., Tamura, T., van Westrum, S. S., Crabbe, T., Clements, J., d'Ortho, M. P., and Murphy, G. (1998) *J. Biol. Chem.* **273,** 871–880
11. Lehti, K., Lohi, J., Valtanen, H., and Keski-Oja, J. (1998) *Biochem. J.* **334,** 345–353
12. Sato, H., Kinoshita, T., Takino, T., Nakayama, K., and Seiki, M. (1996) *FEBS Lett.* **393,** 101–104
13. Maquoi, E., Noel, A., Frankenne, F., Angliker, H., Murphy, G., and Foidart, J. M. (1998) *FEBS Lett.* **424,** 262–266
14. Yana, I., and Weiss, S. J. (2000) *Mol. Biol. Cell* **11,** 2387–2401
15. Strongin, A. Y., Collier, I., Bannikov, G., Marmer, B. L., Grant, G. A., and Goldberg, G. I. (1995) *J. Biol. Chem.* **270,** 5331–5338
16. Itoh, Y., Ito, A., Iwata, K., Tanzawa, K., Mori, Y., and Nagase, H. (1998) *J. Biol. Chem.* **273,** 24360–24367
17. Zucker, S., Drews, M., Conner, C., Foda, H. D., DeClerck, Y. A., Langley, K. E., Bahou, W. F., Docherty, A. J., and Cao, J. (1998) *J. Biol. Chem.* **273,** 1216–1222
18. Jo, Y., Yeon, J., Kim, H. J., and Lee, S. T. (2000) *Biochem. J.* **345,** 511–519
19. Overall, C. M., King, A. E., Sam, D. K., Ong, A. D., Lau, T. T., Wallon, U. M., DeClerck, Y. A., and Atherstone, J. (1999) *J. Biol. Chem.* **274,** 4421–4429
20. Toth, M., Bernardo, M. M., Gervasi, D. C., Soloway, P. D., Wang, Z., Bigg, H. F., Overall, C. M., DeClerck, Y. A., Tschesche, H., Cher, M. L., Brown, S., Mobashery, S., and Fridman, R. (2000) *J. Biol. Chem.* **275,** 41415–41423
21. Madlener, M., Parks, W. C., and Werner, S. (1998) *Exp. Cell Res.* **242,** 201–210
22. Baumann, P., Zigrino, P., Mauch, C., Breitkreutz, D., and Nischt, R. (2000) *Br. J. Cancer* **83,** 1387–1393
23. Nagavarapu, U., Relloma, K., and Herron, G. S. (2002) *J. Invest. Dermatol.* **118,** 573–581
24. Hennings, H., Michael, D., Cheng, C., Steinert, P., Holbrook, K., and Yuspa, S. H. (1980) *Cell* **19,** 245–254
25. Hennings, H., and Holbrook, K. A. (1983) *Exp. Cell Res.* **143,** 127–142
26. Yuspa, S. H., Kilkenny, A. E., Steinert, P. M., and Roop, D. R. (1989) *J. Cell Biol.* **109,** 1207–1217
27. Bikle, D. D., Ng, D., Tu, C. L., Oda, Y., and Xie, Z. (2001) *Mol. Cell. Endocrinol.* **177,** 161–171
28. Menon, G. K., Grayson, S., and Elias, P. M. (1985) *J. Invest. Dermatol.* **84,** 508–512
29. Menon, G. K., Price, L. F., Bommannan, B., Elias, P. M., and Feingold, K. R. (1994) *J. Invest. Dermatol.* **102,** 789–795
30. Mauro, T., Bench, G., Sidderas-Haddad, E., Feingold, K., Elias, P., and Cullander, C. (1998) *J. Invest. Dermatol.* **111,** 1198–1201
31. Kobayashi, T., Hattori, S., Nagai, Y., Tajima, S., and Nishikawa, T. (1998) *Dermatology* **197,** 1–5
32. Kobayashi, T., Hattori, S., Nagai, Y., and Tajima, S. (2000) *IUBMB Life* **50,** 221–226
33. Kobayashi, T., Kishimoto, J., Ge, Y., Jin, W., Hudson, D. L., Ouahes, N., Ehama, R., Shinkai, H., and Burgeson, R. E. (2001) *EMBO Rep.* **2,** 604–608
34. Munshi, H. G., and Stack, M. S. (2002) *Methods Cell Biol.* **69,** 195–205
35. Laemmli, U. K. (1970) *Nature* **227,** 680–685
36. Wong, H., Muzik, H., Groft, L. L., Lafleur, M. A., Matouk, C., Forsyth, P. A., Schultz, G. A., Wall, S. J., and Edwards, D. R. (2001) *Methods Mol. Biol.* **151,** 305–320
37. Neuhaus, E. M., and Soldati, T. (2000) *J. Cell Biol.* **150,** 1013–1026
38. Gospodarowicz, D. (1984) in *Methods for Preparation of Media Supplements and Substrata* (Barnes, D. W., Sirbasku, D. A., and Stao, G. H., eds) pp. 275–293, Alan R. Liss, Inc., New York
39. Gilles, C., Polette, M., Coraux, C., Tournier, J. M., Meneguzzi, G., Munaut, C., Volders, L., Rousselle, P., Birembaut, P., and Foidart, J. M. (2001) *J. Cell Sci.* **114,** 2967–2976
40. Hernandez-Barrantes, S., Bernardo, M., Toth, M., and Fridman, R. (2002) *Semin. Cancer Biol.* **12,** 131–138
41. Toth, M., Hernandez-Barrantes, S., Osenkowski, P., Bernardo, M. M., Gervasi, D. C., Shimura, Y., Meroueh, O., Kotra, L. P., Galvez, B. G., Arroyo, A. G., Mobashery, S., and Fridman, R. (2002) *J. Biol. Chem.* **277,** 26340–26350
42. Azzam, H. S., and Thompson, E. W. (1992) *Cancer Res.* **52,** 4540–4544
43. Seltzer, J. L., Lee, A. Y., Akers, K. T., Sudbeck, B., Southon, E. A., Wayner, E. A., and Eisen, A. Z. (1994) *Exp. Cell Res.* **213,** 365–374
44. Gilles, C., Polette, M., Seiki, M., Birembaut, P., and Thompson, E. W. (1997) *Lab. Invest.* **76,** 651–660
45. Haas, T. L., Davis, S. J., and Madri, J. A. (1998) *J. Biol. Chem.* **273,** 3604–3610
46. Ellerbroek, S. M., Fishman, D. A., Kearns, A. S., Bafetti, L. M., and Stack, M. S. (1999) *Cancer Res.* **59,** 1635–1641
47. Ellerbroek, S. M., Wu, Y. I., Overall, C. M., and Stack, M. S. (2001) *J. Biol. Chem.* **276,** 24833–24842
48. Aznavoorian, S., Moore, B. A., Alexander-Lister, L. D., Hallit, S. L., Windsor, L. J., and Engler, J. A. (2001) *Cancer Res.* **61,** 6264–6275
49. Strongin, A. Y., Marmer, B. L., Grant, G. A., and Goldberg, G. I. (1993) *J. Biol. Chem.* **268,** 14033–14039
50. Will, H., Atkinson, S. J., Butler, G. S., Smith, B., and Murphy, G. (1996) *J. Biol. Chem.* **271,** 17119–17123
51. Kurschat, P., Zigrino, P., Nischt, R., Breitkopf, K., Steurer, P., Klein, C. E., Krieg, T., and Mauch, C. (1999) *J. Biol. Chem.* **274,** 21056–21062
52. Lohi, J., and Keski-Oja, J. (1995) *J. Biol. Chem.* **270,** 17602–17609
53. Simon, C., Goepfert, H., and Boyd, D. (1998) *Cancer Res.* **58,** 1135–1139
54. Yamamoto, M., Tsujishita, H., Hori, N., Ohishi, Y., Inoue, S., Ikeda, S., and Okada, Y. (1998) *J. Med. Chem.* **41,** 1209–1217
55. Rozanov, D. V., Deryugina, E. I., Ratnikov, B. I., Monosov, E. Z., Marchenko, G. N., Quigley, J. P., and Strongin, A. Y. (2001) *J. Biol. Chem.* **276,** 25705–25714
56. Jiang, A., Lehti, K., Wang, X., Weiss, S. J., Keski-Oja, J., and Pei, D. (2001) *Proc. Natl. Acad. Sci. U. S. A.* **98,** 13693–13698
57. Uekita, T., Itoh, Y., Yana, I., Ohno, H., and Seiki, M. (2001) *J. Cell Biol.* **155,** 1345–1356
58. Maquoi, E., Frankenne, F., Baramova, E., Munaut, C., Sounni, N. E., Remacle, A., Noel, A., Murphy, G., and Foidart, J. M. (2000) *J. Biol. Chem.* **275,** 11368–11378

59. Brown, P. D., Bloxidge, R. E., Stuart, N. S., Gatter, K. C., and Carmichael, J. (1993) *J. Natl. Cancer Inst.* **85,** 574–578
60. Nomura, H., Fujimoto, N., Seiki, M., Mai, M., and Okada, Y. (1996) *Int. J. Cancer* **69,** 9–16
61. Liabakk, N. B., Talbot, I., Smith, R. A., Wilkinson, K., and Balkwill, F. (1996) *Cancer Res.* **56,** 190–196
62. Crescimanno, C., Foidart, J. M., Noel, A., Polette, M., Maquoi, E., Birembaut, P., Baramova, E., Kaufmann, P., and Castellucci, M. (1996) *Exp. Cell Res.* **227,** 240–251
63. Deryugina, E. I., Bourdon, M. A., Luo, G. X., Reisfeld, R. A., and Strongin, A. (1997) *J. Cell Sci.* **110,** 2473–2482
64. Makela, M., Larjava, H., Pirila, E., Maisi, P., Salo, T., Sorsa, T., and Uitto, V. J. (1999) *Exp. Cell Res.* **251,** 67–78
65. Itoh, Y., Takamura, A., Ito, N., Maru, Y., Sato, H., Suenaga, N., Aoki, T., and Seiki, M. (2001) *EMBO J.* **20,** 4782–4793
66. Kawata, R., Shimada, T., Maruyama, S., Hisa, Y., Takenaka, H., and Murakami, Y. (2002) *Acta Oto-Laryngol.* **122,** 101–106
67. Overall, C. M., and Sodek, J. (1990) *J. Biol. Chem.* **265,** 21141–21151
68. Yu, M., Sato, H., Seiki, M., and Thompson, E. W. (1995) *Cancer Res.* **55,** 3272–3277
69. Maquoi, E., Frankenne, F., Noel, A., Krell, H. W., Grams, F., and Foidart, J. M. (2000) *Exp. Cell Res.* **261,** 348–359
70. Stanton, H., Gavrilovic, J., Atkinson, S. J., d'Ortho, M. P., Yamada, K. M., Zardi, L., and Murphy, G. (1998) *J. Cell Sci.* **111,** 2789–2798
71. Gilles, C., Bassuk, J. A., Pulyaeva, H., Sage, E. H., Foidart, J. M., and Thompson, E. W. (1998) *Cancer Res.* **58,** 5529–5536
72. Shofuda, K., Moriyama, K., Nishihashi, A., Higashi, S., Mizushima, H., Yasumitsu, H., Miki, K., Sato, H., Seiki, M., and Miyazaki, K. (1998) *J. Biochem. (Tokyo)* **124,** 462–470
73. Koshikawa, N., Giannelli, G., Cirulli, V., Miyazaki, K., and Quaranta, V. (2000) *J. Cell Biol.* **148,** 615–624
74. Nawrocki Raby, B., Polette, M., Gilles, C., Clavel, C., Strumane, K., Matos, M., Zahm, J. M., Van Roy, F., Bonnet, N., and Birembaut, P. (2001) *Int. J. Cancer* **93,** 644–652
75. Takahashi, K., Eto, H., and Tanabe, K. K. (1999) *Int. J. Cancer* **80,** 387–395
76. Giannelli, G., Falk-Marzillier, J., Schiraldi, O., Stetler-Stevenson, W. G., and Quaranta, V. (1997) *Science* **277,** 225–228

THE JOURNAL OF BIOLOGICAL CHEMISTRY
Vol. 277, No. 41, Issue of October 11, pp. 38159–38167, 2002
Printed in U.S.A.

Proteinase Suppression by E-cadherin-mediated Cell-Cell Attachment in Premalignant Oral Keratinocytes*

Received for publication, March 12, 2002, and in revised form, July 16, 2002
Published, JBC Papers in Press, July 23, 2002, DOI 10.1074/jbc.M202384200

Hidayatullah G. Munshi‡§¶‖, Supurna Ghosh¶, Subhendu Mukhopadhyay**, Yi I. Wu**, Ratna Sen**, Kathleen J. Green§ §§, and M. Sharon Stack§**‡‡¶¶**

*From the ‡Division of Hematology/Oncology, Department of Medicine, Departments of **Cell and Molecular Biology, ‡‡Obstetrics and Gynecology, §§Pathology and Dermatology, Feinberg School of Medicine, Northwestern University and the §Robert H. Lurie Comprehensive Cancer Center of Northwestern University, Chicago, Illinois 60611*

The expression and activity of epithelial proteinases is under stringent control to prevent aberrant hydrolysis of structural proteins and disruption of tissue architecture. E-cadherin-dependent cell-cell adhesion is also important for maintenance of epithelial structural integrity, and loss of E-cadherin expression has been correlated with enhanced invasive potential in multiple tumor models. To address the hypothesis that there is a functional link between E-cadherin and proteinase expression, we have examined the role of E-cadherin in proteinase regulation. By using a calcium switch protocol to manipulate junction assembly, our data demonstrate that initiation of *de novo* E-cadherin-mediated adhesive contacts suppresses expression of both relative matrix metalloproteinase-9 levels and net urinary-type plasminogen activator activity. E-cadherin-mediated cell-cell adhesion increases both phosphatidylinositol 3′-kinase (PI3-kinase)-dependent AKT phosphorylation and epidermal growth factor receptor-dependent MAPK/ERK activation. Pharmacologic inhibition of the PI3-kinase pathway, but not the epidermal growth factor receptor/MAPK pathway, prevents E-cadherin-mediated suppression of proteinases and delays junction assembly. Moreover, inhibition of junction assembly with a function-blocking anti-E-cadherin antibody stimulates proteinase-dependent Matrigel invasion. As matrix metalloproteinase-9 and urinary-type plasminogen activator potentiate the invasive activity of oral squamous cell carcinoma, these data suggest E-cadherin-mediated signaling through PI3-kinase can regulate the invasive behavior of cells by modulating proteinase secretion.

Degradation of the extracellular matrix by proteolytic enzymes is necessary for a number of normal and pathological processes, including embryonic development, tissue resorption and remodeling, angiogenesis, and wound healing (1–3). Proteinases have also been implicated in the invasion and metastasis of malignant cells (4–6). Predominant among these enzymes are the matrix metalloproteinases (MMPs)[1] and the plasminogen activator (PA) urinary-type PA (uPA) (7–10). MMPs are a large family of metalloendopeptidases with activity directed against a variety of extracellular matrix substrates (11). MMP-9 (gelatinase B), a 92-kDa gelatinase that efficiently degrades native type IV collagen, has been implicated in tumor dissemination, as evidenced by enhanced MMP-9 expression in tumor samples exhibiting matrix invasion and distant metastases (12). This is supported by studies using tumor-bearing MMP-9-deficient mice, which exhibit decreased propensity to develop metastatic foci, indicating that MMP-9 plays a critical role in tumor development (5). Post-translational regulation of MMP-9 activity is mediated by interaction with tissue inhibitor of metalloproteinases (TIMP)-1 which forms a 1:1 noncovalent inactive enzyme-inhibitor complex (12). Under many conditions, secretion of MMP-9 and TIMP-1 is coordinately regulated (12).

In addition to MMP-9, up-regulation of uPA expression has also been correlated with malignant progression of a wide variety of neoplasms (9). uPA is a serine proteinase that functions in the conversion of the circulating zymogen plasminogen to the active enzyme plasmin (9). Plasmin is a broad spectrum serine proteinase that can directly cleave a number of protein substrates (9), as well as activate many additional proteinase zymogens including pro-MMP-9 (13). uPA is localized to the cell surface via interaction with a glycosylphosphatidylinositol-anchored receptor, designated uPA receptor or uPAR (9). Proteolytic activity is also regulated by the serpin plasminogen activator inhibitor 1 (PAI-1) which forms a covalent enzyme-inhibitor complex with both free and receptor-localized uPA (9). In a number of tumor models, down-regulation of either uPA or its receptor decreases invasion and reduces metastatic potential (14, 15).

Like proteolytic enzymes, dysregulation of adhesion molecules is often observed in malignant cells. Cadherins are a family of cell surface adhesion molecules that participate in Ca^{2+}-dependent cell-cell adhesion (16) and thus are essential for maintenance of tissue integrity. E-cadherin is a widely distributed transmembrane intercellular adhesion molecule

* This work was supported in part by NIDCR Research Grant PO1 DE12328 from the National Institutes of Health (to M. S. S. and K. J. G.) and National Institutes of Health Grant RO1 CA 85870 (to M. S. S.). The costs of publication of this article were defrayed in part by the payment of page charges. This article must therefore be hereby marked "*advertisement*" in accordance with 18 U.S.C. Section 1734 solely to indicate this fact.

¶ Both authors contributed equally to this work.

‖ Supported by NCI Clinical Oncology Research Training Program Grant T32 CA79447 from the National Institutes of Health.

¶¶ To whom correspondence should be addressed: Dept. of Cell and Molecular Biology, Northwestern University Medical School, 303 E. Chicago Ave., Tarry 8-715, Chicago IL 60611. Tel.: 312-908-8216; Fax: 312-503-7912; E-mail: mss130@northwestern.edu.

[1] The abbreviations used are: MMP-9, matrix metalloproteinase 9; TIMP-1, tissue of inhibitor of metalloproteinases 1; uPA, urinary-type plasminogen activator; uPAR, uPA receptor; PAI-1, plasminogen activator inhibitor 1; MEK, mitogen-activated protein kinase/extracellular signal-regulated kinase kinase; MAPK, mitogen-activated protein kinase; ERK, extracellular signal-regulated kinase; PI3-kinase, phosphatidylinositol 3′-kinase; ELISA, enzyme-linked immunosorbent assay; EGFR, epidermal growth factor receptor; PBS, phosphate-buffered saline; pp, phosphoprotein.

(17). In addition to functioning in cell-cell adhesion, the cytoplasmic tail of E-cadherin binds to β- or γ-catenin/plakoglobin, thereby providing a mechanism for association with additional proteins, including signaling molecules such as phosphatidylinositol 3′-kinase (PI3-kinase) and epidermal growth factor receptor (18–21). Loss of E-cadherin expression is frequently observed in carcinomas (22, 23), and transfection of ectopic E-cadherin into breast (24), colon (25), and prostate cancer cells (26) decreases cellular invasion.

In multiple tumor models, loss of E-cadherin expression and increased proteinase activity correlate with more invasive and metastatic tumors (9, 12, 14, 15, 22, 23, 27). To address the hypothesis that there is a functional link between E-cadherin and proteinase expression, in the current study we have examined the role of E-cadherin in the regulation of proteinase expression in premalignant oral keratinocytes. Our data demonstrate that initiation of *de novo* E-cadherin-mediated cell-cell adhesion suppresses both relative MMP-9 levels and net uPA activity in premalignant oral keratinocytes. Concomitant with decreased proteinase expression, secretion of TIMP-1 and PAI-1 is also down-regulated. E-cadherin-mediated cell-cell adhesion increases PI3-kinase-dependent AKT activation and epidermal growth factor receptor (EGFR)-dependent mitogen-activated protein kinase (MAPK)/extracellular signal regulated kinase (ERK) activation. Inhibition of the PI3-kinase pathway, but not the EGFR-MAPK pathway, interferes with formation of adherens junctions and prevents E-cadherin-mediated suppression of proteinases. Furthermore, prevention of junction assembly with a function-blocking E-cadherin antibody stimulates proteinase-dependent Matrigel invasion. Together these data support the hypothesis that E-cadherin-mediated signaling via PI3-kinase can regulate the invasive behavior of cells by modulating proteinase expression.

EXPERIMENTAL PROCEDURES

Materials—Gelatin, cell culture reagents, D-Val-Leu-Lys-*p*-nitroanilide, rat anti-E-cadherin (DECMA clone), and peroxidase-conjugated secondary antibodies were purchased from Sigma. Keratinocyte-SFM was obtained from Invitrogen. Plasminogen was purified by affinity chromatography from outdated human plasma as described previously (28). Anti-mouse E-cadherin (HECD-1 clone) and isotype-specific IgG1 antibodies were obtained from Calbiochem; anti-phosphorylated p42/p44 (MAPK/ERK) was obtained from Promega (Madison, WI); anti-ERK1/2 (anti-p42/p44) antibody and anti-AKT antibody were purchased from Santa Cruz Biotechnology (Santa Cruz, CA); anti-phosphorylated AKT (Thr-308) was obtained from Upstate Biotechnology, Inc.; anti-uPAR antibody (399R) and function-blocking anti-uPA antibody (394) were obtained from American Diagnostica (Greenwich, CT); and Alexa Fluor 594 goat anti-mouse and anti-rat antibodies were from Molecular Probes (Eugene, OR). TIMP-1 and MMP-9 ELISA kits were from Oncogene Research Products (Boston, MA), and PAI-1 ELISA kit was purchased from American Diagnostica. The mitogen-activated protein kinase/extracellular signal-regulated kinase kinase (MEK) inhibitor PD98059, PI3-kinase inhibitor LY294002, and EGFR-specific inhibitor AG1478 were obtained from Calbiochem. The MMP inhibitor GM6001 was purchased from Chemicon (Temecula, CA). Polyvinylidene difluoride membrane was from Amersham Biosciences (Arlington Heights, IL). Supersignal enhanced chemiluminescence (ECL) reagent, EZ-Link Sulfo-NHS-Biotin, and UltraLink Immobilized Streptavadin Gel were obtained from Pierce. Microcon 10 microconcentrators were purchased from Millipore (Bedford, MA).

Cell Cultures—Premalignant oral keratinocytes (pp126 cells) were the gift of Dr. D. Oda (University of Washington, Seattle, WA) (29, 30). Early passage (between 3 and 8) pp126 cells were maintained at 37 °C in a humidified atmosphere of 5% CO_2 in keratinocyte-SFM containing 0.09 mM calcium and supplemented with 100 units/ml penicillin, 100 ng/ml EGF, and 50 μg/ml bovine pituitary extract.

E-cadherin Activation—The calcium switch method was utilized to assess the consequences of *de novo* E-cadherin activation (19–21, 31, 32). Briefly, pp126 cells were seeded at a constant density (1.5×10^6 cells/well) in 12-well tissue culture plates. After 24 h, the cells were starved for 6–8 h, and calcium was removed by incubation with Keratinocyte-SFM containing 4 mM EGTA and 1 mM $MgCl_2$ at 37 °C. After 30 min the calcium-free medium was removed, and Keratinocyte-SFM containing 0.09 mM calcium was immediately added to induce E-cadherin mediated cell-cell interactions (designated "E-cadherin activation +"). In control experiments, cells received fresh media in the absence of EGTA such that original junctions are maintained, but *de novo* activation of E-cadherin is not induced (designated "E-cadherin activation −"). In selected experiments, either anti-E-cadherin antibody (HECD-1 clone) or isotype-specific control antibody was added to the calcium-containing medium at 10 μg/ml. In additional studies, the PI3-kinase inhibitor LY294002 (10 μM), the MEK inhibitor PD98059 (5 μM), the EGFR inhibitor AG1478 (250 nM), or the appropriate vehicle was added to the medium. Conditioned medium was collected for proteinase analysis after 24–36 h.

Immunfluorescence Microscopy—pp126 cells were grown on glass coverslips at 37 °C in Keratinocyte-SFM. Following a 30-min incubation with serum-free medium containing 4 mM EGTA and 1 mM $MgCl_2$, cells were incubated with Keratinocyte-SFM containing 0.09 mM Ca^{2+} in the presence of either control IgG antibody or anti-E-cadherin antibody (HECD-1, 10 μg/ml). In additional studies, the PI3-kinase inhibitor LY294002 (10 μM), the MEK inhibitor PD98059 (5 μM), the EGFR inhibitor AG1478 (250 nM), or the appropriate vehicle was added to the medium. For immunofluorescence staining, cells were washed with PBS and fixed with ice-cold methanol for 2 min or with 3.7% formaldehyde for 5 min followed by 0.5% Triton X-100 for 7 min. After washing with PBS, cells were blocked with 1% bovine serum albumin in PBS and incubated with mouse anti-E-cadherin antibody (HECD-1) or rat anti-E-cadherin antibody (DECMA) for 1 h at 37 °C. After three washes with PBS, cells were incubated for 1 h at room temperature with Alexa Fluor 594-labeled goat anti-mouse or anti-rat antibody. Glass coverslips were washed with PBS three times, mounted, and examined under a UV microscope (Nikon) using the appropriate filter.

Analysis of MMP-9 and TIMP-1 Expression—Gelatinase activities in the conditioned media at 36 h were determined using SDS-PAGE gelatin zymography as described previously (33). Briefly, SDS-PAGE gels (9% acrylamide) were co-polymerized with 0.1% gelatin, and samples were electrophoresed without reduction or boiling using 5× Laemmli sample buffer (34). SDS was removed through a 30-min incubation in 2.5% Triton X-100, and gels were incubated in 20 mM glycine, pH 8.3, 10 mM $CaCl_2$, 1 μM $ZnCl_2$ at 37 °C for 24–36 h. The gels were stained with Coomassie Blue to visualize zones of gelatinolytic activity. MMP-9 levels in the conditioned media were also quantified by ELISA (Oncogene Research Products) following concentration of the conditioned media 25–30-fold with Microcon 10. Levels of TIMP-1 protein in the conditioned media were quantified by ELISA (Oncogene Research Products) according to the manufacturer's specifications.

Analysis of uPA Activity and PAI-1 Protein Levels—Net uPA activity in the conditioned media at 24 h was quantified using a coupled assay to monitor plasminogen activation and resulting hydrolysis of a colorimetric substrate (Val-Leu-Lys-*p*-nitroanilide) as described previously (28). Levels of PAI-1 protein in the conditioned media were quantified by ELISA (American Diagnostica) according to the manufacturer's specifications.

Cell Surface Biotinylation—pp126 cells were grown in a 6-well plate, washed with ice-cold PBS, and incubated at 4 °C with gentle shaking for 30 min with 0.5 mg/ml cell-impermeable Sulfo-NHS-Biotin in ice-cold PBS, followed by washing with 100 mM glycine to quench free biotin. Cells were then detached by scraping, lysed in modified RIPA buffer (50 mM Tris, pH 7.4, 150 mM NaCl, 5 mM EDTA, 1% Triton X-100, and 0.1% SDS) with proteinase inhibitors, and clarified by centrifugation. To isolate biotinylated cell-surface proteins, equal amounts of protein from each of the samples were incubated with streptavidin beads at 4 °C for 14 h, followed by centrifugation. After boiling in Laemmli sample dilution buffer (34) to dissociate streptavidin bead-biotin complexes, the samples were analyzed by SDS-PAGE (9% gels) and immunoblotted for uPAR (1:1000, American Diagnostica, clone 399R).

MAPK and AKT Activation—E-cadherin was activated by the calcium switch method as described above, and at the indicated time points cells were lysed in modified RIPA buffer containing 20 mM sodium fluoride, 10 mM sodium pyrophosphate, 1 mM sodium orthovanadate, 1 μg/ml aprotinin, 1 μM pepstatin, and 10 μM leupeptin. The samples were analyzed by SDS-PAGE (9% gels), and the blots were probed with anti-ERK1/2 antibody (1:1000) or with anti-AKT antibody (1:1000) to detect total ERK1/2 or AKT expression or with anti-phosphorylated ERK1/2 antibody (1:1000) or anti-phosphorylated AKT antibody (1:1000) to detect active (phosphorylated) forms of ERK or AKT.

Analysis of Invasion—Invasive activity was quantified using a Boyden Chamber (8-μm pore size) coated with Matrigel (10 μg). Cells (2×10^5) were added to the chamber in 500 μl of serum-free medium with 25 μg/ml of E-cadherin function-blocking antibody (HECD-1 clone) or isotype-specific control antibody, followed by incubation for 40 h. Nonmigrating cells were removed from the upper chamber with a cotton swab; filters were fixed and stained with Diff-Quik Stain, and migrating cells adherent to the underside of the filter were enumerated using an ocular micrometer and counting a minimum of 10 high-powered fields. Data are expressed as relative migration (number of cells/field). In selected experiments, the proteinase dependence of invasion was determined by quantifying invasion in the presence of the MMP inhibitor GM6001 (2.5 μM) (Chemicon) or the function-blocking anti-uPA antibody (15 μg/ml) (American Diagnostica, clone 394).

RESULTS

Calcium-dependent Cell-Cell Adhesion Modulates Proteinase and Inhibitor Expression—E-cadherin dependent cell-cell adhesion is important for the maintenance of epithelial structural integrity, and the loss of E-cadherin expression has been shown to correlate with increased invasive potential of both carcinoma cell lines and human tumor samples (21, 22, 27, 35). Recent data demonstrate that specific proteinases, including tumor-associated MMPs, can modulate cell-cell adhesion by cleaving E-cadherin (36–38). As E-cadherin itself couples to signal transduction pathways (18–21), the hypothesis that E-cadherin may participate in proteinase regulation was tested in premalignant gingival keratinocytes (pp126 cells). The calcium switch method, in which E-cadherin-mediated cell-cell adhesion was disrupted with EGTA treatment and restored by replacing Ca^{2+}, was utilized to initiate *de novo* adherens junction assembly (19–21, 31, 32). Control cells present a typical pattern of E-cadherin staining at the level of cell-cell contacts (Fig. 1*A*); however, in cells treated with EGTA, E-cadherin is absent from cell junctions (Fig. 1*B*). After addition of calcium, adherens junctions are again formed (Fig. 1*C*), with complete restoration by 1 h of treatment (Fig. 1*D*). To evaluate the effect of E-cadherin activation on proteinase expression, after 24–36 h conditioned media were collected and analyzed. Gelatin zymography demonstrated that calcium-mediated cell-cell adhesion (designated *E-cad Actn* +) decreased relative MMP-9 levels (Fig. 1*E*). This was confirmed using an ELISA kit that recognizes both free and TIMP-1-complexed MMP-9, demonstrating a 6.5-fold decrease in MMP-9 levels in concentrated conditioned media following calcium-mediated cell-cell adhesion (Fig. 1*E*). Concomitant with MMP-9 down-regulation, *net* uPA activity was also decreased by 2–3-fold (Fig. 1*F*). Evaluation of proteinase inhibitor expression by ELISA indicated a coordinate decrease in both TIMP-1 and PAI-1 levels (Table I). Disruption of cell-cell junctions using the calcium switch method did not affect cell proliferation (data not shown).

Proteinase Suppression Following Cell-Cell Adhesion Requires Engagement of E-cadherin—To confirm that proteinase suppression is due to E-cadherin engagement and is not an unrelated consequence of calcium modulation, a function-blocking anti-E-cadherin antibody (HECD-1 clone) was utilized. To verify that the HECD-1 antibody blocked cell-cell attachment following the calcium switch protocol, cells were treated with EGTA to dissociate cell-cell junctions and then incubated for 40 min in calcium-containing medium in the presence of either function-blocking E-cadherin antibody (HECD-1, 10 μg/ml) or isotype-matched control IgG. Cells were then processed for immunofluorescence microscopy using rat anti-E-cadherin antibody (DECMA clone). Similar to the control experiment shown in Fig. 1*B*, no E-cadherin staining is visible at cell-cell junctions following EGTA treatment (Fig. 2*A*). Following calcium restoration, junctional E-cadherin is prevalent in IgG-treated cells (Fig. 2*B*), but not in anti-E-cadherin-treated cells (Fig. 2*C*), demonstrating that the antibody indeed blocks cell-cell attachment. To assess the effect of E-cadherin function blocking antibodies on proteinase suppression, cell-cell junctions were disrupted by calcium chelation, and junction assembly was initiated by the addition of calcium in the presence of

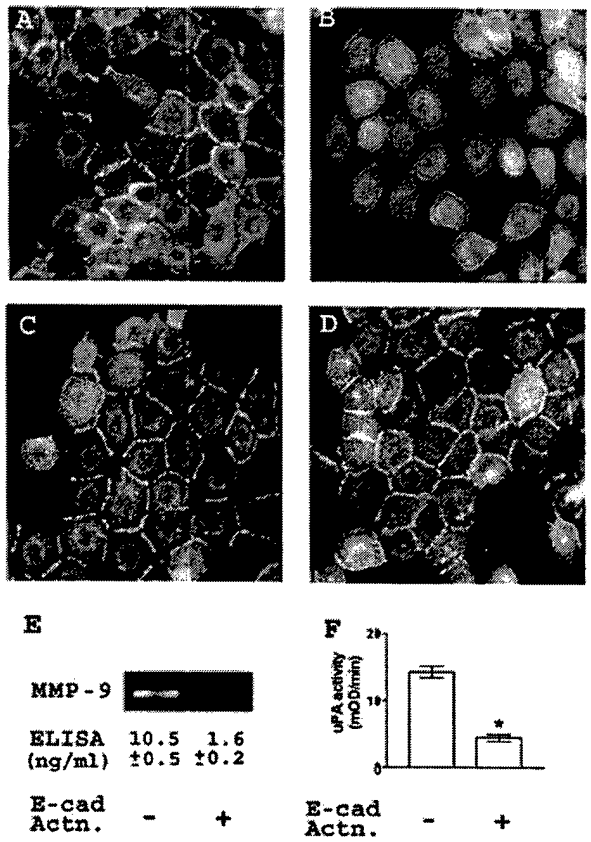

FIG. 1. **Calcium-mediated cell-cell adhesion decreases proteinase expression.** *A–D*, pp126 cells were left untreated (*A*) or treated with 4 mM EGTA for 30 min (*B–D*). To induce E-cadherin activation, the EGTA-containing medium was then replaced with calcium-containing Keratinocyte-SFM (0.09 mM) for 30 min (*C*) or 1 h (*D*). Cells were fixed, incubated with anti-E-cadherin antibody (HECD-1), and detected with Alexa Fluor 594-conjugated anti-mouse antibody. *E*, E-cadherin was activated (designated *E-cad Actn.* +) in pp126 cells using the calcium switch method as described under "Experimental Procedures." Control cells (designated *E-cad Actn.* −) were left untreated. Conditioned media were collected at 36 h and analyzed for MMP-9 expression by gelatin zymography and by ELISA as described under "Experimental Procedures." *F*, uPA activity was analyzed in the conditioned media at 24 h using a coupled colorimetric plasminogen activation assay as described under "Experimental Procedures." The results represent the mean ± S.E. of five different experiments. *, significantly different from control with $p < 0.001$.

TABLE I

Calcium-mediated cell-cell attachment suppresses TIMP-1 and PAI-1

E-cadherin (E-cad)-mediated cell-cell adhesion was disrupted by incubating pp 126 cells with 4 mM EGTA for 30 min and then re-initiated by replacing the medium with calcium-containing keratinocyte-SFM (0.09 mM, designated E-cad activation +). Conditioned media were collected after 24–36 h, and TIMP-1 and PAI-1 levels were analyzed by ELISA according to the manufacturer's specifications. The results represent the mean ± S.E. of three individual experiments.

E-cad activation	TIMP-1	PAI-1
	ng/ml	
−	72 ± 3	40 ± 2
+	45 ± 3[a]	16 ± 1[b]

[a] Value significantly different from control with $p < 0.005$.
[b] Value significantly different from control with $p < 0.001$.

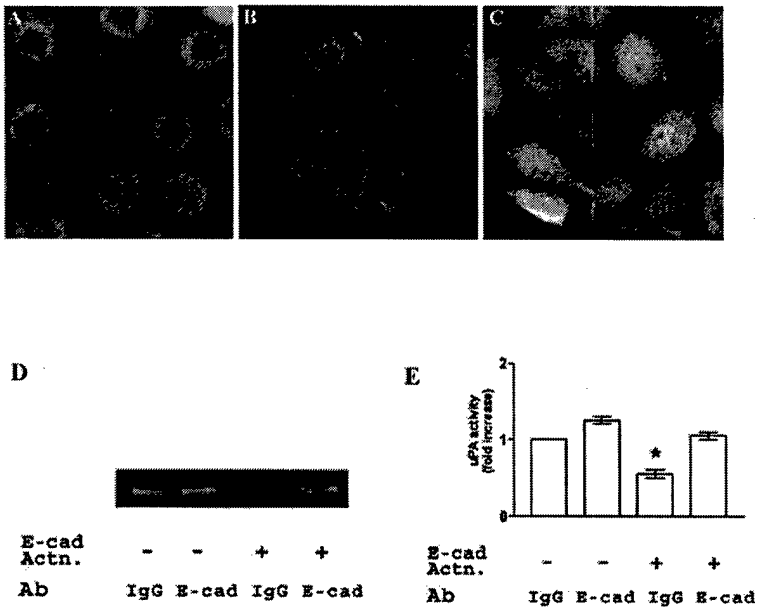

FIG. 2. **Proteinase suppression following cell adhesion requires engagement of E-cadherin.** *A–C*, pp126 cells were treated with 4 mM EGTA for 30 min (*A–C*). The EGTA-containing medium was replaced with Keratinocyte-SFM containing 0.09 mM calcium for 45 min in the presence of control IgG (10 μg/ml) (*B*) or function-blocking anti-E-cadherin antibody (HECD-1, 10 μg/ml) (*C*). Cells were fixed, incubated with anti-E-cadherin antibody (DECMA), and detected with Alexa Fluor 594-conjugated anti-rat antibody. *D* and *E*, cells were either left untreated or underwent activation of E-cadherin using the calcium switch method in the presence of function-blocking anti-E-cadherin antibody (*Ab*) (HECD-1, 10 μg/ml) or isotype-matched IgG (10 μg/ml) as described under "Experimental Procedures." *D*, conditioned media were collected at 36 h and analyzed for MMP-9 activity by gelatin zymography. *E*, uPA activity was analyzed in the conditioned media at 24 h using a coupled colorimetric plasminogen activation assay as described under "Experimental Procedures." The results represent the mean ± S.E. of three different experiments. *, significantly different from control with $p < 0.01$.

blocking antibody (10 μg/ml) to prevent formation of adherens junctions. Control samples contained an equal concentration of isotype-specific IgG. In additional controls, antibodies were added without prior disruption of cell-cell junctions by calcium chelation (designated *E-cad Actn* −). Blocking E-cadherin engagement prevented the adhesion-mediated suppression of both the relative MMP-9 levels (Fig. 2*D*, *4th lane*) and the net uPA activity (Fig. 2*E*). Addition of the function-blocking HECD-1 antibody at 10 μg/ml without prior junction disruption (designated *E-cad Actn* −) was ineffective (Fig. 2, *D*, *2nd lane*, and *E*). Moreover, in IgG-treated control samples, in which junction reformation was not prevented, proteinase expression was suppressed (Fig. 2, *D*, *3rd lane*, and *E*). Similar results were obtained for TIMP-1 and PAI-1, in which suppression of expression by E-cadherin engagement was also blocked by anti-E-cadherin antibody (Table II). In control experiments, treatment of cells with EGTA in the presence or absence of blocking antibody did not alter proliferation (data not shown). Together these data demonstrate that *de novo* E-cadherin engagement suppresses proteinase expression.

Because uPA activity can also be modulated by cell surface association (9), the effect of E-cadherin-mediated cell-cell adhesion on uPAR expression was evaluated. Cell-cell junctions were disrupted by calcium chelation, and the samples were treated with either HECD-1 blocking antibody or control IgG as described above. Cells were then incubated with cell-impermeable NHS-biotin to label surface proteins and lysed in modified RIPA buffer. Following precipitation of surface-labeled proteins with streptavidin beads, samples were electrophoresed and probed for uPAR by immunoblotting. There was no change in uPAR surface expression induced by E-cadherin-mediated cell-cell adhesion (Fig. 3). In addition, there was no change in total cellular uPAR protein levels (surface and cytoplasmic) as measured by Western blot (data not shown). These data suggest that, although the net uPA activity is suppressed, the receptor remains available.

TABLE II
Suppression of TIMP-1 and PAI-1 following cell adhesion requires E-cadherin

E-cadherin (E-cad)-mediated cell-cell adhesion was disrupted by incubating pp 126 cells with 4 mM EGTA for 30 min and then re-initiated by replacing the medium with calcium-containing keratinocyte-SFM (0.09 mM, designated E-cad activation +) in the presence of anti-E-cadherin antibody (HECD-1, 10 μg/ml) or isotype-matched IgG (10 μg/ml). Conditioned media were collected after 24–36 h, and TIMP-1 and PAI-1 levels in the conditioned media were analyzed by ELISA according to the manufacturer's specifications.

Antibody	E-cad activation	TIMP-1	PAI-1
		ng/ml	
IgG	−	94 ± 6	25 ± 2
E-cad	−	83 ± 5	23 ± 2
IgG	+	46 ± 3[a]	13 ± 1[b]
E-cad	+	70 ± 5	21 ± 1

[a] Values significantly different from control with $p < 0.001$.
[b] Values significantly different from control with $p < 0.01$.

Inhibition of MAPK Does Not Block E-cadherin-mediated Suppression of Proteinases—Because we have reported previously (30) that MAPK activation regulates proteinase expression in pp126 cells, levels of phosphorylated (active) ERK1/2 were assessed in pp126 cells following the calcium switch. Cells were lysed at various time points after calcium-induced initiation of junction assembly, and samples were analyzed by Western blotting using antibodies directed against total ERK1/2 or the phosphorylated (active) species of ERK 1/2. A time-dependent phosphorylation of ERK1/2 following *de novo* engagement of E-cadherin was observed in pp126 cells (Fig. 4*A*), with maximal MAPK activation at ~15 min. There was no change in the total amount of ERK1/2 protein (Fig. 4*A*). To confirm that

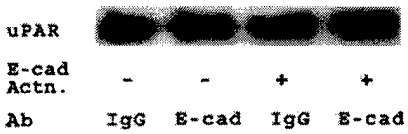

FIG. 3. **E-cadherin-mediated cell-cell adhesion does not affect surface uPAR expression.** Cells were either left untreated (designated *E-cad Actn.* −) or underwent activation of E-cadherin (designated *E-cad Actn.* +) using the calcium switch method in the presence of function-blocking anti-E-cadherin antibody (*Ab*) (HECD-1, 10 μg/ml) or isotype-matched IgG (10 μg/ml) as described under "Experimental Procedures." After 24 h the cells were surface-biotinylated and lysed. Samples were immunoprecipitated with streptavidin beads to isolate cell-surface proteins and electrophoresed on a 9% SDS-polyacrylamide gel. The membranes were immunoblotted with anti-uPAR antibody followed by peroxidase-conjugated secondary antibody and enhanced chemiluminescence detection.

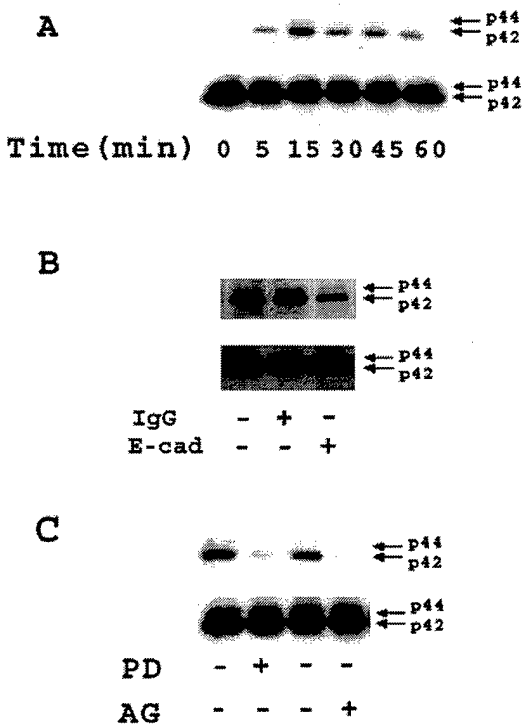

FIG. 4. **E-cadherin-mediated adhesion enhances EGFR-mediated MAPK activity.** *A*, using the calcium switch method, E-cadherin was activated in pp126 cells. The cells were lysed at the indicated times following E-cadherin activation. The lysates were separated by SDS-PAGE (9% gels), transferred to polyvinylidene difluoride membrane, and probed with anti-phospho-ERK1/2 antibody to detect the phosphorylated, active form of ERK (*upper panel*) or with anti-ERK1/2 antibody to detect total ERK1/2 expression (*lower panel*). *B*, pp126 cells underwent activation of E-cadherin using the calcium switch method in the presence of function-blocking anti-E-cadherin antibody (HECD-1, 10 μg/ml) or isotype-matched IgG (10 μg/ml) as described under "Experimental Procedures." The cells were lysed at 15 min after calcium restoration. The lysates were analyzed for phospho-ERK (*upper panel*) or for total ERK expression (*lower panel*). *C*, pp126 cells were treated with the MEK inhibitor, PD98059 (*PD*, 5 μM), EGFR inhibitor, AG1478 (*AG*, 250 nM), or with an equal amount of Me_2SO vehicle as control at the time of disruption of cell-cell junctions as described above. The cells were lysed at 15 min after calcium restoration. The lysates were analyzed for phospho-ERK (*upper panel*) or for total ERK expression (*lower panel*). The results are representative of three independent experiments.

MAPK phosphorylation was a specific consequence of E-cadherin engagement, junction assembly was initiated in the presence of the function-blocking anti-E-cadherin antibody or control IgG as described above. Inhibition of E-cadherin engagement decreased ERK1/2 phosphorylation, indicating that engagement of E-cadherin leads to MAPK activation (Fig. 4*B*). Moreover, E-cadherin-mediated MAPK activation was blocked with the MEK inhibitor PD98059, demonstrating the involvement of the MEK-ERK pathway (Fig. 4*C*). Interestingly, the epidermal growth factor receptor (EGFR)-specific tyrphostin AG1478 also completely abrogated E-cadherin-mediated MAPK activation (Fig. 4*C*), supporting the observation that E-cadherin-mediated activation of MAPK is dependent on EGFR (20).

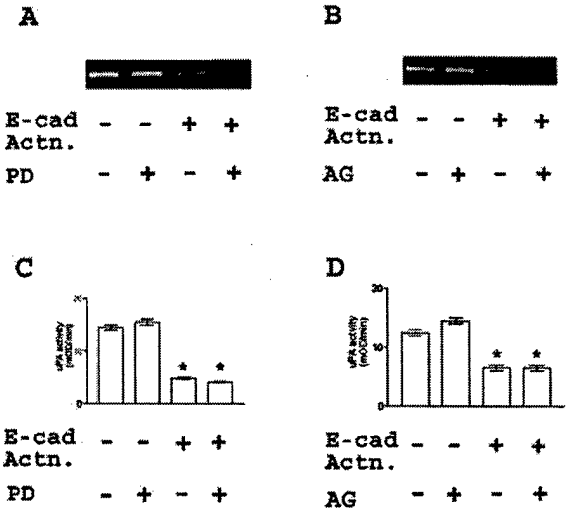

FIG. 5. **EGFR-MAPK pathway is not involved in E-cadherin-mediated suppression of proteinases.** Serum-starved pp126 cells were either left untreated (designated *E-cad Actn.* −) or underwent activation of E-cadherin (designated *E-cad Actn.* +) using the calcium switch method in the presence of 5 μM PD98059 (*PD*), 250 nM AG1478 (*AG*), or an equal volume of Me_2SO as described under "Experimental Procedures." *A* and *B*, conditioned media were collected at 36 h and analyzed for MMP-9 activity by gelatin zymography. *C* and *D*, uPA activity was analyzed in the conditioned media at 24 h using a coupled colorimetric plasminogen activation assay. The results represent the mean ± S.E. of three different experiments. *, significantly different from control with $p < 0.005$.

By using the MEK inhibitor PD98059, the role of MAPK in the E-cadherin mediated suppression of proteinases was evaluated. Cells were incubated with EGTA and 5 μM PD98059 or an equal amount of Me_2SO vehicle for 30 min before the addition of calcium-replete medium containing either 5 μM PD98059 or Me_2SO. Under basal conditions (designated *E-cad Actn* −), PD98059 did not affect the relative MMP-9 levels or the net uPA activity (Fig. 5, *A*, *2nd lane*, and *C*). However following E-cadherin activation by EGTA treatment and calcium restoration, inhibition of MEK activity did not prevent the suppression of proteinase expression (Fig. 5, *A*, *4th lane*, and *C*). Similar results were obtained with TIMP-1 and PAI-1 (data not shown).

To evaluate further the role of MAPK in the control of E-cadherin-regulated proteinase expression, the EGFR kinase-specific inhibitor tyrphostin AG1478 was employed. Cells were treated with EGTA followed by calcium restoration in the presence of AG1478 (250 nM). Under basal conditions (designated *E-cad Actn* −) AG1478 (250 nM) did not affect MMP-9 or uPA expression (Fig. 5, *B*, *2nd lane*, and *D*). Similar to the results obtained with PD98059, specific inhibition of the EGFR kinase also failed to abrogate the suppressive effect of E-cadherin engagement on the relative MMP-9 levels or the net uPA activity (Fig. 5, *B*, *4th lane*, and *D*). Together these data demonstrate that, although E-cadherin engagement can activate

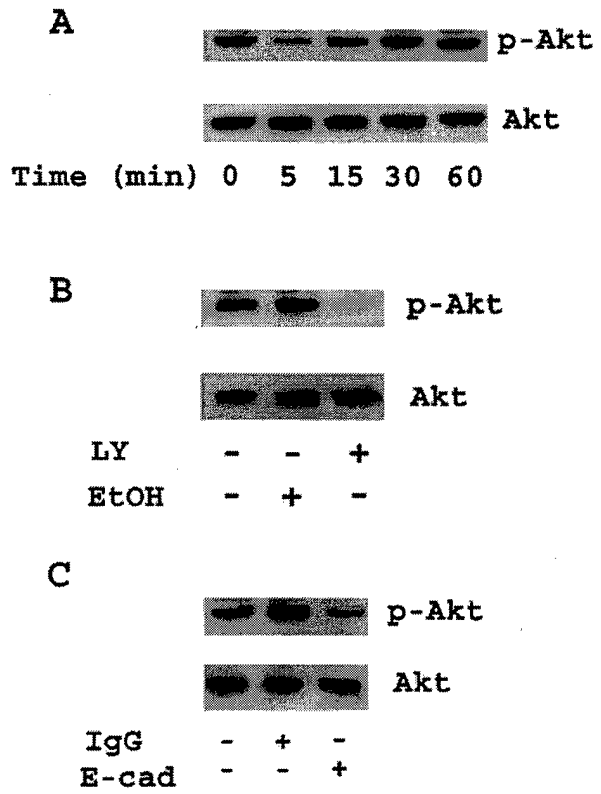

FIG. 6. **E-cadherin-mediated adhesion induces PI3-kinase mediated AKT activity.** *A*, using the calcium switch method, E-cadherin was activated in pp126 cells. The cells were lysed at the indicated times following E-cadherin activation. The lysates were separated by SDS-PAGE (9% gels), transferred to polyvinylidene difluoride membrane, and probed with an antibody that specifically recognizes phosphorylation on Thr-308 (phospho-AKT). The membrane was then reprobed with an antibody against total AKT. *B*, pp126 cells were treated with the PI3-kinase inhibitor, LY294002 (*LY*, 10 μM), or an equal volume of ethanol for 30 min at the time of disruption of cell-cell junctions as described above. The cells were lysed at 30 min after calcium restoration and analyzed for phospho-AKT (*upper panel*) and total AKT (*lower panel*) as described above. *C*, pp126 cells were either left untreated or underwent activation of E-cadherin using the calcium switch method in the presence of function-blocking anti-E-cadherin antibody (HECD-1, 10 μg/ml) or isotype-matched IgG (10 μg/ml) as described under "Experimental Procedures." The cells were lysed at 30 min after calcium restoration and analyzed for phospho-AKT or for total AKT expression as described above. The results are representative of three independent experiments.

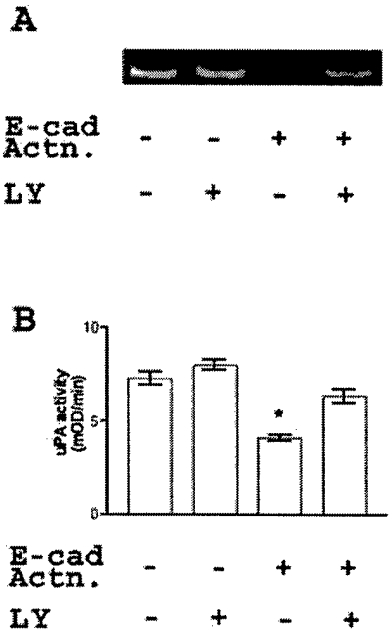

FIG. 7. **Inhibition of PI3-kinase blocks E-cadherin-mediated suppression of proteinases.** Serum-starved pp126 cells were either left untreated (designated *E-cad Actn.* −) or underwent activation of E-cadherin (designated *E-cad Actn.* +) using the calcium switch method in the presence of 10 μM LY294002 (*LY*) or an equal volume of ethanol for 30 min as described under "Experimental Procedures." *A*, conditioned media were collected at 36 h and analyzed for MMP-9 activity by gelatin zymography. *B*, uPA activity was analyzed in the conditioned media at 24 h using a coupled colorimetric plasminogen activation assay. The results represent the mean ± S.E. of three different experiments. * significantly different from control with $p < 0.05$.

MAPK in pp126 cells via a mechanism involving the EGFR kinase, this signaling pathway does not modulate E-cadherin regulation of proteinase expression.

Inhibition of PI3-kinase Blocks E-cadherin-mediated Suppression of Proteinases—Formation of *de novo* E-cadherin-mediated cell-cell contact activates PI3-kinase (19–21, 31, 32, 39–41) and induces physical association of PI3-kinase with E-cadherin (see Refs. 19 and 21 and data not shown). To determine whether PI3-kinase activation may play a role in the E-cadherin regulation of proteinase expression, activation of PI3-kinase was assessed in pp126 cells following calcium-induced adherens junction assembly by evaluating activation (phosphorylation) of the downstream substrate AKT. Cells were lysed at various time points and samples analyzed by Western blotting using antibodies directed against total AKT or the phosphorylated (active) species. A time-dependent phosphorylation of AKT following E-cadherin activation was observed in pp126 cells (Fig. 6*A*, *upper panel*) with no change in total AKT protein (Fig. 6*A*, *lower panel*). AKT activation was blocked with the PI3-kinase inhibitor LY294002, demonstrating the involvement of the PI3-kinase-AKT pathway (Fig. 6*B*). To confirm that AKT activation resulted from E-cadherin engagement, junction assembly was initiated in the presence of the function-blocking anti-E-cadherin antibody or control IgG as described above. Inhibition of E-cadherin engagement decreased AKT activation (Fig. 6*C*), indicating that engagement of E-cadherin leads to PI3-kinase activation.

By using the inhibitor LY294002, the role of PI3-kinase in E-cadherin-mediated suppression of MMP-9 and uPA expression was evaluated. Cells were preincubated with EGTA and LY294002 (10 μM) or an equal amount of ethanol vehicle for 30 min before the addition of calcium-replete medium containing LY294002 or ethanol. Under control conditions when the adherens junctions were not disrupted with EGTA treatment (designated *E-cad Actn* −), LY294002 did not alter the relative MMP-9 levels or the net uPA activity (Fig. 7, *A*, *2nd lane*, and *B*). In EGTA-treated cells, calcium-induced engagement of E-cadherin decreased the relative MMP-9 levels and the net uPA activity, as demonstrated previously (Fig. 7, *A*, *3rd lane*, and *B*). However, concomitant treatment with LY294002 abrogated the E-cadherin-mediated proteinase suppression and restored the relative MMP-9 levels and the net uPA activity (Fig. 7, *A*, *4th lane*, and *B*), implicating PI3-kinase in E-cadherin-mediated proteinase regulation. Similar results were obtained with TIMP-1 and PAI-1 (data not shown).

PI3-Kinase Controls Integrity of Adherens Junctions in pp126 Cells—Recent data indicate that PI3-kinase can regulate either the assembly or maintenance of adherens junctions (21, 32). As both PI3-kinase inhibition (using LY294002) and prevention of E-cadherin junction formation (with blocking an-

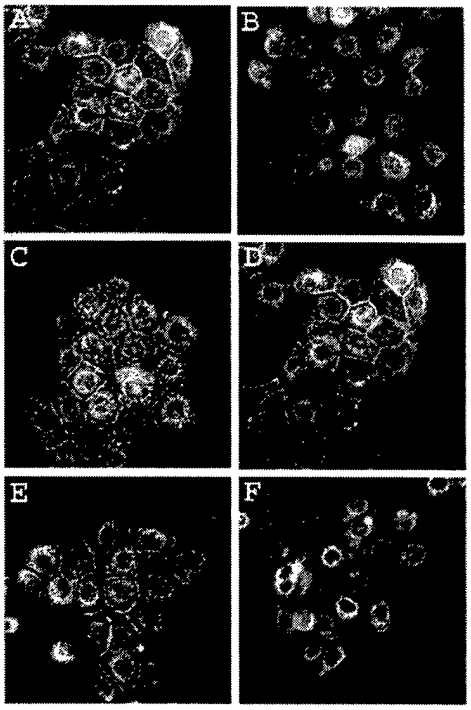

FIG. 8. **PI3-kinase controls the integrity of adherens junctions in pp126 cells.** Serum-starved pp126 cells were either left untreated (*A*) or treated with 4 mM EGTA for 30 min (*B–F*) containing either Me_2SO as control (*A–C*), 5 μM PD98059 (*D*), 250 nM AG1478 (*E*), or 10 μM LY294008 (*F*). The EGTA containing medium was then replaced with Keratinocyte-SFM (0.09 mM Ca^{2+}) containing Me_2SO or the corresponding inhibitor for 45 min. Cells were fixed, incubated with anti-E-cadherin antibody (HECD-1), and detected with Alexa Fluor 594-conjugated anti-mouse antibody.

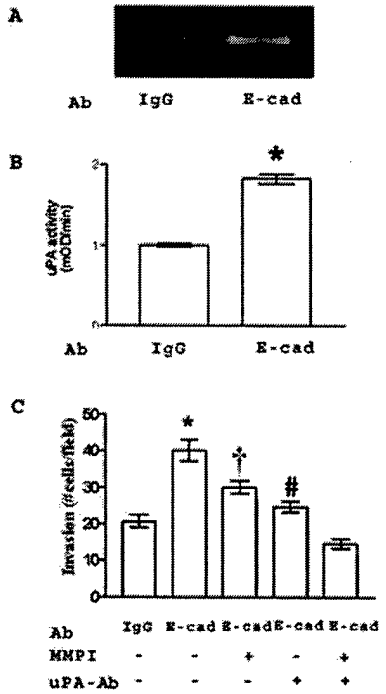

FIG. 9. **Disruption of cell-cell adhesion enhances pp126 cell invasion.** pp126 cells were plated with either control antibody (*Ab*) (*IgG*) or anti-E-cadherin antibody (HECD-1, designated *E-cad*). *A*, conditioned media were collected at 36 h and analyzed for MMP-9 activity by gelatin zymography. *B*, uPA activity was analyzed in the conditioned media at 24 h using a coupled colorimetric plasminogen activation assay. *, significantly different from control with $p < 0.001$. *C*, cells (2×10^5/500 μl) were added to porous polycarbonate filters (8-μm pore) coated with Matrigel (10 μg) in the presence 25 μg/ml of control antibody (*IgG*) or anti-E-cadherin antibody (HECD-1, designated *E-cad*) for 40 h. In wells containing E-cadherin antibody, either MMP inhibitor, GM6001 (2.5 μM), function-blocking uPA antibody (American Diagnostica number 394, 15 μg/ml), or both were added. Nonmigrating cells were removed from the upper chamber, and filters were fixed and stained, and invading cells were enumerated using an ocular micrometer. The results represent the mean ± S.E. of three different experiments. *, significantly different from IgG treated cells with $p < 0.001$. †, significantly different from E-cadherin antibody treated cells with $p < 0.05$. #, significantly different from E-cadherin antibody treated cells with $p < 0.01$.

tibodies) restored proteinase expression, these data suggest that PI3-kinase may participate in regulation of E-cadherin junctions in pp126 cells. To test this hypothesis, the effect of PI3-kinase inhibition (10 μM LY294002) on junction formation was evaluated. Control experiments included inhibitors of EGFR tyrosine kinase (250 nM AG1478) or MEK (5 μM PD98059). Cells were pre-incubated with EGTA in the presence of inhibitor or Me_2SO vehicle for 30 min before the addition of calcium-replete medium containing the specific inhibitor or Me_2SO. After 45 min, cells were processed for immunofluorescence microscopy using anti-E-cadherin antibody. Control cells present a typical pattern of E-cadherin staining at the level of cell-cell contacts (Fig. 8*A*). After 30 min of treatment with EGTA, E-cadherin was absent from sites of cell-cell contact (Fig. 8*B*). Following calcium addition, E-cadherin-mediated adherens junctions were again formed at 45 min (Fig. 8*C*). Similar results were observed in cells treated with PD98059 or AG1478 (Fig. 8, *D* and *E*). In contrast, cells treated with LY294002 showed significantly reduced E-cadherin staining at sites of cell-cell contact (Fig. 8*F*), indicating that PI3-kinase participates in the formation of *de novo* E-cadherin-mediated adherens junctions in pp126 cells.

Prevention of Cell-Cell Adhesion Enhances pp126 Cell Invasion—To assess the functional consequences of E-cadherin-regulated proteinase expression, the impact of preventing cell-cell adhesion on cellular invasive activity was evaluated. pp126 cells were seeded into Boyden chambers overlaid with Matrigel to provide a three-dimensional, protein-rich barrier to invasion in the presence of E-cadherin blocking antibody (HECD-1) or control IgG. Prevention of *de novo* E-cadherin cell-cell contacts resulted in an increase in the relative MMP-9 levels and the net uPA activity (Fig. 9, *A* and *B*). Concomitant with enhanced proteinase expression, inhibition of junction formation significantly increased Matrigel invasion (Fig. 9*C*). The enhanced invasive activity was partially blocked with either a broad spectrum MMP inhibitor (2.5 μM GM6001) or by a function-blocking anti-uPA antibody (15 μg/ml) and was completely abrogated by a mixture of the two inhibitors (Fig. 9*C*), implicating both MMP-9 and uPA in Matrigel invasion by pp126 cells. These data demonstrate that the proteinase up-regulation resulting from inhibition of E-cadherin engagement can promote cellular invasive behavior.

DISCUSSION

Studies using multiple cancer models have demonstrated that loss of E-cadherin-mediated adherens junctions leads to increased invasion and metastases (22, 23, 27, 35, 42). Additional data suggest a correlation between E-cadherin status and proteinase levels. For example, down-regulation of E-cadherin increased MMP-9 secretion in murine skin carcinoma cell lines (43), whereas overexpression of E-cadherin decreased MMP-2 activity in prostate cancer cells (26) and MT1-MMP in squamous cancer cells (44). However a mechanistic examina-

tion of the potential functional link between cell-cell adhesion and proteolysis has not been reported. Our current data demonstrate that E-cadherin plays a direct role in proteinase regulation in premalignant oral keratinocytes. Initiation of *de novo* E-cadherin-mediated cell-cell junctions resulted in suppression of MMP-9 and uPA expression. Conversely, prevention of junction formation enhanced proteinase expression and consequent cellular invasive behavior, suggesting a biochemical mechanism by which down-regulation of E-cadherin may promote metastasis.

The detailed signal transduction pathway through which E-cadherin regulates proteinase gene expression is unknown. However, our data support a role for PI3-kinase activity in the E-cadherin-mediated suppression of MMP-9 and uPA expression. Formation of *de novo* E-cadherin junctions activates PI3-kinase (Fig. 6) (19–21, 31, 32, 39–41) and leads to the physical association of PI3-kinase with E-cadherin (see Refs. 19 and 21 and data not shown). Activation of PI3-kinase recruits the GTP exchange factor Tiam-1 to the adherens junctions, resulting in activation of Rac-GTPase (45). In keratinocytes, Rac-GTPases play an important role in forming and stabilizing adherens junctions by recruiting F-actin to these junctions (46, 47). Supporting this model, inhibition of PI3-kinase blocks the recruitment of F-actin to sites of cell-cell contact in intestinal epithelial cells (21) and destabilizes adherens junctions in mammary epithelial cells (48). Moreover, additional data indicate that PI3-kinase may participate in maturation and maintenance of cadherin-based adhesions (32, 40), in part via regulation of productive adhesive contact formation following initial homophilic ligation (32). Our current data support the hypothesis that PI3-kinase activity also functions to regulate formation of adherens junctions in pp126 cells. Thus, inhibition of PI3-kinase activity with LY294002 destabilizes junctions, thereby abrogating the suppressive effect of E-cadherin engagement on proteinase expression.

In addition to activation of PI3-kinase, E-cadherin engagement has also been shown to enhance MAPK activity through the recruitment and activation of EGFR (20). A similar effect was observed in the current study, wherein junction formation induced maximal MAPK activation in pp126 cells at 15 min. MAPK activation was completely abrogated with the EGFR kinase inhibitor AG1478, implicating EGFR signaling in MAPK activation. However, inhibition of MEK (with PD98059) or EGFR kinase (with AG1478) was insufficient to restore proteinase expression, suggesting that E-cadherin-mediated proteinase regulation does not involve EGFR-initiated MAPK signaling. Furthermore, inhibition of MEK and EGFR kinase activity at the time of calcium switch did not prevent adherens junction re-formation in pp126 cells. It should be noted, however, that the MAPK pathway is important in both growth factor-induced secretion of MMP-9 in carcinoma cells (49) and in integrin-mediated up-regulation of uPA in pp126 cells (30). These data support the hypothesis that the signaling pathways that regulate formation of adherens junctions (PI3-kinase) may also regulate cadherin-mediated suppression of proteinases. This effect may be, in part, due to sequestration of β-catenin at cell-cell junctions as part of E-cadherin-catenin complex (50, 51). β-catenin can translocate to the nucleus and form a complex with proteins of the T cell factor/lymphoid-enhancer factor family (52). T cell factor/lymphoid-enhancer factor proteins act as transcription factors and have been shown to activate genes that are important in cancer progression including MMP-7, MMP-26, and uPAR (50, 51, 53–58). A number of other MMP promoters, including MMP-9, have T cell factor 4-binding sites and, consequently, may be regulated by β-catenin (54, 57). Although we have not formally addressed the potential contribution of β-catenin signaling, no change in uPAR expression was observed following E-cadherin activation in our system, suggesting that additional mechanisms of proteinase regulation are engaged. Thus, it is interesting to speculate that net extracellular proteinase activity may result from a balance between signaling pathways differentially activated by engagement of cell-cell *versus* cell-matrix adhesion molecules.

In addition to enhanced proteinase expression (uPA, MMP-9) induced by E-cadherin disruption, a coordinate increase in the corresponding inhibitors (PAI-1, TIMP-1) was also observed. Although a coordinate regulation of uPA and PAI-1 is apparent, a *net* increase in uPA activity is obtained following E-cadherin disruption, and this functionally contributes to the increased Matrigel invasion. Similarly, the Matrigel invasion data also suggest that a net increase in MMP-9 activity is also likely. It has been shown previously (24) in T47D and MCF-7 breast cancer cells that disruption of cell junctions with anti-E-cadherin antibodies increases uPA expression and collagen invasion. The enhanced collagen invasion was partially blocked using anti-catalytic uPA antibodies; however, the effect of MMP inhibitors was not evaluated (24). The current data demonstrate that Matrigel invasion by pp126 cells is dependent on both uPA and MMP-9, as inhibiting both proteinases simultaneously completely abrogated the increase in Matrigel invasion by pp126 cells.

Recent studies (36–38) have shown that proteinase expression may regulate cell-cell junction integrity by cleaving E-cadherin. Conversely, our data demonstrate that E-cadherin participates in proteinase regulation via a PI3-kinase-dependent mechanism, providing novel evidence for a bi-directional communication between proteinases and cadherins. As proteinases play a central role in a number of important cellular processes, these findings may provide a framework for a more detailed understanding of the mechanism by which E-cadherin-mediated cell-cell contacts regulate both normal epithelial cell behavior and the invasiveness of carcinoma cells.

REFERENCES

1. Werb, Z. (1997) *Cell* **91,** 439–442
2. Sternlicht, M. D., and Werb, Z. (2001) *Annu. Rev. Cell Dev. Biol.* **17,** 463–516
3. Ellis, V., and Murphy, G. (2001) *FEBS Lett.* **506,** 1–5
4. Westermarck, J., and Kahari, V. M. (1999) *FASEB J.* **13,** 781–792
5. Itoh, T., Tanioka, M., Matsuda, H., Nishimoto, H., Yoshioka, T., Suzuki, R., and Uehira, M. (1999) *Clin. Exp. Metastasis* **17,** 177–181
6. Murphy, G., and Gavrilovic, J. (1999) *Curr. Opin. Cell Biol.* **11,** 614–621
7. Nagase, H., and Woessner, J. F., Jr. (1999) *J. Biol. Chem.* **274,** 21491–21494
8. Vu, T. H., and Werb, Z. (2000) *Genes Dev.* **14,** 2123–2133
9. Andreasen, P. A., Kjoller, L., Christensen, L., and Duffy, M. J. (1997) *Int. J. Cancer* **72,** 1–22
10. Ghosh, S., Ellerbroek, S. M., Wu, Y., and Stack, M. S. (2000) *Fibrinolysis Proteolysis* **14,** 87–97
11. Parks, W. C., and Mecham, R. P. (1998) *Matrix Metalloproteinases*, Academic Press, San Diego
12. Vu, T. H., and Werb Z. (1998) in *Matrix Metalloproteinases* (Parks, W. C., and Mecham, R. P., eds) pp. 115–48, Academic Press, San Diego
13. Mignatti, P., and Rifkin, D. B. (2000) *Adv. Cancer Res.* **78,** 103–157
14. Yu, H. R., and Schultz, R. M. (1990) *Cancer Res.* **50,** 7623–7633
15. Kook, Y. H., Adamski, J., Zelent, A., and Ossowski, L. (1994) *EMBO J.* **13,** 3983–3991
16. Angst, B. D., Marcozzi, C., and Magee, A. I. (2001) *J. Cell Sci.* **114,** 629–641
17. Takeichi, M. (1991) *Science* **251,** 1451–1455
18. Provost, E., and Rimm, D. L. (1999) *Curr. Opin. Cell Biol.* **11,** 567–572
19. Pece, S., Chiariello, M., Murga, C., and Gutkind, J. S. (1999) *J. Biol. Chem.* **274,** 19347–19351
20. Pece, S., and Gutkind, J. S. (2000) *J. Biol. Chem.* **275,** 41227–41233
21. Laprise, P., Chailler, P., Houde, M., Beaulieu, J. F., Boucher, M. J., and Rivard, N. (2001) *J. Biol. Chem.* **276,** 21885–21894
22. Noe, V., Chastre, E., Bruyneel, E., Gespach, C., and Mareel, M. (1999) *Biochem. Soc. Symp.* **65,** 43–62
23. Van Aken, E., De Wever, O., Correia da Rocha, A. S., and Mareel, M. (2001) *Virchows Arch.* **439,** 725–751
24. Frixen, U. H., and Nagamine, Y. (1993) *Cancer Res.* **53,** 3618–3623
25. Miyaki, M., Tanaka, K., Kikuchi-Yanoshita, R., Muraoka, M., Konishi, M., and Takeichi, M. (1995) *Oncogene* **11,** 2547–2552
26. Luo, J., Lubaroff, D. M., and Hendrix, M. J. (1999) *Cancer Res.* **59,** 3552–3556
27. Wijnhoven, B. P., Dinjens, W. N., and Pignatelli, M. (2000) *Br. J. Surg.* **87,** 992–1005
28. Stack, S., Gonzalez-Gronow, M., and Pizzo, S. V. (1990) *Biochemistry* **29,** 4966–4970

29. Oda, D., Bigler, L., Lee, P., and Blanton, R. (1996) *Exp. Cell Res.* **226,** 164–169
30. Ghosh, S., Brown, R., Jones, J. C., Ellerbroek, S. M., and Stack, M. S. (2000) *J. Biol. Chem.* **275,** 23869–23876
31. Kim, S. H., Li, Z., and Sacks, D. B. (2000) *J. Biol. Chem.* **275,** 36999–37005
32. Nakagawa, M., Fukata, M., Yamaga, M., Itoh, N., and Kaibuchi, K. (2001) *J. Cell Sci.* **114,** 1829–1838
33. Munshi, H. G., and Stack, M. S. (2002) *Methods Cell Biol.* **69,** 195–205
34. Laemmli, U. K. (1970) *Nature* **227,** 680–685
35. Frixen, U. H., Behrens, J., Sachs, M., Eberle, G., Voss, B., Warda, A., Lochner, D., and Birchmeier, W. (1991) *J. Cell Biol.* **113,** 173–185
36. Noe, V., Fingleton, B., Jacobs, K., Crawford, H. C., Vermeulen, S., Steelant, W., Bruyneel, E., Matrisian, L. M., and Mareel, M. (2001) *J. Cell Sci.* **114,** 111–118
37. Steinhusen, U., Weiske, J., Badock, V., Tauber, R., Bommert, K., and Huber, O. (2001) *J. Biol. Chem.* **276,** 4972–4980
38. Ryniers, F., Stove, C., Goethals, M., Brackenier, L., Noe, V., Bracke, M., Vandekerckhove, J., Mareel, M., and Bruyneel, E. (2002) *Biol. Chem.* **383,** 159–165
39. Li, G., Satyamoorthy, K., and Herlyn, M. (2001) *Cancer Res.* **61,** 3819–3825
40. Kovacs, E. M., Ali, R. G., McCormack, A. J., and Yap, A. S. (2002) *J. Biol. Chem.* **277,** 6708–6718
41. Shinohara, M., Kodama, A., Matozaki, T., Fukuhara, A., Tachibana, K., Nakanishi, H., and Takai, Y. (2001) *J. Biol. Chem.* **276,** 18941–18946
42. Schipper, J. H., Frixen, U. H., Behrens, J., Unger, A., Jahnke, K., and Birchmeier, W. (1991) *Cancer Res.* **51,** 6328–6337
43. Llorens, A., Rodrigo, I., Lopez-Barcons, L., Gonzalez-Garrigues, M., Lozano, E., Vinyals, A., Quintanilla, M., Cano, A., and Fabra, A. (1998) *Lab. Invest.* **78,** 1131–1142
44. Ara, T., Deyama, Y., Yoshimura, Y., Higashino, F., Shindoh, M., Matsumoto, A., and Fukuda, H. (2000) *Cancer Lett.* **157,** 115–121
45. Sander, E. E., van Delft, S., ten Klooster, J. P., Reid, T., van der Kammen, R. A., Michiels, F., and Collard, J. G. (1998) *J. Cell Biol.* **143,** 1385–1398
46. Braga, V. M., Machesky, L. M., Hall, A., and Hotchin, N. A. (1997) *J. Cell Biol.* **137,** 1421–1431
47. Braga, V. M., Del Maschio, A., Machesky, L., and Dejana, E. (1999) *Mol. Biol. Cell* **10,** 9–22
48. Somasiri, A., Wu, C., Ellchuk, T., Turley, S., and Roskelley, C. D. (2000) *Differentiation* **66,** 116–125
49. McCawley, L. J., Li, S., Wattenberg, E. V., and Hudson, L. G. (1999) *J. Biol. Chem.* **274,** 4347–4353
50. Barker, N., and Clevers, H. (2000) *Bioessays* **22,** 961–965
51. Huber, A. H., and Weis, W. I. (2001) *Cell* **105,** 391–402
52. Love, J. J., Li, X., Case, D. A., Giese, K., Grosschedl, R., and Wright, P. E. (1995) *Nature* **376,** 791–795
53. Wong, N. A., and Pignatelli, M. (2002) *Am. J. Pathol.* **160,** 389–401
54. Brabletz, T., Jung, A., Dag, S., Hlubek, F., and Kirchner, T. (1999) *Am. J. Pathol.* **155,** 1033–1038
55. Crawford, H. C., Fingleton, B., Gustavson, M. D., Kurpios, N., Wagenaar, R. A., Hassell, J. A., and Matrisian, L. M. (2001) *Mol. Cell. Biol.* **21,** 1370–1383
56. Crawford, H. C., Fingleton, B. M., Rudolph-Owen, L. A., Goss, K. J., Rubinfeld, B., Polakis, P., and Matrisian, L. M. (1999) *Oncogene* **18,** 2883–2891
57. Marchenko, G. N., Marchenko, N. D., Leng, J., and Strongin, A. Y. (2002) *Biochem. J.* **363,** 253–262
58. Mann, B., Gelos, M., Siedow, A., Hanski, M. L., Gratchev, A., Ilyas, M., Bodmer, W. F., Moyer, M. P., Riecken, E. O., Buhr, H. J., and Hanski, C. (1999) *Proc. Natl. Acad. Sci. U. S. A.* **96,** 1603–1608

Targeting Oestrogen to Kill the Cancer but not the Patient

Joan S. Lewis, Dong Cheng, and V. Craig Jordan

Robert H. Lurie Comprehensive Cancer Center
Feinberg School of Medicine
Northwestern University, Chicago 60611

Short Title: Estrogen Kills Cancer

Supported by: DOD Training Grant in Breast Neoplasia DAMD17-00-1-0386, Training Program in Signal Transduction T32 CA70085-06, SPORE in Breast Cancer P50 CA89018-03, Lynn Sage Breast Cancer Research Foundation and the Avon Foundation.

Contact Information: V. Craig Jordan, OBE, PhD, DSc, Robert H. Lurie Comprehensive Cancer Center, Northwestern University, Feinberg School of Medicine, 303 East Chicago Avenue, Olson Pavilion, Room 8258, Chicago, IL 60611 – vcjordan@northwestern.edu, 312.908.4148 (Telephone), 312.908.1372 (Fax)

Abstract

The link between sex steroids and the development and growth of breast cancer has proved to be an invaluable clue for advances in the prevention and treatment of breast cancer. The identification of the oestrogen receptor (ER) not only allowed advances in the molecular endocrinology of oestrogen action, but also provided a target for antioestrogenic therapeutic agents. However, the application of long-term or indefinite treatment regimens has consequences for the breast cancer. New forms of resistance, based upon enhanced cellular survival networks independent of ER and the suppression of apoptotic mechanisms, develop and then evolve. Remarkably, low concentrations of oestrogen collapse survival pathways and induce apoptosis in completely antihormonally refractory breast cancer. However, recurrent oestrogen stimulated disease is again sensitive to antihormonal therapy. The novel reapplication of the ER as a therapeutic target for apoptosis is emerging as a new strategy for the long-term targeted maintenance treatment of breast cancer and in formulating a targeted strategy for endocrine independent cancer.

There is an expanding clinical database that implicates oestrogen and progestins (hormone replacement therapy, HRT) in the development and growth of breast cancer. Evidence to support this conclusion comes from two major clinical sources: clinical studies of HRT, initially designed to determine the benefits of replacement approaches on postmenopausal women's health (Writing Group for the Women's Health Initiative Investigation, 2002; Million Women Study Collaborators, 2003) and the successful clinical strategy of treating breast cancer by blocking oestrogen action.

The use of HRT increased steadily throughout the 1990's primarily because there was epidemiological evidence (Grady *et al*, 1992) that hormone replacement could reduce the incidence of coronary heart disease (CHD), the major cause of death in postmenopausal women. Nevertheless, publication of a subset of the Women's Health Initiative demonstrated that of 8506 women taking HRT or 8102 women taking placebo for a mean of 5.2 years there was an absolute excess risk per 10,000 healthy person years of 7 more CHD events, 8 more strokes and 8 more pulmonary emboli (Writing Group for the Women's Health Initiative Investigation, 2002). HRT is not recommended for the primary prevention of CHD (Manson *et al*, 2003). Also surprising was an additional 23 cases of dementia per 10,000 women per year (Shumaker *et al,* 2003). Less surprising was the prospective confirmation of an increase in breast cancer associated with HRT (Cheblowski *et al*, 2003; Li *et al*, 2003).

The Million Woman Study provides powerful additional (Million Women Study Collaborators, 2003) information about the actual impact of HRT on the incidence of breast cancer. A total of 1,084,110 UK women aged 50-64 years were recruited to determine the association of HRT use with breast cancer incidence and death. It is

estimated that 10 years use of HRT produces 19 additional breast cancers per 1000 users. These data extrapolate to an estimated total of an excess of 15,000 breast cancers associated with HRT over the past decade in the UK.

In contrast to the effects of hormone replacement on the incidence of breast cancer, the use of either an antioestrogen, tamoxifen, to block the action of oestrogen in breast cancer (EBCTCG,1998) or an aromatase inhibitor, to prevent oestrogen synthesis in postmenopausal patients (ATAC Trialists' Group, 2002), is effective and considered to be the standard treatment strategy for breast cancer. Indeed, the concept of antioestrogenic interventions has been advanced with the reduction of risk from breast cancer by using tamoxifen (Cuzick *et al,* 2003) or raloxifene (Cummings *et al,* 1999), as well as suggestions for the evaluation of a number of aromatase inhibitors as chemopreventives in high risk postmenopausal populations.

To the casual observer, the clinical evidence appears to demonstrate that oestrogen is detrimental to women's health and especially implicated in breast cancer development and growth. However, there have been consequences to current antihormonal strategies and we will propose new concepts about antihormonal drug resistance in breast cancer which can be rapidly incorporated into the treatment plan. In otherwords, there are now opportunities to kill sensitized tumour cells with oestrogen and advance a new innovation in therapeutics.

Classical Concept of Tumour Targeting

The discovery of the ER as a critical component of the oestrogen signal transduction pathway in target tissues (Jensen and Jacobson, 1962) and the utilization of

this knowledge as a target for antihormonal therapy in breast cancer (Jensen and Jordan, 2003) improved the survival prospects for millions of breast cancer patients. However, the advance with antioestrogens occurred not only because of targeting the ER, to prevent oestrogen stimulated tumour growth, but also because of the application of the appropriate duration of treatment. During the 1970's, when tamoxifen was initially being evaluated as an adjuvant therapy in patients, laboratory studies demonstrated that longer durations of complete antihormonal therapy was likely to provide more benefit for patients than shorter durations of therapy (Lerner and Jordan,1990). At the time, the majority of clinical trials elected to use one year of therapy because there was a sincere concern that longer durations would enhance the possibility of premature drug resistance. Following the methodical evaluation of randomized clinical trials, conducted over the past 20 years, it is now clear that one year of adjuvant tamoxifen is only minimally effective but five years of tamoxifen produces an increase in disease-free and overall survival (EBCTCG, 1998). The use of long-term (5 years) adjuvant antihormone therapy is now standard for the treatment of breast cancer therapy.

Clinical trials of adjuvant tamoxifen therapy also provide an invaluable insight into the appropriate duration of an antihormone necessary to prevent primary breast cancer. The Oxford Overview of clinical trials (EBCTCG, 1998) demonstrated that one and two years of adjuvant tamoxifen produce only modest decreases in contralateral breast cancers but five years of adjuvant tamoxifen reduces contralateral breast cancer by 50%. These data are consistent with the findings of the NSABP P-1 trial that 5 years of tamoxifen reduces the incidence of invasive and noninvasive breast cancer in high risk pre- and postmenopausal women by approximately 50% (Fisher *et al,* 1998). Currently

in the United States, appropriately selected high risk women can use a course of 5 years of tamoxifen to reduce their risk of breast cancer.

The treatment of breast cancer has changed dramatically during the past 15 years with patients now all receiving long-term antihormonal therapies whether it is tamoxifen (EBCTCG, 1998), aromatase inhibitors (ATAC Trialists' Group, 2002), or LHRH superagonists plus tamoxifen (Emens and Davidson, 2003). However, the intense laboratory study of nonsteroidal antioestrogens led to the recognition of selective oestrogen receptor modulation (SERM) (Jordan, 2001) and the idea that SERMs could be used to treat and prevent osteoporosis but prevent breast cancer as a beneficial side effect (Lerner and Jordan, 1990). Raloxifene, a molecule related to tamoxifen, is used to treat and prevent osteoporosis with a reduction of breast cancer (Cumming *et al,* 1999). In the wake of the controversy surrounding the negative effects of HRT there are new opportunities to develop novel SERMs to address the prevention of osteoporosis, CHD and breast cancer. Raloxifene is currently being evaluated for the prevention of breast cancer and CHD in high risk postmenopausal women, so it could become the first multifunctional medicine.

Despite the fact that SERMs introduce a new dimension into therapeutics for the prevention of osteoporosis and CHD, the question of unlimited treatment durations with SERMs will have consequences for the national history of breast cancer. Early reductions in the incidence of ER positive disease (Fisher *et al,* 1998; Cumming *et al,* 1999) will potentially result in SERM resistant breast cancers thereby confronting the oncologist with unanticipated and complex treatment decisions in an increasing proportion of women. However, laboratory studies have established a new understanding

of SERM resistance that could potentially convert breast cancer from an acute to a chronic, controllable disease.

Changes in the Understanding of Antihormone Resistance

During the past twenty years there has been an important change in the understanding of drug resistance to the antioestrogen tamoxifen. In the early 1980's, tamoxifen was anticipated to be effective in ER positive breast cancers but ineffective in ER negative disease. Resistance to tamoxifen would develop because the ER positive tumour cells would be controlled but eventually these would be overwhelmed by the outgrowth of ER negative breast cancer cells (Fig. 1A). However, this model was not consistent with the known clinical observation that select patients with metastatic breast cancer could be maintained on successive endocrine therapies for prolonged periods.

It is now clear that there are two types of drug resistance to tamoxifen: intrinsic resistance, where the tumor is either ER negative or ER positive with enhanced survival pathways (HER2/neu plus a coactivator molecule AIB1) (Osborne *et al,* 2003) and acquired resistance where an ER positive tumour that initially responds to treatment now becomes tamoxifen-stimulated and grows in response to either tamoxifen or oestrogen. The laboratory description of acquired resistance forms the scientific basis for the understanding of current therapeutic interventions with aromatase inhibitors or fulvestrant as second line agents following the development of clinical resistance to tamoxifen. Aromatase inhibitors block oestrogen synthesis and fulvestrant destroys the ER to prevent the growth of breast cancers with acquired tamoxifen resistance. However,

despite the remarkable investment in a broad range of antihormonal therapies, the actual advance in improved survival and reduced side effects has been modest.

The successful control of breast cancer with antihormonal therapy requires years of successive treatments. An obstacle to progress in therapeutics is a clear understanding of the changes that occur in the breast cancer cell as a consequence of exhaustive antihormonal therapies. It is presumed that the cancer cell must create a sophisticated survival network and suppress the natural process of apoptosis to subvert the continuous inhibitory signal through the ER. Until recently, no laboratory models replicated the former clinical scenario, but the deficiencies in our knowledge have now been corrected.

Drug resistance to tamoxifen evolves through three phases: Phase I and II both require tamoxifen, or a related SERM (O'Regan *et al,* 2002), to maintain growth but in Phase III the ER positive tumor is refractory to all antihormonal therapies and growth is SERM independent (Jordan *et al.*, 2003).

Remarkably, the response of the breast tumor to oestrogen during the evolution of drug resistance changes dramatically from initially being growth stimulatory to becoming completely inhibitory after five years of antihormonal therapy. Apoptosis is initiated in response to minute concentrations of oestradiol which results in dramatic tumour regression in heterotransplanted athymic mice. When this phenomenon was first noted and reported in the early 1990s (Wolf and Jordan, 1993), it was suggested that a woman's own oestrogen actually destroyed the micrometastases that were presensitized by five years of tamoxifen treatment. In otherwords, stopping tamoxifen at a critical time (five years) was responsible for the long-term survival statistics. While the concept may have some veracity, the knowledge that minute concentrations of oestrogen can have a

dramatic effect on tumour cell death could have important clinical implications for treatment. Indeed, a clear understanding of the mechanism of Phase II and III resistance is becoming increasingly important for the treatment of metastatic breast cancer.

The current focus on exhaustive antiendocrine therapy may in fact be disadvantageous for patients. The antitumour action of oestrogen in Phase II tamoxifen resistance can paradoxically be reversed by fulvestrant (Osipo *et al,* 2003). In otherwords, oestradiol causes rapid tumor regression, fulvestrant causes tumourstasis but a combination of oestradiol and fulvestrant causes robust tumour growth. If Phase II or III drug resistance to tamoxifen can be shown to occur in patients, then an oestrogen rich environment would subvert the actions of fulvestrant. Obviously one could enhance the probability of a response to fulvestrant by administering an aromatase inhibitor but perhaps oestrogen should be pursued as a targeted alternative. To advance this idea it would be valuable to examine whether the observations in the laboratory with the evolution of tamoxifen drug resistance apply to other SERMs and to breast cancer cells that have adapted to oestrogen deprivation i.e.: as an expression of resistance to aromatase inhibitors.

Expansion of the Concept of Oestrogen-induced Apoptosis

Song and coworkers (Song *et al,* 2001) were the first to demonstrate that oestradiol causes apoptosis in breast cancer cells that have been adapted to grow in an oestrogen-free environment for prolonged periods. These investigators suggested that their data provided an explanation for the effectiveness of high dose diethylstilboestrol formally used to treat breast cancer in elderly postmenopausal women i.e.: women who

were 10-25 years after menopause. Thus a switch occurs in the cancer cell from oestrogen stimulated growth but following prolonged oestrogen deprivation cell death occurs in response to oestrogen. However and perhaps more importantly, the apoptotic effect occurs with low concentrations of oestradiol. We illustrate the principle in Figure 2B by comparing and contrasting the action of oestradiol in wild type breast cancer cells and an ER positive progesterone receptor negative, oestrogen-deprived clone referred to as MCF-7 5C (Jiang *et al,* 1992). Of interest is the observation that alterations in the media can enhance the actions of oestradiol as an apoptotic agent. Clearly, this is an area of research activity worthy of pursuit as the proposed therapeutic use of long-term aromatase inhibition can potentially reconfigure the cellular response to oestrogen.

The other relevant clinical scenario is the response of occult breast cancer cells to indefinite raloxifene administration for the treatment and prevention of osteoporosis. Long-term culture of breast cancer cells in 1μM raloxifene results in adaptation of cell survival mechanisms and raloxifene resistance. Transplantation of cells into athymic mice demonstrates Phase II SERM resistance; tamoxifen or raloxifene stimulates growth, no treatment (no ER binding ligand) results in no growth, but oestradiol causes apoptosis and rapid tumour regression (Liu *et al,* 2003). Thus a general principle is emerging that merits investigation in the laboratory to discover mechanisms that could be targeted and amplified.

Molecular Mechanisms

The target site specific actions of SERMs is not well understood but there is an emerging understanding of the modulation of the SERM ER complex in breast cancer

(Figure3). Antioestrogenic action appears to be dominant in a cancer cell with no cell surface signaling and the SERM ER complex binds preferentially to corepressor molecules to prevent gene activation and cell replication (Figure 3A). In contrast, the oestrogen-like actions of a SERM become dominant in acquired resistance when cells are selected with enhanced cell surface signaling, reduced corepressors but increased coactivator molecules (Figure 3B). This molecular mechanism could serve as a working model for Phase I drug resistance. It is plausible that the subsequent evolution of drug resistance into Phase II results from an enhanced sophistication in establishing survival pathways during continuing selection in an oestrogen deprived environment. Ultimately, the ER appears to become redundant for growth in Phase III drug resistance (Jordan *et al.*, 2003). However, it is the remarkable switch from oestrogen-stimulated growth in breast cancer to oestrogen-stimulated death that merits investigation. Song and coworkers (Song *et al*, 2001) first focused attention on the fas, fas ligand pathway as a potential mechanism of oestrogen-induced apoptosis in oestrogen deprived breast cancer cells. Study of molecular mechanisms for oestrogen-induced tumor regression have recently been extended with the demonstration that oestrogen simultaneously collapses survival mechanisms (HER2/neu NFκB) in the Phase II SERM resistant tumour and enhances the expression of the fas receptor (Osipo *et al.,* 2003; Liu *et al.*, 2003) (Figure 3C,D). Clearly, much needs to be done to understand the new molecular endocrinology of oestrogen action but the knowledge now creates opportunities for novel applications in therapeutics.

Clinical Correlations

Current clinical practice is focused on the premise that oestrogen is the principal growth stimulator in select ER positive breast cancers. The application of this principle over the past 30 years has been at the forefront of targeted therapeutics and has undoubtedly saved lives. However, clinical clues are emerging that the practice of exhaustive antihormonal therapy is not always appropriate, and useful palliation can occur with an application of the obsolete modality of pharmacological oestrogen treatment (diethylstilboestrol, 5 mg three times a day). Renewed interest in re-treating endocrine refractory disease with high dose oestrogen has demonstrated improvement in the anecdotal patient (Ingle *et al.,* 2002) and remarkable responses in metastatic breast cancer patients treated exhaustively with antihormonal therapies (Lonning *et al.*, 2001). Out of 32 evaluable patients, four had complete response, six had partial response and two had stable disease. These encouraging data require confirmation, before any change in medical practice can be recommended, but for the individual patient with completely refractory disease the potential for palliation is clear. More importantly, there is now a renewed conversation between the laboratory and the clinic that offers opportunities not only to enhance the duration of responses based on retargeting the ER, but also to improve the proportion of response rates based on an enhanced understanding of the survival and death pathways that could potentially be manipulated.

Opportunities for Targeting Oestrogen to the Tumour

Professor Paul Erlich established the foundation for targeted therapeutics by describing the successful process for treating infectious disease. An effective treatment is based on selective toxicity to destroy the disease and not the patient. To achieve that

goal, an appropriate laboratory model for the disease in question should be used to identify active synthetic molecules that will selectively destroy the disease *in vivo* under laboratory conditions. The successful chemotherapeutic candidate can subsequently be evaluated in clinical trials to establish "real world" efficacy and selectivity. The process has been remarkably successful during the past Century with the development of a diverse range of antibacterial agents and drugs to either prevent or palliate parasitic disorders. Unfortunately, the realization of the goal of targeting cancer selectively has, until recent times, remained elusive. Not that there has not been a sincere attempt to achieve the goal. One hundred years ago, Professor Paul Erhlich was the first to apply the principles of chemotherapeutic drug discovery to cancer cures. His approach was not successful. He declared, "I have wasted 15 years of my live in experimental cancer research", the year before he died on 20th August 1915.

What has become increasingly clear is that establishing target site specificity is not simple, especially in cancer, and that for the application of the Erhlich method in general, there are consequences of launching an attack that is not complete – drug resistance. The success in targeting breast cancer initially developed slowly by the reinvention and retargeting of existing molecules that had not succeeded in their primary applications. Tamoxifen, discovered in a fertility control program, was reinvented as a breast cancer drug and subsequently targeted to the ER (Jordan, 2003). Raloxifene, discovered in a breast cancer program and targeted to the ER, was reinvented as a preventive for osteoporosis with breast and uterine safety. After thirty years of clinical usage, the ubiquitous application of SERMs has now provided clues to progress by retargeting the ER with oestrogen in SERM resistant disease. However, rather than

returning to the therapeutic modality of the 1960's by reintroducing high dose oestrogen therapy for a few select patients, the new knowledge emerging from the laboratory now creates novel scientific and clinical opportunities to target the ER and extend response rates, cycle antihormonal therapies, enhance response rates and determine the precise molecular mechanism of ER mediated apoptosis so the knowledge could potentially be exported to kill ER negative tumour cells.

There are at least two dimensions to consider when applying the targeted action of oestrogen to the tumour: the nature of the oestrogen ER complex and the length of time that oestrogen must be administered to initiate the apoptotic cascade. The ER can bind an enormous range of ligands with diverse shapes and structures. To date, laboratory and clinical studies of ER mediated apoptosis have only used either oestradiol or DES. However, recent studies of the molecular biology of oestrogen action have defined two classes of ER complex. This is because the shape of the ligand preprograms the actual external shape of the ER complex (Bentrem *et al.*, 2003). The planar oestrogens, oestradiol, DES and the phyto-oestrogens genistein and coumestrol are class I oestrogens that rely on helix 12 in the ligand binding domain to seal the oestrogen molecule into the hydrophobic pocket (Bentrem *et al.*, 2003). This causes activating function (AF) 2 to be triggered and synergise with AF-1 at the other end of the complex during the formation of a gene transcription complex. In contrast , a non-planar oestrogen such as an oestrogenic triphenylethylene or the metabolites of the insecticide methoxychlor bind in the ligand binding domain but prevent activation of AF-2. Helix 12 cannot seal the ligand in the hydrophobic pocket and the transcription complex occurs through the triple site interaction of AF-1, D351 and select acidic amino acids in helix 12 (Bentrem *et al.*,

2003). The comparative testing of a range of phytoestrogens and the active constituents of conjugated equine oestrogen, equilin and equilenin, for their activity as apoptotic agents in Phase II and III antihormone drug resistance will establish which types of oestrogen could be used in clinical studies.

An important laboratory observation is that the apoptic response of SERM resistant breast cancer occurs, not with pharmacologic doses of oestrogen but physiologic oestradiol in the postmenopausal range (Yao *et al*, 2000). The majority of SERM resistant tumours regress completely but the few that regress but regrow, are again completely responsive to tamoxifen that prevents oestradiol stimulated growth. Based on these laboratory findings, a clinical program to determine the value of short or extended conjugated equine oestrogen or high phytoestrogen containing diets could establish new standards of clinical care to extend, initially, the effectiveness of antihormonal therapies for metastatic breast cancer and, subsequently, the consideration of rotating adjuvant antihormones with an "oestrogen purge" to improve survival through extending the duration of disease free survival.

The next two challenges have the potential to expand the value of the developing knowledge on ER induced cellular apoptosis. Half of the ER positive tumours do not respond to antihormonal therapy, therefore, any strategy to target the ER in endocrine refractory tumours would ultimately double response rates in breast cancer. Endocrine refractory disease appears to have developed survival pathways that are independent of regulation by ER. One potential strategy could be to convert an endocrine nonresponsive tumour to become responsive to oestrogen induced apoptosis by blocking the survival pathways with the expanding list of tyrosine kinase inhibitors and antibodies that block

cell surface signaling. The goal would be to prevent cell survival, but then create a subcellular environment so that there is no choice but to induce apoptosis when the survival pathway is blocked. There would also be the possibility that the oestradiol ER complex could synergise with traditional inducers of apoptosis e.g. chemotherapy in cells paralysed with select cell survival inhibitors.

The ultimate goal of the basic research will be to identify the molecular mechanism that permits the oestradiol ER complex from switching from being a survival mechanism through replication to a death signal. How does the ER complex know when it must induce the death of an aberrant cell? Clues are already available since the expression of ectopic ER in ER negative cells prevents replication (Jiang and Jordan., 1992) so the next step will be to identify critical pathways in the ER negative cell that can convert inhibition of replication to the induction of apoptosis.

Conclusions

New knowledge about the ability of low concentrations of oestrogens to cause apoptosis in exhaustively treated breast tumour has the potential to advance targeted therapeutics not only in breast cancer but also in other cancers. The remarkable ability of the oestradiol ER complex, a natural signal transduction pathway, to discriminate between a growth and a death environment is unique. Application of the new knowledge has immediate relevance for the treatment of metastatic breast cancer and the eventual maintenance of breast cancer patients for decades using cycles of antihormones but with regular "oestrogen purges" to kill resistant cells, and subsequently reactivate antihormonal therapy. Most importantly, the new knowledge will establish a strategic

plan to integrate novel survival blockers into a logical treatment strategy and simultaneously utilize the emerging power of the "omics" technologies to identify specific targets for future apoptotic therapy.

References:

ATAC Trialists' Group. (2002) Anastrozole alone or in combination with tamoxifen versus tamoxifen alone for adjuvant treatment of postmenopausal women with early breast cancer: first results of the ATAC randomized trial. *Lancet* **359**:2131-39.

Bentrem, D., Fox, J.E., Pearce, S.T., Liu, H., Pappas, S., Kupfer, D., Zapf, J.W. & Jordan, V.C. (2003). Distinct moleular conformations of the estrogen receptor alpha complex exploited by environmental estrogens. *Cancer Res*, **(in press)**.

Chlebowski, R.T., Hendrix, S.L., Langer, R.D., Stefanick, M.L., Gass, M., Lane, D., Rodabough, R.J., Gilligan, M.A., Cyr, M.G., Thomson, C.A., Khandekar, J., Petrovitch, H. & McTiernan, A. (2003) Influence of estrogen plus progestin on breast cancer and mammography in healthy postmenopausal women. *JAMA* **289**:3243-53.

Cuzick, J., Powles, T., Veronesi, U., Forbes, J., Edwards, R., Ashley, S. & Boyle, P. (2003). Overview of the main outcomes in breast-cancer prevention trials. *Lancet*, **361,** 296-300.

Cummings, S.R., Eckert, S., Krueger, K.A., Grady, D., Powles, T.J., Cauley, J.A., Norton, L., Nickelsen, T., Bjarnason, N.H., Morrow, M., Lippman, M.E., Black, D., Glusman, J.E., Costa, A. & Jordan, V.C. (1999). The effect of raloxifene on risk of breast cancer in postmenopausal women: results from the MORE randomized trial. Multiple Outcomes of Raloxifene Evaluation. *JAMA*, **281,** 2189-97.

EBCTCG. (1998). Tamoxifen for early breast cancer: an overview of the randomised trials. *Lancet*, **351,** 1451-67.

Emens, L.A. & Davidson, N.E. (2003) Adjuvant hormonal therapy for premenopausal women with breast cancer. *Clinical Cancer Research* **9**:486s-94s.

Fisher, B., Costantino, J.P., Wickerham, D.L., Redmond, C.K., Kavanah, M., Cronin, W.M., Vogel, V., Robidoux, A., Dimitrov, N., Atkins, J., Daly, M., Wieand, S., Tan-Chiu, E., Ford, L. & Wolmark, N. (1998). Tamoxifen for prevention of breast cancer: report of the National Surgical Adjuvant Breast and Bowel Project P-1 Study. *J Natl Cancer Inst*, **90,** 1371-88.

Grady, D., Rubin, S.M., Petitti, D.B., Fox, C.S., Black, D., Ettinger, B., Ernster, V.L. & Cummings, S.R. (1992). Hormone therapy to prevent disease and prolong life in postmenopausal women. *Ann Intern Med*, **117,** 1016-37.

Ingle, J.N. (2002). Estrogen as therapy for breast cancer. *Breast Cancer Res*, **4,** 133-6.

Jensen, E.V. & Jacobson, H.I. (1962). Basic guides to the mechanism of estrogen action. *Recent Prog Horm Res*, **18,** 387-414.

Jensen, E.V. & Jordan, V.C. (2003). The estrogen receptor: a model for molecular medicine. The Dorothy P. Landon AACR Prize for Translational Research. *Clin Cancer Res*, **9,** 1980-1989.

Jiang, S.Y. & Jordan, V.C. (1992). Growth regulation of estrogen receptor-negative breast cancer cells transfected with complementary DNAs for estrogen receptor [see comments]. *J Natl Cancer Inst*, **84,** 580-91.

Jiang, S.Y., Wolf, D.M., Yingling, J.M., Chang, C. & Jordan, V.C. (1992). An estrogen receptor positive MCF-7 clone that is resistant to antiestrogens and estradiol. *Mol Cell Endocrinol*, **90,** 77-86.

Jordan, V.C. (2001). Selective estrogen receptor modulation: a personal perspective. *Cancer Res*, **61,** 5683-5687.

Jordan, V.C. (2003). Tamoxifen: a most unlikely pioneering medicine. *Nature Reviews Drug Discovery*, **2,** 205-213.

Jordan, V.C., Osipo, C., MacGregor Schafer, J., Cheng, D. & Liu, H. (2003). Changing role of the oestrogen receptor (ER) in the life and death of breast cancer. *The Breast*, **(in press).**

Kinsinger, L.S., Harris, R., Woolf, S.H., Sox, H.C. & Lohr, K.N. (2002) Chemoprevention of breast cancer: a summary of the evidence for the U.S. preventive services task force. *Annals of Internal Medicine* **137**: 59-69.

Lerner, L.J. & Jordan, V.C. (1990). The development of antiestrogens for the treatment of breast cancer: Eighth Cain Memorial Award Lecture. *Cancer Res*, **50,** 4177-4189.

Li, C.I., Malone, K.E., Porter, P.L., Weiss, N.S., Tang, M., Cushing-Haugen, K.L. & Daling, J.R. (2003) Relationship between long durations and different regimens of hormone therapy and risk of breast cancer. *JAMA* **289**:3254-3263.

Liu, H., Lee, E.-S., Gajdos, C., Pearce, S.T., Chen, B., Osipo, C., Loweth, J., McKian, K., De los Reyes, A., Wing, L. & Jordan, V.C. (2003). Apoptotic action of 17 beta-estradiol in raloxifene resistant MCF-7 cells *in vitro* and *in vivo*. *J Natl Cancer Inst*, (in press).

Lonning, P.E., Taylor, P.D., Anker, G., Iddon, J., Wie, L., Jorgensen, L.M., Mella, O. & Howell, A. (2001). High-dose estrogen treatment in postmenopausal breast cancer patients heavily exposed to endocrine therapy. *Breast Cancer Res Treat*, **67,** 111-6.

Manson, J.E., Hsia, J., Johnson, K.C., Rossouw, J.E., Assaf, A.R., Lasser, N.L., Trevisan, M., Black, H.R., Heckbert, S.R., Detrano, R., Strickland, O.L., Wong, N.D. Crouse, J.R., Stein, E. & Cushman, M. (2003) Estrogen plus progestin and the risk of coronary heart disease. *NEJM* **349**:523-34.

Million Women Study Collaborators. (2003) Breast cance and hormone-replacement therapy in the Million Women Study. *Lancet* **362**:419-427.

O'Regan, R.M., Gajdos, C., Dardes, R.C., De Los Reyes, A., Park, W., Rademaker, A.W. & Jordan, V.C. (2002). Effects of raloxifene after tamoxifen on breast and endometrial tumor growth in athymic mice. *J Natl Cancer Inst*, **94,** 274-83.

Osborne, C.K., Bardou, V., Hopp, T.A., Chamness, G.C., Hilsenbeck, S.G., Fuqua, S.A., Wong, J., Allred, D.C., Clark, G. & Schiff, R. (2003). Role of the estrogen receptor coactivator AIB1 (SRC3) and HER2/neu in tamoxifen resistance in breast cancer. *J Natl Cancer Inst*, **95,** 353-361.

Osipo, C., Gajdos, C., Liu, H., Chen, B. & Jordan, V.C. (2003). Paradoxical action of fulvestrant on estradiol-induced regression of tamoxifen-stimulated breast cancer. *J Natl Cancer Inst*, **in press**.

Shumaker, S.A., Legault, C., Rapp, S., Thal, L., Wallace, R.B., Ockene, J.K., Hendrix, S.L., Jones, B.N., Assaf, A.R., Jackson, R.D., Kotchen, J.M., Wassertheil-Smoller, S. & Wactawski-Wende, J. (2003) Estrogen plus progestin and the incidence of dementia and mild cognitive impairment in postmenopausal women. *JAMA* **289**:2651-62.

Song, R.X., Mor, G., Naftolin, F., McPherson, R.A., Song, J., Zhang, Z., Yue, W., Wang, J. & Santen, R.J. (2001). Effect of long-term estrogen deprivation on apoptotic responses of breast cancer cells to 17beta-estradiol. *J Natl Cancer Inst*, **93,** 1714-23.

Wolf, D.M. & Jordan, V.C. (1993). A laboratory model to explain the survival advantage observed in patients taking adjuvant tamoxifen therapy. *Recent Results Cancer Res*, **127,** 23-33.

Writing Group for the Women's Health Initiative Investigators. (2002) Risks and benefits of estrogen plus progestin in healthy postmenopausal women. *JAMA* **288**: 321-33.

Yao, K., Lee, E.S., Bentrem, D.J., England, G., Schafer, J.I., O'Regan, R.M. & Jordan, V.C. (2000). Antitumor action of physiological estradiol on tamoxifen-stimulated

breast tumors grown in athymic mice [In Process Citation]. *Clin Cancer Res*, **6,** 2028-36.

Figure Legends

Figure 1 The evolution of antihormonal resistance.

A. Twenty years ago, it was believe that oestrogen receptor positive (ER+) tumours would usually be expected to respond to oestrogen withdrawal of a selective (o)estrogen receptor modulator (SERM) such as tamoxifen but eventually resistance would occur because ER- cells would overgrow the tumour. **B.** Currently, it is recognized that SERMs cause the development of acquired resistance where both oestradiol (E_2) or a tamoxifen stimulate growth. These ER positive tumours respond a second time to an aromatase inhibitor that prevents oestrogen synthesis or fulvestrant that destroys the ER. **C.** Emerging laboratory and clinical evidence suggests that SERM resistance evolves from acquired resistance (Phase I) to Phase II where any SERM will maintain growth, whereas, unliganded ER does not provoke growth. However, oestrogen at physiological levels causes rapid apoptosis. In Phase III, tumours are completely resistant to all antihormonal therapies and grow spontaneously. Nevertheless, physiological concentrations of oestrogen causes rapid apoptosis.

Figure 2 Oestradiol inhibits the growth of MCF-7:5C cells and induces apoptosis. MCF-7:5C cells were cloned from wild-type MCF-7:WS8 cells following long-term growth (~ 1 year) in oestrogen-free RPMI medium containing 10% (v/v) dextran charcoal-stripped (DCC) fetal bovine serum (FBS), 2 MM glutamine, 100 units/ml penicillin-streptomycin, 6ng/ml bovine insulin, and 1X non=essential amino acids.

A. For DNA assays, MCF-7:5C cells were seeded into 12-well plates at a density of ~ 20,000 cells per well in RPMI medium. The cells were left for 24 h to acclimatize and then treated with 0.1, 1, or 10nM oestradiol (E_2) for a total of 6 days with the control cells receiving <0/1% ethanol vehicle. Cells were re-fed on days 3 and 5. Total DNA (μg)/well was used to measure cell growth. The data represent the average of five separate experiments. **B.** Apoptotic cells were identified/quantified by double staining with recombinant FITC-conjugated annexin V and propidium iodide (PI), using the Annexin V-FITC kit (Immunotech, Beckman Coulter). For experiments, MCF-7:WS8 and MCF-7:5C cells were seeded in 100mm plates at a density of 1×10^6 per plate in either oestrogen-free RPMI medium containing 10% DCC stripped fetal bovine serum (SFS) or MEM containing 5% DCC stripped calf serum (SCS). The cells were left for 24 h to acclimatize and then treated with either 1 nM E_2 or less that 0.1% ethanol vehicle (control) for 72 h. Data shown represent three separate experiments. It should be noted that oestradiol treatment of MCF-7:WS8 cells in oestrogen-free MEM media containing 5% SCS did not have any significant effect on apoptosis (data not shown).

Figure 3 The development of tamoxifen (TAM) resistant breast cancer and the changing role of oestradiol (E_2) in the life and death of oestrogen receptor (ER) positive cancer cells.

A. E_2 stimulated growth is inhibited by the use of an aromatase inhibitor to block oestrogen synthesis or TAM to block the ER and prevent oestrogen-stimulated gene transcription. Optimal antioestrogenic effects occur in the absence of preexisting cell surface signaling mechanisms. **B.** Prolonged use of TAM promotes an increase in HER2/neu cell surface signaling that creates a survival pathway phosphorylating the TAM ER complex and coactivator proteins. The transcription complex becomes activated to enhance gene activation and TAM stimulated growth. If this is Phase I resistance then oestrogen will also promote growth so an aromatase inhibitor is an appropriate second line therapy. If it is Phase II resistance, E_2 causes apoptosis. **C.** In Phase II tamoxifen resistance, the E_2 ER complex collapses the survival mechanisms by dramatically reducing the level of cell surface signaling by preventing HER2/neu mRNA transcription and the nuclear level of NFκB, a transcription factor. **D.** In Phase II tamoxifen resistance, the E_2 ER complex also enhances the synthesis of Fas receptor mRNA and protein which, in the presence of Fas ligand (FasL) activates caspase 8 and a cascade of events resulting in apoptosis.

CHEMOPREVENTION OF BREAST CANCER: LABORATORY PRINCIPLES

Joan S. Lewis and V. Craig Jordan

INTRODUCTION

Considerable progress has been made in understanding the mechanisms of breast tumor growth and progression. Application of effective treatment practices has resulted in significant decreases in morbidity and mortality.[1] Nevertheless, the National Cancer Institute (NCI) estimates that about 1 in 8 women in the United States (approximately 12.5 percent) will develop breast cancer during her lifetime. Excluding nonmelanoma skin cancers, breast cancer is the most common form of cancer among women in the United States and it accounts for up to one third of all new cases of women's cancer in North America.[2] The American Cancer Society has estimated that in 2002, about 203,500 new cases of breast cancer will be diagnosed among women in the United States and that ~ 40,000 women will die from the disease.[3] Breast cancer is the second leading cause of cancer death in women, exceeded only by lung cancer. On a global scale, it is estimated that breast cancer will affect five million women worldwide over the next decade, and the incidence of the disease is increasing on an average of about 1% per year in industrialized countries and at a greater rate in developing countries.[2,4,5] Clearly a strategy not only to treat but also to prevent breast cancer is required to control the disease.

Although the exact etiology of breast cancer is not known, the presence of a significant family history is considered the most important risk factor for developing the disease. However, only a minority (~10%) of women with breast cancer report such a history. Aggregate analyses suggest that a woman with a family history of breast cancer has between 1.5 and 2.5 times the risk of a woman without such a history.[6,7] Women with familial breast cancer have a higher probability of carrying a germline mutation in either the BRCA1 or the BRCA2 susceptibility genes. Germline mutations in BRCA1 and BRCA2 genes have been identified in 15-20% of women with a family history of breast cancer and 60-80% of women with a family history of

both breast and ovarian cancer.[8,9,10] The lifetime risk of breast cancer risk in women who carry a deleterious BRCA1 or BRCA2 mutation is estimated to be approximately 80%,[8,11,12] and in the ten-year period following a diagnosis of breast cancer, the risk of contralateral breast cancer is about 35%. Several studies indicate that BRCA1 and BRCA2 are involved in the repair of double-stranded DNA breaks and maintenance of chromosome integrity.[13] Because hereditary breast cancer typically occurs at an early age (between the ages of 40-45), it is recommended that prevention strategies be directed to women from their early twenties in order to minimize the burden of the disease.

Current strategies for reducing the risk of breast cancer in BRCA carriers include prophylactic mastectomy, oophorectomy, and chemoprevention. Bilateral risk-reducing mastectomy has been reported to be at least 90% effective in reducing breast cancer incidence and mortality in women with a family history of breast cancer, and this approach appears to be effective in women with BRCA mutations.[14] Despite its effectiveness, however, the acceptance of risk-reducing mastectomy has been modest, presumably because of the significant physical and psychological morbidity of the procedure. Another surgical option for BRCA-mutation carriers is oophorectomy. Oophorectomy was recently shown to reduce the risk of breast cancer in BRCA1-mutation carriers by 61%, however, this procedure did not significantly reduce the risk of BRCA2-mutation carriers.[15,16] Non-surgical options for the prevention of hereditary breast cancer are currently limited. Tamoxifen was shown in a case-control study to reduce the risk of new contralateral breast primaries in women taking the drug for their initial breast cancer diagnosis.[17,18] However, a subset analysis of the prospective Breast Cancer Prevention Trial, carried out in unaffected women at risk, failed to demonstrate a significant risk reduction in BRCA mutation carriers.[19] Additionally, selective estrogen receptor modulators such as

tamoxifen and raloxifene do not appear to reduce the incidence of estrogen receptor-negative tumors,[20,21] which BRCA1 heterozygotes, are at risk to develop. Until further data become available, the use of tamoxifen and similar drugs for the prevention of BRCA-associated breast cancer should be considered investigational.

Apart from a family history or genetic predisposition, there is a plethora of evidence which suggest that steroid hormones also play a major role in both the development and progression of breast cancer, with the risk of developing malignancies related to the cumulative exposure of the breast to endogenous and exogenous estrogens.[22-25] Early menarche, late menopause, and late age at birth of first child or nulliparity, have all been shown to increase the risk of breast cancer, while completion of a full-term pregnancy before the age of 24 years has been shown to effectively reduce the risk.[23,26-28] Exogenous estrogens, either from oral contraceptives or hormone replacement therapy (HRT), have also been shown to confer increased risks of breast cancer.[28] The estrogen dependency of breast cancer thus represents a unique feature of the disease that can be manipulated to effectively control growth and/or prevent tumor development, possibly through the use of chemopreventive agents. Unfortunately, the inability to predict precisely who will develop breast cancer (due to its complex etiologies) has required broad, population-based strategies to prevent the disease. A successful chemopreventive strategy must therefore be effective and acceptable (i.e. well tolerated with limited side-effects) to the majority of treated women who will not develop the disease. Over the past ten years, this goal has proven to be both difficult and controversial. This chapter provides a synthesis of laboratory principles and, where possible, translation into humans. Clinical results will illustrate the progress in the chemoprevention of breast cancer.

RATIONALE FOR CHEMOPREVENTION

Sporn and Newton[29] first defined chemoprevention as "prevention of cancer by the use of pharmacological agents (natural or synthetic) to inhibit or reverse the process of carcinogenesis". A fundamental issue that needs to be addressed in developing a strategy for breast cancer prevention, however, is understanding when or how carcinogenesis occurs. In laboratory models of mammary cancer, the timing of the carcinogenic insult is critical, and tumor development is influenced by the hormonal milieu. A series of experiments performed over 40 years in different strains of rats using different carcinogens have shown that mammary cancer can be induced only by carcinogen administration during the first few months of puberty (Fig. 1).[30-34] Unfortunately, the nature and timing of the carcinogenic insult in women are not known. Most of the current knowledge about carcinogenesis in the breast is based on small epidemiologic studies of known cancer-causing agents. Data from women exposed to radiation suggest a long period of promotion after initiation at a young age. Among survivors of the atomic bombings, the greatest increase in breast cancer incidence was seen in women exposed during their early teens. Breast cancer development in these women, however, did not occur at an early age.[35] Additional support for the concept of a long period of hormonal promotion after an early carcinogenic insult is found in the data for female infants undergoing thymic irradiation[36] and adolescent girls irradiated during fluoroscopy for tuberculosis.[37] In both groups, a significant increase in breast cancer incidence was observed. Hopefully, the characterization of specific genes responsible for the hereditary risk of common cancers will enable the development of clinical tests designed to identify at-risk individuals so that chemopreventive strategies can be implemented at an early stage. For the majority of women who lack germline mutations but have an elevated risk of

developing breast cancer, the strategy for an effective intervention with chemoprevention is much more complex.

STRATEGY TO PREVENT MAMMARY CANCER IN THE LABORATORY AND EXTRAPOLATION TO THE CLINIC

The observation that early oophorectomy retards the development of mammary cancer[38] prompted Lacassagne to suggest in 1936 that, because breast cancer appears to be due to a special hereditary sensitivity to estrogen, perhaps a therapeutic agent to inhibit estrogen accumulation could be found to prevent breast cancer.[39] Regrettably, no therapeutic inhibitor was available at that time, and all of Lacassagne's suggestions were based on the use of ablation endocrine surgery. Prior to its approval by the FDA in 1999 as a chemopreventive agent, tamoxifen was first examined in mouse and rat models of carcinogenesis to evaluate its chemopreventive potential. Studies[40,41] demonstrated that long-term treatment of tamoxifen, suppressed mammary tumorigenesis in virgin or once pregnant C3H/OUJ female mice, an effect that was consistently more effective than early ovariectomy, which only delayed tumorigenesis.

The administration of chemical carcinogens to sensitive strains of young female rats causes mammary tumorigenesis.[30] Unlike in mice, pregnancy or the administration of a suitable combination of progesterone and estrogen can prevent mammary carcinogenesis in rats if this occurs at the time of the carcinogenic insult or soon after.[42-44] However, later pregnancy or progesterone administration can reduce the latency of rat mammary carcinogenesis and increase the growth rate of some tumors.[45,46] As in mice, oophorectomy can interfere with the process of chemical carcinogenesis in rats[47] (Fig. 2). The earlier it is performed after the carcinogenic insult, the more effective is oophorectomy. Similarly, the administration of antiestrogens for different times around the time of carcinogen administration can alter carcinogenesis.[48,49] Short-

term (4 week) administration of tamoxifen a month after carcinogen administration not only delays carcinogenesis, but also reduces the number of mammary tumors produced.[50] In contrast, long-term treatment with low dosages of tamoxifen after the carcinogenic insult can almost completely prevent the development of mammary tumors.[51,52] These laboratory findings presaged and complemented studies with tamoxifen in the clinic on the duration of tamoxifen and the incidence of contralateral breast cancer. The longer the treatment between 1 and 5 years, the more effective tamoxifen was found to be.[53]

Overall, the animal model systems demonstrate that intervention soon after initiation of the carcinogenic insult is the most effective form of breast cancer prevention. In addition, changes in the hormonal milieu can affect the process of carcinogenesis, either by altering the receptivity of the epithelial tissue to carcinogens or by preventing the process of promotion to produce an invasive carcinoma.

Currently, four major clinical breast cancer prevention trials have reported on the efficacy of tamoxifen in reducing the incidence of ER-positive breast cancer in women at increased risk.[20,54-56] Results from the National Surgical Adjuvant Breast and Bowel Project (NSABP) P1 trial[20] showed that tamoxifen reduced the risk of invasive breast cancer by 49% and DCIS by 50% in high-risk women. The International Breast Cancer Intervention Study (IBIS) I trial closely replicated the findings of the NSABP P1 trial.[56] The overall reduction in the risk of developing breast cancer when comparing women taking tamoxifen with those taking placebo was 33%.[57] In the Italian Randomized Trial, tamoxifen was also shown to reduce the incidence of breast cancer in high-risk women; however, it did not have any significant protective effect in the low-risk group.[58] It should be noted that tamoxifen was only effective in reducing the incidence of breast cancer in women with ER-positive tumors, not ER-negative tumors. Clearly,

progress in chemoprevention has occurred, however, the current overall goal of chemoprevention is to advance further ideas from the laboratory to the clinic and improve efficacy and reduce the incidence of side effects.

TARGET PROBLEMS

Potential agents for breast cancer prevention must have a strong scientific basis for action and minimal toxicity. Ideally, a true preventive agent would block the carcinogenic insult in readily identifiable individuals and would have minimal side effects. Although this goal is not attainable at present, several broad approaches/strategies are being suggested.

Figure 3 illustrates a sequence of events that can be exploited in a prevention strategy. In general, an intervention must be given over a prolonged period to protect the individual from repeated carcinogenic insults. The agent could either prevent metabolic activation of the carcinogen or change the hormonal balance necessary for the epithelium to be receptive to the carcinogen. Estrogen is key to consolidating the carcinogenic insult through promotion of the transformed cell. At this stage, the dividing cell population is directly or indirectly sensitive to estrogen stimulation through the estrogen receptor. As tumorigenesis progresses, however, the genetic instability of the transformed cells results in a mixed population of receptor-positive and receptor-negative breast cancer cells. The presence or absence of these receptors in breast tumors determines their responsiveness to hormonal manipulations.[59] Based on this knowledge, a number of endocrine strategies (Fig. 4) have been proposed and studied in the laboratory or in clinical trials. The use of a contraceptive that could protect young women from pregnancy and breast cancer would be the most effective strategy because, based on all existing knowledge, it would be applied at the correct time during the process of tumorigenesis. Unfortunately, there are no examples of the successful use of a contraceptive strategy to reduce breast cancer risk.

Nevertheless, there are attempts to exploit the protective effects of pregnancy by studying hormonal variations.

PSEUDOPREGNANCY

Several studies have reported that nulliparous women have a higher risk (2-fold) of breast cancer compared with women who complete full-term pregnancies early in life (i.e. before the age of 20 years).[60,61] The protective effect of pregnancy is universal, and pregnancy is the only normal physiological condition that consistently prevents breast cancers among all ethnic groups worldwide.[60] The phenomenon of parity protection against mammary carcinogenesis is not species-specific and has been observed in rats and mice. For example, Moon[62] previously demonstrated that parous rats exposed to chemical carcinogens developed fewer cancers compared with virgin rats. Medina and Smith[63] have also demonstrated the protective effects of pregnancy against mammary carcinogenesis in mouse models. Furthermore, studies by Russo et al.[64] showed that short-term administration of the placental hormone human chorionic gonadotropins (hCG) either before or after treatment with the chemical carcinogen, 7,12-dimethylbenz[α]anthracene (DMBA), inhibited both the initiation and progression of mammary carcinogenesis in rats. At present, the mechanism by which parity protects against the development of mammary carcinogenesis is not known. It is suggested that this protective effect could result from the pregnancy-driven terminal differentiation of a subpopulation of target cells at increased risk for carcinogenesis, from the preferential loss of target cells during postlactational involution, or from a permanent endocrine change that indirectly decreases breast cancer risk by altering either the hormonal environment or the hormonal responsiveness of cells in the mammary gland.[65-69] To date, however, little evidence exists at the cellular or molecular level to support any of these hypotheses. Recently, D'Cruz et al.[70] reported using high-density

oligonucleotide microarrays to analyze the impact of early first full-term pregnancy on global gene expression profiles within the murine mammary gland. They found that parity resulted in the persistent down-regulation of multiple genes encoding growth factors, such as amphiregulin, pleiotrophin, and IGF-1, as well as the persistent up-regulation of the growth-inhibitory molecule, TGF-β3, and several of its transcriptional targets. Parity also resulted in a persistent increase in the differentiated state of the mammary gland as well as lifelong changes in the hematopoietic cell types resident within the gland. Clearly, knowledge about the early protective effects of hormonal changes on the breast tissue could serve as targets and be applied to select individuals to prevent breast cancer.

BUILDING ON THE LINK BETWEEN ESTROGEN AND AN INCREASE IN BREAST CANCER RISK

The application of laboratory knowledge with an antiestrogenic drug, tamoxifen, to prevent breast cancer in high risk women[20] is an important advance. However, despite the fact that tamoxifen has been investigated so thoroughly it was never designed for its current applications.[71] Current laboratory efforts seek to refine the results with tamoxifen by increasing effectiveness and decreasing side effects. Several approaches are being advanced. Firstly, the idea that estrogen itself might be a carcinogenic agent is being vigorously investigated. This is not to suggest that all estrogen must be removed from all women at an early age, but it is possible that some women have specific metabolic pathways that could enhance their susceptibility to estrogen. In other words, estrogen becomes a cause as well as a promoter of cancer. Secondly, agents that could be superior to tamoxifen are being evaluated in women at risk. It is clear that tamoxifen dramatically reduces the incidence of benign breast disease in premonopausal women compared to postmenopausal women[72] which perhaps illustrates the idea

that early intervention will be better than later interventions. Nevertheless, careful selection of postmenopausal women with high estrogen levels[73] could have a profound effect on the reduction of breast cancer incidence. The knowledge of selective estrogen receptor modulator or SERMs is a good current example of laboratory work that has extrapolated to the clinic.[74] New SERMs are currently being evaluated to prevent multiple diseases.[75]

ESTROGEN METABOLITES AS A CAUSE OF BREAST CANCER

Estrogens are known for their proliferative effects on estrogen-sensitive tissues resulting in tumorigenesis. Results of experiments in multiple laboratories over the last 20 years have shown that a large part of the cancer-inducing effect of estrogen involves the formation of active metabolites of estrogen, especially 16-alpha-hydroxyestrone (16α-OHE_1) and 4-hydroxyestradiol (4-OHE_2).[76-81] Other metabolites, such as 2-hydroxyestrone (2-OHE_1), 2-hydroxyestradiol (2-OHE_2), and 2-methoxyestradiol ($2ME_2$) are suggested to offer protection against the estrogen-agonist effects of 16α-OHE_1 and 4-OHE_2, due to their antagonistic effects in estrogen target tissues.[82-84] Indeed, alterations in estrogen metabolism in favor of increased 16α-hydroxylation have been reported in postmenopausal patients with breast cancer compared with healthy control subjects.[85] Enhanced 16α-hydroxylation has also been detected in healthy women at high risk for breast cancer.[86]

Several studies have reported that 16α-OHE_1 stimulates the growth of ER-positive MCF-7 breast cancer cells with potency similar to that of E_2.[87,88] There is also evidence that 16α-OHE_1 binds to and activates the ER.[89] 16α-OHE_1 treatments have also been shown to increase unscheduled DNA synthesis and anchorage-independent growth of mouse mammary epithelial cells in culture, thus suggesting possible genotoxicity for this metabolite.[90] In addition, animal studies have shown that in several different strains of mice with varying incidence of

spontaneous mammary tumors, the extent of 16α-hydroxylation is positively correlated with their mammary tumor incidence.[91] 16α-OHE_1, however, lacks substantial carcinogenicity in the estrogen-induced hamster kidney tumor model.[92] Similar to 16α-OHE_1, 4-OHE_2 is also capable of binding to and activating the ER.[93] 4-OHE_2 is hormonally active for stimulating uterine growth when injected into animals,[94] but its uterotropic potency is slightly weaker than that of E_2 and 16α-OHE_1.[81] Several studies have reported that 4-OHE_2 undergoes metabolic redox cycling to generate free radicals such as superoxide and the chemically reactive estrogen semiquinone/quinone intermediates.[92,95-97] These metabolic intermediates may damage DNA and other cellular constituents,[98] induce cell transformation and initiate tumorigenesis.[99,100] Indeed, 4-OHE_2 has been shown to be a strong carcinogen towards the hamster kidney (~100% tumor incidence).[101,102]

In contrast to the growth-stimulatory effects of 16α-OHE_1 and 4-OHE_2, the catecholestrogens, 2-OHE_1 and 2-OHE_2, exert anti-proliferative effects in ER-positive MCF-7 breast cancer cells. There is also evidence that suggest that 2-OHE_1 is capable of partially blocking E_2-induced growth stimulation.[103-105] 2-OHE_1 and 2-OHE_2 also have little or no tumorigenic activity toward the male Syrian hamster kidney.[101] Furthermore, some studies indicate that treatment of rodents with certain inducers of estradiol 2-hydroxylation (i.e. indole-3-carbinol) may actually decrease spontaneous tumorigenesis in estrogen-sensitive tissues.[106,107] Although the mechanism by which the 2-hydroxyestrogens inhibit growth *in vivo* is not known, one plausible explanation might be metabolic conversion to 2-methoxyestrogens. Several studies have reported that 2-methoxyestradiol (2-ME_2), the metabolic by-product of 2-hydroxyestradiol, is a potent inhibitor of tumor cell proliferation[104, 105] and angiogenesis.[82,108,109] 2-ME_2 is also capable of inhibiting the growth of transplanted meth-A sarcoma and B16 melanoma in C3H

mice,[108] and oral administration of this drug has been shown to inhibit the growth of an ER-negative human breast cancer cell line in immunodeficient mice.[82] Recently, 2-ME_2 was shown to inhibit the growth of MNU-induced rat mammary carcinoma at high doses, with minimal side effects.[110] These findings have led to the suggestion that 2-ME_2 might be a promising anticancer agent.[111,112] Currently, 2-ME_2 is in Phase I clinical trials for breast cancer and Phase II trials for prostate cancer and multiple myeloma.

Overall, these findings suggest that endogenous estradiol metabolites have the ability to stimulate and inhibit the growth of various tumors, and current clinical studies are in place to address the importance of estrogen metabolism to predict breast cancer risk. Alternatively, the detailed description of the physiology of the metabolites could be used to design new therapeutic agents.

SERMS

Selective ER modulators (SERMs) are an expanding class of structurally diverse drugs that bind to ERs.[71,74,75,113] SERMs can retain some of the positive effects of estrogen while preventing some of its adverse effects, namely the proliferative effects on reproductive tissues. Three clinically useful drugs that belong to the SERM drug class are tamoxifen (Nolvadex®), toremifene (Fareston®), and raloxifene (Evista®). Tamoxifen is currently available for risk reduction in pre- and post-menopausal women with an elevated risk of breast cancer.[20] Despite the beneficial effects of tamoxifen however, preclinical evidence indicate that this drug has genotoxic properties. Animal studies show that tamoxifen induces liver tumors in rats,[114,115] and initially the concern was raised that tamoxifen had the potential to induce hepatocellular carcinoma in women. Studies demonstrate, however, that the metabolic pathways necessary to produce DNA adducts are unique to the rat.[116] No DNA adducts have been noted in human liver

in patients receiving tamoxifen,[117] and no increase has been reported in hepatocellular carcinoma in patients taking tamoxifen.[20] Laboratory[118] and clinical data[20] also indicate that long-term use of tamoxifen increases the risk of secondary endometrial cancer and thromboembolic disease in postmenopausal women. Based on these findings it is clear that an alternative to tamoxifen is needed; preferably a drug that has all the benefits of tamoxifen but none of its side effects.

RATIONALE FOR RALOXIFENE

The knowledge that nonsteroidal antiestrogens had SERM actions, i.e. were estrogen-like in the bones and lowered cholesterol but were antiestrogenic in the breast raised the possibility that alternatives to tamoxifen could be found that would prevent osteoporosis and coronary heart disease in postmenopausal women in good health and prevent breast cancer as a beneficial side effect.[119] Based on existing laboratory data, the result is the introduction of raloxifene to treat and prevent osteoporosis but with breast and endometrial safety.

Raloxifene (originally known as LY156,758 or keoxifene) is an antiestrogen in the rodent uterus, and the compound has a high binding affinity for ER.[120] Unlike tamoxifen, raloxifene is much less estrogenic in the rat and mouse uterus,[120] and it shows antitumor activity to prevent rat mammary tumorigenesis.[52,121] Most importantly, like tamoxifen, raloxifene was demonstrated to maintain bone density in ovariectomized rats[122] which, following confirmation,[123] resulted in clinical trials which showed prevention of osteoporotic fractures,[124] reduction in cholesterol and homocysteine,[125,126] and in select patients reduction in coronary heart disease.[127]

Raloxifene is currently approved for the prevention of osteoporosis and is being tested for risk reduction in coronary heart disease in a prospective placebo-controlled clinical trial referred to as Raloxifene Use for the Heart (*RUTH*). Raloxifene is also being evaluated in the STAR (Study of Tamoxifen and Raloxifene) trial to compare its effectiveness with tamoxifen in

reducing the incidence of invasive breast cancer in postmenopausal women.[128] This trial was initiated based on the positive results obtained from the MORE trial in which raloxifene was shown to cause a 76% reduction in the incidence of ER-positive breast cancer in postmenopausal women with osteoporosis without the increased risk of endometrial cancer.[21,129]

In addition to tamoxifen and raloxifene (FIG. 5), several newer SERMs are currently being developed for the treatment of breast cancer and are potential agents for chemoprevention.[75] These include LY 353,381.HCL,[130,131] EM-652,[132] GW-5638,[133] and SP500263(FIG. 5).[134] Preclinical studies indicate that LY 353,381.HCl (arzoxifene) is a long-acting raloxifene analogue and it protects against bone loss and reduces serum cholesterol levels in ovariectomized rats.[135,136] Arzoxifene is also highly effective for prevention of mammary cancer induced in the rat by the carcinogen nitrosomethylurea and is significantly more potent than raloxifene in this regard.[137] Furthermore, arzoxifene is devoid of the uterotrophic effects of tamoxifen.[137] A similar finding was reported with EM-652, the active compound derived from the inactive precursor EM-800. Martel and coworkers[138] reported that EM-652 was as effective as raloxifene in preventing bone loss and reducing serum cholesterol in the ovariectomized rat without having any negative effects on the endometrium. The tamoxifen analogue, GW-5638, has also been shown to function as a full ER agonist in bone and the cardiovascular system in ovariectomized rats, with minimal uterotropic activity.[133] Lastly, SP500263 represents a novel SERM with a structure unrelated to other SERMs currently in clinical development. SP500263 was discovered in a screen using a small molecule compound library to identify estrogen agonists in bone.[134] This compound has high affinity for both ERs (ER-α and ER-β) but functionally acts through ER-α only.[134] Recently it was reported that SP500263 acts as an antiestrogen in MCF-7 *in vitro* proliferation assay and that it effectively reduces estrogen-

stimulated tumor growth in a murine breast cancer xenograft model.[139] The efficacy of SP500263 was comparable to tamoxifen and superior to raloxifene. Also, SP500263 lacks the ability to stimulate uterine wet weight in immature rats and adult OVX rats, and it prevents bone loss, however it does not have any cholesterol or triglyceride-lowering effects.[140] Despite the positive effects of these SERMs in preclinical studies, however, additional in vivo efficacy and safety studies are required to advance these SERMs as anticancer or preventive agents.

AROMATASE INHIBTORS

It is suggested that aromatase activity, by increasing local estrogen synthesis, may play an early role in breast cancer carcinogenesis.[141] Indeed, *in vivo* models have shown that aromatase expression in breast tissue can induce the development of premalignant lesions.[142] A major treatment strategy for breast cancer is directed at completely abolishing the effects of estrogen and its metabolites on the breast by using aromatase inhibitors.[143-145] Aromatase is the enzyme complex responsible for the final step in estrogen synthesis, via the conversion (in peripheral tissues) of the androgens androstenedione and testosterone to the estrogens estrone and estradiol. Aromatase inhibitors function by blocking the aromatase enzyme; which results in the depletion/reduction of estrogen and its metabolites in target tissues. The aromatase inhibitors such as anastrozole, letrozole, and vorozole are very potent suppressors of serum estradiol, with limited toxicities.[146,147] Prevention of tumor formation in carcinogen induced (i.e. MNU- and DMBA-induced rat mammary carcinomas) and spontaneous breast tumor animal bearing models (i.e. Sprague-Dawley rats) has been well demonstrated with aromatase inhibitors.[148-151] In these animal models, aromatase inhibitors were given either before or after carcinogen administration to determine their chemopreventive potential.

Several large randomized trials have compared the third-generation aromatase inhibitors to tamoxifen for first-line treatment of ER-positive metastatic breast cancer. Overall, these trials have demonstrated that the aromatase inhibitors have similar or slightly superior clinical efficacy as compared with tamoxifen.[152-154] On the basis of these trials, both letrozole and anastrozole have gained FDA approval for first-line treatment of metastatic breast cancer. In addition, many clinical trials are currently underway evaluating aromatase inhibitors in the adjuvant setting. The aim of these studies is to determine which hormonal therapy leads to the lowest rates of breast cancer recurrence and produces the most favorable side effect profile. Presently, only one trial comparing a third-generation aromatase inhibitor and tamoxifen in the adjuvant setting has been reported. Preliminary results[155] from the Anastrozole or Tamoxifen Alone or in Combination (ATAC) trial indicated that anastrozole was superior to tamoxifen regarding disease-free survival in the overall population and particularly in the receptor-positive subpopulation of patients, as well as in terms of reducing the incidence of contralateral breast cancer in the overall population. Patients receiving anastrozole also reported significantly lower incidence of hot flashes, vaginal bleeding, vaginal discharge, and venous thromboembolism and a significantly higher incidence of musculoskeletal symptoms and fractures than those receiving tamoxifen.[155,156] The IBIS group is also conducting a study of women with newly diagnosed ductal carcinoma *in situ* (DCIS), comparing tamoxifen alone and anastrozole alone, and also a study of placebo versus anastrozole alone in postmenopausal women. Currently, short-term chemoprevention trials of aromatase inhibitors in postmenopausal women are planned.[157]

Based on the clinical data, aromatase inhibitors appear to be superior in efficacy to tamoxifen both in terms of the treatment of breast cancer in the metastatic setting and in the preoperative neoadjuvant setting. This, combined with their lower toxicity profile (short-term),

makes these compounds very attractive as chemopreventives. Nevertheless, the long-term effects of aromatase inhibitors on osteoporosis, dementia, and cardiovascular disease must be carefully monitored in clinical studies (please see Chapter X of book chapter for further details about the clinical aspects of aromatase inhibitors).

RETINOIDS

Retinoids, the natural and synthetic derivatives of vitamin A (Fig. 6), have been extensively investigated for their effectiveness as both cancer chemopreventive and chemotherapeutic agents. These compounds have been shown to modulate a wide variety of cellular processes including proliferation, differentiation, malignant transformation and apoptosis.[158-160] Retinoids also act, pharmacologically, to restore regulation of differentiation and growth in certain premalignant and malignant cells *in vitro* and *in vivo*.[161] Numerous studies with various experimental animal models have subsequently shown that retinoids are highly effective in preventing a variety of epithelial cancers, including mammary cancer.[162-164] However, chronic treatment with retinoids is limited by side effects, such as mucocutaneous toxicity, hypertriglyceridemia, and teratogenicity.[165] By modifying the basic retinoid structure, analogs with reduced toxicity have been developed.

The synthetic amide of retinoic acid, fenretinide or N-(4-hydroxyphenyl)-retinamide, (4-HPR) (Fig. 6), was synthesized in the late 60s, and its biological activity was measured by Moon and coworkers,[166] who also showed the preferential accumulation of this drug in the breast instead of the liver. The inhibition of chemically-induced mammary carcinogenesis in rats by fenretinide was first described in 1979.[166] Since then, as a result of promising in vitro data and a favorable toxicity profile compared with other retinoids, fenretinide has been extensively studied in various clinical trials involving chemoprevention of cancers of the breast.[167] However, results

from a large controlled trial in which women with stage I breast cancer were randomized to fenretinide or placebo indicated that fenretinide did not significantly reduce the risk of contralateral breast cancers 5 years after follow-up, although there was some beneficial effects in premenopausal women.[168] The feasibility of tamoxifen and fenretinide combination chemoprevention is also under investigation. Tamoxifen and 4-HPR has been shown to be additive or synergistic in both the growth inhibition of the breast cancer cell line MCF-7,[169] and the prevention of *N*-methyl-*N*-nitrosourea-induced mammary carcinoma in the rat.[170,171] In human studies, the combination of tamoxifen and 4-HPR has been shown to be safe and well tolerated.[172] Overall, these findings suggest that the role of fenretinide in breast cancer prevention needs to be further elucidated.

There is also evidence that the retinoid X receptor-selective ligand LGD1069 (Fig. 6) has both chemotherapeutic and chemopreventive efficacy in the NMU-induced mammary carcinoma model.[173] In this animal model, LGD1069 eradicated primary tumors and prevented the appearance of additional new tumors. This compound showed superior efficacy to tamoxifen in both therapy and prevention. In addition, LGD1069 has been shown to be extremely well tolerated, with little or no traditional retinoid-associated toxicities in PhaseI/IIA human clinical cancer trials.[174] Recently, it was reported that LGD1069 effectively suppressed mammary tumorigenesis in C3(1)-SV40 Tag transgenic mice,[175] and ER-negative tumor development in MMTV-erbB2 transgenic mice with minimal toxicity.[176] Overall, these studies suggest that receptor-selective retinoids are promising chemopreventive agents and that they may be particularly useful in preventing ER-negative breast cancer. Currently, several selective retinoids and rexinoids are completing phase I and phase II studies and appear to be promising.[177]

PROGRESS IN CHEMOPREVENTION

Effective strategies for treatment and prevention currently involve the use of drugs that block estrogen action in the breast. The success of the antiestrogen tamoxifen as a treatment of breast cancer opened the door for the testing of this drug (in terms of its worthiness) to reduce breast cancer incidence in high-risk women and in postmenopausal women aged 60 and older. It is clear from reported clinical studies,[56,57] that tamoxifen is particularly effective in women with high risk. Despite its many benefits however, there are negative effects associated with long-term use of tamoxifen (i.e. endometrial cancer and thromboembolic disorders). The discovery of the SERM raloxifene, which functions as a potent antiestrogen in the breast but an ER agonist in the bone and cardiovascular system, with very little uterotropic activity, provides an alternative strategy to the targeted use of tamoxifen. Raloxifene is currently being tested as a breast cancer preventive in the STAR trial against tamoxifen. If raloxifene can be given long term, the prevention of breast cancers may be further advanced. Indeed, a newer generation of SERMs such as EM-652, LY 353,381.HCl, GW-5638, and SP500263 also has potential for chemoprevention.[71,75] The aromatase inhibitors appear to be superior in efficacy to tamoxifen both in terms of the treatment of breast cancer in the metastatic setting and in a preoperative neoadjuvant setting. Common toxicities and serious but rare adverse effects that are usually associated with long-term tamoxifen use appear to be of less concern with the aromatase inhibitors. At present however, full-scale randomized trials evaluating aromatase inhibitor use for primary breast cancer risk reduction are only starting so the improvements in chemoprevention are unknown. Nevertheless, it is important that the long-term effects of aromatase inhibitors on bone and lipid metabolism, cognitive function and other estrogen dependent organs are carefully evaluated. Despite these concerns however, it is more than likely

that aromatase inhibitors will be used not only to treat postmenopausal women with early onset disease but also in the chemopreventive setting in select postmenopausal women.

It should be noted that the benefit of tamoxifen in preventing breast cancer is only observed, at present, in ER-positive breast cancers. Hence, there is an urgent need for a chemopreventive agent for ER-negative tumors. Possible candidates include the non-steroidal anti-inflammatory agent, especially the COX-2 inhibitors[178] (Fig. 7). It has been shown that the selective COX-2 inhibitor, celecoxib, has growth inhibitory effects on breast cancer cell lines and induces regression of DMBA-induced mammary tumors in rats.[179] Celecoxib has also been shown to protect against HER-2/neu-induced breast cancer in MMTV-erbB2 transgenic mice.[180] COX-2 inhibitors are also capable of reducing the development of carcinogen-induced mammary tumors in several in vivo mouse models, a finding which substantiates their chemopreventive potential.[181,182] Currently, several phase I and phase II chemoprevention trials are planned to evaluate the COX-2 inhibitors in the context of breast cancer chemoprevention. Other promising agents for the prevention of ER-negative breast cancers include receptor tyrosine kinase (RTK) inhibitors or monoclonal antibodies.[183-185] Recently, the EGFR inhibitor ZD1839 (Iressa) has been reported to suppress the development of ER-negative mammary tumors in transgenic mice.[186] The epidermal growth factor receptor (EGFR) family serves as an excellent example for therapeutic targets based on studies of tumor formation. EGFR overexpression correlates inversely with ER status. Inhibition of EGFR function by either monoclonal antibodies (mAB) or small-molecule tyrosine kinase inhibitors (KI) (Fig. 7) has anti-tumor effects in breast carcinoma cell lines and many EGFR-specific compounds and monoclonal antibodies are currently in clinical trials. The second member of the EGFR family, ERBB2 (HER-2) is considered one of the most important oncogenes in invasive breast cancer. ERRB2 overexpression correlates with a

lack of response to endocrine therapy and chemotherapeutic agents. Based on the discovery of aberrant HER-2 overexpression in breast cancer, the monoclonal antibody against HER-2, trastuzumab, was developed (Fig. 7). Telomerase inhibitors,[187] isoflavonoids,[188] polyamine biosynthesis inhibitors (DFMO),[189,190] and 2-ME_2[108] are additional examples of potential chemoprevention agents (Fig. 7).

To summarize, we have highlighted the chemopreventive potential of several compounds and have identified some of the target population that would most likely benefit from clinical chemoprevention trials with these agents. However, the fundamental question still remains as to when chemical intervention should occur in the target population. It is known that genetic alterations and molecular changes occur during the multi-step carcinogenic process; hence, to achieve effective breast cancer chemoprevention development, it is extremely important to identify specific molecular abnormalities that can be monitored as biological endpoint biomarkers during specific pharmacological interventions. Currently, there are no validated substitute endpoint biomarkers for breast cancer in the context of chemoprevention trials with invasive cancer as the definitive end points; therefore, the development of intermediate biomarkers as surrogate endpoints for clinical chemoprevention trials for breast cancer is extremely important. Because of the shorter latency to intermediate biomarker end points and the smaller cohorts required for treatment, planning short term prevention trials and evaluating potential biomarkers in this setting is critical to the progress of chemoprevention. It is clear that the better selection of the target populations (i.e. high-risk women, BRCA mutation carriers; pre- or post-menopausal women, etc) that would most likely benefit from these intervention trials is an important consideration in any successful chemoprevention strategy.

REFERENCES

1. Jatoi I, Miller AB. Why is breast-cancer mortality declining? *Lancet Oncol* 2003; 4:251.

2. Landis SH, Murray T, Bolden S, Wingo PA. Cancer statistics. *CA Cancer J Clin* 1999;49:8.

3. Jemal A, Thomas A, Murray T, Thun M. Cancer statistics. *CA Cancer J Clin* 2002;52:23.

4. Mettlin C. Global breast cancer mortality statistics. *CA Cancer J Clin* 1999;49:138.

5. Edwards BK, Howe HL, Ries LA, Thun MJ, Rosenberg HM, Yancik R, et al. Annual report to the nation on the status of cancer, 1973-1999, featuring implications of age and aging on U.S. cancer burden. *Cancer* 2002;94:2766.

6. Narod SA. Modifiers of risk of hereditary breast and ovarian cancer. *Nat Rev Cancer* 2002;2:113.

7. Boucher KM, Kerber RA. Measures of familial aggregation as predictors of breast-cancer risk. *J Epidemiol Biostat* 2001;6:377.

8. Nathanson KL, Wooster R, Weber BL, Nathanson KN. Breast cancer genetics: what we know and what we need. *Nat Med* 2001;7:552.

9. Martin AM, Blackwood MA, Antin-Ozerkis D, Shih HA, Calzone K, Colligon TA, et al. Germline mutations in BRCA1 and BRCA2 in breast-ovarian families from a breast cancer risk evaluation clinic. *J Clin Oncol* 2001;19:2247.

10. Newman B, Austin MA, Lee M, King MC. Inheritance of human breast cancer: evidence for autosomal dominant transmission in high-risk families. *PNAS* 1988;85:3044.

11. Easton DF, Bishop DT, Ford GP, Crockford GP. Genetic linkage analysis in familial breast and ovarian cancer: results from 214 families. The Breast Cancer Linkage Consortium. *American Journal of Human Genetics* 1993;52:678.

12. Struewing JP, Hartge P, Wacholder S, Baker SM, Berlin M, McAdams M, et al. The risk of cancer associated with specific mutations of BRACA1 and BRCA2 among Ashkenazi Jews. *New England Journal of Medicine* 1997;336:1401.

13. Chen JJ, Silver D, Cantor S, Livingston DM, Scully R. BRCA1, BRCA2, and Rad51 operate in a common DNA damage response pathway. *Cancer Res* 1999;59 Suppl 7:S1752.

14. Hartmann LC, Sellers TA, Schaid DJ, Frank TS, Soderberg CL, Sitta DL, Frost MH, et al. Efficacy of bilateral prophylactic mastectomy in BRCA1 and BRCA2 gene mutation carriers. *J Natl Cancer Inst* 2001;93:1633.

15. Anderson WF, Brawley OW, Chang S. Oophorectomy in carriers of BRCA mutations. *N Engl J Med* 2002;347:1037.

16. Rebbeck TR, Lynch HT, Neuhausen SL, Narod SA, Van't Veer L, Garber JE, et al. Prophylactic oophorectomy in carriers of BRCA1 or BRCA2 mutations. *N Engl J Med.* 2002;346:1616.

17. Robson M. Tamoxifen for primary breast cancer prevention in BRCA heterozygotes. *Eur J Cancer* 2002;38 Suppl 6:S18.

18. Narod SA. Hormonal prevention of hereditary breast cancer. *Ann N Y Acad Sci* 2001;952:36.

19. King MC, Wieand S, Hale K, Lee M, Walsh T, Owens K, Tait J, Ford L, et al. Tamoxifen and breast cancer incidence among women with inherited mutations in BRCA1 and BRCA2: National Surgical Adjuvant Breast and Bowel Project (NSABP-P1) Breast Cancer Prevention Trial. *JAMA* 2001;286:2251.

20. Fisher B, Costantino JP, Wickerham DL, Redmond CK, Kavanah M, Cronin WM, et al. Tamoxifen for prevention of breast cancer: report of the National Surgical Adjuvant Breast and Bowel Project P-1 Study. *J Natl Cancer Inst* 1998;90:1371.

21. Cummings SR, Eckert S, Krueger KA, Grady D, Powles TJ, Cauley JA, et al. The effect of raloxifene on risk of breast cancer in postmenopausal women: results from the MORE randomized trial. Multiple Outcomes of Raloxifene Evaluation. *JAMA* 1999;281:2189.

22. Bernstein L. Epidemiology of endocrine-related risk factors for breast cancer. *J Mammary Gland Biol Neoplasia* 2002;7:3.

23. Fentiman IS. How do endogenous oestrogens affect breast cancer? *Eur J Cancer* 2002;38 Suppl 6:S59.

24. Henderson BE, Ross R, Bernstein L. Estrogens as a cause of human cancer: the Richard and Hinda Rosenthal Foundation award lecture. *Cancer Res* 1988;48:246.

25. Russo IH, Russo J. Role of hormones in mammary cancer initiation and progression. *J Mammary Gland Biol Neoplasia* 1998;3:49.

26. Sivaraman L, Medina D. Hormone-induced protection against breast cancer. *J Mammary Gland Biol Neoplasia* 2002;7:77.

27. Pike MC, Spicer DV, Dahmoush L, Press MF. Estrogens, progestogens, normal breast cell proliferation, and breast cancer risk. *Epidemiol Rev* 1993;15:17.

28. Wagner JD, Kaplan JR, Burkman RT. Reproductive hormones and cardiovascular disease mechanism of action and clinical implications. *Obstet Gynecol Clin North Am* 2002;29:475.

29. Sporn MB, Newton DL. Chemoprevention of cancer with retinoids. *Fed Proc* 1979;38:2528.

30. Huggins C, Grand LC, Brillantes FP. Mammary cancer induced by a single feeding of polynuclear hydrocarbons and their suppression. *Nature* 1961;189:204.

31. Dao TL. Mammary cancer induction by 7,12 dimethylbenzanthracene: relation to age. *Science* 1969;165:810.

32. Grubbs CJ, Peckham JC, Cato KD. Mammary carcinogenesis in rats in relation to age at time of nitroso-N-methyl urea administration. *J Natl Cancer Inst* 1983;70:209.

33. Mehta RG. Experimental basis for the prevention of breast cancer. *Eur J Cancer* 2000; 36:1275.

34. Russo J, Lareef H, Tahin Q, Russo IH. Pathways of carcinogenesis and prevention in the human breast. *Eur J Cancer* 2002;38 Suppl 6:S31.

35. Tokanaga M, Land CE, Yamamoto T, et al. Incidence of female breast cancer among atomic bomb survivors: Hiroshima and Nagasaki 1950-1980. *Radiat Res* 1987;112:243.

36. Hildreth N, Shore R, Dvukresteski P, et al. The risk of breast cancer after irradiation of the thymus in infancy. *N Engl J Med* 1989;321:1281.

37. Miller AB, How G, Sherman G, et al. The risk of breast cancer after irradiation during fluoroscopic examinations in patients being treated for tuberculosis. *N Engl J Med* 1989;321:1285.

38. Lathrop AE, Loeb L. Further investigations on the origins of tumors in mice III on the part played by internal secretions in the spontaneous development of tumors. *J Cancer Res* 1916;1:1.

39. Lacassagne A. Hormonal pathogenesis of adenocarcinoma of the breast. *Am J Cancer* 1936;27:713.

40. Jordan VC, Labadidi MK, Mirecki DM. The antiestrogens and anti-tumor properties of prolonged tamoxifen therapy in C3H/OUJ mice. *Eur J Cancer* 1990;26:718.

41. Jordan VC, Labadidi MK, Langen-Fahey S. Suppression of mouse mammary tumoigenesis by long-term tamoxifen therapy. *J Natl Cancer Inst* 1991;83:492.

42. Dao TL, Sutherland H. Mammary carcinogenesis by 3-methylcholanthrene. 1. Hormonal aspects in tumor induction and growth. *J Natl Cancer Inst* 1959;23:567.

43. Dao TL, Bock FG, Greiner MJ. Mammary carcinogenesis by 3-methylcholanthrene. 2. Inhibitory effects of pregnancy and lactation on tumor induction. *J Natl Cancer Inst* 1959;23:567.

44. Huggins C, Moon R, Morii S. Extinction of experimental mammary cancer. 1. Estradiol-17 and progesterone. *Proc Natl Acad Sci U S A* 1962;48:379.

45. Jabara AC, Toyne PH, Harcourt AG. Effects of time and duration of progesterone administration on mammary tumors induced by 7,12-dimethylbenzanthracene in Sprague-Dawley rats. *Br J Cancer* 1973;27:63.

46. Grubbs CJ, Hill DL, McDonough KC, et al. N-nitroso-N-methylurea-induced mammary carcinogenesis: effect of pregnancy on preneoplastic cells. *J Natl Cancer Inst* 1983;71:625.

47. Dao TL. The role of ovarian hormones in initiating the induction of mammary cancer in rats by polynuclear hydrocarbons. *Cancer Res* 1962;22:973.

48. Jordan VC. Effect of tamoxifen (ICI 46,474) on initiation and growth of DMBA-induced rat mammary carcinoma. *Eur J Cancer* 1976;12:419.

49. Tsai TLS, Katzenellenbogen BS. Antagonism of development and growth of 7,12 dimethylbenzanthracene-induced rat mammary tumors by the anti-estrogen U23,469 and effects on estrogen and progesterone receptors. *Cancer Res* 1977;37:1537.

50. Jordan VC, Allen KE. Evaluation of the antitumor activity of the non-steroidal antioestrogen monohydroxytamoxifen in the DMBA-induced rat mammary carcinoma model. *Eur J Cancer* 1980;16:239.

51. Jordan VC, Allen KE, Dix CJ. Pharmacology of tamoxifen in laboratory animals. *Cancer Treat Rep* 1980;64:745.

52. Gottardis MM, Jordan VC. Antitumor actions of keoxifene and tamoxifen in the N-nitrosomethylurea-induced rat mammary carcinoma model. *Cancer Res* 1987;47:4020.

53. Tamoxifen for early breast cancer: an overview of the randomised trials. Early Breast Cancer Trialists' Collaborative Group. *Lancet* 1998;351:1451.

54. Powles T, Eeles R, Ashley S, Easton D, Chang J, Dowsett M, Tidy A, et al. Interim analysis of the incidence of breast cancer in the Royal Marsden Hospital tamoxifen randomised chemoprevention trial. *Lancet* 1998;352:98.

55. Veronesi U, Maisonneuve P, Costa A, Sacchini V, Maltoni C, et al. Prevention of breast cancer with tamoxifen: preliminary findings from the Italian randomised trial among hysterectomised women. Italian Tamoxifen Prevention Study. *Lancet* 1998;352:93.

56. IBIS investigators. First results from the International Breast Cancer Intervention Study (IBIS-I): a randomised prevention trial. *Lancet* 2002;360:817.

57. Cuzick J, Powles T, Veronesi U, Forbes J, Edwards R, Ashley S, Boyle P. Overview of the main outcomes in breast-cancer prevention trials. *Lancet* 2003;361:296.

58. Veronesi U, Maisonneuve P, Rotmensz N, Costa A, Sacchini V, Travaglini R, et al. Italian randomized trial among women with hysterectomy: tamoxifen and hormone-dependent breast cancer in high-risk women. *J Natl Cancer Inst* 2003;95:160.

59. Bundred NJ. Prognostic and predictive factors in breast cancer. *Cancer Treat Rev* 2001;27:137.

60. MacMahon B, Cole P, Lin TM, Lowe CR, Mirra AP, et al. Age at first birth and breast cancer risk. *Bull World Health Organ* 1970;43:209.

61. Henderson BE, Powell D, Rosario I, Keys C, et al. An epidemiologic study of breast cancer. *J Natl Cancer Inst* 1974;53:609.

62. Moon RC. Relationship between previous reproductive history and chemically induced mammary cancer in rats. *Int J Cancer* 1969;4:312.

63. Medina D, Smith GH. Chemical carcinogen-induced tumorigenesis in parous, involuted mouse mammary glands. *J Natl Cancer Inst* 1999:91:967.

64. Russo IH, Koszalka M, Gimotty PA, et al. Protective effect of chorionic gonadotropin on DMBA-induced mammary carcinogenesis. *Br J Cancer* 1990;62:243.

65. Russo IH, Russo J. Developmental stage of the rat mammary gland as determinant of its susceptibility to 7,12-dimethylben(a)anthracene. *J Natl Cancer Inst* 1978;61:1439.

66. Russo J, Tay LK, Russo IH. Differentiation of the mammary gland and susceptibility to carcinogenesis. *Breast Cancer Res Treat* 1982;2:5.

67. Swanson SM, Guzman RC, Collins G, Tafoya P, et al. Refractoriness to mammary carcinogenesis in the parous mouse is reversible by hormonal stimulation induced by pituitary isografts. *Cancer Lett* 1995;90:171.

68. Thordarson G, Van Horn K, Guzman RC, Nandi S, Talamantes F. Parous rats regain high susceptibility to chemically induced mammary cancer after treatment with various mammotropic hormones. *Carcinogenesis* 2001;22:1027.

69. Guzman RC, Yang J, Rajkumar L, Thordarson G, Chen X, Nandi S. Hormonal prevention of breast cancer mimicking the protective effect of pregnancy. *Proc Natl Acad Sci USA* 1999;96:2520.

70. D'Cruz CM, Moody SE, Master SR, Hartman JL, Keiper EA, et al. Persistent parity-induced changes in growth factors, TGF-b3, and differentiation in the rodent mammary gland. *Mol Endocrinology* 2002;16:2034.

71. Jordan VC. Tamoxifen: a most unlikely pioneering medicine. *Nat Rev Drug Discov* 2003;2:205.

72. Tan-Chiu E, Wang J, Costantino JP, Paik S, Butch C, Wickerham DL, et al. Effects of tamoxifen on benign breast disease in women at high risk for breast cancer. *J Natl Cancer Inst* 2003;95:302.

73. Cummings SR, Duong T, Kenyon E, Cauley JA, Whitehead M, Krueger KA; Multiple Outcomes of Raloxifene Evaluation (MORE) Trial. Serum estradiol level and risk of breast cancer during treatment with raloxifene. *JAMA* 2002;287:216.

74. Jordan VC. Selective estrogen receptor modulation: a personal perspective. *Cancer Res* 2001;61:5683.

75. Jordan VC. Antiestrogens and selective estrogen receptor modulators as multifunctional medicines. 2. Clinical considerations and new agents. *J Med Chem* 2003;46:1081.

76. Martucci C, Fishman J. Direction of estradiol metabolism as a control of its hormonal action--uterotrophic activity of estradiol metabolites. *Endocrinology* 1977;101:1709.

77. Liehr JG, Avitts TA, Randerath E, Randerath K. Estrogen-induced endogenous DNA adduction: possible mechanism of hormonal cancer. *Proc Natl Acad Sci U S A* 1986;83:5301.

78. Zhu BT, Conney AH. Functional role of estrogen metabolism in target cells: review and perspectives. *Carcinogenesis* 1998;19:1.

79. Lippert TH, Seeger H, Mueck AO. The impact of endogenous estradiol metabolites on carcinogenesis. *Steroids* 2000;65:357.

80. Cavalieri EL, Rogan EG, Chakravarti D. Initiation of cancer and other diseases by catechol ortho-quinones: a unifying mechanism. *Cell Mol Life Sci* 2002;59:665.

81. Mueck A, Seeger H, Lippert T. Estradiol metabolism and malignant disease. *Maturitas* 2002;43:1.

82. Klauber N, Parangi S, Flynn E, Hamel E, D'Amato RJ. Inhibition of angiogenesis and breast cancer in mice by the microtubule inhibitors 2-methoxyestradiol and taxol. *Cancer Res* 1997;57:81.

83. Zhu BT, Conney AH. Is 2-methoxyestradiol an endogenous estrogen metabolite that inhibits mammary carcinogenesis? *Cancer Res* 1998;58:2269.

84. Lippert C, Seeger H, Mueck AO. The effect of endogenous estradiol metabolites on the proliferation of human breast cancer cells. *Life Sci* 2003;72:877.

85. Fishman J, Schneider J, Hershcope RJ, Bradlow HL. Increased estrogen-16 alpha-hydroxylase activity in women with breast and endometrial cancer. *J Steroid Biochem* 1984;20:1077.

86. Raju U, Bradlow HL, Skidmore FD, Levitz M. The concentration of 16α-hydroxy androgens in serum and cyst fluid of women with gross cystic disease of the breast. *Steroids* 1989;54:101.

87. Gupta M, McDougal A, Safe S. Estrogenic and antiestrogenic activities of 16alpha- and 2-hydroxy metabolites of 17beta-estradiol in MCF-7 and T47D human breast cancer cells. J *Steroid Biochem Mol Biol* 1998 Dec;67:413.

88. Lewis JS, Thomas TJ, Klinge CM, Gallo MA, Thomas T. Regulation of cell cycle and cyclins by 16alpha-hydroxyestrone in MCF-7 breast cancer cells. *J Mol Endocrinol* 2001;27:293.

89. Fishman J, Martucci C. Biological properties of 16 alpha-hydroxyestrone: implications in estrogen physiology and pathophysiology. *J Clin Endocrinol Metab* 1980;51:611.

90. Telang NT, Suto A, Wong GY, Osborne MP, Bradlow HL. Induction by estrogen metabolite 16 alpha-hydroxyestrone of genotoxic damage and aberrant proliferation in mouse mammary epithelial cells. *J Natl Cancer Inst* 1992;84:634.

91. Bradlow HL, Hershcopf RJ, Martucci CP, Fishman J. Estradiol 16 alpha-hydroxylation in the mouse correlates with mammary tumor incidence and presence of murine mammary tumor virus: a possible model for the hormonal etiology of breast cancer in humans. *Proc Natl Acad Sci U S A* 1985;82:6295.

92. Liehr JG, Fang WF, Sirbasku DA, Ari-Ulubelen A. Carcinogenicity of catechol estrogens in Syrian hamsters. *J Steroid Biochem* 1986;24:353.

93. Ball P, Knuppen R. Catecholoestrogens (2-and 4-hydroxyoestrogens): chemistry, biogenesis, metabolism, occurrence and physiological significance. *Acta Endocrinol Suppl* (Copenh) 1980;232:1.

94. Franks S, MacLusky NJ, Naftolin F. Comparative pharmacology of oestrogens and catechol oestrogens: actions on the immature rat uterus in vivo and in vitro. *J Endocrinol* 1982;94:91.

95. Liehr JG, Roy D. Free radical generation by redox cycling of estrogens. *Free Radic Biol Med* 1990;8:415.

96. Liehr JG. Genotoxic effects of estrogens. *Mutat Res* 1990;238:269.

97. Liehr JG. Genotoxicity of the steroidal oestrogens oestrone and oestradiol: possible mechanism of uterine and mammary cancer development. *Hum Reprod Update* 2001;7:273.

98. Nutter LM, Ngo EO, Abul-Hajj YJ. Characterization of DNA damage induced by 3,4-estrone-o-quinone in human cells. *J Biol Chem* 1991;266:16380.

99. Yager JD, Liehr JG. Molecular mechanisms of estrogen carcinogenesis. *Annu Rev Pharmacol Toxicol* 1996;36:203.

100. Liehr JG. Dual role of oestrogens as hormones and pro-carcinogens: tumour initiation by metabolic activation of oestrogens. *Eur J Cancer Prev* 1997;6:3.

101. Li JJ, Li SA. Estrogen carcinogenesis in Syrian hamster tissues: role of metabolism. *Fed Proc* 1987;46:1858.

102. Yagi E, Barrett JC, Tsutsui T. The ability of four catechol estrogens of 17beta-estradiol and estrone to induce DNA adducts in Syrian hamster embryo fibroblasts. *Carcinogenesis* 2001;22:1505.

103. Schneider J, Huh MM, Bradlow HL, Fishman J. Antiestrogen action of 2-hydroxyestrone on MCF-7 human breast cancer cells. *J Biol Chem* 1984;259:4840.

104. Seegers JC, Aveling ML, Van Aswegen CH, Cross M, Koch F, Joubert WS. The cytotoxic effects of estradiol-17 beta, catecholestradiols and methoxyestradiols on dividing MCF-7 and HeLa cells. *J Steroid Biochem* 1989;32:797.

105. Lottering ML, Haag M, Seegers JC. Effects of 17 beta-estradiol metabolites on cell cycle events in MCF-7 cells. *Cancer Res* 1992;52:5926.

106. Jellinck PH, Michnovicz JJ, Bradlow HL. Influence of indole-3-carbinol on the hepatic microsomal formation of catechol estrogens. *Steroids* 1991;56:446.

107. Bradlow HL, Michnovicz J, Telang NT, Osborne MP. Effects of dietary indole-3-carbinol on estradiol metabolism and spontaneous mammary tumors in mice. *Carcinogenesis* 1991;12:1571.

108. Fotsis T, Zhang Y, Pepper MS, Adlercreutz H, Montesano R, Nawroth PP, et al. The endogenous oestrogen metabolite 2-methoxyoestradiol inhibits angiogenesis and suppresses tumour growth. *Nature* 1994;368:237.

109. Cushman M, He HM, Katzenellenbogen JA, Varma RK, Hamel E, Lin CM, et al. Synthesis of analogs of 2-methoxyestradiol with enhanced inhibitory effects on tubulin polymerization and cancer cell growth. *J Med Chem* 1997;40:2323.

110. Lippert TH, Adlercreutz H, Berger MR, Seeger H, Elger W, Mueck AO. Effect of 2-methoxyestradiol on the growth of methyl-nitroso-urea (MNU)-induced rat mammary carcinoma. *J Steroid Biochem Mol Biol* 2003;84:51.

111. Lakhani NJ, Sarkar MA, Venitz J, Figg WD. 2-Methoxyestradiol, a promising anticancer agent. *Pharmacotherapy* 2003 Feb;23:165.

112. Hayashi T, Hideshima T, Anderson KC. Novel therapies for multiple myeloma. *Br J Haematol* 2003;120:10.

113. Jordan VC. Antiestrogens and selective estrogen receptor modulators as multifunctional medicines. 1. Receptor interactions. *J Med Chem* 2003;46:883.

114. White IN, de Matteis F, Davies A, Smith LL, Crofton-Sleigh C, et al. Genotoxic potential of tamoxifen and analogues in female Fischer F344/n rats, DBA/2 and C57BL/6 mice and in human MCL-5 cells. *Carcinogenesis* 1992;13:2197.

115. Greaves P, Goonetilleke R, Nunn G, Topham J, Orton T. Two-year carcinogenicity study of tamoxifen in Alderley Park Wistar-derived rats. *Cancer Res* 1993;53:3919.

116. Phillips DH. Understanding the genotoxicity of tamoxifen? *Carcinogenesis* 2001;22:839.

117. Martin EA, Rich KJ, White IN, Woods KL, Powles TJ, Smith LL. ^{32}P-postlabelled DNA adducts in liver obtained from women treated with tamoxifen. *Carcinogenesis* 1995;16:1651.

118. Gottardis MM, Robinson SP, Satyaswaroop PG, Jordan VC. Contrasting actions of tamoxifen on endometrial and breast tumor growth in the athymic mouse. *Cancer Res* 1988;48:812.

119. Lerner LJ, Jordan VC. Development of antiestrogens and their use in breast cancer: eighth Cain memorial award lecture. *Cancer Res* 1990;50:4177.

120. Black LJ, Jones CD, Falcone JF. Antagonism of estrogen action with a new benzothiophene derived antiestrogen. *Life Sci* 1983;32:1031.

121. Anzano MA, Peer CW, Smith JM, Mullen LT, Shrader MW, Logsdon DL, Driver CL, Brown CC, Roberts AB, Sporn MB. Chemoprevention of mammary carcinogenesis in the rat: combined use of raloxifene and 9-cis-retinoic acid. *J Natl Cancer Inst* 1996;88:123.

122. Jordan VC, Phelps E, Lindgren JU. Effects of anti-estrogens on bone in castrated and intact female rats. *Breast Cancer Res Treat* 1987;10:31.

123. Black LJ, Sato M, Rowley ER, Magee DE, Bekele A, Williams DC, Cullinan GJ, Bendele R, Kauffman RF, Bensch WR, et al. Raloxifene (LY139481 HCI) prevents bone loss and reduces serum cholesterol without causing uterine hypertrophy in ovariectomized rats. *J Clin Invest* 1994;93:63.

124. Ettinger B, Black DM, Mitlak BH, Knickerbocker RK, Nickelsen T, et al. Reduction of vertebral fracture risk in postmenopausal women with osteoporosis treated with raloxifene: results from a 3-year randomized clinical trial. Multiple Outcomes of Raloxifene Evaluation (MORE) Investigators. *JAMA* 1999;282:637.

125. Walsh BW, Kuller LH, Wild RA, Paul S, Farmer M, Lawrence JB, Shah AS, Anderson PW. Effects of raloxifene on serum lipids and coagulation factors in healthy postmenopausal women. *JAMA* 1998;279:1445.

126. Walsh BW, Paul S, Wild RA, Dean RA, Tracy RP, Cox DA, Anderson PW. The effects of hormone replacement therapy and raloxifene on C-reactive protein and homocysteine in healthy postmenopausal women: a randomized, controlled trial. *J Clin Endocrinol Metab* 2000;85:214.

127. Barrett-Connor E, Grady D, Sashegyi A, Anderson PW, Cox DA, Hoszowski K, et al. Raloxifene and cardiovascular events in osteoporotic postmenopausal women: four-year results from the MORE (Multiple Outcomes of Raloxifene Evaluation) randomized trial. *JAMA* 2002;287:847.

128. Vogel VG, Costantino JP, Wickerham DL, Cronin WM, Wolmark N. The study of tamoxifen and raloxifene: preliminary enrollment data from a randomized breast cancer risk reduction trial. *Clin Breast Cancer* 2002;3:153.

129. Cauley JA, Norton L, Lippman ME, Eckert S, Krueger KA, Purdie DW, et al. Continued breast cancer risk reduction in postmenopausal women treated with raloxifene: 4-year results from the MORE trial. Multiple outcomes of raloxifene evaluation. *Breast Cancer Res Treat* 2001;65:125.

130. Sato M, Turner CH, Wang T, Adrian MD, Rowley E, Bryant HU. LY353381.HCl: a novel raloxifene analog with improved SERM potency and efficacy in vivo. *J Pharmacol Exp Ther* 1998;287:1.

131. Munster PN, Buzdar A, Dhingra K, Enas N, Ni L, Major M, et al. Phase I study of a third-generation selective estrogen receptor modulator, LY353381.HCL, in metastatic breast cancer. *J Clin Oncol* 2001;19:2002.

132. Gutman M, Couillard S, Roy J, Labrie F, Candas B, Labrie C. Comparison of the effects of EM-652 (SCH57068), tamoxifen, toremifene, droloxifene, idoxifene, GW-5638 and raloxifene on the growth of human ZR-75-1 breast tumors in nude mice. *Int J Cancer* 2002;99(2):273.

133. Willson TM, Henke BR, Momtahen TM, Charifson PS, Batchelor KW, et al. 3-[4-(1,2-Diphenylbut-1-enyl)phenyl]acrylic acid: a non-steroidal estrogen with functional selectivity for bone over uterus in rats. *J Med Chem* 1994;37:1550.

134. Brady H, Doubleday M, Gayo-Fung LM, Hickman M, Khammungkhune S, Kois A, et al. Differential response of estrogen receptors alpha and beta to SP500263, a novel potent selective estrogen receptor modulator. *Mol Pharmacol* 2002;61:562.

135. Sato M, Zeng GQ, Rowley E, Turner CH. LY353381.HCl (arzoxifene): an improved benzothiophene analog with bone efficacy complementary to parathyroid hormone-(1-34). *Endocrinology* 1998;139:4642.

136. Ma YL, Bryant HU, Zeng Q, Palkowitz A, Jee WS, Turner CH, Sato M. Long-term dosing of arzoxifene lowers cholesterol, reduces bone turnover, and preserves bone quality in ovariectomized rats. *J Bone Miner Res* 2002;17:2256.

137. Suh N, Glasebrook AL, Palkowitz AD, Bryant HU, Burris LL, Starling JJ, Pearce HL, Williams C, Peer C, Wang Y, Sporn MB. Arzoxifene, a new selective estrogen receptor modulator for chemoprevention of experimental breast cancer. *Cancer Res* 2001;61:8412.

138. Martel C, Picard S, Richard V, Belanger A, Labrie C, Labrie F. Prevention of bone loss by EM-800 and raloxifene in the ovariectomized rat. *J Steroid Biochem Mol Biol* 2000;74:45.

139. Brady H, Desai S, Gayo-Fung LM, Khammungkhune S, McKie JA, O'Leary E, Pascasio L, Sutherland MK, Anderson DW, Bhagwat SS, Stein B. Effects of SP500263, a novel, potent antiestrogen, on breast cancer cells and in xenograft models. *Cancer Res* 2002;62:1439.

140. Sutherland KM, Brady H, Gayo-Fung LM, Leisten J, Lipps SG, et al. Effects of SP500263, a Novel Selective Estrogen Receptor Modulator, on Bone, Uterus, and Serum Cholesterol in the Ovariectomized Rat. *Calcif Tissue Int* 2003 Mar 6; [epub ahead of print].

141. Bulun SE, Price TM, Aitken J, Mahendroo MS, Simpson ER. A link between breast cancer and local estrogen biosynthesis suggested by quantification of breast adipose tissue aromatase cytochrome P450 transcripts using competitive polymerase chain reaction after reverse transcription. *J Clin Endocrinol Metab* 1993;77:1622.

142. Tekmal RR, Ramachandra N, Gubba S, Durgam VR, Mantione J, et al. Overexpression of int-5/aromatase in mammary glands of transgenic mice results in the induction of hyperplasia and nuclear abnormalities. *Cancer Res* 1996;56:3180.

143. Brodie AM, Njar VC. Aromatase inhibitors and breast cancer. *Semin Oncol* 1996;23:10-20.

144. Goss PE, Strasser K. Aromatase inhibitors in the treatment and prevention of breast cancer. J *Clin Oncol* 2001;19:881.

145. Chen S, Zhou D, Okubo T, Kao YC, Eng ET, et al. Prevention and treatment of breast cancer by suppressing aromatase activity and expression. *Ann N Y Acad Sci* 2002;963:229.

146. Yates RA, Dowsett M, Fisher GV, Selen A, Wyld PJ. Arimidex (ZD1033): a selective, potent inhibitor of aromatase in postmenopausal female volunteers. *Br J Cancer* 1996;73:543.

147. Decoster G, Stein G, Holdener EE. Responses and toxic deaths in phase I clinical trials. *Ann Oncol* 1990;1:175.

148. De Coster R, Van Ginckel RF, Callens MJ, Goeminne NK, Janssens BL. Antitumoral and endocrine effects of (+)-vorozole in rats bearing dimethylbenzanthracene-induced mammary tumors. *Cancer Res* 1992;52:1240.

149. Schieweck K, Bhatnagar AS, Batzl C, Lang. Anti-tumor and endocrine effects of non-steroidal aromatase inhibitors on estrogen-dependent rat mammary tumors. *J Steroid Biochem Mol Biol* 1993;44:633.

150. Lubet RA, Steele VE, Casebolt TL, Eto I, Kelloff GJ, Grubbs CJ. Chemopreventive effects of the aromatase inhibitors vorozole (R-83842) and 4-hydroxyandrostenedione in the methylnitrosourea (MNU)-induced mammary tumor model in Sprague-Dawley rats. *Carcinogenesis* 1994;15:2775.

151. Gunson DE, Steele RE, Chau RY. Prevention of spontaneous tumours in female rats by fadrozole hydrochloride, an aromatase inhibitor. *Br J Cancer* 1995;72:72.

152. Bonneterre J, Thurlimann B, Robertson JF, Krzakowski M, Mauriac L, et al. Anastrozole versus tamoxifen as first-line therapy for advanced breast cancer in 668 postmenopausal women: results of the Tamoxifen or Arimidex Randomized Group Efficacy and Tolerability study. *J Clin Oncol* 2000;18:3748.

153. Bonneterre J, Buzdar A, Nabholtz JM, Robertson JF, Thurlimann B, et al. Anastrozole is superior to tamoxifen as first-line therapy in hormone receptor positive advanced breast carcinoma. *Cancer* 2001;92:2247.

154. Mouridsen H, Gershanovich M, Sun Y, Perez-Carrion R, Boni C, Monnier A, et al. Superior efficacy of letrozole versus tamoxifen as first-line therapy for postmenopausal

women with advanced breast cancer: results of a phase III study of the International Letrozole Breast Cancer Group. *J Clin Oncol* 2001;19:2596.

155. ATAC Trialists' Group. Arimidex, tamoxifen alone or in combination. Anastrozole alone or in combination with tamoxifen versus tamoxifen alone for adjuvant treatment of postmenopausal women with early breast cancer: first results of the ATAC randomised trial. *Lancet* 2002;359:2131.

156. Baum M. A vision for the future? *Br J Cancer* 2001;85 Suppl 2:15.

157. Chlebowski RT, Col N, Winer EP, Collyar DE, Cummings SR, Vogel VG 3rd, et al. American Society of Clinical Oncology technology assessment of pharmacologic interventions for breast cancer risk reduction including tamoxifen, raloxifene, and aromatase inhibition. *J Clin Oncol* 2002;20:3328.

158. Lotan R. Retinoids and apoptosis: implications for cancer chemoprevention and therapy. *J Natl Cancer Inst* 1995;87:1655.

159. Chambon P. A decade of molecular biology of retinoic acid receptors. *FASEB J* 1996;10:940.

160. Ulukaya E, Wood EJ. Fenretinide and its relation to cancer. *Cancer Treat Rev* 1999;25:229.

161. Lippman SM, Benner SE, Fritsche HA Jr, Lee JS, Hong WK. The effect of 13-cis-retinoic acid chemoprevention on human serum retinol levels. *Cancer Detect Prev* 1998;22:51.

162. Abou-Issa H, Duruibe VA. Anticarcinogenic effect of retinoids on 7,12-dimethylbenz(a)anthracene-induced mammary tumor induction, and its relationship to cyclic AMP-dependent protein kinase. *Biochem Biophys Res Commun* 1986;135:116.

163. Moon RC. Vitamin A, retinoids and breast cancer. *Adv Exp Med Biol* 1994;364:101.

164. Costa A, Formelli F, Chiesa F, Decensi A, De Palo G, Veronesi U. Prospects of chemoprevention of human cancers with the synthetic retinoid fenretinide. *Cancer Res* 1994;54 Suppl 7:S2032.

165. Lippman SM, Benner SE, Hong WK. Cancer chemoprevention. *J Clin Oncol* 1994;12:851.

166. Moon RC, Thompson HJ, Becci PJ, Grubbs CJ, Gander RJ, Newton DL, Smith JM, et al. N-(4-Hydroxyphenyl)retinamide, a new retinoid for prevention of breast cancer in the rat. *Cancer Res* 1979;39:1339.

167. Kelloff GJ, Crowell JA, Boone CW, Steele VE, Lubet RA, Greenwald P, Alberts DS, et al. Clinical development plan: N-(4-hydroxyphenyl)retinamide. *J Cell Biochem Suppl* 1994;20:176.

168. Veronesi U, De Palo G, Marubini E, Costa A, Formelli F, Mariani L, Decensi A, et al. Randomized trial of fenretinide to prevent second breast malignancy in women with early breast cancer. *J Natl Cancer Inst* 1999;91:1847.

169. Fontana JA. Interaction of retinoids and tamoxifen on the inhibition of human mammary carcinoma cell proliferation. *Exp Cell Biol* 1987;55:136.

170. Ratko TA, Detrisac CJ, Dinger NM, Thomas CF, Kelloff GJ, Moon RC. Chemopreventive efficacy of combined retinoid and tamoxifen treatment following surgical excision of a primary mammary cancer in female rats. *Cancer Res* 1989;49:4472.

171. Moon RC, Kelloff GJ, Detrisac CJ, Steele VE, Thomas CF, Sigman CC. Chemoprevention of MNU-induced mammary tumors in the mature rat by 4-HPR and tamoxifen. *Anticancer Res* 1992;12:1147.

172. Conley B, O'Shaughnessy J, Prindiville S, Lawrence J, Chow C, Jones E, et al. Pilot trial of the safety, tolerability, and retinoid levels of N-(4-hydroxyphenyl) retinamide in combination with tamoxifen in patients at high risk for developing invasive breast cancer. *J Clin Oncol* 2000;18:275.

173. Bischoff ED, Gottardis MM, Moon TE, Heyman RA, Lamph WW. Beyond tamoxifen: the retinoid X receptor-selective ligand LGD1069 (TARGRETIN) causes complete regression of mammary carcinoma. *Cancer Res* 1998;58:479.

174. Miller VA, Benedetti FM, Rigas JR, Verret AL, Pfister DG, Straus D, Kris MG, et al. Initial clinical trial of a selective retinoid X receptor ligand, LGD1069. *J Clin Oncol* 1997;15:790.

175. Wu K, Kim HT, Rodriquez JL, Hilsenbeck SG, Mohsin SK, Xu XC, Lamph WW, et al. Suppression of mammary tumorigenesis in transgenic mice by the RXR-selective retinoid, LGD1069. *Cancer Epidemiol Biomarkers Prev* 2002;11:467.

176. Wu K, Zhang Y, Xu XC, Hill J, Celestino J, Kim HT, Mohsin SK, Hilsenbeck SG, et al. The retinoid X receptor-selective retinoid, LGD1069, prevents the development of estrogen receptor-negative mammary tumors in transgenic mice. *Cancer Res* 2002;62:6376.

177. Paik J, Blaner WS, Sommer KM, Moe R, Swisshlem K. Retinoids, retinoic acid receptors, and breast cancer. *Cancer Invest* 2003;21:304.

178. Howe LR, Subbaramaiah K, Brown AM, Dannenberg AJ. Cyclooxygenase-2: a target for the prevention and treatment of breast cancer. *Endocr Relat Cancer* 2001;8:97.

179. Alshafie GA, Abou-Issa HM, Seibert K, Harris RE. Chemotherapeutic evaluation of Celecoxib, a cyclooxygenase-2 inhibitor, in a rat mammary tumor model. *Oncol Rep* 2000;7:1377.

180. Howe LR, Subbaramaiah K, Patel J, Masferrer JL, Deora A, et al. Celecoxib, a selective cyclooxygenase 2 inhibitor, protects against human epidermal growth factor receptor 2 (HER-2)/neu-induced breast cancer. *Cancer Res* 2002;62:5405.

181. Harris RE, Alshafie GA, Abou-Issa H, Seibert K. Chemoprevention of breast cancer in rats by celecoxib, a cyclooxygenase 2 inhibitor. *Cancer Res 2000*;60:2101.

182. Davies G, Martin LA, Sacks N, Dowsett M. Cyclooxygenase-2 (COX-2), aromatase and breast cancer: a possible role for COX-2 inhibitors in breast cancer chemoprevention. *Ann Oncol* 2002;13:669.

183. Ciardiello F. Epidermal growth factor receptor tyrosine kinase inhibitors as anticancer agents. *Drugs* 2000;60:25-32.

184. Mendelsohn J, Baselga J. The EGF receptor family as targets for cancer therapy. *Oncogene* 2000;19:6550.

185. Bange J, Zwick E, Ullrich A. Molecular targets for breast cancer therapy and prevention. *Nat Med* 2001;7:548.

186. Lu C, Speers C, Zhang Y, Xu X, Hill J, Steinbis E, Celestino J, Shen Q, Kim H, Hilsenbeck S, Mohsin SK, Wakeling A, Osborne CK, Brown PH. The EGFR inhibitor ZD1839 (Gefitinib, 'Iressa') suppresses the development of estrogen receptor-negative mammary tumors in transgenic mice. *JNCI* 2003 (in press).

187. Herbert BS, Wright AC, Passons CM, Wright WE, Ali IU, et al. Effects of chemopreventive and antitelomerase agents on the spontaneous immortalization of breast epithelial cells. *J Natl Cancer Inst* 2001;93:39.

188. Sarkar FH, Li Y. Mechanisms of cancer chemoprevention by soy isoflavone genistein. *Cancer Metastasis Rev* 2002;21:265.

189. Meyskens FL Jr, Gerner EW. Development of difluoromethylornithine (DFMO) as a chemoprevention agent. *Clin Cancer Res* 1999;5:945.

190. Fabian CJ, Kimler BF, Brady DA, Mayo MS, Chang CH, Ferraro JA, et al. A phase II breast cancer chemoprevention trial of oral alpha-difluoromethylornithine: breast tissue, imaging, and serum and urine biomarkers. *Clin Cancer Res* 2002;8:3105.

Article

Formation of filopodia-like bundles in vitro from a dendritic network

Danijela Vignjevic,[1] Defne Yarar,[2] Matthew D. Welch,[2] John Peloquin,[1] Tatyana Svitkina,[1] and Gary G. Borisy[1]

[1]Department of Cell and Molecular Biology, Northwestern University Medical School, Chicago, IL 60611
[2]Department of Molecular and Cell Biology, University of California, Berkeley, CA 94720

We report the development and characterization of an in vitro system for the formation of filopodia-like bundles. Beads coated with actin-related protein 2/3 (Arp2/3)–activating proteins can induce two distinct types of actin organization in cytoplasmic extracts: (1) comet tails or clouds displaying a dendritic array of actin filaments and (2) stars with filament bundles radiating from the bead. Actin filaments in these bundles, like those in filopodia, are long, unbranched, aligned, uniformly polar, and grow at the barbed end. Like filopodia, star bundles are enriched in fascin and lack Arp2/3 complex and capping protein. Transition from dendritic to bundled organization was induced by depletion of capping protein, and add-back of this protein restored the dendritic mode. Depletion experiments demonstrated that star formation is dependent on Arp2/3 complex. This poses the paradox of how Arp2/3 complex can be involved in the formation of both branched (lamellipodia-like) and unbranched (filopodia-like) actin structures. Using purified proteins, we showed that a small number of components are sufficient for the assembly of filopodia-like bundles: Wiskott-Aldrich syndrome protein (WASP)–coated beads, actin, Arp2/3 complex, and fascin. We propose a model for filopodial formation in which actin filaments of a preexisting dendritic network are elongated by inhibition of capping and subsequently cross-linked into bundles by fascin.

Introduction

Lamellipodia and filopodia are the two major types of protrusive organelles in crawling cells. Multiple lines of evidence indicate that lamellipodial protrusion occurs by a dendritic nucleation/array treadmilling model (Mullins et al., 1998; Borisy and Svitkina, 2000). In this model, members of the Wiskott-Aldrich syndrome protein (WASP)* family activate the actin-related protein 2/3 (Arp2/3) complex and nucleate the formation of actin filaments on preexisting filaments, which function as coactivators (Higgs and Pollard, 2001). Repeated dendritic nucleation generates a branched array of filaments, as found at the leading edge of cells (Svitkina et al., 1997; Svitkina and Borisy, 1999) or in comet tails (Cameron et al., 2001). Capping protein functions to cap excessive barbed ends (Cooper and Schafer, 2000), thus channeling actin polymerization close to the membrane.

Whereas lamellipodia seem designed for protrusion over a smooth surface, filopodia seem designed for exploring the extracellular matrix and surfaces of other cells. Filopodia, in contrast to the branched network of lamellipodia, contain an unbranched bundle of actin filaments that are aligned axially, packed tightly together, and of uniform polarity (Small et al., 1978; Lewis and Bridgman, 1992). Unlike lamellipodia, the Arp2/3 complex is excluded from filopodia (Svitkina and Borisy, 1999), and filaments in filopodia are relatively long and do not turn over rapidly (Mallavarapu and Mitchison, 1999). The roots of filopodia extend well into the cell lamellipodium. As proposed by the filament treadmilling model (Small et al., 1994), filaments elongate with their barbed ends oriented toward the leading edge, pushing the membrane and at the same time continuously depolymerizing from the pointed ends.

A major question in understanding filopodial formation is how they are initiated. One member of the WASP family, N-WASP, facilitates Cdc42-induced filopodia formation in cells (Miki et al., 1998), suggesting that Arp2/3-mediated nucleation of actin filaments plays a role in generating parallel bundles. How might Arp2/3 complex be involved in the formation of unbranched actin structures? One possibility is that the nucleation and branching activities of Arp2/3 complex can be separated, resulting in the production of dendritic

Address correspondence to Danijela Vignjevic, Northwestern University Medical School, Department of Cell and Molecular Biology, 303 E. Chicago Ave., Ward 8-063, Chicago, IL 60611. Tel.: (312) 503-2854. Fax: (312) 501-7912. E-mail: nele@northwestern.edu

*Abbreviations used in this paper: Arp2/3, actin-related protein 2/3; BB, brain buffer; Ena/VASP, enabled/vasodilator-stimulated phosphoprotein; REF, rat embryo fibroblast; VCA, verprolin-homology/connecting/acidic domain of WASP; WASP, Wiskott-Aldrich syndrome protein.

Key words: filopodia; actin; Arp2/3; capping protein; fascin

The Journal of Cell Biology, Volume 160, Number 6, March 17, 2003 951–962
http://www.jcb.org/cgi/doi/10.1083/jcb.200208059

The Journal of Cell Biology

or parallel actin structures, depending on the way in which it is activated. Another possibility is that the dendritic array initially produced by Arp2/3-mediated nucleation is subsequently transformed into parallel bundles of actin filaments.

Valuable insights into the mechanism of lamellipodial formation and protrusion have been obtained using bacterial- and bead-based in vitro motility systems (Theriot et al., 1994; Loisel et al., 1999; Cameron et al., 2000). Filopodial formation is less understood, one reason being that a similar in vitro approach is lacking. In this study, we report the development of in vitro systems for producing filopodia-like bundles, one of which employs cytoplasmic extracts and another that reconstitutes filopodia-like bundles from purified proteins. Using these systems, we provide evidence that filopodia-like bundles are formed by reorganization of the dendritic array.

Results

Formation of bead-associated actin bundles in extracts

Because filopodia are especially abundant in neuronal cell growth cones, we reasoned that brain cytoplasmic extracts might be a good source of filopodia-promoting factors, even though such extracts have previously been demonstrated to support comet tail motility (Laurent et al., 1999; Yarar et al., 1999). WASP-coated beads were introduced into rat brain extracts along with rhodamine–actin. Strikingly different structures were found associated with the beads depending on their position on the coverslip. In the center of the coverslip, beads were associated with a cloud of actin filaments or a typical comet tail (Fig. 1 A). In contrast, at the edge of the coverslip, straight actin bundles radiated from a bead in a star-like configuration (Fig. 1, A and B). These stars represented 84 ± 10% (n = 1,030) of all bead-associated actin structures at the edges of the coverslips (outermost third of the coverslip radius). No stars were found in the center of the coverslips (innermost third of the radius). In the transition zone between the center and edge of the coverslip, we observed large actin clouds and chimeras, structures intermediate between tails and stars (Fig. 1 A).

To determine whether star formation somehow resulted from special conditions at the coverslip edge, we altered the geometry of sample preparation. In the previous experiment, a 1-μl drop of assay mix was placed on a glass slide, and a coverslip was applied such that the drop spread outward from the coverslip's center. Here, the coverslip was applied such that one edge contacted the drop of assay mix, which was then forced to spread toward the coverslip's center. With this design, stars were not observed at the initial contacting edge of the coverslip (n = 527), whereas in the center of the coverslip, stars were abundant (83 ± 10%, n = 675), and in the transition zone, they represented 2 ± 2% (n = 745) of all structures. Thus, star formation was not a result of proximity to the coverslip edge. Rather, star formation correlated with distance of spreading across the glass surface.

One possible explanation for the formation of stars instead of comet tails was depletion of some protein(s) by adsorption to the glass during sample spreading. We tested this idea by blocking and preadsorption experiments. Pretreat-

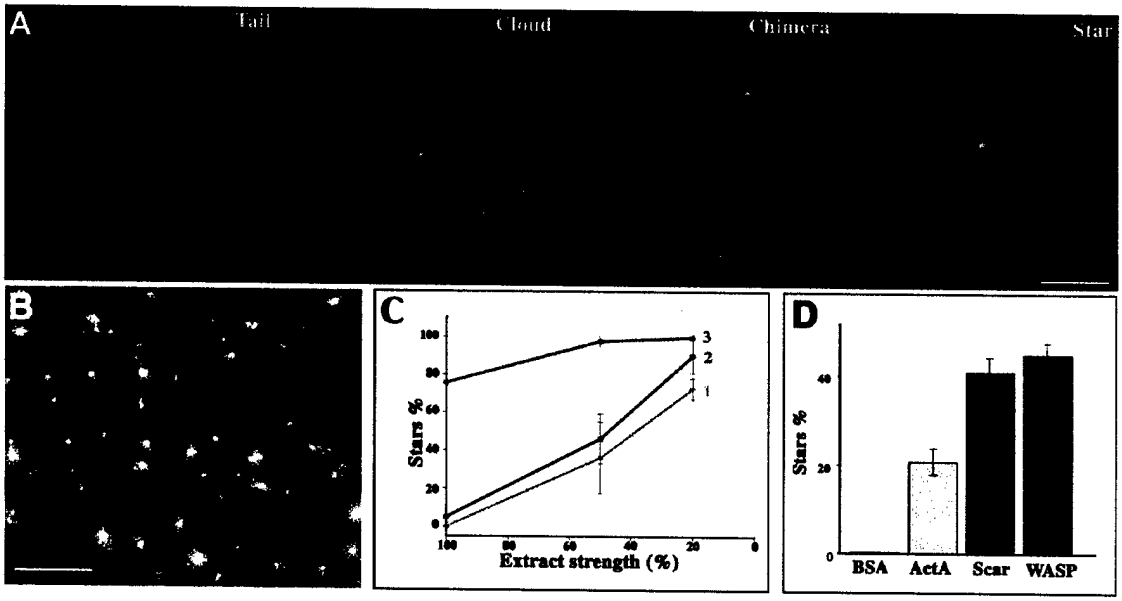

Figure 1. **Different actin structures are assembled on the beads.** Actin assembly was assayed on Arp2/3 activator-coated beads in brain extract supplemented with rhodamine-labeled actin. (A) The pattern of actin assembly depends on the location of the bead on the coverslip. In the center of the coverslip, beads induce the formation of tails. Halfway between the center and edge of the coverslip, actin clouds and chimeras are formed. At the edge of the coverslip, star-like structures are associated with the beads. Beads are shown in yellow. Bar, 5 μm. (B) Stars are the dominant actin structure at the edge of the sample. Low magnification view of a field at the edge of a coverslip. Bar, 50 μm. (C) Percentage of stars increases with extract dilution. 1, center of the coverslip; 2, transitional zone; 3, edge of the coverslip. (D) Percentage of stars produced at the edge of the coverslip in undiluted rat brain extract by beads coated with different Arp2/3-activating proteins.

ment of the coverslip with 1% BSA blocked star formation, whereas other actin structures (tails and clouds) did form (unpublished data), suggesting that protein adsorption to glass plays a critical role in star formation. Preadsorption was performed by mixing extract with ground glass to simulate protein depletion during sample spreading, followed by centrifugation to collect the unadsorbed fraction. Glass-depleted extracts supported star formation throughout the entire coverslip, not only at the edges. Further, glass-depleted extracts also supported the formation of stars on WASP-coated beads in plastic tubes. If absorption to glass reduced the concentration of some star-inhibiting factor(s), then simple dilution of the extract might be sufficient to induce stars. Indeed, as shown in Fig. 1 C, when extracts were diluted fivefold with buffer, stars formed across the entire coverslip. The percentage of stars at the center of the coverslip increased from 0% (n = 1603), for undiluted extracts, to 73 ± 6% (n = 542), for extracts diluted fivefold. Thus, the formation of stars could be induced by lowering the concentration of some factor(s) in the extract. Star formation was not limited to rat brain extracts. Extracts of *Xenopus* oocytes and rat embryo fibroblasts (REFs) also supported star formation (unpublished data), but required greater dilution than rat brain extracts. 10% *Xenopus* oocyte extracts and 50% REF extracts were comparable to full-strength brain extracts in their ability to produce stars.

Star formation in extracts is an Arp2/3-dependent process

The formation of bundles in association with WASP-coated beads suggested the involvement of the Arp2/3 complex. To investigate the role of Arp2/3 complex in star assembly, it was depleted from brain extracts by GST–verprolin-homology/connecting/acidic domain of WASP (VCA) sepharose beads. At least 90% depletion was achieved, as assayed by immunoblotting (Fig. 2 A). In control and mock-depleted extracts, stars were present throughout the entire coverslip, 96% (n = 126) and 90% (n = 138), respectively (Fig. 2, B and C). In Arp2/3-depleted extracts (Fig. 2 D), actin assembly around the beads was completely abolished (0%, n = 213). Only spontaneously polymerized filaments could be observed in the background. Add-back of pure Arp2/3 complex to the depleted brain extracts restored star formation (Fig. 2 E) (84%, n = 170), although stars were slightly smaller than in control samples. Based on our immunoblotting experiments, the concentration of Arp2/3 complex necessary to rescue star formation (0.5 μM) was similar to that calculated to be present in glass-depleted extracts (0.45 μM). Lower concentrations of added Arp2/3 complex induced the formation of branched filaments on the background or actin clouds on the beads. We conclude that star formation is mediated by the Arp2/3 complex.

We next assayed whether star formation would be supported by different Arp2/3 activators. Beads were coated with either the bacterial protein ActA or cellular proteins WASP or Scar1. All activator-coated beads induced star formation in rat brain extracts, whereas beads coated with BSA did not (Fig. 1 D). COOH-terminal domains of WASP and Scar (pVCA) proteins, which were sufficient for Arp2/3 activation (Higgs and Pollard, 2001), also induced stars in extracts. We also tested whether star formation depended on beads or could also occur on bacteria. Stars assembled on *Listeria* expressing ActA and on *Escherichia coli* expressing the *Shigella* protein IcsA (unpublished data), indicating that

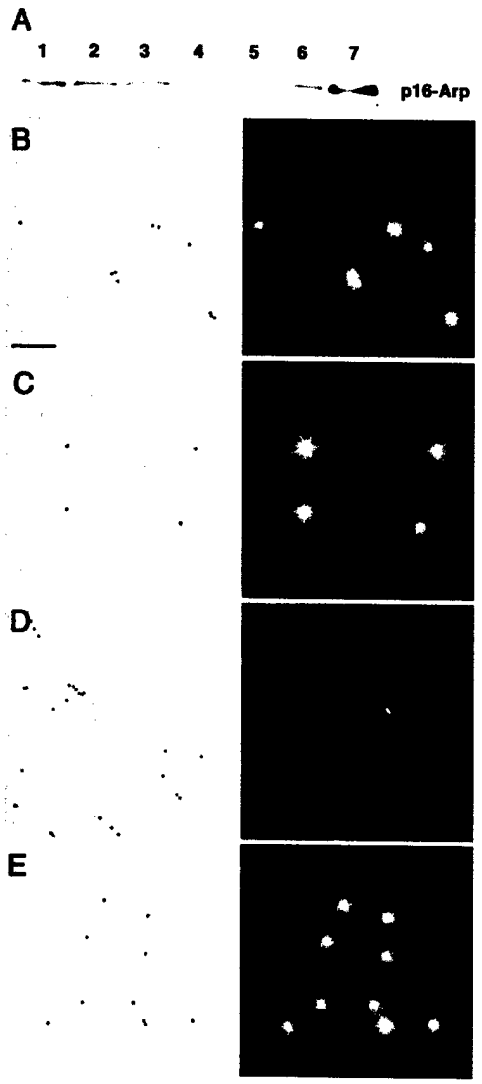

Figure 2. **Arp2/3 complex is essential for star formation.** (A) Arp2/3 complex depletion in brain extract. Glutathione-Sepharose or glutathione-Sepharose–coupled GST–VCA beads were incubated with 40 μl of brain extract. Arp2/3 depletion was monitored by immunoblotting using anti-p16 polyclonal antibody. Lane 1, 10 μl of untreated extract; lane 2, 10 μl of glass-depleted extract; lane 3, 10 μl of mock-depleted extract; lane 4, 10 μl of Arp2/3-depleted extract; lane 5, Arp2/3 associated with glutathione-Sepharose beads; lane 6, Arp2/3 associated with GST–VCA beads; lane 7, pure Arp2/3 from bovine brain, 4 μg. (B–E) Star assembly in Arp2/3-depleted brain extract. (B) Control, glass-depleted extract. (C) Mock-depleted extract. (D) Arp2/3-depleted extract; stars do not form. (E) Arp2/3-depleted extract rescued by add-back of 0.64 μM pure Arp2/3 complex; star formation is restored. Left panels, phase contrast. Individual 0.5-μm beads are visible. Right panels, fluorescence. Bright stars are evident on a background of faint individual filaments in B, C, and E. Only faint filaments are seen in D. Bar, 10 μm.

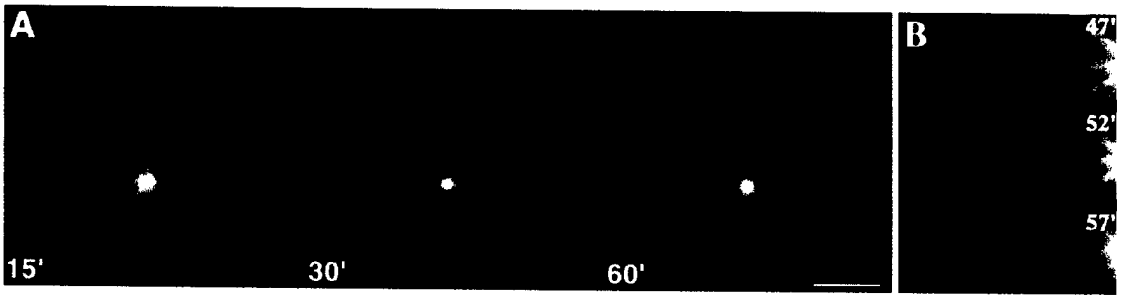

Figure 3. **Kinetics of star formation.** (A) Time-lapse sequence of star assembly in rat brain extract. Bar, 5 μm. (B) Actin bundle zippering. Two bundles zipper together in a centrifugal direction. Time shown in min.

the formation of stars was not restricted to coated synthetic beads. Because *Shigella* protein IcsA is known to recruit N-WASP from the extracts (Egile et al., 1999), this result also suggests that N-WASP supports star formation. Thus, star formation required active Arp2/3 complex but did not depend on a specific Arp2/3 activator.

Stars display both lamellipodial and filopodial types of actin organization

The radial bundles comprising stars bear a superficial similarity to filopodia in cells. To test whether these two kinds of structures have a deeper similarity, we analyzed the kinetics of star formation, their structural organization, sites of actin incorporation, and protein composition. Star development was observed by time-lapse microscopy. Initially, a diffuse actin cloud was formed around the bead (Fig. 3 A, 15 min). As time progressed, radial actin bundles appeared and began to elongate, with an average rate of 0.15 μm/min. Finally, we observed long stable actin bundles radiating from the bead-associated cloud. Some bundles in the course of star formation fused together by zippering in a proximal–distal direction, producing thicker bundles (Fig. 3 B). Zippering in a distal–proximal direction was also observed (unpublished data).

The structural organization of stars was examined by EM of platinum replicas (Fig. 4 A). Proximal to the bead, actin filaments formed a dendritic network, similar to that in lamellipodia. Many long unbranched filaments emanated from this network and, distal to the bead, gradually merged into bundles structurally similar to filopodia. Because one of the hallmarks of native filopodial bundles is uniform polarity of actin filaments, we performed myosin S1 decoration of actin filaments in stars to determine their polarity. The high density of filaments near the bead prevented determination of filament polarity in this region as well as in tight bundles. However, in the looser bundles distal to the bead (>1 μm), 93% (n = 429) of actin filaments had uniform polarity with their barbed ends pointing away from the bead (Fig. 4 B). Thus, stars display both lamellipodial (dendritic network) and filopodial (parallel bundle) types of actin organization, with the transition from one to the other occurring with distance away from the bead. The transition appeared as bundling of long filaments arising from the dendritic network.

Sites of actin polymerization in stars were analyzed by pulse-labeling experiments. After allowing stars to form, the distribution of newly incorporated rhodamine-labeled actin was determined relative to total actin, which was labeled with fluorescein-conjugated phalloidin (Fig. 4 C). Two major sites of actin incorporation were found: near the bead and at the tips of actin bundles. We interpret bead-associated sites to represent the growth of branches nucleated by WASP-activated Arp2/3 complex. In contrast, we interpret the incorporation at tips of radial bundles to represent elongation from preexisting, uncapped barbed ends, because no branched filaments were observed by EM at the tips of bundles. Actin incorporation was sometimes seen along the bundle, distant from its tip, consistent with EM data showing that some filaments in the bundle are shorter than others. This may result from unequal elongation of filaments or zippering of bundles of unequal length. Thus, stars display two modes of actin polymerization: Arp2/3-mediated nucleation at the bead, similar to that in lamellipodia, and barbed-end elongation at the tips of bundles, like that in filopodia.

Lamellipodia and comet tails, on the one hand, and filopodia in cells, on the other hand, have distinct protein composition (Goldberg, 2001; Small et al., 2002). For example, the Arp2/3 complex and capping protein are present in lamellipodia and comet tails but have not been found in filopodia (Svitkina and Borisy, 1999; Svitkina et al., 2003), whereas fascin is enriched in filopodia and less abundant in lamellipodia (Kureishy et al., 2002). α-Actinin has been found in lamellipodia (Langanger et al., 1984) but only in the roots of filopodia (Svitkina et al., 2003). We determined the localization of these proteins in stars by immunofluorescence staining or by incorporation of the labeled protein (Fig. 5). Arp2/3 complex and capping protein were found in the dendritic network proximal to the bead but not in actin bundles. α-Actinin was clearly enriched around the bead but could be faintly detected in bundles when a high amount of exogenous protein was added. In contrast, fascin was strongly localized to actin bundles but was diminished in the network surrounding the bead. Thus, by structural, kinetic, and biochemical criteria, our data demonstrate that the proximal dendritic network and radial bundles of stars are similar to the actin organization of lamellipodia and filopodia, respectively.

Parallel bundle formation can be shifted to dendritic network formation by capping protein

The absorption and dilution experiments indicated that reduced levels of factor(s) in the extract are critical in shifting

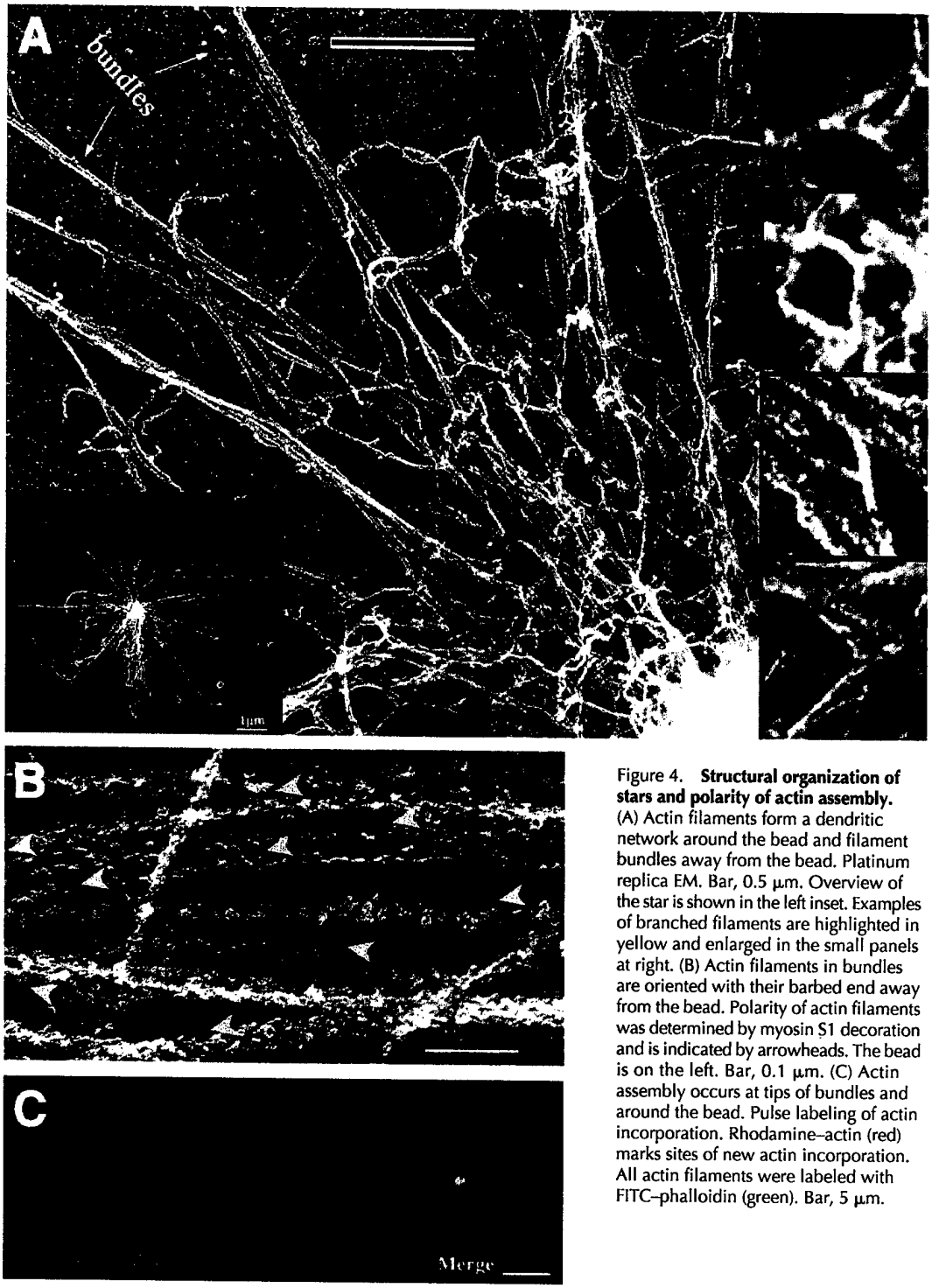

Figure 4. **Structural organization of stars and polarity of actin assembly.** (A) Actin filaments form a dendritic network around the bead and filament bundles away from the bead. Platinum replica EM. Bar, 0.5 μm. Overview of the star is shown in the left inset. Examples of branched filaments are highlighted in yellow and enlarged in the small panels at right. (B) Actin filaments in bundles are oriented with their barbed end away from the bead. Polarity of actin filaments was determined by myosin S1 decoration and is indicated by arrowheads. The bead is on the left. Bar, 0.1 μm. (C) Actin assembly occurs at tips of bundles and around the bead. Pulse labeling of actin incorporation. Rhodamine–actin (red) marks sites of new actin incorporation. All actin filaments were labeled with FITC–phalloidin (green). Bar, 5 μm.

the balance from a dendritic organization toward parallel bundles of actin. Several considerations suggest that one likely candidate for this role is capping protein. First, it has been shown (DiNubile et al., 1995) that increasing the concentration of neutrophil extract, and thus concentration of added capping protein, inhibited the extent and rate of polymerization of actin on spectrin–actin seeds. Conversely, we interpret that in our system, star formation after dilution or glass depletion might be due to decreased capping protein concentration. Second, when bacterial motility was reconstituted from purified proteins, suboptimal concentrations of capping protein (35 nM) produced comet tails with a fish-bone appearance (Pantaloni et al., 2000), similar to chimeras observed in our samples in the transitional zone (Fig. 1 A).

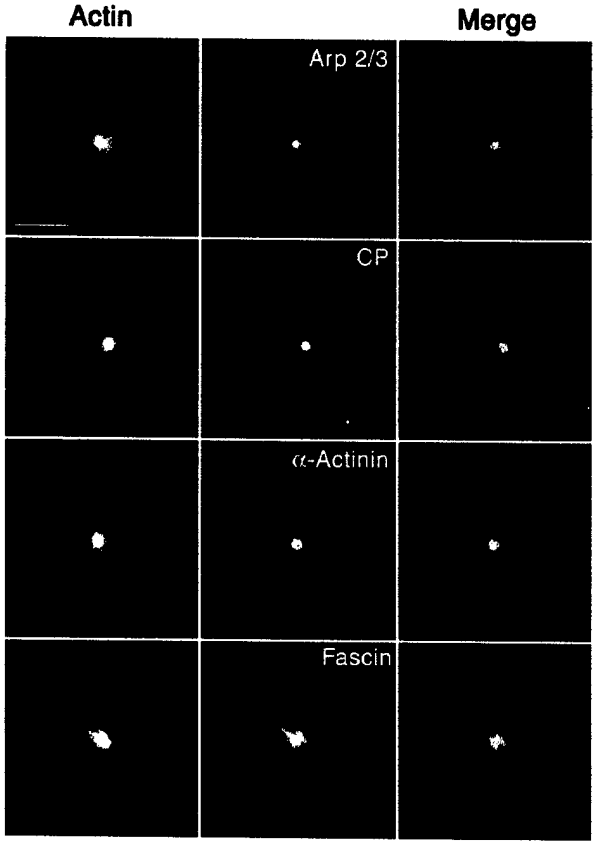

Figure 5. **Localization of actin binding proteins in stars.** Arp2/3 complex, capping protein, and α-actinin are enriched near the beads but not in bundles, whereas fascin is enriched in bundles but is not prominent at beads. Stars were labeled with rhodamine–actin (green) and FITC–α-actinin (red) during assembly. Immunostaining for Arp2/3 (p16 Arc), capping protein (β2), or fascin (red) was performed after fixation of stars. Bar, 5 μm.

Third, immunostaining for capping protein detected high levels of fluorescence on the coverslip (Fig. 3), suggesting that capping protein was adsorbed to the glass and thus depleted from the extract. Therefore, we investigated whether star formation was dependent on the concentration of capping protein in the extract.

Capping protein concentration was estimated in terms of a chicken capping protein standard by immunoblotting. Rat brain extracts contained 3.8 ng/μl (58 nM) and REF extracts contained 8 ng/μl (122 nM) capping protein (Fig. 6 A). The twofold higher concentration of capping protein in REF extracts was consistent with the twofold dilution of this extract required to produce stars. We were unable to estimate the concentration of capping protein in *Xenopus* oocyte extracts because of a lack of cross-reactivity of the antibodies used. The initial total protein concentration for all tested extracts was similar: brain extract, 16 mg/ml; REF, 21 mg/ml; and *Xenopus* oocyte, 24 mg/ml. Next, we examined how much capping protein was depleted from brain extract by its adsorption on ground glass. As assayed by immunoblotting, 35% of capping protein was depleted (Fig. 6 B), whereas actin was not depleted (0%) (Fig. 6 B), Arp2/3 was 18% depleted (Fig. 2 A), and fascin was only 8% depleted (unpublished data). These results demonstrate that glass absorbs motility proteins differentially and that capping protein is preferentially depleted.

Next, we supplemented 50% diluted brain extract with increasing amounts of exogenous capping protein. Capping protein inhibited star formation and facilitated cloud formation in a concentration-dependent manner (Fig. 6 C). In a kinetic analysis using time-lapse observation, addition of 50 nM capping protein to the extract (which normally produced mostly stars) blocked bundle formation around beads but allowed for continuous growth of actin clouds up to 20 times the bead diameter (Fig. 6 D). EM analysis of such clouds showed that actin filaments were organized into an extended dendritic network (Fig. 6 E). Higher concentrations of added capping protein, as expected, inhibited the extensive growth of clouds (unpublished data). At 400 nM capping protein, the diameter of the cloud was reduced to approximately twice the bead diameter. These results show that parallel bundle formation can be shifted to extended dendritic network formation by an optimal level of capping protein. As a specificity control, other proteins known to participate in actin dynamics were added to glass-depleted and diluted brain extracts. Addition of actin (7.5 μM), Arp2/3 complex (0.05, 0.1, and 0.6 μM), profilin (1.0, 2.5, and 10 μM), cofilin (2.5, 5.0, and 10 μM), and α-actinin (0.15, 0.25, 0.35, and 0.5 μM) did not affect star formation, whereas addition of 50 nM capping protein blocked star formation but allowed growth of actin clouds. These results show that capping protein was specific in antagonizing star formation.

Reconstitution of filopodia-like bundles using pure proteins

We tried to define a minimal set of components necessary for star assembly. Because data obtained with extracts indicated that Arp2/3 complex was necessary and capping protein had to be depleted, initial reconstitution experiments were performed with WASP-coated beads, actin, and Arp2/3 complex. Concentrations of proteins were based on published data for reconstitution of comet tails (Loisel et al., 1999). Beads coated with WASP were put into physiological ionic strength buffer solution, pH 7, containing rhodamine-labeled actin (6.9 μM) and increasing amounts of Arp2/3 complex over the range 0.1–0.9 μM. At 0.7 μM Arp2/3 complex and above, actin polymerization at the bead surface resulted in clouds within 15 min (Fig. 7 A). Clouds were ~3.2 mm in diameter (measured as full width at 1/e of maximum fluorescence) and were azimuthally homogeneous in intensity except for apparently stochastic fluctuations. Lower concentrations of Arp2/3 did not generate clouds or did so more slowly.

Because Arp2/3 alone was insufficient to induce stars, we then introduced a bundling protein. Fascin was selected to complement the reconstitution system because it is the major bundler in filopodia and in star bundles formed in extracts. Recombinant fascin was used in these experiments. Fascin was added to samples of WASP-coated beads preincubated with Arp2/3 complex (0.7 μM) and actin (6.9 μM)

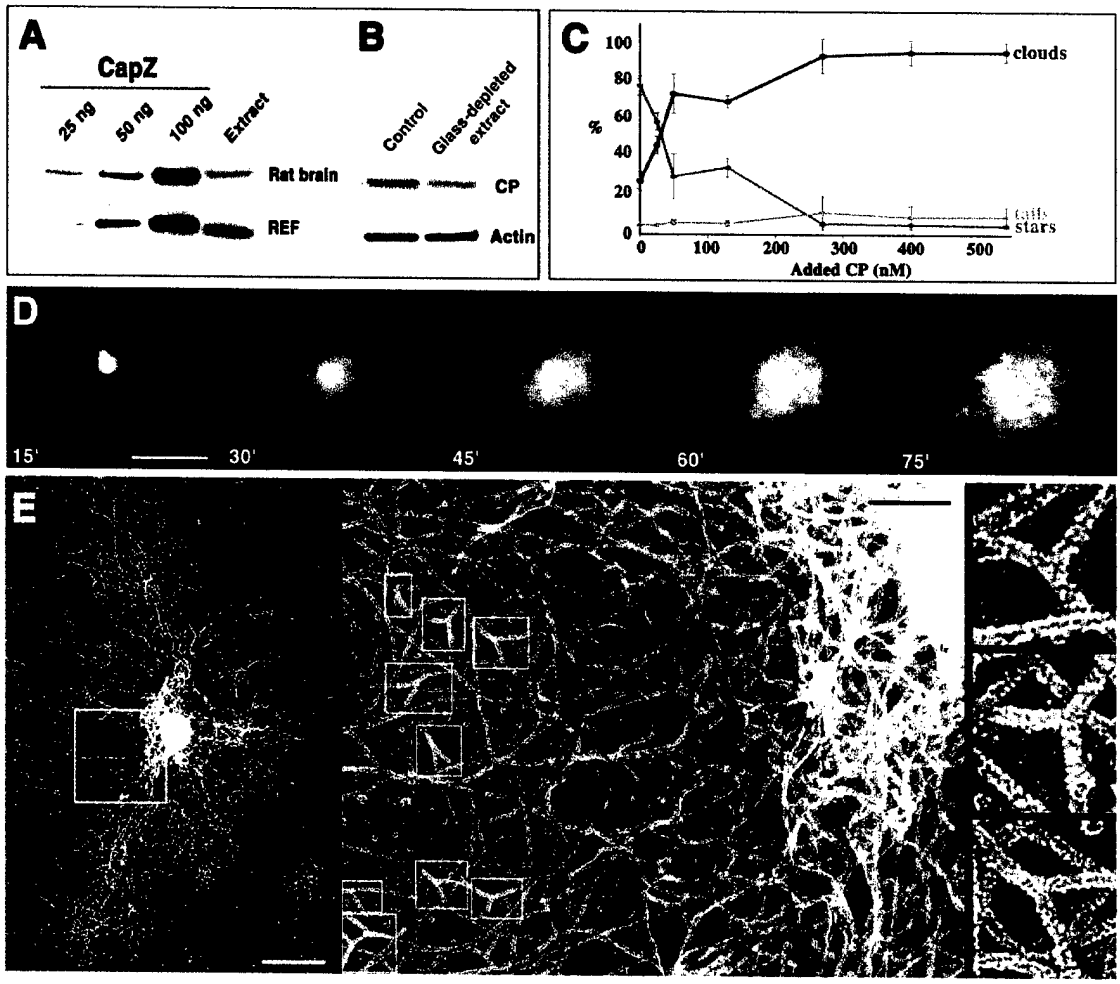

Figure 6. **Formation of stars depends on the concentration of capping protein.** (A) Capping protein concentration in rat brain and REF extracts (7.5 μl per lane) was determined by Western blotting. Purified CapZ was used as a standard at concentrations shown above the respective lanes. (B) Capping protein and actin concentration in control and glass-depleted brain extract. (C) Addition of capping protein inhibits star formation. Percentage of the indicated bead-associated structure (Y axis) is shown versus concentration of added capping protein (X axis) to the 50% diluted rat brain extract. (D) Addition of capping protein induces growth of clouds. Time-lapse sequence of actin assembly around a WASP-coated bead in 50% brain extract supplemented with 50 nM capping protein. Bar, 5 μm. (E) Dendritic organization of clouds formed after the addition of 50 nM capping protein to the 50% brain extract. Bar, 0.2 μm. Overview of the cloud is shown in the left panel. Bar, 1 μm. Examples of branched filaments are highlighted in boxes and enlarged in small right panels.

on ice for 20 min, and star formation was evaluated within 15 min incubation at RT. Increasing amounts of fascin promoted bundle formation both on beads and of filaments in the background. At 3.1 μM fascin, >95% of the beads showing actin polymerization displayed stars with straight, needle-like rays (Fig. 7 B). EM demonstrated that the star bundles formed in the presence of fascin were composed of long actin filaments that were packed tightly together (Fig. 7 C), similar to those of filopodia and bundles made in extracts. The actin cross-linking protein, α-actinin, also generated star-like structures, but they were qualitatively different from those induced by fascin. The bundles of α-actinin stars were wavy, not straight, and EM showed them to consist of loosely packed and cross-linked filaments (unpublished data), as previously reported for mixtures of α-actinin and actin (Jockusch and Isenberg, 1982). The reconstitution experiments demonstrate that in the absence of barbed-end capping, four components, WASP-coated beads, Arp2/3 complex, actin, and fascin, are sufficient for star formation.

Discussion

Formation of filopodia-like structures in vitro and initiation of filopodia in the cellular context (Svitkina et al., 2003) reveal remarkable similarities. A comparison of these two processes is presented in Fig. 8. The initial step, dendritic nucleation of actin filaments, is essentially the same in both cases. Nucleation is driven by activation of the Arp2/3 complex and results in the formation of new branches on preexisting filaments. Under conditions where capping activity is favored, filaments not specifically protected become terminated soon after nucleation, resulting in an overall dendritic organization, forming tails or clouds in the bead assay (Fig. 8, top left) and lamellipodia in cells

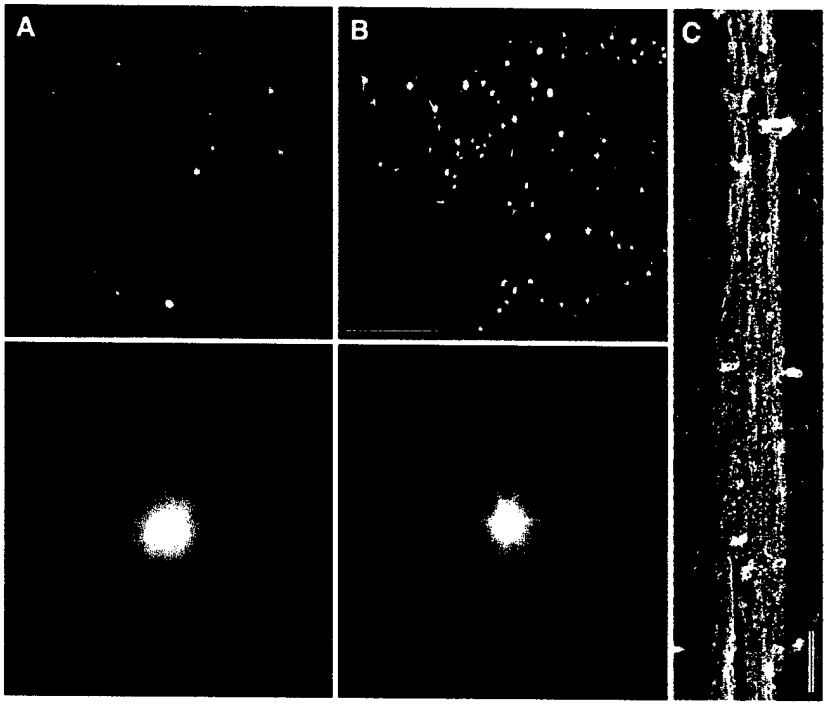

Figure 7. **Reconstitution of filopodia-like bundles from pure proteins.** Samples of WASP-coated beads preincubated on ice with 6.9 μM rhodamine-labeled actin and 0.7 μM Arp2/3 complex were brought to RT to allow for actin assembly. (A) Actin clouds formed in the absence of fascin. (B) Addition of 3.1 μM fascin to the sample before incubation at RT produced stars. Low magnification panels (top row) show distinctive pattern of actin assembly under each condition. (C) EM of star bundles formed in the presence of fascin as in B. Bars: (top row) 50 μM; (bottom row) 5 μm; (C) 100 nm.

(top right). In the in vitro system, using activator-coated beads, a reduced concentration of capping protein allows filaments to remain uncapped and continue elongation, followed by cross-linking into bundles to form stars (Fig. 8, bottom left). In the cellular context, where the cytoplasmic concentration of capping protein is presumably high, we postulate that filaments with barbed ends at the membrane are protected from capping, allowing them to elongate and be bundled to form filopodia (bottom right). Thus, we recognize three processes to be necessary for star or filopodia formation: nucleation, elongation, and bundling. These three processes and the molecules likely to be involved in them are discussed in turn.

Nucleation

The Arp2/3 complex is thought to play a role in filopodia formation because one of its activators, N-WASP, induces filopodia in cells (Miki et al., 1998). Because Arp2/3 is absent from established filopodia (Svitkina and Borisy, 1999; Svitkina et al., 2003), one may infer that it likely participates in initiation, not in steady-state elongation of filopodia. The question then becomes precisely how the Arp2/3 complex is involved in the initiation process. We suggest that our in vitro system for producing filopodia-like bundles reflects the situation in vivo and provides insights into the mechanism. First, formation of filopodia-like bundles, as well as dendritic clouds, depended on the presence and activity of the Arp2/3 complex. These findings agree with the observations in vivo, that perturbation of Arp2/3 complex function inhibits the formation of both lamellipodia and filopodia (Machesky and Insall, 1998; Li et al., 2002). Localization of Arp2/3 in stars was also analogous to the in vivo situation; it was present in dendritic arrays at the base of bundles, but not in bundles per se.

One possibility for how the action of the Arp2/3 complex can be explained is that it promotes dendritic or filopodial initiation depending upon the specific Arp activator. This

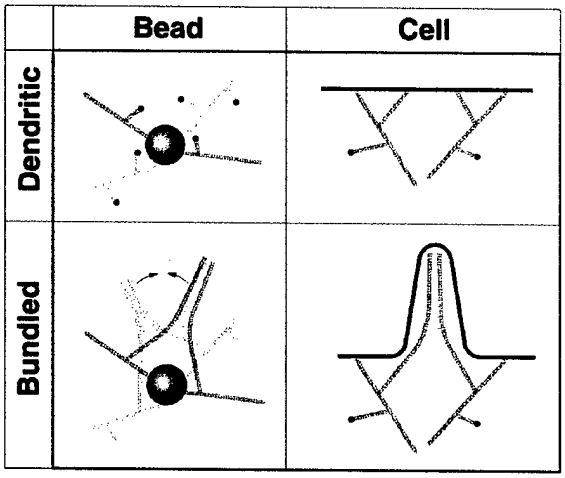

Figure 8. **Model for the formation of filopodial bundles.** We propose that filopodia are formed from a preexisting dendritic network by barbed-end elongation of actin filaments and their subsequent cross-linking into bundles. At normal levels of capping activity, clouds and tails are formed around the bead in the in vitro system (top left), and lamellipodia are formed in cells (top right). If the concentration of capping protein is lowered in the in vitro system, filaments elongate and become bundled by cross-linking proteins, e.g., fascin (bottom left). Two examples of cross-linking are presented. Thin bundles may further zipper into the thicker bundles (arrows). In the cell, some filament barbed ends at the membrane become protected from capping, perhaps by Ena/VASP proteins, so that they can elongate and be cross-linked to form bundles in filopodia (bottom right).

idea is consistent with findings that different members of the WASP family vary in their ability to activate the Arp2/3 complex (Zalevsky et al., 2001). However, we found no significant differences in the process of star formation when they were induced by a variety of Arp2/3 activators, including ActA, WASP, Scar, N-WASP, and the pVCA COOH-terminal domains of WASP and Scar. ActA was active both as endogenous bacterial protein and as a recombinant protein at the bead surface. Thus, our data do not support a model that Arp2/3 complex produces different arrays depending on the specific activator.

Our data are in agreement with a model in which the Arp2/3 complex, irrespective of its activator, produces a normal dendritic array, which subsequently becomes reorganized into bundles. Time-lapse observations showed that diffuse clouds with dendritic organization preceded the formation of bundles. Structural studies demonstrated a gradual transition from dendritic arrays around the bead to distal radial bundles. Both results suggest that a normal dendritic network serves as a precursor for bundles. These results are in close agreement with recent results elucidating the in vivo mechanism of filopodial initiation (Svitkina et al., 2003). We propose that the role of the Arp2/3 complex in the in vitro system is to supply barbed ends. The high local concentration of barbed ends created by activator-coated beads and the high concentration of Arp2/3 in solution were essential for bundle formation. A similar method may be used by cells if Arp2/3 activators (or molecules recruiting them) are not evenly distributed along the leading edge, but exist in clusters. A high local concentration of barbed ends could also be created by the clustering of some barbed end–binding molecules at the membrane. Possible candidates for such a role are members of the enabled/vasodilator-stimulated phosphoprotein (Ena/VASP) family (Bear et al., 2002; Svitkina et al., 2003) and formins (Pruyne et al., 2002), which have recently been shown to bind barbed ends but allow for filament elongation. Formins can also nucleate unbranched actin filaments (Pruyne et al., 2002; Sagot et al., 2002b) and thus are candidates for an alternative, Arp2/3-independent pathway of bundle initiation, similar to how actin cables in yeast are formed (Evangelista et al., 2002; Sagot et al., 2002a). However, this mechanism does not account for the N-WASP induction of filopodia.

Elongation

After filaments are nucleated, they have to elongate and encounter each other before they can form a bundle. A priori, elongation of filaments could be facilitated by increasing the concentration of an "elongation" factor or by decreasing the concentration of a "termination" factor. The main arguments in favor of the latter possibility are that star formation was induced in extracts by depletion of capping protein and was antagonized specifically by add-back of capping protein. A key point here is that add-back of capping protein to depleted extracts did not simply block all actin polymerization. Rather, it induced the formation of clouds as opposed to stars. Our interpretation is that cloud formation was the result of the termination of filament elongation shortly after branch nucleation under conditions when active Arp2/3 complex continuously nucleates new filaments. This process results in short filaments and a dense dendritic network. The fact that stars could be reconstituted in a pure protein system lacking barbed-end capping proteins but allowing for filament nucleation, elongation, and bundling is consistent with the interpretation that star formation was facilitated by decreasing a termination factor.

In the cellular context, the cytoplasmic concentration of capping protein is high (Huang et al., 1999). In lamellipodia where barbed ends are constantly being produced, the high concentration of capping protein can be understood as necessary to cap unproductive barbed ends. In filopodia where filaments elongate continuously, their barbed ends need to be protected from capping. Protection may be provided by Ena/VASP family proteins because they are present at the extreme leading edge, bind to barbed ends, and can antagonize capping in vitro and in vivo (Bear et al., 2002). Ena/VASP proteins are also enriched at the tips of filopodia (Lanier et al., 1999; Rottner et al., 1999) and become gradually accumulated at the tips of filopodial precursors during the filopodial initiation (Svitkina et al., 2003). It is attractive to speculate that the presence of Ena/VASP at the filopodial tips in the cellular context prevents filament termination and allows filopodial elongation. Consistent with this idea, our results showing that the level of capping protein controls the transition between two types of actin arrays in vitro match the observations that the level of Ena/VASP proteins performs analogous control in vivo, but in the opposite direction. That is, a low level of Ena/VASP induced short branched filaments, and an excess of Ena/VASP promoted the formation of long filaments (Bear et al., 2002).

In our in vitro system, the rates of bundle elongation in stars were ~0.15 μm/min, similar to the reported rates of comet tail motility in undiluted brain extracts (0.2–0.3 μm/min) (Laurent et al., 1999; Yarar et al., 1999). Whereas in *Xenopus* oocyte extract or during leading edge protrusion in cells, the rates of actin array assembly are at least an order of magnitude higher (Mallavarapu and Mitchison, 1999). These observations indicate that additional factors may contribute to the overall performance of actin machinery, but balance between nucleation and elongation seems to be critical for the determination of supramolecular organization of the actin array.

Bundling

Bundling is necessary to allow long filaments to push efficiently without buckling under the cell surface. The leading candidate for filament bundling in filopodia is fascin. It shows the greatest enrichment in filopodial bundles in cells (Kureishy et al., 2002), where it significantly prevails over α-actinin (Svitkina et al., 2003), and it is essential for the maintenance of filopodia (Yamashiro et al., 1998; Adams et al., 1999; Cohan et al., 2001).

Consistent with in vivo data, we found that fascin was the major bundling protein present in stars assembled in cytoplasmic extracts. Fascin was also sufficient to form filopodia-like bundles in a reconstitution system in which fascin represented the only bundling protein. The straightness of the fascin-induced star bundles suggests that they were quite rigid, similar to filopodia. In contrast to fascin, the other actin filament cross-linker, α-actinin, was more abundant in

the dendritic network surrounding beads and was absent from star bundles. Although α-actinin was also able to drive star assembly in a reconstitution system, the resulting star bundles had wavy rays and a dendritic, not parallel bundled, organization. Thus, α-actinin did not recapitulate filopodia formation in vitro. These results suggest that the two cross-linkers may be specialized with respect to the particular actin filament array that they stabilize. Segregation of fascin and α-actinin to bundles and the dendritic network, respectively, correlates with the biochemical properties of these two cross-linkers: fascin is a short cross-linker that makes tight parallel bundles (Yamashiro-Matsumura and Matsumura, 1985) and α-actinin is a longer molecule that, when combined with actin, makes loose bundles with both parallel and antiparallel filament orientation. The absence of α-actinin in filopodial bundles in more complex systems, such as extracts or cells, when both proteins are present may be explained as fascin outcompeting α-actinin because of a slightly higher affinity or, possibly, specific recruitment to areas of filopodial assembly.

In the course of star formation, we frequently observed zippering of radial bundles, an effect that superficially resembles fusion of filopodia during their normal dynamics in cells. However, distinctions between these two phenomena should be noted. In cells, the fusion site moves backward because of treadmilling and retrograde flow of the whole assembly, but no actual displacement of bundles, with respect to each other, occurs. In stars, we did not find independent indications of retrograde flow, suggesting that zippering in vitro actually brings distant bundles together. A likely reason for the difference between the two systems is that the movement of bundles in vivo is precluded by the more crowded conditions and cross-linking occurring in the cytoplasm, compared with extracts. Nevertheless, the similarity of the systems suggests that cross-linking molecules, presumably fascin, have a potential for zippering and may accomplish this function under permissive circumstances, for formation of bundles in vitro and for filopodia in vivo.

In summary, our results suggest that an Arp2/3-mediated pathway is compatible with filopodia formation, and that it is not necessary to postulate unusual properties of WASP family members to stimulate a nonbranching mode of actin filament formation. Filopodia-like structures can be accounted for as a transformation from a dendritic organization by a combination of elongation and bundling.

Materials and methods

Proteins

Actin was purified from rabbit muscle as previously described (Spudich and Watt, 1971). Rhodamine–actin was prepared by labeling actin with *N*-hydroxy succinimido-rhodamine (Molecular Probes) as previously described (Isambert et al., 1995) and stored at −80°C. Before use, labeled G-actin was recycled by polymerization for 2 h on ice in the presence of 50 mM KCl, 2 mM $MgCl_2$, and 1 mM ATP, sedimentation at 100,000 *g* for 1.5 h at 4°C, resuspension in cold G buffer (2 mM Tris-Cl, 0.2 mM $CaCl_2$, 0.2 mM ATP, and 0.5 mM DTT) to a final concentration of 2 mg/ml, and dialysis overnight against G buffer using microdialysis buttons (Hampton Research) and dialysis tubing (Pierce Chemical Co.).

DNA encoding WASP tagged at its NH_2 terminus with both Met, Arg, Gly, Ser (MRGS) 6xHis and FLAG epitopes was amplified by PCR from a human WASP cDNA (a gift of Arie Abo, PPD Discovery, Menlo Park, CA) and subcloned into pFastBac1 (Life Technologies; Amersham Biosciences). DNA encoding human Scar1 was amplified by PCR and subcloned into the WASP-pFastbac1 vector in the place of the WASP DNA. Recombinant WASP and Scar1 proteins were expressed in Sf9 cells using the baculovirus system. Baculovirus strains were generated and used for infections according to the Bac-to-Bac baculovirus expression system (Life Technologies). After 72 h of infection, cells were harvested by centrifugation at 500 *g* for 10 min at 25°C, resuspended in lysis buffer (50 mM NaH_2PO_4, pH 8.0, 300 mM KCl) with protease inhibitors (1 mM PMSF and 10 μg/ml leupeptin, pepstatin, and chymostatin [LPC]), and frozen in liquid N_2. To prepare the lysate, cells were thawed and centrifuged at 200,000 *g* for 15 min at 4°C.

To purify the recombinant proteins, Sf9 lysates were supplemented with 20 mM imidazole, incubated with Ni-NTA agarose (QIAGEN) resin for 45 min at 4°C, washed with 50 mM NaH_2PO_4, pH 8.0, 300 mM KCl, 20 mM imidazole, and eluted with 200 mM imidazole, 50 mM NaH_2PO_4, pH 8.0, 300 mM KCl, and protease inhibitors. Eluted proteins were further purified by gel filtration chromatography on a Superdex-200 column (Amersham Biosciences) equilibrated with 20 mM MOPS, pH 7.0, 100 mM KCl, 2 mM $MgCl_2$, 5 mM EGTA, 1 mM EDTA, 0.2 mM ATP, 0.5 mM DTT, 10% vol/vol glycerol. Full-length recombinant WASP has constitutive ability to activate Arp2/3 complex (Higgs and Pollard, 2001).

DNA encoding human fascin was amplified by PCR and sublcloned into the pGEX-4T-3 vector (Amersham Biosciences) using BamH1/Xho I sites. Recombinant human fascin was prepared by a modification of the method of Ono et al. (1997). *E. coli* carrying the plasmid was grown at 37°C until the A600 reached 0.6. Protein expression was induced by adding 0.1 mM IPTG at 20°C for 4 h. Cells were harvested by centrifugation and extracted with B-PER in phosphate buffer (Pierce Chemical Co.) plus 1 mM PMSF and 1 mM DTT. The lysate was centrifuged at 20,000 *g* for 20 min, and the supernatant was mixed for 1 h at RT with 2 ml glutathione–Sepharose 4B (Amersham Biosciences) equilibrated with PBS plus 1 mM DTT. The glutathione-Sepharose was poured into a column and washed with 20 ml of PBS plus 1 mM DTT. 80 μl of thrombin (Amersham Biosciences) was added, and digestion was allowed to proceed overnight at 4°C. Flowthrough fractions were collected in 2 mM PMSF and concentrated by Centricon 10 (Amicon).

Arp2/3 was purified from bovine brain as described by Laurent et al. (1999). Recombinant chicken CapZ (Soeno et al., 1998; Palmgren et al., 2001) was provided by John Cooper (Washington University School of Medicine, St. Louis, MO). FITC-labeled α-actinin was provided by Marion Greaser (University of Wisconsin, Madison, WI). ActA protein (Cameron et al., 1999) was provided by Julie Theriot (Stanford University School of Medicine, Stanford, CA). Recombinant human cofilin and human profilin were purchased from Cytoskeleton, Inc.

Cytoplasmic extracts

Rat brain extract was prepared as previously described (Laurent et al., 1999). Metaphase *Xenopus* oocyte extract was prepared as previously described (Murray, 1991) and kept frozen at −80°C. Before use, it was centrifuged at 100,000 *g* for 1 h at 4°C, and the supernatant was used for experiments. Rat embryonic fibroblast extract was prepared as described by Saoudi et al. (1998).

Actin polymerization bead assay

Carboxylated polystyrene beads (Polysciences) were coated with ActA as previously described (Cameron et al., 1999). For coating beads with WASP/Scar proteins, we took 15 μl of 0.5 μM WASP or Scar proteins, mixed up with 15 μl of brain buffer (BB) (Laurent et al., 1999) or *Xenopus* buffer (Murray, 1991) and 0.5 μl of 0.5-μm carboxylated polystyrene beads. This mixture was incubated at RT for 1 h. Beads were washed twice with the appropriate buffer and resuspended in 10 μl of buffer. For longer storage, beads were supplemented with 50% glycerol and placed at −80°C.

Coated beads (0.5 μl) were introduced into 10 μl of cell extract supplemented with energy mix (15 mM creatine phosphate, 2 mM ATP, and 2 mM $MgCl_2$) and 1.25 μM rhodamine-labeled actin. In experiments to evaluate the effect of capping protein concentration, the assay mix was supplemented with increasing amounts of capping protein. The assay mix was incubated on ice for 1 h before preparation for observation.

For reconstitution system, 0.5 μl of coated beads was introduced in 1× KME buffer (50 mM KCl, 1 mM $MgCl_2$, 1 mM EGTA, 10 mM imidazole, pH 7) supplemented with Arp2/3 complex. After incubation for 5 min at RT, 6.9 μM actin was added, and the mixture was incubated on ice for 20 min before the addition of fascin and allowing for actin assembly at RT.

Microscopy

For light microscopy, a 1-μl sample was removed and pressed tightly between a microscope slide and a 22-mm square glass to create a chamber ~5

μm thick, which was then sealed with vaseline/lanolin/paraffin (at 1:1:1). Samples were incubated at RT for 15 min and then observed with a Nikon Eclipse inverted microscope equipped with phase contrast and epifluorescence optics. Time-lapse images were acquired with a back-thinned CCD camera (CH250; Photometrics) using METAMORPH (Universal Imaging Corp.) software. Fluorescence images were recorded every 5 min for 2 h.

For EM, samples were prepared as described by Cameron et al. (2001). After incubation for 2 h at RT in a humid environment, chambers were opened into solution containing 0.2% Triton X-100 and 2 μM phalloidin in BB. Although some stars were washed out during this procedure, some remained attached to the coverslip. Coverslips were washed with 2 μM phalloidin in BB, fixed with 2% glutaraldehyde, and processed for EM. Procedures for S1 decoration and EM were as previously described (Svitkina and Borisy, 1998). Polarity of filaments, determined in blind experiments by two independent observers, gave similar results.

Immunostaining

Rabbit polyclonal antibody to the Arc p16 subunit of the Arp2/3 complex was prepared against the RFRKVDVDEYDENKFVDEED peptide of the human sequence. By Western blotting, the affinity-purified antibody recognized in rat brain extract a doublet of closely spaced bands in the16-kD range, supposedly corresponding to two isoforms of Arc p16 (Millard et al., 2003). Polyclonal rabbit antibody against capping protein (R22) was provided by Dorothy A. Schafer (University of Virginia, Charlottesville, VA). Mouse monoclonal α-actinin antibody was from Sigma-Aldrich, and mouse monoclonal fascin antibody was from DakoCytomation. Immunostaining was performed in perfusion chambers. Solutions were applied on one side of the chamber with a pipet and withdrawn from the other side with filter paper. A 4-μl assay sample was sandwiched between a glass slide and a coverslip (22 × 22 mm) separated by two strips of teflon tape and sealed. Stars were allowed to form for 2 h at RT in humid conditions. 10 μl of BB containing 0.2% Triton X-100 and 2 μM phalloidin was perfused through the chamber, followed by 10 μl of 2 μM phalloidin in BB. For most immunostaining experiments, stars were fixed with 0.2% glutaraldehyde for 20 min at RT, washed with PBS, and quenched for 20 min with 2 mg/ml of $NaBH_4$ in PBS supplemented with 0.1% Tween 20. For fascin staining, samples were fixed with methanol for 10 min at −20°C.

Pulse-labeling assay

Stars were allowed to form for 1 h in a perfusion chamber containing 4 μl of assay sample without labeled actin. Then 1 μl of 1.8 μM rhodamine–actin was added by diffusion from the edge. After 10 min, FITC–phalloidin was added in the same way to label all actin filaments. The chamber was sealed, and observations were made after 10 min of incubation at RT.

Glass depletion experiment

30 μl of brain extract was applied to 70 mg of ground glass coverslip in a mini filtration tube (0.65 μm; UltraFree-MC; Millipore), and the filtrate was collected by centrifugation twice for 1 min at 11,000 *g*.

Depletion of Arp2/3 complex

Arp2/3 complex was depleted from glass-depleted brain extract using a variation of the method described by Egile et al. (1999). 15 μl of glutathione-Sepharose–coupled GST–VCA beads was incubated with 40 μl of brain extract for 30 min at 4°C on a rotating wheel. Beads were pelleted at 10,000 *g* for 2 min. Mock depletion is performed by the same amount of glutathione-Sepharose beads. Depletion of the Arp2/3 complex was monitored by Western blotting of aliquots of extracts and beads. The add-back experiment was performed using the Arp2/3 complex purified from bovine brain. For the microscopy assay, we scored the percentage of stars assembled on all beads.

Quantification of capping protein in cell extracts by Western blotting

Different amounts of rat brain and rat embryonic fibroblast extracts were subjected to SDS-PAGE (4–20% polyacrylamide) and immunoblotting with anti-CapZ. The amount of capping protein present was evaluated by comparing the intensity of the bands of each sample with the chicken CapZ standard by densitometry using NIH image software.

We thank Drs. Julie Theriot, Dorothy Schafer, John Cooper, Marie-France Carlier, Josephine Adams, Marion Greaser, and Elena S. Nadezhdina for generous gifts of reagents and bacterial strains. We also thank Dr. Tom Keating and members of the Borisy laboratory for constructive discussions.

This work was supported by United States Army USAMRMC grant DAMD 17-00-1-0386 (D. Vignjevic), National Institutes of Health (NIH) grant GM 62431 (G.G. Borisy), and NIH Glue Grant on Cell Migration IU 54 GM 63126.

Submitted: 12 August 2002
Revised: 24 January 2003
Accepted: 24 January 2003

References

Adams, J.C., J.D. Clelland, G.D. Collett, F. Matsumura, S. Yamashiro, and L. Zhang. 1999. Cell-matrix adhesions differentially regulate fascin phosphorylation. *Mol. Biol. Cell.* 10:4177–4190.

Bear, J.E., T.M. Svitkina, M. Krause, D.A. Schafer, J.J. Loureiro, G.A. Strasser, I.V. Maly, O.Y. Chaga, J.A. Cooper, G.G. Borisy, and F.B. Gertler. 2002. Antagonism between Ena/VASP proteins and actin filament capping regulates fibroblast motility. *Cell.* 109:509–521.

Borisy, G.G., and T.M. Svitkina. 2000. Actin machinery: pushing the envelope. *Curr. Opin. Cell Biol.* 12:104–112.

Cameron, L.A., M.J. Footer, A. van Oudenaarden, and J.A. Theriot. 1999. Motility of ActA protein-coated microspheres driven by actin polymerization. *Proc. Natl. Acad. Sci. USA.* 96:4908–4913.

Cameron, L.A., P.A. Giardini, F.S. Soo, and J.A. Theriot. 2000. Secrets of actin-based motility revealed by a bacterial pathogen. *Nat. Rev. Mol. Cell Biol.* 1:110–119.

Cameron, L.A., T.M. Svitkina, D. Vignjevic, J.A. Theriot, and G.G. Borisy. 2001. Dendritic organization of actin comet tails. *Curr. Biol.* 11:130–135.

Cohan, C.S., E.A. Welnhofer, L. Zhao, F. Matsumura, and S. Yamashiro. 2001. Role of the actin bundling protein fascin in growth cone morphogenesis: localization in filopodia and lamellipodia. *Cell Motil. Cytoskeleton.* 48:109–120.

Cooper, J.A., and D.A. Schafer. 2000. Control of actin assembly and disassembly at filament ends. *Curr. Opin. Cell Biol.* 12:97–103.

DiNubile, M.J., L. Cassimeris, M. Joyce, and S.H. Zigmond. 1995. Actin filament barbed-end capping activity in neutrophil lysates: the role of capping protein-β2. *Mol. Biol. Cell.* 6:1659–1671.

Egile, C., T.P. Loisel, V. Laurent, R. Li, D. Pantaloni, P.J. Sansonetti, and M.F. Carlier. 1999. Activation of the CDC42 effector N-WASP by the *Shigella flexneri* IcsA protein promotes actin nucleation by Arp2/3 complex and bacterial actin-based motility. *J. Cell Biol.* 146:1319–1332.

Evangelista, M., D. Pruyne, D.C. Amberg, C. Boone, and A. Bretscher. 2002. Formins direct Arp2/3-independent actin filament assembly to polarize cell growth in yeast. *Nat. Cell Biol.* 4:32–41.

Goldberg, M.B. 2001. Actin-based motility of intracellular microbial pathogens. *Microbiol. Mol. Biol. Rev.* 65:595–626 (table of contents).

Higgs, H.N., and T.D. Pollard. 2001. Regulation of actin filament network formation through ARP2/3 complex: activation by a diverse array of proteins. *Annu. Rev. Biochem.* 70:649–676.

Huang, M., C. Yang, D.A. Schafer, J.A. Cooper, H.N. Higgs, and S.H. Zigmond. 1999. Cdc42-induced actin filaments are protected from capping protein. *Curr. Biol.* 9:979–982.

Isambert, H., P. Venier, A.C. Maggs, A. Fattoum, R. Kassab, D. Pantaloni, and M.F. Carlier. 1995. Flexibility of actin filaments derived from thermal fluctuations. Effect of bound nucleotide, phalloidin, and muscle regulatory proteins. *J. Biol. Chem.* 270:11437–11444.

Jockusch, B.M., and G. Isenberg. 1982. Vinculin and α-actinin: interaction with actin and effect on microfilament network formation. *Cold Spring Harb. Symp. Quant. Biol.* 46:613–623.

Kureishy, N., V. Sapountzi, S. Prag, N. Anilkumar, and J.C. Adams. 2002. Fascins, and their roles in cell structure and function. *Bioessays.* 24:350–361.

Langanger, G., J. de Mey, M. Moeremans, G. Daneels, M. de Brabander, and J.V. Small. 1984. Ultrastructural localization of α-actinin and filamin in cultured cells with the immunogold staining (IGS) method. *J. Cell Biol.* 99:1324–1334.

Lanier, L.M., M.A. Gates, W. Witke, A.S. Menzies, A.M. Wehman, J.D. Macklis, D. Kwiatkowski, P. Soriano, and F.B. Gertler. 1999. Mena is required for neurulation and commissure formation. *Neuron.* 22:313–325.

Laurent, V., T.P. Loisel, B. Harbeck, A. Wehman, L. Grobe, B.M. Jockusch, J. Wehland, F.B. Gertler, and M.F. Carlier. 1999. Role of proteins of the Ena/VASP family in actin-based motility of *Listeria monocytogenes*. *J. Cell Biol.* 144:1245–1258.

Lewis, A.K., and P.C. Bridgman. 1992. Nerve growth cone lamellipodia contain

two populations of actin filaments that differ in organization and polarity. *J. Cell Biol.* 119:1219–1243.

Li, Z., E.S. Kim, and E.L. Bearer. 2002. Arp2/3 complex is required for actin polymerization during platelet shape change. *Blood.* 99:4466–4474.

Loisel, T.P., R. Boujemaa, D. Pantaloni, and M.F. Carlier. 1999. Reconstitution of actin-based motility of *Listeria* and *Shigella* using pure proteins. *Nature.* 401: 613–616 (see comments).

Machesky, L.M., and R.H. Insall. 1998. Scar1 and the related Wiskott-Aldrich syndrome protein, WASP, regulate the actin cytoskeleton through the Arp2/3 complex. *Curr. Biol.* 8:1347–1356.

Millard, T.H., B. Behrendt, S. Launay, K. Futterer, and L.M. Machesky. 2003. Identification and characterisation of a novel human isoform of Arp2/3 complex subunit p16-ARC/ARPC5. *Cell Motil. Cytoskeleton.* 54:81–90.

Mallavarapu, A., and T. Mitchison. 1999. Regulated actin cytoskeleton assembly at filopodium tips controls their extension and retraction. *J. Cell Biol.* 146: 1097–1106.

Miki, H., T. Sasaki, Y. Takai, and T. Takenawa. 1998. Induction of filopodium formation by a WASP-related actin-depolymerizing protein N-WASP. *Nature.* 391:93–96.

Mullins, R.D., J.A. Heuser, and T.D. Pollard. 1998. The interaction of Arp2/3 complex with actin: nucleation, high affinity pointed end capping, and formation of branching networks of filaments. *Proc. Natl. Acad. Sci. USA.* 95: 6181–6186.

Murray, A.W. 1991. Cell cycle extracts. *Methods Cell Biol.* 36:581–605.

Ono, S., Y. Yamakita, S. Yamashiro, P.T. Matsudaira, J.R. Gnarra, T. Obinata, and F. Matsumura. 1997. Identification of an actin binding region and a protein kinase C phosphorylation site on human fascin. *J. Biol. Chem.* 272: 2527–2533.

Palmgren, S., P.J. Ojala, M.A. Wear, J.A. Cooper, and P. Lappalainen. 2001. Interactions with PIP2, ADP-actin monomers, and capping protein regulate the activity and localization of yeast twinfilin. *J. Cell Biol.* 155:251–260.

Pantaloni, D., R. Boujemaa, D. Didry, P. Gounon, and M.F. Carlier. 2000. The Arp2/3 complex branches filament barbed ends: functional antagonism with capping proteins. *Nat. Cell Biol.* 2:385–391.

Pruyne, D., M. Evangelista, C. Yang, E. Bi, S. Zigmond, A. Bretscher, and C. Boone. 2002. Role of formins in actin assembly: nucleation and barbed-end association. *Science.* 297:612–615.

Rottner, K., B. Behrendt, J.V. Small, and J. Wehland. 1999. VASP dynamics during lamellipodia protrusion. *Nat. Cell Biol.* 1:321–322.

Sagot, I., S.K. Klee, and D. Pellman. 2002a. Yeast formins regulate cell polarity by controlling the assembly of actin cables. *Nat. Cell Biol.* 4:42–50.

Sagot, I., A.A. Rodal, J. Moseley, B.L. Goode, and D. Pellman. 2002b. An actin nucleation mechanism mediated by Bni1 and profilin. *Nat. Cell Biol.* 4:626–631.

Saoudi, Y., R. Fotedar, A. Abrieu, M. Doree, J. Wehland, R.L. Margolis, and D. Job. 1998. Stepwise reconstitution of interphase microtubule dynamics in permeabilized cells and comparison to dynamic mechanisms in intact cells. *J. Cell Biol.* 142:1519–1532.

Small, J.V., G. Isenberg, and J.E. Celis. 1978. Polarity of actin at the leading edge of cultured cells. *Nature.* 272:638–639.

Small, J.V., M. Herzog, M. Haner, and U. Abei. 1994. Visualization of actin filaments in keratocyte lamellipodia: negative staining compared with freeze-drying. *J. Struct. Biol.* 113:135–141.

Small, J.V., T. Stradal, E. Vignal, and K. Rottner. 2002. The lamellipodium: where motility begins. *Trends Cell Biol.* 12:112–120.

Soeno, Y., H. Abe, S. Kimura, K. Maruyama, and T. Obinata. 1998. Generation of functional β-actinin (CapZ) in an *E. coli* expression system. *J. Muscle Res. Cell Motil.* 19:639–646.

Spudich, J.A., and S. Watt. 1971. The regulation of rabbit skeletal muscle contraction. I. Biochemical studies of the interaction of the tropomyosin-troponin complex with actin and the proteolytic fragments of myosin. *J. Biol. Chem.* 246:4866–4871.

Svitkina, T.M., and G.G. Borisy. 1998. Correlative light and electron microscopy of the cytoskeleton of cultured cells. *Methods Enzymol.* 298:570–592.

Svitkina, T.M., and G.G. Borisy. 1999. Arp2/3 complex and actin depolymerizing factor/cofilin in dendritic organization and treadmilling of actin filament array in lamellipodia. *J. Cell Biol.* 145:1009–1026.

Svitkina, T.M., A.B. Verkhovsky, K.M. McQuade, and G.G. Borisy. 1997. Analysis of the actin-myosin II system in fish epidermal keratocytes: mechanism of cell body translocation. *J. Cell Biol.* 139:397–415.

Svitkina, T.M., Bulanova E.A., Chaga O.Y., Vignjevic D., Kojima S., Vasiliev J.M., and Borisy G.G. 2003. Mechanism of filopodia initiation by reorganization of a dendritic network. *J. Cell Biol.* 160:409–421.

Theriot, J.A., J. Rosenblatt, D.A. Portnoy, P.J. Goldschmidt-Clermont, and T.J. Mitchison. 1994. Involvement of profilin in the actin-based motility of *L. monocytogenes* in cells and in cell-free extracts. *Cell.* 76:505–517.

Yamashiro, S., Y. Yamakita, S. Ono, and F. Matsumura. 1998. Fascin, an actin-bundling protein, induces membrane protrusions and increases cell motility of epithelial cells. *Mol. Biol. Cell.* 9:993–1006.

Yamashiro-Matsumura, S., and F. Matsumura. 1985. Purification and characterization of an F-actin-bundling 55-kilodalton protein from HeLa cells. *J. Biol. Chem.* 260:5087–5097.

Yarar, D., W. To, A. Abo, and M.D. Welch. 1999. The Wiskott-Aldrich syndrome protein directs actin-based motility by stimulating actin nucleation with the Arp2/3 complex. *Curr. Biol.* 9:555–558.

Zalevsky, J., L. Lempert, H. Kranitz, and R.D. Mullins. 2001. Different WASP family proteins stimulate different Arp2/3 complex-dependent actin-nucleating activities. *Curr. Biol.* 11:1903–1913.

Article

Mechanism of filopodia initiation by reorganization of a dendritic network

Tatyana M. Svitkina,[1] Elena A. Bulanova,[2] Oleg Y. Chaga,[1] Danijela M. Vignjevic,[1] Shin-ichiro Kojima,[1] Jury M. Vasiliev,[2] and Gary G. Borisy[1]

[1]Department of Cell and Molecular Biology, Northwestern University Medical School, Chicago, Illinois 60611
[2]Institute of Mechanisms of Carcinogenesis, Cancer Research Center of Russian Federation, 115478 Moscow, Russia

A filopodium protrudes by elongation of bundled actin filaments in its core. However, the mechanism of filopodia initiation remains unknown. Using live-cell imaging with GFP-tagged proteins and correlative electron microscopy, we performed a kinetic-structural analysis of filopodial initiation in B16F1 melanoma cells. Filopodial bundles arose not by a specific nucleation event, but by reorganization of the lamellipodial dendritic network analogous to fusion of established filopodia but occurring at the level of individual filaments. Subsets of independently nucleated lamellipodial filaments elongated and gradually associated with each other at their barbed ends, leading to formation of cone-shaped structures that we term Λ-precursors. An early marker of initiation was the gradual coalescence of GFP-vasodilator-stimulated phosphoprotein (GFP-VASP) fluorescence at the leading edge into discrete foci. The GFP-VASP foci were associated with Λ-precursors, whereas Arp2/3 was not. Subsequent recruitment of fascin to the clustered barbed ends of Λ-precursors initiated filament bundling and completed formation of the nascent filopodium. We propose a convergent elongation model of filopodia initiation, stipulating that filaments within the lamellipodial dendritic network acquire privileged status by binding a set of molecules (including VASP) to their barbed ends, which protect them from capping and mediate association of barbed ends with each other.

Introduction

The crawling movement of a cell involves protrusion of its leading edge coordinated with translocation of its cell body. Protrusion is driven by polymerization of actin within two organelles, lamellipodia and filopodia, which have strikingly different designs of the actin polymerization machinery and are regulated by different signaling pathways (Hall, 1998; Svitkina and Borisy, 1999b).

In lamellipodia, which are broad, flat protrusions, actin filaments form a branched network (Svitkina et al., 1997; Svitkina and Borisy, 1999a). The current model for lamellipodial dynamics (Borisy and Svitkina, 2000; Pollard et al., 2000) suggests that treadmilling of the branched actin filament array consists of repeated cycles of dendritic nucleation, elongation, capping, and depolymerization of filaments. Dendritic nucleation is mediated by the Arp2/3 complex, which is activated by members of WASP family (Higgs and Pollard, 2001). During a period of elongation after nucleation, the filament pushes the membrane. When a filament elongates beyond the efficient length for pushing, its growth is thought to be terminated by capping protein (Cooper and Schafer, 2000). Depolymerization is assisted by proteins of the ADF/cofilin family (Bamburg, 1999). Other proteins play supporting roles in this process. Profilin targets filament elongation to barbed ends (Carlier and Pantaloni, 1997), enabled/vasodilator-stimulated phosphoprotein (Ena/VASP)* family proteins protect elongating barbed ends from capping (Bear et al., 2002), cortactin stabilizes branches (Weaver et al., 2001), and filamin A (Flanagan et al., 2001) and α-actinin stabilize and consolidate the whole network.

In filopodia, which are thin cellular processes, actin filaments are long, parallel, and organized into tight bundles (Small, 1988; Lewis and Bridgman, 1992; Small et al., 2002). Other cellular structures, such as microspikes and retraction fibers, bear similarities to filopodia and may be related to them. Microspikes are parallel actin bundles within the lamellipodium. Retraction fibers are long, thin cellular processes that remain attached to the substratum after cell withdrawal.

Address correspondence to Tatyana M. Svitkina, Department of Cell and Molecular Biology, Northwestern University Medical School, 303 E. Chicago Ave., Ward 8-063, Chicago, IL 60611. Tel.: (312) 503-2854 Fax: (312) 501-7912. E-mail: t-svitkina@northwestern.edu

Key words: actin; Arp2/3; VASP; fascin; lamellipodia

*Abbreviations used in this paper: EM, electron microscopy; Ena/VASP, enabled/vasodilator-stimulated phosphoprotein.

The Journal of Cell Biology, Volume 160, Number 3, February 3, 2003 409–421
http://www.jcb.org/cgi/doi/10.1083/jcb.200210174

The Journal of Cell Biology

They also contain a parallel bundle of actin filaments (Small, 1988; Lewis and Bridgman, 1992; Svitkina et al., 1997). Filopodial protrusion is thought to occur by a filament treadmilling mechanism, which was originally proposed for both filopodia and lamellipodia (Small, 1994). According to this model, all actin filaments within a bundle elongate at their barbed ends and release subunits from their pointed ends. Existing experimental data support this model of filopodial elongation. Structurally, actin filaments in filopodia are long and unbranched (Svitkina and Borisy, 1999a), suggesting that assembly occurs by elongation, not by branched nucleation. Dynamic observations (Mallavarapu and Mitchison, 1999) revealed that labeled actin incorporated at the filopodial tips, moved backward, and dissipated at the rear (as predicted by a treadmilling mechanism), and that actin turnover in filopodia was slow; consistent with the idea of long filaments adding or losing subunits only at their ends. A frequent event in filopodial behavior is their fusion, which frequently occurs as elongating oblique bundles collide and subsequently grow as a single unit (Katoh et al., 1999b; Small et al., 2002).

A set of molecules essential for filopodial protrusion has not been explicitly determined. However, some proteins are enriched in filopodia, suggesting that they play important roles. One of them is a cross-linking protein (fascin) that mediates filament bundling (Bartles, 2000; Kureishy et al., 2002). Many different proteins are enriched at filopodial tips (Small et al., 2002), including Ena/VASP proteins (Lanier et al., 1999; Rottner et al., 1999), N-WASP and CR16 (Ho et al., 2001), myosin X (Berg and Cheney, 2002), talin (DePasquale and Izzard, 1991), syndapin I (Qualmann and Kelly, 2000), Abl interactor proteins (Stradal et al., 2001), and Vav (Kranewitter et al., 2001). Roles for these proteins remain largely unknown with the exception of Ena/VASP proteins. In lamellipodia, GFP-VASP forms a thin line along the extreme leading edge (Rottner et al., 1999), and in filopodia it appears as a bright dot at filopodial tips (Lanier et al., 1999; Rottner et al., 1999). Ena/VASP proteins bind barbed ends of actin filaments and protect them from capping at the leading edge of lamellipodia, which results in formation of longer filaments within the lamellipodial dendritic network (Bear et al., 2002). These data suggest that Ena/VASP proteins that are enriched at filopodial tips may mediate continuous elongation of filopodial actin filaments.

The major gap in our understanding of filopodia behavior is the mechanism of their initiation. The filament treadmilling model refers to the steady state of an established organelle, but does not explain how it arose in the first place. A small GTPase, Cdc42, is a well-known signaling molecule inducing filopodia in cells (Kozma et al., 1995; Nobes and Hall, 1995). One of its downstream effectors, N-WASP, is an ubiquitous activator of the Arp2/3 complex (Rohatgi et al., 1999, 2000), which significantly facilitates Cdc42-induced filopodial formation (Miki et al., 1998), suggesting that the Arp2/3 complex may be involved in filopodial protrusion. This suggestion has been supported experimentally by perturbing Arp2/3 function in permeabilized platelets with an inhibitory antibody (Li et al., 2002), and in HeLa cells by expressing VCA domain of N-WASP (Qualmann and Kelly, 2000). Because the Arp2/3 complex is absent from established filopodia (Svitkina and Borisy, 1999a), we hypothesized that it plays a role during filopodia initiation. One possibility for how the Arp2/3 complex induces filopodial bundles is that it forms a "nucleation center" which starts a bundle and subsequently dissociates. Another possibility is that the normal dendritic array produced by Arp2/3-mediated nucleation is rearranged into parallel bundles. In this work, we investigated the mechanism of filopodia initiation in B16F1 mouse melanoma cells and found that filopodial bundles were initiated by reorganization of the dendritic network in a process that involved elongation and convergence of subsets of privileged barbed ends.

Results

Filopodia, microspikes, and retraction fibers

Crawling cells elaborate filopodia, microspikes, and retraction fibers in the course of cycles of protrusion and withdrawal. These have been considered as distinct entities, but because of their structural similarities, we investigated whether they were truly distinct or interconvertible. Determining whether they were functionally related was important to define the scope of our study.

We followed the kinetics of peripheral actin bundles by phase contrast or fluorescence microscopy in untransfected or GFP-actin–expressing cells, respectively. We observed many examples of transition between filopodia, microspikes, and retraction fibers (Fig. 1). The predominant order of transitions was from microspike to filopodium to retraction fiber. Transitions in the opposite direction were also observed. For each type of structure, the filament bundle was able to protrude, suggesting that the actin polymerizing machinery was functional in each morphological state. The protrusive activity of the surrounding lamellipodium seemed to be an important factor determining the transitions between these organelles. Depending on whether the lamellipodium advanced as fast as or slower than an actin bundle elongated, the bundle appeared as a microspike or a filopodium. If the lamellipodium withdrew while the actin bundle remained stable or elongated, the bundle appeared as a retraction fiber. Increased net protrusion of an actin bundle also contributed to the transition from microspikes to filopodia, especially after fusion of two microspikes. Thus, filopodia, microspikes, and retraction fibers are interconvertible organelles, which may transform one into another because of a disparity in the protrusion velocity of the bundles themselves and of the surrounding lamellipodium. Therefore, in this paper, we will consider these types of peripheral actin bundles together and will refer to them collectively as "filopodia," because this is the most commonly used term.

Kinetics of filopodia initiation

To approach the central question of the mechanism of filopodia initiation, we first investigated the kinetics of spontaneous filopodia initiation using GFP-tagged structural proteins. If filopodia were initiated by an Arp2/3-containing nucleation center, one would expect a nascent filopodium to arise from a distinct fluorescent dot of actin or Arp2/3 complex, whereas the rearrangement model pre-

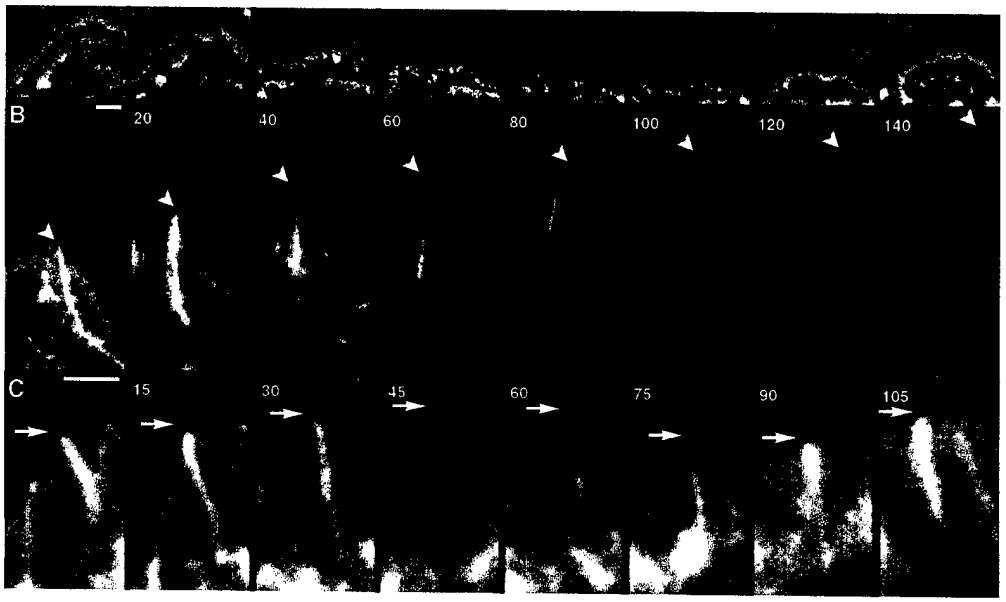

Figure 1. **Interconversion between microspikes, filopodia, and retraction fibers.** Time-lapse sequences of untransfected (A, phase contrast) or GFP-actin expressing (B and C, fluorescence) cells. Time in seconds. (A) Lamellipodium containing several microspikes (triple arrow and arrowhead in first frame) retracts leaving microspikes in the form of retraction fibers (240 s), some of which continue to protrude (240–400 s, arrow). At ~400 s, lamellipodium resumes protrusion and absorbs retraction fibers, some of which disappear, one becoming a filopodium (560 s, arrow), and another becoming a microspike (560 s, arrowhead). (B) Transition of a microspike (0 and 20 s) to filopodium (20–60 s) to retraction fiber (60–140 s). Actin bundle displayed continuous elongation, whereas surrounding lamellipodium initially kept up with the bundle (0–20 s), paused (40 s), and then withdrew (60–140 s). (C) Transition of microspike (0–30 s) to filopodium (45–75 s) and back to microspike (90–105 s) as a result of uncoordinated protrusive behavior of the bundle and the lamellipodium. Bars, 2 μm.

dicts a gradual condensation of actin fluorescence into a filopodial bundle.

Filopodia in GFP-actin–expressing cells displayed a broad range of lengths and fluorescence intensities. Histories of large filopodia revealed that they were formed by fusion of smaller filopodia, which in turn were the result of fusion at an even finer scale (Fig. 2 A). Events of true filopodia initiation were recognized as the appearance of thin, faint nascent filopodia contained within the lamellipodial network. In most cases (81%, $n = 124$), they arose from fishtail-shaped actin densities within the lamellipodium (Fig. 2, B and C). These densities, which we will call Λ-precursors because of their shape, were just slightly brighter than the surrounding lamellipodium at their vertices, but gradually diffused into a lamellipodial network at their bases (Fig. 2 D). Although hardly distinguishable from the rest of the lamellipodial network, Λ-precursors could be consistently recognized, after contrast enhancement, by tracing back in time the sequences of newly formed filopodia. In the remaining cases of filopodial initiation (19%), Λ-precursors were not visible, possibly because of insufficient temporal resolution or contrast. Nascent filopodia subsequently fused with each other (Fig. 2, B and C) or with other filopodia, and thus increased in size. Fusion produced Λ-configurations of filopodial bundles reminiscent of the shape of Λ-precursors, but with more distinct individual branches. Over time, these Λ-shaped bundles treadmilled backward at the root of the fused filopodium (Fig. 2 C) until they disappeared in the course of depolymerization. The observed actin kinetics appears more consistent with the idea of network reorganization as a mechanism of filopodia initiation.

The Arp2/3 complex is predicted to be enriched in the hypothetical filopodial nucleation center. Therefore, we performed kinetic analysis of GFP-Arp3–expressing cells (Fig. 3 A). Because filopodial bundles were invisible in GFP-Arp3 images, we acquired phase contrast images at the beginning and at the end of the sequence to detect nascent filopodia initiated during the sequence. Filopodia were observed to appear by phase microscopy and GFP-Arp3 was present throughout the lamellipodium, but no increase in GFP-Arp3 intensity was detected to spatially and temporally correlate with filopodial initiation. The essentially uniform distribution of the GFP-Arp3 signal does not support the hypothesis of an Arp2/3-based nucleation center for filopodial initiation.

To obtain insight into the actual mechanism of filopodia initiation, we next analyzed the kinetics of proteins enriched in filopodia, i.e., fascin and VASP. In GFP-fascin–expressing cells, a majority of nascent filopodia (66%, $n = 207$) first appeared as a bright dot or short rod on a dark background (Fig. 3, B and C). In other cases (34%), a bright dot of GFP-fascin rather suddenly appeared at the tip of a very faint Λ-shaped density in lamellipodia (Fig. 3 C, inset in 16 s frame). Both kinds of nascent fascin dots subsequently elongated to form a filopodium. Fusion of mature fascin-containing filopodia was also frequently seen (Fig. 3 C). Because fascin is present in lamellipodia, albeit at much lower concentration than in filopodia, the faint Λ-shaped fascin densities might correspond to Λ-precursors, suggesting that in the course of filopodia initiation, fascin initially appears at the tips of the Λ-precursors (see next section). In GFP-VASP sequences, we followed the formation of brighter dots corre-

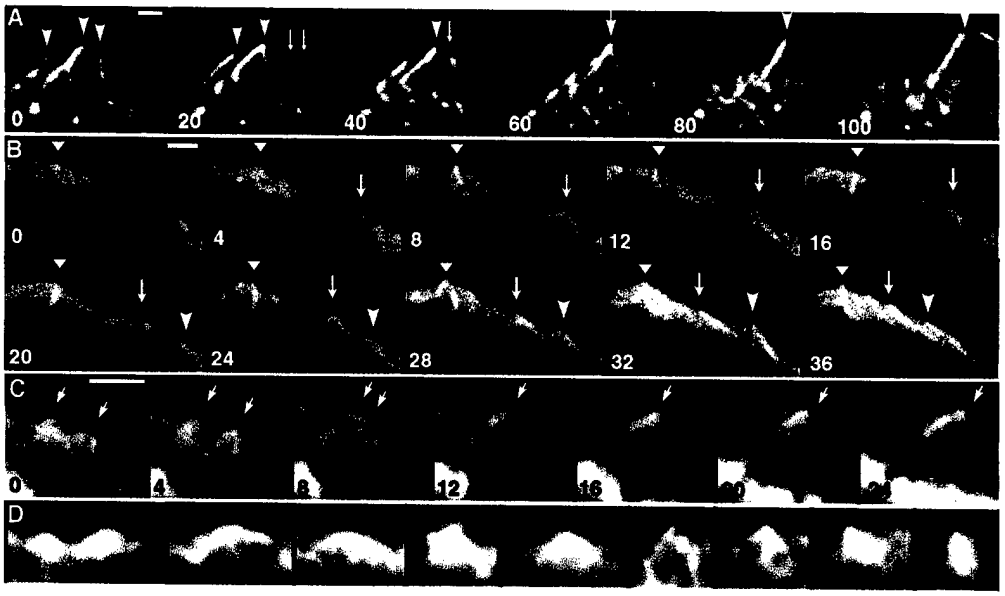

Figure 2. **Actin kinetics during filopodia initiation.** (A–C) Time-lapse sequences of GFP-actin–expressing B16F1 cells. Time in seconds; individual features marked by arrows and arrowheads. Nascent filopodia are marked starting from the frame preceding the appearance of the recognizable precursor. (A) Three established filopodia (0 s, arrowheads) fuse with each other (0–60 s). Two Λ-precursors (arrows) appear (20 s), and fuse with each other (40 s), forming a nascent filopodium that subsequently (60 s) joins the fusing older filopodia. (B) Several nascent filopodia form from Λ-precursors that appear within lamellipodium. (C) Two Λ-precursors existing at 0 s (arrows) fuse with each other (12 s), producing a nascent filopodium with a Λ-shaped root. The fusion point treadmills backward while the filopodium protrudes forward. (D) Gallery of Λ-precursors. First four examples represent enlarged and enhanced Λ-precursors from A (20 s), B (8 s), B (24 s), and C (0 s), respectively. Remaining examples are from other sequences. Bars, 2 μm.

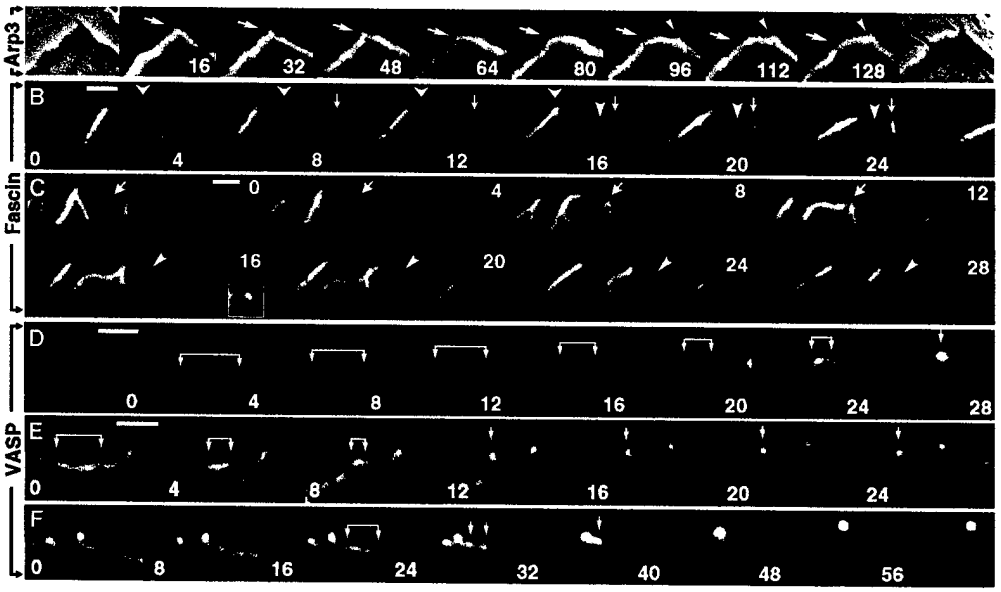

Figure 3. **Kinetics of marker proteins during filopodia initiation.** Time-lapse sequences of GFP-Arp3 (A), GFP-fascin (B and C), or GFP-VASP (D–F). (A) Two flanking phase contrast frames (0 and 164 s) demonstrate formation of a new filopodium during the sequence. Positions of preexisting (arrow) and nascent (arrowhead) filopodia are indicated. No focal enrichment of Arp3 was seen during formation of the nascent filopodium. (B and C) Most nascent filopodia arise from bright GFP-fascin dots without obvious Λ-precursors. In some cases, a bright dot localizes to the tip of a faint Λ-shaped density, as in the inset in 16 s frame in C, which shows the region indicated by arrowhead in this frame after enlargement and adjustment of contrast to reveal weak fluorescence. Filopodia fusion occurs in C (arrows). (D–F) Bright GFP-VASP dots corresponding to nascent filopodia arise by gradual coalescence of the initially even line of leading-edge fluorescence. Brackets indicate regions of brighter GFP-VASP fluorescence that shrink into dots over time. In F, two smaller dots (24 s) are formed during coalescence of the shrinking region, which subsequently fuse with each other (32 s) and with the adjacent preexisting dot (40 s). Bars, 2 μm.

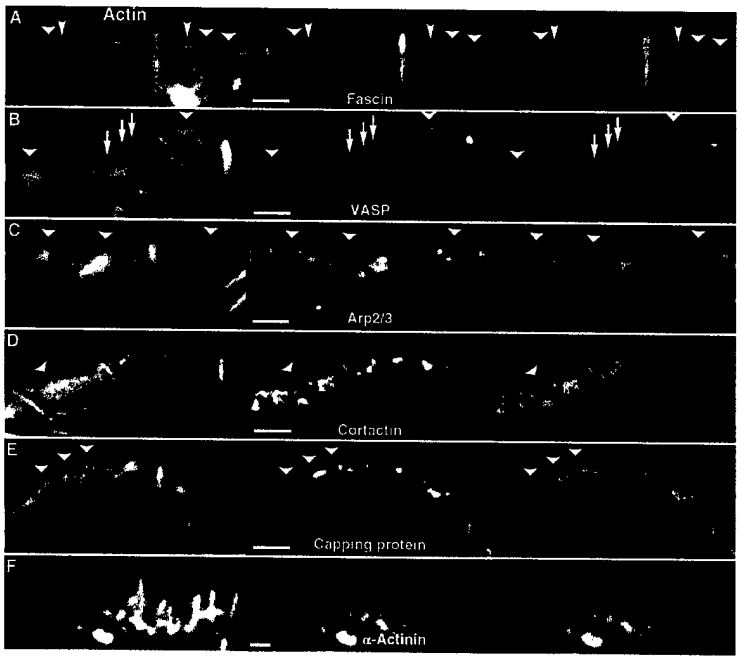

Figure 4. **Localization of filopodial and lamellipodial markers in Λ-precursors.** Left column; actin revealed by Texas Red-phalloidin (A, B, and F) or by GFP-actin expression (C–E). Central column; actin-binding proteins (as indicated) revealed by expression of GFP-fusion proteins (A, B, and F) or by immunostaining (C–E). Right column; merged images. Λ-precursors are indicated by arrowheads. (A) Fascin is strongly enriched in established filopodia and localizes to the distal section of some Λ-precursors (wide arrowheads), but not others (narrow arrowheads). (B) VASP forms bright dots at the tips of filopodia and Λ-precursors. Additional dots can be seen along the leading edge (arrows), which apparently do not correspond to Λ-precursors. (C–E) Lamellipodial markers, Arp2/3 complex (C), cortactin (D), and capping protein (E), are excluded from filopodia and are partially depleted from Λ-precursors. (F) α-Actinin localizes to proximal parts of lamellipodia and filopodia. Bars, 2 μm.

sponding to filopodial tips among the weaker fluorescence of the lamellipodial edge. The major pathway for filopodia initiation (Fig. 3, D–F) was a gradual coalescence of VASP to ultimately produce a bright dot. The first sign detected was a slight elevation of GFP-VASP fluorescence intensity within a small domain (2–4 μm) along the leading edge. Then, this region gradually shrank into a dot concurrently increasing its intensity. In some cases, the condensing region became discontinuous during shrinkage (Fig. 3 F), suggesting intermediate formation of smaller filopodia. Because Ena/VASP proteins bind barbed ends and protect them from capping (Bear et al., 2002), these data suggest that elongating barbed ends from the lamellipodial network gradually segregate into a small region, which becomes a filopodial tip.

Protein composition of Λ-precursors

Our kinetic analysis identified Λ-precursors as intermediates in filopodial initiation. Next, we examined whether molecular markers that discriminate between lamellipodia and filopodia are present in Λ-precursors (Fig. 4). Expression of GFP-actin or staining with labeled phalloidin was used to visualize actin. Putative Λ-precursors were identified in the actin channel based on their characteristic shape, and slightly increased actin density. Immunostaining or expression of GFP-tagged proteins was used to localize the second protein.

Fascin and VASP were used as filopodial markers. In GFP-fascin–expressing cells, putative Λ-precursors either did not contain significant amount of fascin (Fig. 4 A, arrows; also see Fig. 6), or they had fascin enriched only at the tip (Fig. 4 A, arrowheads), suggesting that fascin was recruited to the tips of the preformed Λ-precursors. In GFP-VASP–expressing cells (Fig. 4 B), VASP fluorescence at the leading edge became less uniform after extraction, perhaps revealing more strongly associated protein. The brightest VASP dots corresponded to established filopodia. The majority of Λ-precursors contained a distinct VASP dot at their vertex (Fig. 4 B, arrowheads). Weak VASP dots were also evident without recognizable Λ-precursors (Fig. 4 B, arrows). These may represent fluctuations in density of actin filament barbed ends within the lamellipodium or Λ-precursors not detected in the actin channel.

As lamellipodial markers, we used Arp2/3 complex, cortactin, and capping protein. Previously, we have shown that Arp2/3 complex is excluded from filopodial bundles (Svitkina and Borisy, 1999a). Here, we report that cortactin and capping protein are also excluded from filopodia (Fig. 4, D and E). In Λ-precursors, these proteins were partially depleted, especially close to the vertex, but not completely absent (Fig. 4, C–E), suggesting that gradual depletion of lamellipodial proteins occurs during formation of Λ-precursors and filopodia initiation. No enrichment of Arp2/3 complex was detected at filopodial roots.

We also investigated the ability of α-actinin to discriminate between filopodia and lamellipodia. Previously, α-actinin has been shown to localize to lamellipodia (Langanger et al., 1984), but its localization in filopodia is unclear. GFP-tagged α-actinin associated with both lamellipodia and filopodia (Fig. 4 F), but appeared in these organelles with delay and, consequently, localized to the base of the fast-protruding lamellipodia and filopodia. Thus, α-actinin is a late marker for actin bundling in filopodia and is apparently not involved in filopodia initiation.

Together, the molecular marker analysis suggests that Λ-precursors represent a transitional structure displaying enrichment of filopodial markers and partial depletion of lamellipodial proteins. Dual-channel correlation of actin distribution with that of filopodial markers suggested that VASP accumulation occurred early in the process of formation of Λ-precursors, and that fascin appeared at the tips of established Λ-precursors.

Structure of Λ-precursors

Light microscopic analysis suggested a gradual reorganization of the lamellipodial network into bundles through intermediate formation of Λ-precursors. This hypothesis was analyzed using a higher resolution technique; platinum replica electron microscopy (EM). Treadmilling behavior of filopodia has a remarkable consequence in that the history of the actin array is imprinted in its structure (Katoh et al., 1999a), so that moving from the leading edge in a proximal direction in space is analogous to traveling back in time. To understand the mechanism of filopodia initiation, we first focused on the analysis of filopodial roots. In this work, we were most interested in analyzing young filopodia, which are usually thin and short according to our kinetic study.

The majority of apparently young filopodial bundles were splayed apart at their roots into smaller bundles or individual filaments (Fig. 5), suggesting that the bundles were formed by convergence of the composing elements. Filopodial roots consisting of two or more smaller bundles are consistent with an event of filopodial fusion in the recent history of that filopodium (Fig. 5 B). More importantly, we observed many examples of filopodial bundles whose roots suggested the convergence of individual filaments originating from distant places in the surrounding lamellipodial network and entering the bundle at different levels. In some cases, it was possible to track filaments back from the bundle toward their origin as a branch on another filament in the surrounding network (Fig. 5 C). These findings suggest that filaments comprising filopodial bundles were asynchronously recruited from the dendritic network. Remarkably, filaments entering filopodial bundles were long compared with the branched network near the leading edge (Fig. 5, inset in A). Older filopodia, which could be recognized by their length and thickness, either had their actin bundles rooted deeply in the cytoplasm, which impeded visualization, or had tapered (not splayed) roots. This is consistent with depolymerization from the pointed ends of the composing filaments causing progressive elimination of the original splayed roots.

Splayed filopodial roots apparently corresponded to aged Λ-precursors that treadmilled backward during filopodium growth. To identify Λ-precursors at a stage when they had not yet produced a filopodium, we performed correlative light microscopy and EM (Fig. 6). Putative Λ-precursors were identified in cells by fluorescence microscopy and relocalized after EM processing of the same cells. For these experiments, we used cells expressing GFP-fascin, which allowed us to compare parts of the Λ-precursor containing and not containing fascin.

Λ-precursors lacking fascin clearly displayed features of dendritic organization, such as short filaments, branching filaments, and numerous free filament ends (Fig. 6). Also, consistent with the idea of the transitional character of Λ-precursors, we found many rather long filaments within Λ-precursors, whereas long filaments were not frequent in the dendritic network outside Λ-precursors (Fig. 6, A and C). These long filaments apparently became enriched during transition of Λ-precursors into splayed filopodial roots, perhaps because of faster depolymerization of short filaments. The actin array in fascin-positive parts (Fig. 6 B) had a clearly bundled organization with densely packed filaments.

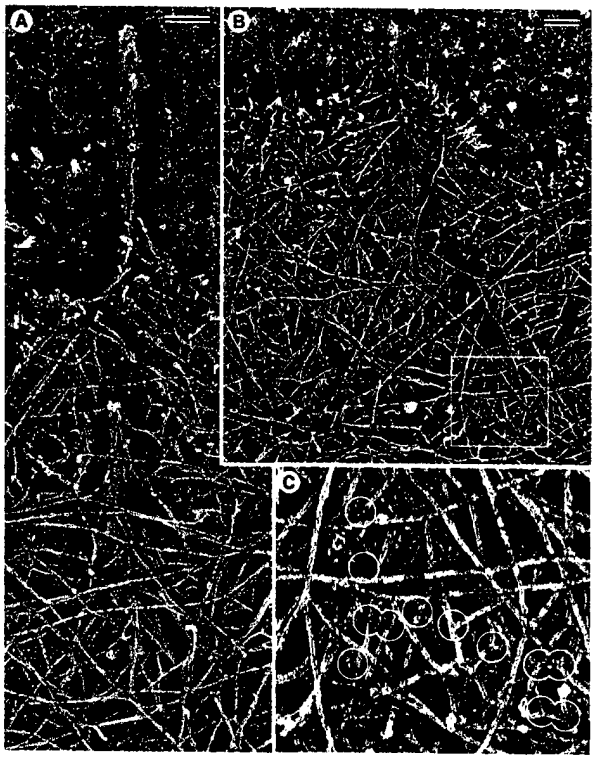

Figure 5. **Filopodial filaments originate from the surrounding dendritic network.** Platinum replica EM. (A) Filopodium contains a tight bundle of actin filaments that splays apart at its root and becomes an integral part of the surrounding network. Filaments in the roots are long compared with the branching network of the adjacent lamellipodium (inset). (B) Recently fused filopodium consists of two sub-bundles, each of which has a splayed root; the boxed region at the root of the right sub-bundle is enlarged in C and shows many branches (encircled) at which filopodial filaments originate. Rough background outside the cell edge is due to laminin coating of the glass coverslip. Bars, 0.2 μm.

The more proximal parts of actin bundles were not significantly enriched in fascin and displayed long, loosely aligned filaments (Fig. 6 B), suggesting that fascin-mediated bundling was delayed compared with accumulation of long filaments in the forming bundle. Thus, structural analysis of Λ-precursors and filopodial roots demonstrated enrichment of long filaments in these structures that apparently occurred before fascin-mediated bundling.

Structural organization of filopodia with known history

Because not every Λ-precursor produced a filopodium in kinetic studies, we performed correlative EM for cells with known history. For this purpose, we acquired time-lapse sequences of GFP-actin–expressing cells. After extraction and fixation, we prepared those cells for EM and analyzed filopodia formed in the course of the sequence (Fig. 7). Fig. 7 A illustrates the correlation between the last live image of one such cell, the image of the lysed cell, and the EM image of the same cell taken at low magnification comparable with that of light microscopy. During the 19-s interval between the last live image and the image of the lysed cell, the lamellipodium protruded ~0.9 μm, which is evident in the su-

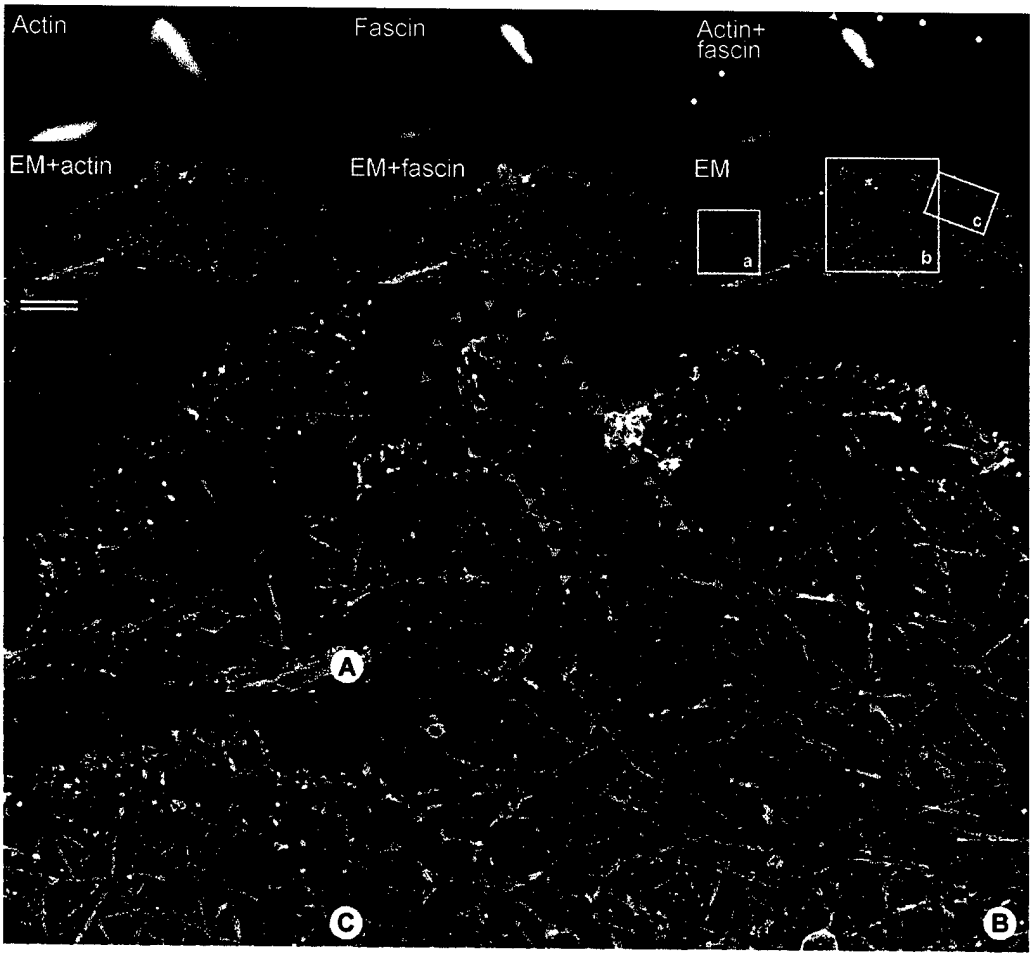

Figure 6. **Actin filament organization in Λ-precursors.** Correlative fluorescence and EM of the same cell. First row; fluorescence microscopy of the leading edge showing Texas Red-phalloidin labeled actin (left), GFP-fascin (middle), and merged image (right). White dots in the merged image mark putative Λ-precursors, and the arrowhead indicates a filopodium, which have been analyzed by EM. Second row; EM of the same region (right) overlaid with fluorescence images of actin in red (left) and fascin in green (middle). Boxed regions (a–c) are enlarged in the bottom panels, labeled respectively. Red outlines in enlarged panels denote areas of increased actin density in the fluorescence image that represent putative Λ-precursors or filopodia. Λ-precursors contain relatively long filaments, some of which are highlighted in cyan in A and C, along with short branching filaments highlighted in magenta; adjacent lamellipodium (C) contains mostly short branching filaments highlighted in magenta. Yellow outline denotes region enriched in fascin in the established filopodium. This region contains tightly bundled filaments. Bar, 0.2 μm.

perimposed image. The subsequent processing for EM did not introduce significant distortions into the structure of the lamellipodium because extracted light and low power EM images could be almost perfectly overlapped. Coincidence of light and EM features could also be seen at higher magnification, where brighter areas in fluorescence corresponded to denser actin arrays in EM (Fig. 7 B).

Several filopodia were spontaneously formed during the total period of 35 s of this sequence. Fig. 7 C illustrates the history of three nascent filopodia of different age, which are color coded in yellow, blue, and green for convenience of description. The filopodium marked with a yellow arrow was the oldest one. This filopodium was formed in the course of fusion of two faint, converging linear densities existing at the beginning of the sequence. A bright spot of actin fluorescence, which appeared in the filopodium shaft in the second frame, allows one to recognize treadmilling and retrograde flow in this filopodium. The filopodium marked with the blue arrow was not visible in the first frame; at 4 s, it appeared as a Λ-precursor, which at 8 s could be seen near the edge, and which produced a faint filopodium by 12 s. The filopodium marked with the green arrow is the youngest one. It was formed from a Λ-precursor first visible at 12 s. Tips of all three filopodia converged by the end of the sequence, suggesting that they began fusing at the moment of extraction.

The detailed structural organization of the region containing all three filopodia is shown in Fig. 7 D. The root of the "yellow" filopodium consisted of two thin, fusing bundles corresponding to two converging lines in the first frame of the sequence. Each of these sub-bundles, when followed backward, splayed into individual filaments originating from the surrounding dendritic network (not depicted). The Λ-precursor of the "blue" filopodium that

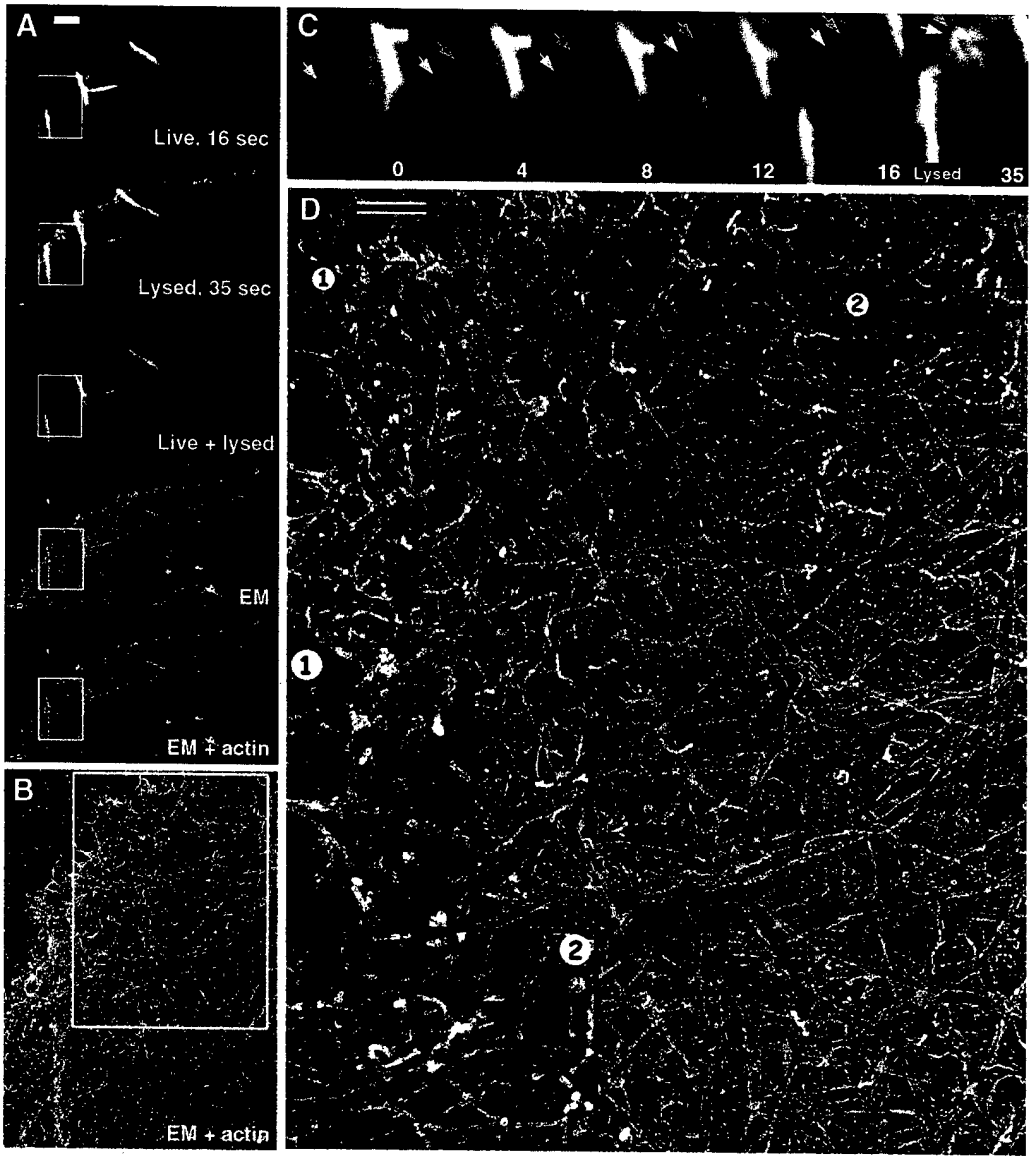

Figure 7. **Structural organization of filopodia with known history.** Correlative live imaging and EM. (A) Overview of the cell lamellipodium at different stages of sample processing. GFP-actin fluorescence images taken just before (live, 16 s) and immediately after (lysed, 35 s) cell lysis were merged (live + lysed) in green and red channels, respectively; cell advance during the 19 s between images appears as red strip at the leading edge. Low magnification EM image of the same region (EM) is overlaid with actin fluorescence image of the lysed cell (EM + actin). (B) Boxed region in A is enlarged in B to show correlation between light and EM in more detail. Brighter areas in fluorescence image correspond to denser actin arrays in EM. (C) Detailed history of the boxed region in A. Time in seconds. The 35 s frame is taken from the lysed cell. Arrows of different color indicate position of individual nascent filopodia. (D) Enlarged EM of the boxed region in B showing the structure of nascent filopodia, whose history is presented in C; individual nascent filopodia are outlined in colors corresponding to colors of arrows in C. Some filaments converging into the bundle of the "blue" filopodium are highlighted in shades of blue. Boxes 1 and 2 are further enlarged in corresponding insets and show organization of the filopodial tip (1) and of the root of "green" filopodium (2); branching filaments are highlighted in green in the inset (2). See detail in text. Bars, 2 μm (A) and 0.2 μm (D).

treadmilled backward during the sequence was identified with the splayed root of the blue filopodium in the EM image, indicating that splayed roots of filopodia indeed represent former Λ-precursors. Like in other EM images, filaments were collected into the bundle of the blue filopodium from the wide surrounding area (Fig. 7 D). In fluorescence images (Fig. 7 C), the splayed root became invisible already in 12 s frame, probably because of low fluorescence intensity. The root of the youngest "green" filopodium displayed many features of the dendritic organization of Λ-precursors. It had relatively high network density, many short filaments, frequent branching, and numerous free barbed ends (Fig. 7, inset 2 in D). Some filaments originating as a branch on another filament could be seen to enter the bundle of the green filopodium. These data support the idea that Λ-precursors initially represent a part of

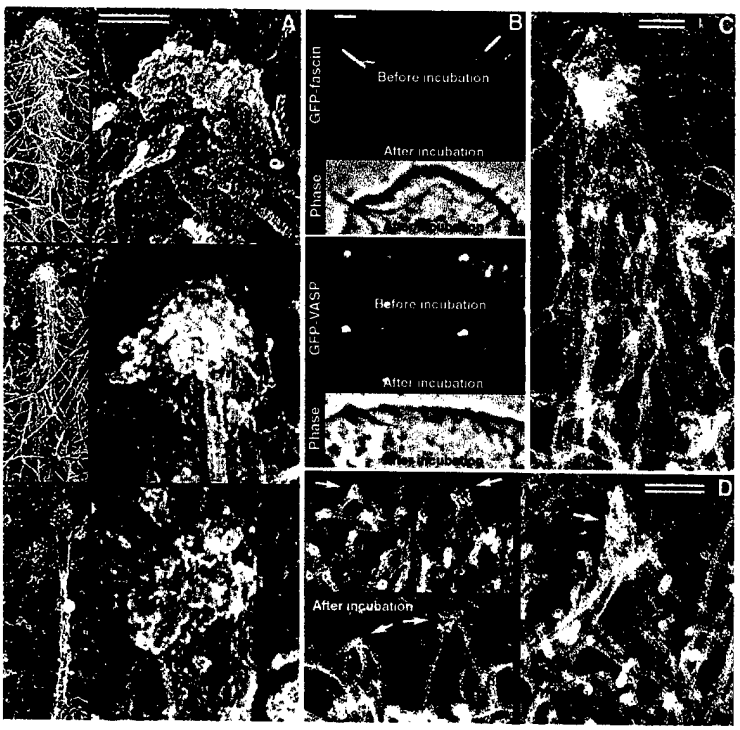

Figure 8. **Filopodial tip complex.** (A) Structure of tip complex in three filopodia seen by replica EM. Lower magnification, left; higher magnification, right. (B) Incubation of lysed cells in buffer causes dissociation of fascin (top) but not VASP (bottom) from filopodia. Phase contrast and GFP fluorescence images of cells transiently expressing indicated fusion proteins were taken immediately after cell lysis ("before incubation" phase images are not depicted) and after overnight incubation in phalloidin-containing buffer ("after incubation"). Acquisition and processing of fluorescence images was identical for each pair. (C) Filopodial bundle and tip complex after overnight incubation of the lysed cell in phalloidin-containing buffer. Replica EM. Filopodial tip complex keeps barbed ends of filopodial filaments together, whereas filaments within the bundle become loose. (D) Junctions between barbed ends of lamellipodial filaments (arrows) immediately after lysis or after incubation in buffer like in B or C ("after incubation"). Bars: 0.1 μm (A, C, and D), and 2 μm (B).

the dendritic network, but lose short filaments with age. An interesting feature of the green filopodium was that it was barely recognizable in the EM image because its filaments, although long, were not well-aligned, suggesting that filament cross-linking is not an early event during filopodial formation, in agreement with delayed recruitment of fascin to Λ-precursors.

In contrast to delayed bundling, the filament barbed ends at filopodial tips were in register, suggesting they were interacting with each other, even though they supposedly encountered each other just a few seconds before extraction. A substantial amount of granular material was associated with the tip of the fused filopodium (Fig. 7, inset 1 in D). The presence of tip-associated material may play an important role in filopodial formation, and we therefore investigated it in more detail.

Filopodial tip complex

In EM images, many filopodial tips were associated with a distinct structure, which had a rough granular surface and variable shape and size (Fig. 8 A). To test whether this tip complex was involved in physical association of filopodial barbed ends with each other, we incubated lysed cells overnight in phalloidin-containing buffer. Phalloidin prevented depolymerization of actin filaments during incubation, whereas dissociation of other proteins was allowed. We monitored dissociation of fascin or VASP using cells expressing GFP-fusion proteins. Although lysis removed soluble and weakly bound proteins, lysed cells initially retained most of filopodia-associated fascin and VASP. However, fascin was completely gone after incubation, whereas VASP remained (Fig. 8 B). EM of incubated cells revealed that filopodial bundles became loose, consistent with the loss of fascin, but the tip complexes were mostly preserved, consistent with retention of VASP, and filament barbed ends remained associated with each other and with the filopodial tip complex (Fig. 8 C). These results suggest that the tip complex physically links barbed ends in filopodia independently of fascin. Occasionally, the tip complex detached partially or completely during incubation. In such cases, released filopodial filaments completely splayed apart.

The next question we addressed was the origin of the tip complex. Because filopodia formation seemed to occur by gradual convergence of filaments from the dendritic network, we wondered whether smaller tip complexes existed in lamellipodia. Careful examination of the leading edge of lamellipodia indeed revealed junctions between barbed ends of two or more lamellipodial filaments (Fig. 8 D). Occasionally, additional material could be seen at the junction points, which may correspond to the tip complex of established filopodia. Association between filament-barbed ends was retained even after overnight incubation in the phalloidin-containing buffer (Fig. 8 D).

Discussion

Our kinetic and structural investigation of filopodial initiation in B16F1 melanoma cells demonstrated that filopodial bundles were formed by gradual reorganization of the lamellipodial dendritic network in a process that involved elongation of a subset of lamellipodial filaments, self-segregation of these filaments into filopodial precursors, and initiation of bundling at the tips of the precursors (Fig. 9). We propose that the mechanism of filopodia initiation is analogous to filopodial fusion, but that it begins at the level of individual filaments and gradually propagates to the fusion of thick bundles. We now discuss this hypothesis in detail.

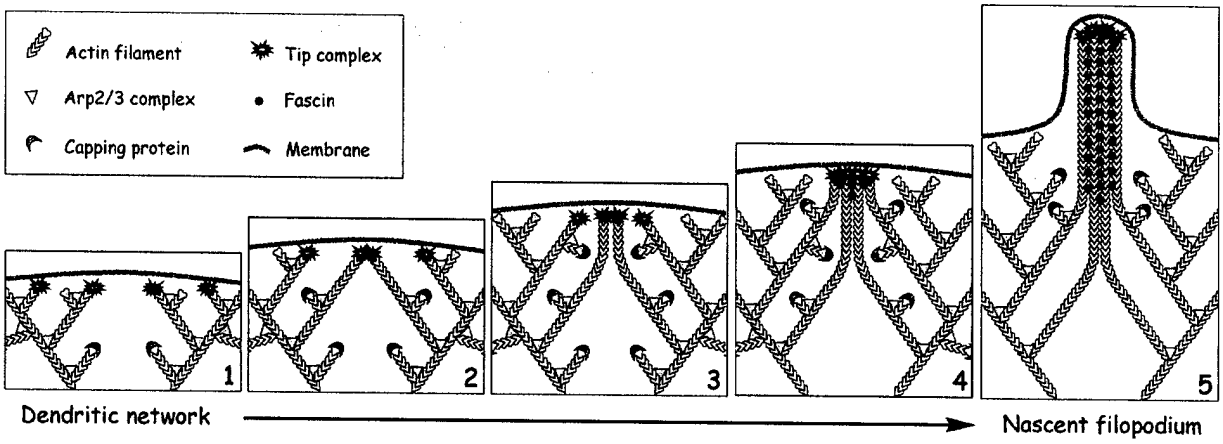

Figure 9. **Convergent elongation model for filopodia initiation.** (1) Lamellipodial network is formed by Arp2/3-mediated dendritic nucleation. Elongation of some barbed ends in the network is terminated by capping protein, but other barbed ends acquire a privileged status by binding a complex of molecules (tip complex) that allows them to elongate continuously. Ena/VASP proteins are likely members of the tip complex mediating protection from capping. (2) Privileged barbed ends drift laterally during elongation and collide with each other. Tip complex mediates clustering of privileged barbed ends upon collision. (3) Converged filaments with linked barbed ends continue to elongate together. Other laterally drifting barbed ends encounter and join the initial cluster of tip complexes. Multiple collisions of barbed ends during elongation lead to gradual clustering of their barbed ends, multimerization of associated tip complexes, and convergence of filaments. (4) The multimeric filopodial tip complex initiates filament cross-linking by recruiting and/or activating fascin, which allows the bundling process to keep up with the elongation and guarantee efficient pushing. (5) In the nascent filopodium, the filopodial tip complex retains its functions of promoting coordinated filament elongation and bundling, as well as fusion with other filopodia.

Dendritic network as a source of filopodial filaments

Arp2/3 complex has been suspected to play a role in filopodia initiation, but paradoxically, is not present in filopodial bundles. Our data do not support the idea of filopodial bundles arising from a nucleation center, but indicate that Arp2/3 complex produces a normal dendritic array which then becomes rearranged into parallel bundles through intermediate formation of Λ-precursors. Considering the ability to fuse displayed by filopodial bundles of all sizes, one can deduce that fusion may also occur below the resolution limit of the light microscope. Fusion of submicroscopic bundles or individual filaments may represent a mechanism of formation of Λ-precursors and explain their Λ-shape. The structure of Λ-precursors and filopodial roots was consistent with this idea, and showed that filaments composing bundles were collected from the surrounding area in an asynchronous manner, suggesting that Arp2/3-mediated actin filament nucleation provides a source of filaments to be rearranged into a bundle by gradual fusion.

Formation of long filaments as a prerequisite of filopodia initiation

The major difference between actin filament arrays in filopodia and lamellipodia is that filopodial filaments elongate continuously, reaching lengths of many micrometers, whereas lamellipodial filaments become capped after a brief period of elongation, and consequently, are relatively short (~100 nm). Extensive elongation of filopodial filaments would seem to require a way to antagonize or protect against capping activity in the cytoplasm. A mechanism for protection is likely to involve proteins of the Ena/VASP family because these proteins are enriched at filopodial tips (Lanier et al., 1999; Rottner et al., 1999), they antagonize the terminating activity of capping protein in vitro, and their depletion from or targeting to the membrane leads to shorter or longer filaments, respectively (Bear et al., 2002). Our data support an idea that distributed filaments with prebound Ena/VASP proteins are gradually brought together to form a filopodium. The kinetics of GFP-VASP demonstrated a correlation between coalescence of VASP and filopodia initiation. At present, it is not clear whether VASP remains associated with the same barbed end for a long time or frequently switches its protégé. The persistence of VASP at the leading edge and filopodial tips after overnight incubation in buffer is evidence that at least some actin filaments can remain tightly associated with VASP. However, in a living cell, the association of VASP with barbed ends may be subject to regulation that affects the degree of protection it confers against capping.

On the assumption that GFP-VASP reports on the behavior of the population of privileged barbed ends, the gradual coalescence of VASP to the tips of Λ-precursors reflects the gradual segregation of longer filaments into Λ-precursors. Consistent with this coalescence process, actin arrays within Λ-precursors were enriched in long filaments and depleted in the lamellipodial markers, Arp2/3 complex, cortactin, and capping protein. Long filaments became more clearly visible when Λ-precursors treadmilled away from the leading edge and became filopodial roots. Long filaments in lamellipodia have been also observed by other EM techniques (Small, 1988; Lewis and Bridgman, 1992; Resch et al., 2002), although no distinction has been made between Λ-precursors and other parts of lamellipodia.

Other studies have indicated that Ena/VASP family members contribute to the formation of filopodia, but the mechanism of their involvement has not been elucidated. In *Dictyostelium*, the VASP family homologue (DdVASP) is essential for filopodia formation (Han et al., 2002). Induction

of filopodia by Irs53 involved recruitment of a member of the Ena/VASP family, Mena (Krugmann et al., 2001). Our data suggest that the mechanism of action of Ena/VASP proteins is through the formation of privileged filaments that can elongate persistently.

Clustering of barbed ends as a mechanism of segregation of filopodial filaments

The persistent elongation of filaments by itself would not result in their local accumulation unless they were able to associate with each other. Consistent with this idea, we found structural interaction between filament barbed ends that was mediated by the filopodial tip complex in a fascin-independent manner. This result suggests that bundling and barbed-end interaction are mediated by different molecules. In addition, we detected formation of junctions between filament barbed ends at the extreme leading edge. Similar to filopodial tips, these junctions were stable even after overnight incubation in buffer and were frequently associated with additional material. The filopodial tip complexes described here may be similar to the material associated with distal filament ends in filopodia and lamellipodia of fibroblasts (Small et al., 1982) and neuronal growth cones (Lewis and Bridgman, 1992). Interaction between barbed ends appears to be responsible for the Λ-configuration of actin arrays at different scales from junctions between individual filaments to Λ-precursors to fusing bundles.

Privileged barbed ends seem to combine the ability for continuous elongation with multimerization potential. The cross-linking molecules mediating junction formation between barbed ends remain unclear, but they are likely to be components of the filopodial tip complex. The molecular composition of the filopodial tip complex remains to be established. However, proteins previously found to localize specifically to filopodial tips (see Introduction), including Ena/VASP proteins, are predicted to be members of this complex. One possibility is that Ena/VASP proteins, which mediate protection of barbed ends from capping, may also work as barbed end "glue" because of their ability to oligomerize (Bachmann et al., 1999). In support of this idea, a domain mediating oligomerization of Mena has been shown to be required for full function of Mena in cell motility (Loureiro et al., 2002). Another possibility is that additional (yet unidentified) molecules within the filopodial tip complex mediate interaction between barbed ends. These possibilities are not mutually exclusive, and the hypothetical barbed end linking molecules may act indirectly through Ena/VASP proteins, which would have the benefit of rendering the anti-capping and clustering capabilities to the same subset of filaments.

The combination of continuous elongation and self-association properties of privileged barbed ends allows one to explain how the privileged filaments in the dendritic network become gradually self-segregated during filopodia initiation. The lamellipodial filaments, on average, have a diagonal orientation of about ±35 degrees with respect to the leading edge (Maly and Borisy, 2001). During elongation, the barbed ends of diagonally oriented filaments drift laterally along the edge, which increases chances of their collision. Such lateral drift of lamellipodial filaments was proposed to mediate formation of filopodia due to activity of bundling proteins (Small et al., 1982, 1998). We propose that the cross-linking molecules at the barbed ends of colliding privileged filaments cause them to associate with each other and travel together. Multiple collisions lead to clustering of barbed ends of filaments and multimerization of individual barbed-end–associated molecular complexes, producing a filopodial tip complex.

Filament bundling as a mechanism of stabilization

Individual long actin filaments are not efficient at pushing. Because of their low persistence length, they bend rather than push. Filament cross-linking along the length is thought to be a solution for this problem (Mogilner and Oster, 1996). The existing evidence suggests that fascin is the major actin cross-linking protein in filopodia (Bartles, 2000; Kureishy et al., 2002) that is required for filopodia maintenance. In support of this idea, we found that fascin enrichment in actin arrays correlated with tight bundling of actin filaments, and fascin dissociation from filopodial bundles resulted in filament unbundling. To allow for efficient pushing, cross-linking of growing filaments is predicted to occur soon in the course of actin polymerization so that the effective length of the filament after the last cross-link remains short. Indeed, fascin is enriched in the distal section of filopodia (Cohan et al., 2001, and this paper) suggesting that its association with the growing actin bundles occurs in parallel with actin assembly. In contrast, association of α-actinin with fast-protruding filopodia and lamellipodia is detected toward their rear, indicating that the role of α-actinin is not to provide the pushing efficiency to growing filaments.

Fascin recruitment during filopodia initiation was not the earliest event. Instead, GFP-fascin rather abruptly appeared at the vertex of a preformed Λ-precursor. We suggest that recruitment and/or activation of fascin to tips of Λ-precursors cross-links the long filaments accumulated there, thus completing the initiation of filopodial bundle formation.

Convergent elongation mechanism of filopodium initiation

Based on our findings, we propose a convergent elongation model for filopodial initiation (Fig. 9), which stipulates that filopodia are formed by reorganization of the dendritic network formed in an Arp2/3-dependent manner. The key assumption of this model is that some filaments within the lamellipodial dendritic network acquire privileged status by binding a set of molecules to their barbed ends, which protect them from capping, and mediate association of barbed ends with each other on collision. Ena/VASP proteins are likely candidates for the role of protection from capping. The glue molecule remains to be established. Multiple collisions of privileged filaments during elongation lead to gradual clustering of their barbed ends and multimerization of associated barbed-end complexes. A set of privileged filaments originating from distant sites of the dendritic network and converging to the same spot forms a Λ-precursor, and aggregated barbed-end complexes form the tip complex of the future filopodium. The filopodial tip complex initiates filament cross-linking by recruiting and/or activating fascin, which allows the bundling process to keep up with elongation and

guarantee efficient pushing. Initiated filopodia elongate and attain steady-state by the filament treadmilling mechanism. The filopodial tip complex remains associated with the growing tip, allowing for continuous elongation of filopodial filaments and mediating filopodia fusion on collision.

Initiation of filopodial bundles within the lamellipodial network necessarily leads to their birth in the form of microspikes. They die either during ruffling or in the form of retraction fibers, when a cell decides to move in a different direction. In between, the microspikes may at some point elongate faster than lamellipodial advance to form a conventional filopodium. Additional evidence for the relatedness of these structures comes from the fact that Cdc42 induces cell retraction and formation of retraction fibers along with formation of genuine filopodia (Kozma et al., 1995). Consequently, the three morphological types of peripheral actin bundle, microspikes, filopodia, and retraction fibers, may be considered as transient states of the same core structure differing primarily in their relationship to the membrane and in the state of their cycle. Also, they may differ in protein composition and dynamics. Filopodia and retraction fibers are predicted to contain actin–membrane linkers, like ERM proteins, which are unnecessary for microspikes. The remote position of barbed ends in filopodia and retraction fibers may require a myosin motor, for example, myosin X (Berg and Cheney, 2002), to deliver building components to the tip.

The pathway of filopodia initiation established in this paper has a remarkable similarity to the mechanism of formation of filopodial-like bundles in vitro (unpublished data). In that work, we found that beads coated with Arp2/3-activating proteins induced formation of radial actin bundles when capping activity in cytoplasmic extracts was decreased. In vitro bundles displayed many filopodial characteristics; they had uniform polarity, grew at the barbed end, were enriched in fascin, and lacked Arp2/3 complex, capping protein, and α-actinin. As in the present paper, individual filaments in bundles in vitro originated from the dendritic network near the bead, and a decreased rate of capping in the extracts allowed them to elongate and be bundled by fascin.

A tightly packed parallel actin bundle, which is a hallmark of filopodia, can also be found in other organelles across tissues and organisms (Bartles, 2000; DeRosier and Tilney, 2000). Our findings that filopodia in B16F1 cells during normal locomotion were formed by reorganization of the dendritic network raises the possibility of a similar pathway for initiation of other parallel bundles, but does not exclude other mechanisms of bundle formation in other cells types or under other circumstances. For example, proteins of the formin family have recently been shown to nucleate actin filaments in vitro (Pruyne et al., 2002; Sagot et al., 2002b) and induce actin cables in yeast in vivo in the absence of the Arp2/3 complex (Evangelista et al., 2002; Sagot et al., 2002a). Thus, it remains an open question whether Arp2/3- or formin-dependent mechanisms operate in other cases, and whether they are exclusive or can cooperate.

In conclusion, we investigated the pathway of filopodia initiation in B16F1 cells and formulated the convergent elongation model for filopodia formation. Although many assumptions of this model remain to be tested, it provides a conceptual framework for further studies aimed at explicitly identifying participating molecules and their precise roles.

Materials and methods

Cells and reagents

Mouse melanoma B16F1 cell line stably expressing EGFP-β-actin, as well as untransfected B16F1 cells, were provided by Dr. C. Ballestrem (Weizmann Institute of Science, Rehovot, Israel) and were cultured as described previously (Ballestrem et al., 1998). For experiments, cells were plated onto coverslips coated with 10–25 μg/ml laminin (Invitrogen) and blocked with 0.1 μg/ml heat-inactivated BSA. For live imaging, cells were transferred from DME into L-15 medium at least 2 h before observation.

EGFP-VASP–expressing construct was obtained from Drs. J. Bear and F. Gertler (Massachusetts Institute of Technology, Cambridge, MA). EGFP-fascin (Adams and Schwartz, 2000) was provided by Dr. J. Adams (Cleveland Clinic Foundation, Cleveland, OH). EGFP-α-actinin (Edlund et al., 2001) was obtained from Dr. C. Otey (University of North Carolina, Chapel Hill, NC). For transient protein expression, cells were transfected with FuGENE™ 6 (Roche) according to the manufacturer's recommendation.

The following primary antibodies were used for immunostaining: affinity-purified rabbit antibody to ARPC5 subunit of Arp2/3 (unpublished data), capping protein antibody (Schafer et al., 1994; provided by Dr. D.A. Schafer, University of Virginia, Charlottesville, VA), and mouse monoclonal cortactin antibody, clone 4F11 (Upstate Biotechnology). Secondary TRITC-conjugated antibodies were purchased from Sigma-Aldrich.

Microscopy

Light microscopy was performed using an inverted microscope (Eclipse or Diaphot 300; Nikon) equipped with a Plan 100×, 1.3 NA objective and a back-illuminated cooled CCD camera (model CH250; Roper Scientific) or a slow-scan cooled CCD camera (model CH350; Photometrics), respectively, driven by MetaMorph® imaging software (Universal Imaging Corp.). FITC filter set was used for GFP-fusion protein observations, and Cy3 and Texas Red filter sets were used for rhodamine and Texas Red imaging, respectively. For live imaging, cells were kept on the microscope stage at 36–37°C during observation.

Immunostaining was performed after cell extraction for 3–10 min with 1% Triton X-100 in PEM buffer (100 mM Pipes, pH 6.9, 1 mM $MgCl_2$, and 1 mM EGTA), containing 4% polyethylene glycol, mol wt 40,000 (SERVA), and 2 μM phalloidin (Sigma-Aldrich), followed by fixation with 0.2% glutaraldehyde and quenching with $NaBH_4$. For phalloidin staining, 0.033 μM Texas Red phalloidin (Molecular Probes, Inc.) was added to the extraction solution instead of unlabeled phalloidin. GFP-fascin–expressing cells were stained with Texas Red phalloidin after fixation of unextracted cells, followed by permeabilization with 1% Triton X-100 in PBS.

For determination of protein dissociation from the cytoskeletons, GFP-fascin or GFP-VASP cells were grown on locator coverslips, extracted as for immunostaining, and images of cells expressing fusion proteins were acquired within 20 min after extraction. Then cells were washed twice with PEM containing 2 μM phalloidin and left in this buffer overnight at RT. After incubation, another set of images of the same cells was acquired. Platinum replica EM and correlative light EM were performed as described previously (Svitkina and Borisy, 1998).

We thank Drs. C. Ballestrem, J. Bear, F. Gertler, J. Adams, C. Otey, and D.A. Schafer for gifts of reagents and Dr. M. Mejillano, Dr. A. Biyasheva, and I. Maly for critical reading of the manuscript.

Supported by NIH Grants GM 62431 and IU 54 GM 63126 to G.G. Borisy.

Submitted: 31 October 2002
Revised: 23 December 2002
Accepted: 23 December 2002

References

Adams, J.C., and M.A. Schwartz. 2000. Stimulation of fascin spikes by thrombospondin-1 is mediated by the GTPases Rac and Cdc42. *J. Cell Biol.* 150: 807–822.

Bachmann, C., L. Fischer, U. Walter, and M. Reinhard. 1999. The EVH2 domain of the vasodilator-stimulated phosphoprotein mediates tetramerization, F-actin binding, and actin bundle formation. *J. Biol. Chem.* 274:23549–23557.

Ballestrem, C., B. Wehrle-Haller, and B.A. Imhof. 1998. Actin dynamics in living

mammalian cells. *J. Cell Sci.* 111:1649–1658.

Bamburg, J.R. 1999. Proteins of the ADF/cofilin family: essential regulators of actin dynamics. *Annu. Rev. Cell Dev. Biol.* 15:185–230.

Bartles, J.R. 2000. Parallel actin bundles and their multiple actin-bundling proteins. *Curr. Opin. Cell Biol.* 12:72–78.

Bear, J.E., T.M. Svitkina, M. Krause, D.A. Schafer, J.J. Loureiro, G.A. Strasser, I.V. Maly, O.Y. Chaga, J.A. Cooper, G.G. Borisy, and F.B. Gertler. 2002. Antagonism between Ena/VASP proteins and actin filament capping regulates fibroblast motility. *Cell.* 109:509–521.

Berg, J.S., and R.E. Cheney. 2002. Myosin-X is an unconventional myosin that undergoes intrafilopodial motility. *Nat. Cell Biol.* 4:246–250.

Borisy, G.G., and T.M. Svitkina. 2000. Actin machinery: pushing the envelope. *Curr. Opin. Cell Biol.* 12:104–112.

Carlier, M.F., and D. Pantaloni. 1997. Control of actin dynamics in cell motility. *J. Mol. Biol.* 269:459–467.

Cohan, C.S., E.A. Welnhofer, L. Zhao, F. Matsumura, and S. Yamashiro. 2001. Role of the actin bundling protein fascin in growth cone morphogenesis: localization in filopodia and lamellipodia. *Cell Motil. Cytoskeleton.* 48:109–120.

Cooper, J.A., and D.A. Schafer. 2000. Control of actin assembly and disassembly at filament ends. *Curr. Opin. Cell Biol.* 12:97–103.

DePasquale, J.A., and C.S. Izzard. 1991. Accumulation of talin in nodes at the edge of the lamellipodium and separate incorporation into adhesion plaques at focal contacts in fibroblasts. *J. Cell Biol.* 113:1351–1359.

DeRosier, D.J., and L.G. Tilney. 2000. F-actin bundles are derivatives of microvilli: What does this tell us about how bundles might form? *J. Cell Biol.* 148:1–6.

Edlund, M., M.A. Lotano, and C.A. Otey. 2001. Dynamics of alpha-actinin in focal adhesions and stress fibers visualized with alpha-actinin-green fluorescent protein. *Cell Motil. Cytoskeleton.* 48:190–200.

Evangelista, M., D. Pruyne, D.C. Amberg, C. Boone, and A. Bretscher. 2002. Formins direct Arp2/3-independent actin filament assembly to polarize cell growth in yeast. *Nat. Cell Biol.* 4:32–41.

Flanagan, L.A., J. Chou, H. Falet, R. Neujahr, J.H. Hartwig, and T.P. Stossel. 2001. Filamin A, the Arp2/3 complex, and the morphology and function of cortical actin filaments in human melanoma cells. *J. Cell Biol.* 155:511–517.

Hall, A. 1998. Rho GTPases and the actin cytoskeleton. *Science.* 279:509–514.

Han, Y.H., C.Y. Chung, D. Wessels, S. Stephens, M.A. Titus, D.R. Soll, and R.A. Firtel. 2002. Requirement of a vasodilator-stimulated phosphoprotein family member for cell adhesion, the formation of filopodia, and chemotaxis in *Dictyostelium*. *J. Biol. Chem.* 277:49877–49887.

Higgs, H.N., and T.D. Pollard. 2001. Regulation of actin filament network formation through ARP2/3 complex: activation by a diverse array of proteins. *Annu. Rev. Biochem.* 70:649–676.

Ho, H.Y., R. Rohatgi, L. Ma, and M.W. Kirschner. 2001. CR16 forms a complex with N-WASP in brain and is a novel member of a conserved proline-rich actin-binding protein family. *Proc. Natl. Acad. Sci. USA.* 98:11306–11311.

Katoh, K., K. Hammar, P.J. Smith, and R. Oldenbourg. 1999a. Arrangement of radial actin bundles in the growth cone of *Aplysia* bag cell neurons shows the immediate past history of filopodial behavior. *Proc. Natl. Acad. Sci. USA.* 96: 7928–7931.

Katoh, K., K. Hammar, P.J. Smith, and R. Oldenbourg. 1999b. Birefringence imaging directly reveals architectural dynamics of filamentous actin in living growth cones. *Mol. Biol. Cell.* 10:197–210.

Kozma, R., S. Ahmed, A. Best, and L. Lim. 1995. The Ras-related protein Cdc42Hs and bradykinin promote formation of peripheral actin microspikes and filopodia in Swiss 3T3 fibroblasts. *Mol. Cell. Biol.* 15:1942–1952.

Kranewitter, W.J., C. Danninger, and M. Gimona. 2001. GEF at work: Vav in protruding filopodia. *Cell Motil. Cytoskeleton.* 49:154–160.

Krugmann, S., I. Jordens, K. Gevaert, M. Driessens, J. Vandekerckhove, and A. Hall. 2001. Cdc42 induces filopodia by promoting the formation of an IRSp53:Mena complex. *Curr. Biol.* 11:1645–1655.

Kureishy, N., V. Sapountzi, S. Prag, N. Anilkumar, and J.C. Adams. 2002. Fascins, and their roles in cell structure and function. *Bioessays.* 24:350–361.

Langanger, G., J. de Mey, M. Moeremans, G. Daneels, M. de Brabander, and J.V. Small. 1984. Ultrastructural localization of alpha-actinin and filamin in cultured cells with the immunogold staining (IGS) method. *J. Cell Biol.* 99:1324–1334.

Lanier, L.M., M.A. Gates, W. Witke, A.S. Menzies, A.M. Wehman, J.D. Macklis, D. Kwiatkowski, P. Soriano, and F.B. Gertler. 1999. Mena is required for neurulation and commissure formation. *Neuron.* 22:313–325.

Lewis, A.K., and P.C. Bridgman. 1992. Nerve growth cone lamellipodia contain two populations of actin filaments that differ in organization and polarity. *J. Cell Biol.* 119:1219–1243.

Li, Z., E.S. Kim, and E.L. Bearer. 2002. Arp2/3 complex is required for actin polymerization during platelet shape change. *Blood.* 99:4466–4474.

Loureiro, J.J., D.A. Rubinson, J.E. Bear, G.A. Baltus, A.V. Kwiatkowski, and F.B. Gertler. 2002. Critical roles of phosphorylation and actin binding motifs, but not the central proline-rich region, for Ena/vasodilator-stimulated phosphoprotein (VASP) function during cell migration. *Mol. Biol. Cell.* 13: 2533–2546.

Mallavarapu, A., and T. Mitchison. 1999. Regulated actin cytoskeleton assembly at filopodium tips controls their extension and retraction. *J. Cell Biol.* 146: 1097–1106.

Maly, I.V., and G.G. Borisy. 2001. Self-organization of a propulsive actin network as an evolutionary process. *Proc. Natl. Acad. Sci. USA.* 98:11324–11329.

Miki, H., T. Sasaki, Y. Takai, and T. Takenawa. 1998. Induction of filopodium formation by a WASP-related actin-depolymerizing protein N-WASP. *Nature.* 391:93–96.

Mogilner, A., and G. Oster. 1996. Cell motility driven by actin polymerization. *Biophys. J.* 71:3030–3045.

Nobes, C.D., and A. Hall. 1995. Rho, rac, and cdc42 GTPases regulate the assembly of multimolecular focal complexes associated with actin stress fibers, lamellipodia, and filopodia. *Cell.* 81:53–62.

Pollard, T.D., L. Blanchoin, and R.D. Mullins. 2000. Molecular mechanisms controlling actin filament dynamics in nonmuscle cells. *Annu. Rev. Biophys. Biomol. Struct.* 29:545–576.

Pruyne, D., M. Evangelista, C. Yang, E. Bi, S. Zigmond, A. Bretscher, and C. Boone. 2002. Role of formins in actin assembly: nucleation and barbed-end association. *Science.* 297:612–615.

Qualmann, B., and R.B. Kelly. 2000. Syndapin isoforms participate in receptor-mediated endocytosis and actin organization. *J. Cell Biol.* 148:1047–1062.

Resch, G.P., K.N. Goldie, A. Krebs, A. Hoenger, and J.V. Small. 2002. Visualisation of the actin cytoskeleton by cryo-electron microscopy. *J. Cell Sci.* 115: 1877–1882.

Rohatgi, R., L. Ma, H. Miki, M. Lopez, T. Kirchhausen, T. Takenawa, and M.W. Kirschner. 1999. The interaction between N-WASP and the Arp2/3 complex links Cdc42-dependent signals to actin assembly. *Cell.* 97:221–231.

Rohatgi, R., H.Y. Ho, and M.W. Kirschner. 2000. Mechanism of N-WASP activation by CDC42 and phosphatidylinositol 4, 5-bisphosphate. *J. Cell Biol.* 150:1299–1310.

Rottner, K., B. Behrendt, J.V. Small, and J. Wehland. 1999. VASP dynamics during lamellipodia protrusion. *Nat. Cell Biol.* 1:321–322.

Sagot, I., S.K. Klee, and D. Pellman. 2002a. Yeast formins regulate cell polarity by controlling the assembly of actin cables. *Nat. Cell Biol.* 4:42–50.

Sagot, I., A.A. Rodal, J. Moseley, B.L. Goode, and D. Pellman. 2002b. An actin nucleation mechanism mediated by Bni1 and profilin. *Nat. Cell Biol.* 4:626–631.

Schafer, D.A., Y.O. Korshunova, T.A. Schroer, and J.A. Cooper. 1994. Differential localization and sequence analysis of capping protein beta-subunit isoforms of vertebrates. *J. Cell Biol.* 127:453–465.

Small, J.V. 1994. Lamellipodia architecture: actin filament turnover and the lateral flow of actin filaments during motility. *Semin. Cell Biol.* 5:157–163.

Small, J.V. 1988. The actin cytoskeleton. *Electron Microsc. Rev.* 1:155–174.

Small, J.V., G. Rinnerthaler, and H. Hinssen. 1982. Organization of actin meshworks in cultured cells: the leading edge. *Cold Spring Harb. Symp. Quant. Biol.* 46:599–611.

Small, J.V., K. Rottner, I. Kaverina, and K.I. Anderson. 1998. Assembling an actin cytoskeleton for cell attachment and movement. *Biochim. Biophys. Acta.* 1404:271–281.

Small, J.V., T. Stradal, E. Vignal, and K. Rottner. 2002. The lamellipodium: where motility begins. *Trends Cell Biol.* 12:112–120.

Stradal, T., K.D. Courtney, K. Rottner, P. Hahne, J.V. Small, and A.M. Pendergast. 2001. The Abl interactor proteins localize to sites of actin polymerization at the tips of lamellipodia and filopodia. *Curr. Biol.* 11:891–895.

Svitkina, T.M., and G.G. Borisy. 1998. Correlative light and electron microscopy of the cytoskeleton of cultured cells. *Methods Enzymol.* 298:570–592.

Svitkina, T.M., and G.G. Borisy. 1999a. Arp2/3 complex and actin depolymerizing factor/cofilin in dendritic organization and treadmilling of actin filament array in lamellipodia. *J. Cell Biol.* 145:1009–1026.

Svitkina, T.M., and G.G. Borisy. 1999b. Progress in protrusion: the tell-tale scar. *Trends Biochem. Sci.* 24:432–436.

Svitkina, T.M., A.B. Verkhovsky, K.M. McQuade, and G.G. Borisy. 1997. Analysis of the actin-myosin II system in fish epidermal keratocytes: mechanism of cell body translocation. *J. Cell Biol.* 139:397–415.

Weaver, A.M., A.V. Karginov, A.W. Kinley, S.A. Weed, Y. Li, J.T. Parsons, and J.A. Cooper. 2001. Cortactin promotes and stabilizes Arp2/3-induced actin filament network formation. *Curr. Biol.* 11:370–374.

The Journal of Cell Biology

An improved silencing vector co-expressing GFP and small hairpin RNA

Shin-ichiro Kojima*, Danijela Vignjevic and Gary G. Borisy

Department of Cell and Molecular Biology, Feinberg School of Medicine, Northwestern University

303 E. Chicago Ave., Chicago, IL 60611, USA

*Address correspondence to:

E-mail: s-kojima@northwestern.edu

Key words: siRNA, green fluorescence protein, pG-SUPER, quantitative immunofluorescence, gene replacement

Abstract

Small interfering RNA (siRNA) is a powerful tool for the specific silencing of gene expression. We developed an improved vector, pG-SUPER, that coexpresses GFP and small hairpin RNA simultaneously to facilitate analysis of silencing at the level of individual cells. As a test system, we analyzed laminA/C knock down in HeLa cells. The GFP signal was a reliable reporter (93-98%) of strong knockdown (90%) over a wide range of GFP intensities. The GFP reporter made possible the application of fluorescent activated cell sorting (FACS) to purify the knockdown cell population. Such populations facilitated Western blotting analysis to determine depletion of the target protein. pG-SUPER was also applied to evaluate gene replacement by exogenous genes rendered refractory to siRNA by introducing silent mutations. Recovery of laminA was linearly correlated to the expression level of the rescue gene. pG-SUPER will expand plasmid-based siRNA applications through the easy and reliable detection of knock down and rescued cells.

Introduction

RNA interference (RNAi) has emerged recently as a powerful method for gene silencing or knockdown of gene expression. In this technique, double stranded RNA induces the degradation of cognate message sequences resulting ultimately in depletion of the encoded protein (1). At the first step of RNA interference, a double-stranded RNA-dependent ribonuclease known as DICER processes double-stranded RNA into approximately 21-23 nucleotide (nt) fragments known as small interfering RNAs (siRNAs) (2-4). The siRNAs bind to the RNA-induced silencing complex (RISC) and guide that multicomponent nuclease complex to its substrate through base-pairing (2,5). RISC cleaves the hybrid complex of the siRNA and the target RNA (4,5), thus leading to target degradation and knockdown of gene expression.

There are two common ways to introduce siRNA into cells. One is the in vitro synthesis of siRNA followed by transfection (6). The other way is by expression of a DNA plasmid encoding an siRNA precursor. In the in vitro approach, a 19-nt sequence, which should be unique in the genome, is selected from the gene to be silenced. Sense and antisense RNA oligonucleotides are chemically synthesized together with an additional 2-nt at their 3'-termini. Annealing of the sense and antisense oligonucleotides makes functional siRNA, in which the 19-nt double-stranded RNA has 2-nt 3'-overhangs in both strands. The resultant siRNA is then transfected to cells by liposome-mediated methods. In vitro studies have shown that such a form of siRNA is the most effective (7). In the DNA plasmid approach, a short RNA fragment is expressed under an RNA polymerase III promoter (8-10). In commonly used methods, the expressed RNA contains the 19 nt target, which is followed by a 6-9 nt spacer, then the complementary sequence of the target and, finally, is terminated with UU. The self-

complementarity causes the expressed short RNA to form a hairpin shape. Constructed expression plasmids are transfected into cells by conventional methods. In the cells, the expressed small hairpin RNA is processed by DICER to become functional siRNA (11) which is integrated into RISC to cause specific degradation of the target mRNA of interest.

At present, there are several technical issues to the application of siRNA. Some issues arise from the fact that many cell types can be transfected only with low efficiency, resulting unavoidably in a large fraction of untransfected cells that contaminate the population. For studies of putative knockdown phenotypes in individual cells, transfectants need to be identified easily and unambiguously in mixed populations. This is particularly acute for studies involving live cell imaging. For mass analysis, such as Western blotting, it is critical to obtain pure transfectant populations since untransfected cells will otherwise mask the knockdown effect.

Other critical issues involve the persistence of the knockdown effect, the design of proper controls and the opportunity to develop a true "cellular genetics". Plasmid-based siRNA systems potentially offer many applications when combined with conventional molecular biological methods. Since RNA interference is very sensitive to base mismatch, an siRNA-refractory gene can be prepared by mutations of the target sequence that do not alter the encoded amino acid residues. Such an altered gene containing silent mutations would allow for "rescue" when introduced to cells in which the endogenous gene expression was silenced. Rescue provides a stringent control for the specificity of targeting by siRNA. More interestingly, it may be possible to replace an endogenous gene with mutants with amino acid substitutions or truncations, and to analyze their phenotypes. Although such cellular genetic approaches sound attractive at the hypothetical level, significant technical problems remain to be examined or solved.

Here we report the construction of an improved vector, pG-SUPER, that coexpresses green fluorescence protein (GFP) and small hairpin RNA simultaneously. The GFP serves as a reporter for expression of knockdown at the single cell level and allows for FACS purification of the knockdown population. We used laminA/C in HeLa cells as a model system to evaluate quantitatively the correlation of GFP expression with gene knockdown. We report the use of pG-SUPER for single cell phenotype analysis, FACS purification and gene replacement.

Materials & methods

Cell Culture and transfection

HeLa cells were obtained from American Type Culture Collection (ATCC) and grown in MEM supplemented with 0.15% Na-bicarbonate, 1 mM Na-pyuravte, 1x Non-essential amino acids (Mediatech) and 10% fetal calf serum. FuGENE6 (Roche) was used for transfection of plasmid DNA. Usually 3-4 μl of FuGENE6 was used per 1 μg of plasmid DNA. Electroporation was carried out as described (12).

Plasmid construction

pSUPER was a gift from Dr. R. Agami (The Netherlands Cancer Institute). pME18S-f1 was provided by Dr. K. Fujiwara (Univ. Rochester). pEYFP-laminA was given by Dr. R. Goldman (Northwestern Univ.).

DNA encoding EGFP was extracted from pEGFP-N1 (Clontech) with EcoRI and Not I, and then inserted into pME18S-f1 (named pME-EGFP). pSUPER was digested with XbaI and XhoI, and then blunted with Klenow large fragment. The extracted H1 RNA promoter fragment

was inserted to pME-EGFP that was digested with SspI and HindIII, and blunted with the Klenow large fragment (named pG-SUPER). pG-SUPER-hLaminA and -mFascin1 were constructed according to (10). The targeting sequences are nt 820-838 of human laminA/C (NM_005572) and nt 819-837 of mouse fascin1 (NM_007984).

pCMV-myc-laminA, which expresses N-terminally myc-tagged human laminA1, was created by removal of the EYFP part from pEYFP-laminA with NheI-SpeI digestion and self-ligation. pCMV-myc-laminA* with two base pair mismatches within the target sequence was prepared by QuikChange® II Site-Directed Mutagenesis Kit (Stratagene). Nucleotides C^{828} and G^{831} were substituted with T and A respectively. These point mutations did not change encoding amino acids. Control empty vector, pCMV, was prepared from pEGFP-C1 that was digested with AgeI and BspEI and subjected to self-ligation. pCMV contains the CMV promoter but not any gene.

Immunofluorescence

After 3-9 days culture, cells were fixed with 4% formaldehyde for 30 min, and permeabilized with 1% Triton X-100 for 5 min. Mouse monoclonal anti-laminA/C (clone 636, Santa Cruz) was used as a primary antibody at 1:100 dilution. For the rescue experiments, rabbit anti-myc antibody (Covance Research Products) were simultaneously reacted at 1:500 dilution. Tetramethylrhodamine isothiocyanate (TRITC)-conjugated anti-mouse IgG (Jackson) and Cy5-conjugated anti-rabbit IgG (Jackson) antibodies were used as secondary antibodies. DNA was stained with 10 μg/ml of Hoechst 33258. Cell preparations were imaged with a Nikon Diaphot 300 inverted microscope equipped with a Fluor 20x, 0.75 NA dry objective and a slow scan

cooled CCD camera CH350 (Photometrics). MetaMorph imaging software (Universal Imaging) was used for image acquisition and data analysis.

Image analysis

Multispectral fluorescence imaging was performed with a quad filter set (Chroma, 86000). GFP expressing cells were randomly selected in the FITC channel and then DNA, GFP and TRITC images were recorded. For the rescue experiments, Cy5 images were additionally acquired. The excitation and emission filters were changed using a Lambda 10-2 Optical Filter Controller (Sutter Instrument). For interphase cells, nuclear regions were defined by manual tracing of the Hoechst 33258 staining areas. Then the mean intensity of GFP, TRITC and Cy5 (if necessary) were measured in individual cell nuclei. Then the background level of GFP and TRITC were measured in regions where cell nuclei were not present. The corrected GFP and TRITC were defined as;

$$I_{corrected}=I_{raw}-I_{background}$$

The TRITC intensity was normalized by the mean value of GFP-negative cells. As a result, laminA/C amounts were represented as percentages of the average level in a normal population. For Cy5 images, there was some nonspecific signal to cell nuclei. Thus, for each image, the mean value ($I_{nonspec}$) of the Cy5 intensity was calculated for cells that did not express myc-laminA (~90% of cells). Then the corrected values were defined as;

$$I_{corrected}=I_{raw}-I_{nonspec}$$

Immunoblotting

Cells were lysed with 50 μL of Lysis Buffer (31.25 mM Tris-HCl, 2% SDS and 10% glycerol, pH6.8). Protein concentration was determined by the BCA protein assay procedure (Pierce). The protein samples were subjected to SDS-PAGE on 4-20% gradient gels and then transferred to nitrocellulose membranes (PROTRAN, Schleicher & Schuell). After blocking with 5% skim milk, mouse anti-laminA/C (clone 636, Santa Cruz) or mouse anti-myc (clone 9E10, Santa Cruz) was reacted with the membrane at a dilution of 1:500 and 1:1000 respectively. After incubation with horseradish peroxidase-conjugated anti-mouse IgG, signal was detected on an X-ray film (CL-Xposure, Pierce) by chemical luminescence (ECL Western Blotting Detection Reagents, Amersham). The films were scanned with Adobe Photoshop software and then analyzed with NIH Image1.6 software. To control for loading on the gels, antibody was stripped from the membranes by Restore Western Blot Stripping Buffer (Pierce) and the stripped membranes were re-assayed by using mouse anti-α-tubulin (clone B-5-1-2, Sigma-Aldrich) at 1:10000 dilution.

Results

Construction of pG-SUPER

In order to make it possible to identify cells that express hairpin-siRNA, we constructed a new vector, pG-SUPER (Fig. 1A). This vector contains two expression units. One is the expression cassette of hairpin siRNA under the human H1 RNA promoter as originally reported for pSUPER. In pG-SUPER, the same restriction enzyme sites (BglII-HindIII) as in pSUPER are used for insertion of in vitro annealed DNA oligonucleotide primers. In addition, pG-SUPER contains the enhanced green fluorescent protein (EGFP) expression cassette that is driven under

the SRα promoter (13). Therefore, cells that receive pG-SUPER-based silencing constructs can be detected by fluorescence of GFP.

In order to test whether pG-SUPER works as predicted, we used laminA/C silencing in HeLa cells as a model system. Lamins A and C are major components of the nuclear lamina underlying the inner nuclear membrane. These two major isoforms are translated from spliced variants of a single gene (14). Since laminA/C is dispensable in tissue culture cells (6,15), we could avoid potential bias from killing or compromising transfectants by silencing the target gene. The selected target 19-nt is located at nt 820-838 (NM_005572), which is identical to what has been reported to function by using in vitro synthesized siRNA (6). We designed and inserted DNA oligoduplex following the criteria of Brummelkamp et al (10). The resulting human laminA/C targeting construct was termed pG-SUPER-hLaminA/C. Six days after transfection to HeLa cells, endogenous laminA/C was assayed by immunofluorescence (Fig. 1B). In the GFP-positive cells, the laminA/C amount was significantly reduced as compared with neighboring GFP-negative cells. This qualitative result supports the initial idea that pG-SUPER will work for identifying individual knockdown cells by GFP expression.

Establishing quantitative immunofluorescence assay

The relationship between the knockdown effect and GFP expression was analyzed quantitatively. For this purpose, we first optimized experimental conditions. To detect low levels of GFP expression, fixation methods were explored. We found that formaldehyde fixation preserved GFP fluorescence without enhancing cellular fluorescence better than methanol or glutaraldehyde fixation (data not shown). The line scan in Fig. 1C shows that cellular autofluorescence (GFP-negative cells in Fig. 1B) is negligibly low in the GFP-channel (green

line). More precisely, the mean fluorescence intensity of the nuclear region was ~10±20 arbitrary units (AU) for GFP-negative cells in our assay, whereas the maximum GFP intensity exceeded 60,000 AU in GFP-positive cells 3 days after transfection. We defined 70 AU as the threshold of the real GFP signal. In practical terms, 70 AU was too dim to be detected by eye looking through the oculars. For quantification of laminA/C protein levels, we used immunofluorescence with mouse monoclonal antibody (clone 636, Santa Cruz) visualized by tetramethylrhodamine isothiocyanate (TRITC)-labeled anti-mouse IgG antibody. Cross-reaction of the primary and secondary antibodies was checked. In immunofluorescence with the second antibody alone, no significant signal was observed (data not shown). For the primary antibody, line scan analysis (Fig. 1C) revealed that the anti-laminA/C antibody had negligible crossreaction in the cytoplasmic region. The specificity of the primary antibody was also confirmed by Western blotting. Only two bands corresponding to laminA and C were detected (data not shown). These results indicate that even low levels of both GFP and laminA/C can be detected in our assay system without significant interference by background fluorescence.

The procedure for quantifying fluorescence consisted of first randomly choosing view fields containing GFP positive cells. Then images of DNA, GFP and LaminA/C were taken in the blue, green and red channels, respectively, at prefixed exposure times. The nuclear regions were determined in the DNA image and used to measure the mean intensity of GFP and TRITC for each cell. After subtraction of the background level of signal, the corrected GFP and TRITC intensity represent protein levels of GFP and laminA/C respectively. Since immunofluorescence gave slightly different staining levels for each specimen even by following the same procedure, we normalized the TRITC intensity to the average level of the GFP-negative cells in the same specimen. After normalization, the laminA/C level of each cell is represented as the percentage

of the average in the non-silenced cell population. By using this assay, we obtained results reproducibly.

Correlation between knockdown and GFP expression

Figure 2 shows the results of HeLa cells 6 days post-transfection of pG-SUPER-hLaminA/C and two negative controls. We analyzed more than 100 GFP-positive cells for each sample. The fluorescence range of GFP was from 70 AU to 13,000 AU, suggesting that expression level per cell differed by a factor of 185. The mean level of endogenous laminA/C in GFP-positive cells of pG-SUPER-hLaminA/C transfection was reduced to 12.4% of non transfected cells. However, the silencing effect might be underestimated, since the possible crossreaction of the primary antibody to other nuclear proteins was not considered. To confirm that the observed silencing was due to expression of hairpin siRNA against laminA/C, we performed the same analysis with pG-SUPER empty vector and pG-SUPER-mFascin1. pG-SUPER-mFascin1 contained the mouse fascin1-targeting sequence, which does not exist in the human genome. Therefore pG-SUPER-mFascin1 would provide siRNA, which was functional for mouse fascin1 (Vignjevic, manuscript in preparation) but not for any human genes. In both negative controls, the laminA/C amounts were indistinguishable between the GFP-positive and -negative populations. The results indicate that inclusion of the GFP reporter cassette did not compromise the silencing capability of the parent vector, pSUPER.

The "penetrance" of the knockdown effect in the whole population of GFP-positive cells was evaluated statistically. Untransfected HeLa cells showed heterogeneity in laminA/C amount with a standard deviation, σ, = 22.5% with respect to the mean value, m, defined as 100%. For an objective definition of silencing, we compared the laminA/C level of each GFP-positive cell

to m and σ. Only 2% of GFP-positive cells had a laminA/C amount within the range [m-σ, m+σ], representing no silencing effect. In contrast, the laminA/C amounts of 93% of GFP-positive cells were below m-3σ, implying statistically significant reduction of laminA/C. Therefore the penetrance of pG-SUPER-hLaminA/C was estimated as 93-98%, indicating strong correlation between knock down and GFP expression.

Does the GFP-negative cell population contain significant numbers of false negatives that display the knockdown effect? We think this is not the case for the following reason. The standard deviation for laminA/C content in GFP-negative cells was 19.8% and 22.5% for pG-SUPER empty vector and pG-SUPER-mFascin1 respectively. This indicates that ~20% is a usual standard deviation for laminA/C amount in the normal HeLa cell population. Importantly, these values are substantially the same as that observed for GFP-negative cells in transfection of pG-SUPER-hLaminA/C (22.5%), indicating that a statistically negligible fraction of GFP-negative cells had the silencing effect when pG-SUPER-laminA/C was transfected. Taking the results together, we conclude that the pG-SUPER approach does not lead to appreciable false positives or false negatives.

Kinetics of knockdown

The tight correlation between GFP and knockdown in pG-SUPER allowed us to determine the time course of silencing (Fig. 3A). Protein levels of laminA/C fell rapidly after the 3rd day and by 7 days reached a low plateau of about 10% of the initial mean level. The relationship between the extent of silencing and the level of EGFP expression was determined by evaluating scatterplots of levels in individual cells (Fig. 3B-D). In these figures, red and green dots correspond to individual GFP-negative and -positive cells respectively. GFP intensity values are

taken to be an indicator of the amount of small hairpin RNA. However, it should be noted that the relationship may not be completely proportional because of unidentified factors that might affect transcription efficiency.

Fig. 3B shows that silencing at 3 days after transfection was partial (46.1±21.0%). The partial silencing was observed over the whole range of GFP intensity and the silencing effect did not show a clear correlation to the GFP intensity. Therefore, shortage of siRNA is unlikely to be the reason for partial knockdown on the third day. Instead, it is more likely that remaining laminA/C protein that was synthesized before transfection had not yet been fully cleared from the cells and this residual protein masked the effect of degradation of laminA/C mRNA.

The knockdown effect was surprisingly persistent. It lasted to at least the 9th day after transfection. After that, the GFP signal became too dim to perform quantitative analysis. GFP-expressing cells not showing silencing were rare (1-2%). The rare lack of silencing seemed unrelated to GFP expression level since it was observed at both low and high GFP intensity values. More importantly, the overwhelming number of cells showed fairly uniform silencing over a wide range of GFP intensity (Figs. 3C & D). The small variance in silencing was not correlated to GFP intensity. Therefore, the knock down effect was likely saturated by a rather small amount of small hairpin RNA. We conclude that, to a first approximation, GFP-positive cells have homogenous silencing independent of GFP expression level in the pG-SUPER system.

Purification of knockdown cells by FACS

Fluorescence activated cell sorting (FACS) was used to purify GFP-positive cells 24 hr post-transfection. Under our conditions, the initially sorted population was >99% pure and one week after FACS, more than 80% of the cells still had GFP signal (Fig. 4A). In contrast, without

FACS, the fraction of GFP-positive cells was 15-20%. It should be noted that the threshold for GFP in FACS was higher than that in counting cells by fluorescence microscopy in order to minimize contamination with non-transfectants. Extracts of sorted cells analyzed by Western blotting 7 days post FACS showed that neither pG-SUPER empty vector nor pG-SUPER-mFascin1 caused any reduction in levels of laminA/C (Fig. 4B) as compared to non-transfected cells. However, transfection with pG-SUPER-hLaminA/C, caused substantial depletion of laminA/C. By comparison with diluted untransfected cell extracts, we estimated that the level of laminA/C in the population was reduced to <25%. Taking into account that ~20% of the cells at 7 days post FACS were GFP-negative, the level of laminA/C in the GFP-positive cells was reduced to <10%, which is consistent with the immunofluorescence results. Reduction of laminA/C was not readily detected in the unsorted population presumably because non-transfected cells masked the knockdown effect.

Gene replacement of laminA/C

Gene rescue or replacement provides a stringent control for the specificity of silencing. We prepared a laminA cDNA refractory to siRNA by introducing mutations within the target sequence. Two nucleotide substitutions were introduced to an expression construct of myc-tagged human laminA1 (Fig. 5A). These were silent mutations so that the expressed laminA had no amino acid changes. During optimization of the rescue experiment, we found that electroporation was an efficient way of gene delivery to HeLa cells, resulting in more than 90% of cells expressing GFP when assayed 5-7 days later. Subsequent to knockdown (4 days after electroporation), the myc-laminA rescue construct was transfected to the cell population with FuGENE6 and allowed to express for an additional 2 days of culture. Western blotting (Fig. 5B)

showed that the rescue construct (*) expressed higher levels of laminA than the wild type (WT) construct, indicating that a two base mismatches provided resistance to knockdown by siRNA.

Gene replacement was also analyzed at the individual cell level. Cells were immunostained with mouse anti-laminA/C and rabbit anti-myc antibodies to reveal total laminA/C and replacement laminA, respectively (Fig. 5C). GFP-expressing cells showed remarkable reduction of laminA/C as compared with GFP-negative cells except for those cells also positive for the myc tag (arrows). These cells corresponded to rescued individuals expressing exogenous myc-laminA. Rescue was quantified by scatterplot analysis of ~1000 GFP-positive cells each for the rescue construct and empty vector (Fig. 5D). When the empty vector was used for the second transfection, laminA/C levels were knocked-down as previously shown (Fig. 3C), demonstrating that sequential plasmid-delivery (electroporation and liposome-mediated transfection) did not disturb the knockdown process. However, when using the rescue construct, many GFP-expressing cells showed an increased amount of laminA/C and these cells expressed myc-tagged laminA at levels close to the normal range (20-170% of normal cells; blue dots in Fig. 5D lower panel). This result is consistent with the immunoblot results that two point mutations were sufficient to render the mutant laminA refractory to siRNA. Importantly, the rescue was observed over a wide range of GFP intensity. Levels of total laminA/C correlated linearly with levels of the myc-tagged rescue laminA (Fig. 5E). This provides strong evidence indicating that the observed recovery was caused by introduction of the exogenous gene. Extrapolation of the least squares regression line in Fig. 5E to zero knockdown gave a value for residual endogenous laminA/C of ~10%, consistent with the value for non-rescued cells. The results demonstrate that endogenous laminA/C can be knocked-down substantially by pG-

SUPER encoded siRNA and replaced to approximately normal levels by a construct refractory to silencing.

Discussion

Properties of pG-SUPER

We report here a new vector, pG-SUPER, for coexpressing GFP and small hairpin RNA. The correlation between GFP expression and gene silencing was tight (93-98%), with rare (2%) false positives. Although we have quantified silencing in detail only for HeLa cells, similar knockdown results have been obtained for B16F1 melanoma cells and two other gene products--fascin and capping protein β (Vignjevic, Mejillano, unpublished results). Thus, although the "penetrance" of the silencing effect by pG-SUPER should be checked for other cell lines, at present we suppose that efficient silencing will be generally observed. Maximal knockdown levels were around 10% which is similar to reported values either by in vitro synthesized siRNA or by plasmid-based siRNA (6,9), indicating that addition of the GFP expression cassette does not disturb small hairpin RNA expression.

Another important feature of pG-SUPER is that the silencing effect approaches saturation at rather small amounts of DNA. Although we have not determined the minimum level sufficient for knockdown, the silencing effect was not dependent on GFP intensity over a wide range of values. Possibly, the siRNA machineries, such as DICER and RISC, are limiting factors. Further considerations in the design of knockdown experiments are the stability and amount of proteins synthesized before expressing small hairpin RNA. Usually, siRNA effects are assayed 48-72 hr after transfection, but at such times preexisting laminA/C partially masked

the silencing effect. Even after 96 hr, the knock down became gradually stronger upon prolonged cell culture. As a generalization, it is reasonable to assume that long-lived proteins will need 4 days or longer in culture to achieve full knockdown. For such proteins, vector-based siRNA expression offers advantages over in vitro synthesized siRNA, since plasmid DNA provides siRNA continuously.

Applications of pG-SUPER

The independence of the silencing effect on the intensity of the GFP signal over a wide range of values suggests additional applications. One is live cell imaging. Simply by GFP-signal, we can easily identify knockdown cells and analyze their phenotypes by bright field or fluorescence microscopy. Even for fixed samples, pG-SUPER will be superior to the conventional silencing vector. By conventional siRNA techniques, knockdown at the individual cell level needs to be confirmed by immunofluorescence. But, in some cases, an antibody may work for Western blotting but not for immunofluorescence. pG-SUPER will give a solution for such cases. Instead of immunofluorescence, the effectiveness of the constructs can be checked by Western blotting of the FACS sorted population. After confirmation, the GFP-positive transfectants can be used for assays of the gene-silenced population.

Again relying on the GFP signal as an indicator, FACS becomes a powerful tool to purify the gene-silenced cells. In our assays, FACS was carried out 24 hr after transfection, allowing collection of transfectants before the silencing effect appears. Thus, FACS-based collection is useful for analysis of essential genes whose knockdown would not allow continued cell propagation. Another important point is that, once selected, the cell population retains the plasmid DNA for a long time--at least 9 days, indicating that FACS-based collection will work

for knocking down of stable proteins. Biochemical experiments critically need pure knocked-down populations. At present, such population analysis is almost impossible in gene silencing by plasmid-based siRNA except for a few cell lines that have extremely high transfection efficiency. By using pG-SUPER combined with FACS, gene silencing will be applicable to many experiments in a wide range of cell types.

Strategy of rescue and gene replacement

Rescue of knockdown and replacement of endogenous laminA/C with myc-tagged laminA was achieved by expression from a cDNA refractory to siRNA. Rescue genes, to be made refractory to silencing, should contain mutations within the target sequence of siRNA. It is not yet certain how accurately siRNA recognizes its target mRNA. Some groups have reported that only 1 base mismatch was enough to abrogate the knockdown effect (7,10). On the other hand, recent papers commented that siRNA might be able to silence gene expression even if 2 or 3 bases were mismatched (16,17). For laminA/C, we found that two nucleotide changes gave successful resistance to siRNA. In our other studies, we examined 2 and 3 base mismatches for capping protein β and fascin (Mejillano, Vignjevic, unpublished results) and found that a 2 base mismatch was sufficient both to abrogate knockdown and to generate a refractory cDNA, which is now our standard procedure.

A critical point in rescue experiments is to identify the rescued cells in a population that, in general, contains normal cells. A related issue is whether a tagged protein is indeed a functional substitute for the endogenous protein. Fluorescence tagging of the rescue protein is, in principle, a convenient way to identify the rescued cells, but the activity of the tagged protein is rarely evaluated. We attempted to rescue the laminA/C knockdown with a YFP-laminA

construct. Unfortunately, the YFP-laminA tended to aggregate, precluding successful rescue. Consequently, we resorted to a myc-tagged construct for rescue of laminA/C knockdown. However, in other experiments, we have successfully rescued fascin and capping protein β knockdown with YFP-tagged constructs (Vignjevic, Mejillano, unpublished results). One of advantages of pG-SUPER is that the fluorescence expression unit can be easily changed for different colors by conventional DNA methods. A rescue construct could be designed to use YFP-tagged protein and the GFP in pG-SUPER could be replaced with CFP. A combination of GFP and DsRed could also be used. Such flexibility of marking color in the pG-SUPER system allows one to use a variety of cell sorting and microscopic techniques.

Expression knockdown and gene replacement with the pG-SUPER system facilitates an equivalent to "cellular genetics". Knockdown of gene product is substantial and reasonably persistent. Rescue allows for stringent evaluation of the specificity of knockdown. Gene replacement provides for a way of evaluating modified gene products in the absence of endogenous protein. Instead of overexpression on a background of endogenous products or expression of dominant negatives, gene replacement at the cellular level offers the opportunity to analyze protein function with the specificity previously afforded only by classical genetics.

Acknowledgments

We thank Drs. R. Agami (The Netherlands Cancer Institute), K. Fujiwara (Rochester Univ.) and R. Goldman (Northwestern Univ.) for pSUPER, pME18S-f1 and pEYFP-laminA/C plasmids respectively. We also acknowledge Dr. Mary Paniagua in the Flow Cytometry Core Facility of Northwestern Univ. for fluorescence activated cell sorting. This research was supported by NIH grant GM 25062 to GGB and the Uehara Memorial Foundation Fellowship to SK.

References

1. **Fire, A., S. Xu, M.K. Montgomery, S.A. Kostas, S.E. Driver and C.C. Mello.** 1998. Potent and specific genetic interference by double-stranded RNA in Caenorhabditis elegans. Nature *391*:806-811.
2. **Hammond, S.M., E. Bernstein, D. Beach and G.J. Hannon.** 2000. An RNA-directed nuclease mediates post-transcriptional gene silencing in Drosophila cells. Nature *404*:293-296.
3. **Bernstein, E., A.A. Caudy, S.M. Hammond and G.J. Hannon.** 2001. Role for a bidentate ribonuclease in the initiation step of RNA interference. Nature *409*:363-366.
4. **Elbashir, S.M., W. Lendeckel and T. Tuschl.** 2001. RNA interference is mediated by 21- and 22-nucleotide RNAs. Genes Dev *15*:188-200.
5. **Martinez, J., A. Patkaniowska, H. Urlaub, R. Luhrmann and T. Tuschl.** 2002. Single-stranded antisense siRNAs guide target RNA cleavage in RNAi. Cell *110*:563-574.
6. **Elbashir, S.M., J. Harborth, W. Lendeckel, A. Yalcin, K. Weber and T. Tuschl.** 2001. Duplexes of 21-nucleotide RNAs mediate RNA interference in cultured mammalian cells. Nature *411*:494-498.
7. **Elbashir, S.M., J. Martinez, A. Patkaniowska, W. Lendeckel and T. Tuschl.** 2001. Functional anatomy of siRNAs for mediating efficient RNAi in Drosophila melanogaster embryo lysate. Embo J *20*:6877-6888.
8. **Sui, G., C. Soohoo, B. Affar el, F. Gay, Y. Shi and W.C. Forrester.** 2002. A DNA vector-based RNAi technology to suppress gene expression in mammalian cells. Proc Natl Acad Sci U S A *99*:5515-5520.
9. **Paul, C.P., P.D. Good, I. Winer and D.R. Engelke.** 2002. Effective expression of small interfering RNA in human cells. Nat Biotechnol *20*:505-508.
10. **Brummelkamp, T.R., R. Bernards and R. Agami.** 2002. A system for stable expression of short interfering RNAs in mammalian cells. Science *296*:550-553.
11. **Paddison, P.J., A.A. Caudy, E. Bernstein, G.J. Hannon and D.S. Conklin.** 2002. Short hairpin RNAs (shRNAs) induce sequence-specific silencing in mammalian cells. Genes Dev *16*:948-958.
12. **Yoon, K.H., M. Yoon, R.D. Moir, S. Khuon, F.W. Flitney and R.D. Goldman.** 2001. Insights into the dynamic properties of keratin intermediate filaments in living epithelial cells. J Cell Biol *153*:503-516.
13. **Takebe, Y., M. Seiki, J. Fujisawa, P. Hoy, K. Yokota, K. Arai, M. Yoshida and N. Arai.** 1988. SR alpha promoter: an efficient and versatile mammalian cDNA expression system composed of the simian virus 40 early promoter and the R-U5 segment of human T-cell leukemia virus type 1 long terminal repeat. Mol Cell Biol *8*:466-472.
14. **Moir, R.D., T.P. Spann and R.D. Goldman.** 1995. The dynamic properties and possible functions of nuclear lamins. Int Rev Cytol *162B*:141-182.

15. **Sullivan, T., D. Escalante-Alcalde, H. Bhatt, M. Anver, N. Bhat, K. Nagashima, C.L. Stewart and B. Burke.** 1999. Loss of A-type lamin expression compromises nuclear envelope integrity leading to muscular dystrophy. J Cell Biol *147*:913-920.
16. **Jackson, A.L., S.R. Bartz, J. Schelter, S.V. Kobayashi, J. Burchard, M. Mao, B. Li, G. Cavet and P.S. Linsley.** 2003. Expression profiling reveals off-target gene regulation by RNAi. Nat Biotechnol *21*:635-637.
17. **Semizarov, D., L. Frost, A. Sarthy, P. Kroeger, D.N. Halbert and S.W. Fesik.** 2003. Specificity of short interfering RNA determined through gene expression signatures. Proc Natl Acad Sci U S A *100*:6347-6352.

Figure Legends

Figure 1

An improved hair-pin siRNA vector, pG-SUPER, and its application to silencing of laminA/C in HeLa cells.

A. A schematic drawing of pG-SUPER. Total nucleotide length is 3911 bp. The EGFP coding sequence from pEGFP-N1 is inserted after the SRα promoter, a modified SV40 promoter. Human H1 RNA promoter from pSUPER is oriented in the opposite direction adjacent to SRα promoter. Facing arrows represent oligonucelotide to be inserted after the H1 promoter at BglII and HindIII sites of the vector.

B. Immunofluorescence of HeLa cells 6 days after transfection with pG-SUPER-hLaminA/C. A phase contrast and three epi-fluorescence images (DAPI, FITC and TRITC channels) were taken for the same viewfield. LaminA/C was stained with mouse monoclonal anti-laminA/C. DNA was stained with Hoechst33258. Yellow line indicates line scan shown in C. Scale bar: 20 μm

C. Line scan analysis. Blue, green and red lines represent the intensity profiles of DNA, GFP and laminA/C signals, respectively.

Figure 2

Quantification of laminA/C silencing at the individual cell level.

HeLa cells were transfected with pG-SUPER-hLaminA/C, -mFascin1 or empty vector. Quantitative immunofluorescence was carried out 6 days post-transfection. The laminA/C amounts were normalized to the average of the GFP-negative population (100%). The results were summarized as histograms. Black and gray bars represent GFP-positive and -negative

cells, respectively. The averages (m) and standard deviations (σ) are shown in histograms as $m \pm \sigma$.

Figure 3

Kinetics of silencing of laminA/C.

A. Time course of reduction of laminA/C. The average and standard deviation of laminA/C amount [%] is plotted vs time after transfection.

B-D. Scatterplots of laminA/C amount (%) and GFP intensity (arbitrary units, AU). Each dot corresponds to an individual cell. Red and green represent GFP-negative and -positive populations respectively. ~100 cells were counted for each population. B: 3 days; C: 6 days; D: 9 days after transfection with pG-SUPER-hLaminA/C.

Figure 4

FACS-purification of knockdown cells allows analysis of silencing at the population level by immunoblotting.

A. Fraction of GFP-positive cells in total population with or without FACS. 8 days after transfection, 140-300 cells were counted under a fluorescence microscope. -: pG-SUPER empty; hLam: pG-SUPER-hlaminA/C; mFas: pG-SUPER-mFascin1. FACS was carried out one day after transfection.

B. Western blotting of cell extracts. 4 μg of total lysate was loaded to each lane. LaminA/C was detected by mouse monoclonal anti-laminA/C. The same membrane was analyzed with anti-α-tubulin to confirm that equal amounts of proteins were loaded.

Figure 5

Rescue of laminA silencing.

A. Design of laminA/C refractory to siRNA. Two point mutations, highlighted in red, were introduced within the target sequence.

B. Western blotting of HeLa cell extracts with mouse anti-myc antibody (clone 9E10). The extracts were prepared from the rescue experiments with pCMV-myc-laminA* (*) or pCMV-myc-laminA without mutation (WT). Extract from untreated HeLa cells was used as control. 10 μg protein was loaded per lane.

C. Immunofluorescence of HeLa cells in the rescue experiment. 4 days after electroporation with pG-SUPER-hLaminA/C, the rescue construct (pCMV-myc-laminA*) was transfected by FuGENE6. Transfectants were cultured 2 days more, and immunostained with mouse anti-laminA/C (clone 636) and rabbit anti-myc antibodies. In the merged image, green and red represent EGFP and laminA/C respectively. Arrows indicate the rescued cells. Scale bar: 20 μm.

D. Scatterplots of laminA/C amount [%] and EGFP intensity. 4 days after electroporation, pCMV (empty vector) or pCMV-myc-laminA* (myc-laminA*). Red and green dots represent GFP-negative and -positive cells not expressing myc-tagged laminA. Blue dots represent cells that coexpressed GFP and myc-laminA.

E. Plot of total laminA/C amounts [%] vs myc-laminA amount [arbitrary units, AU]. Total laminA/C level [%] was estimated by using mouse anti-laminA/C antibody that recognizes both endogenous and exogenous laminA/C. Myc-laminA level was evaluated from immunostaining with rabbit anti-myc antibody that binds only exogenous laminA.

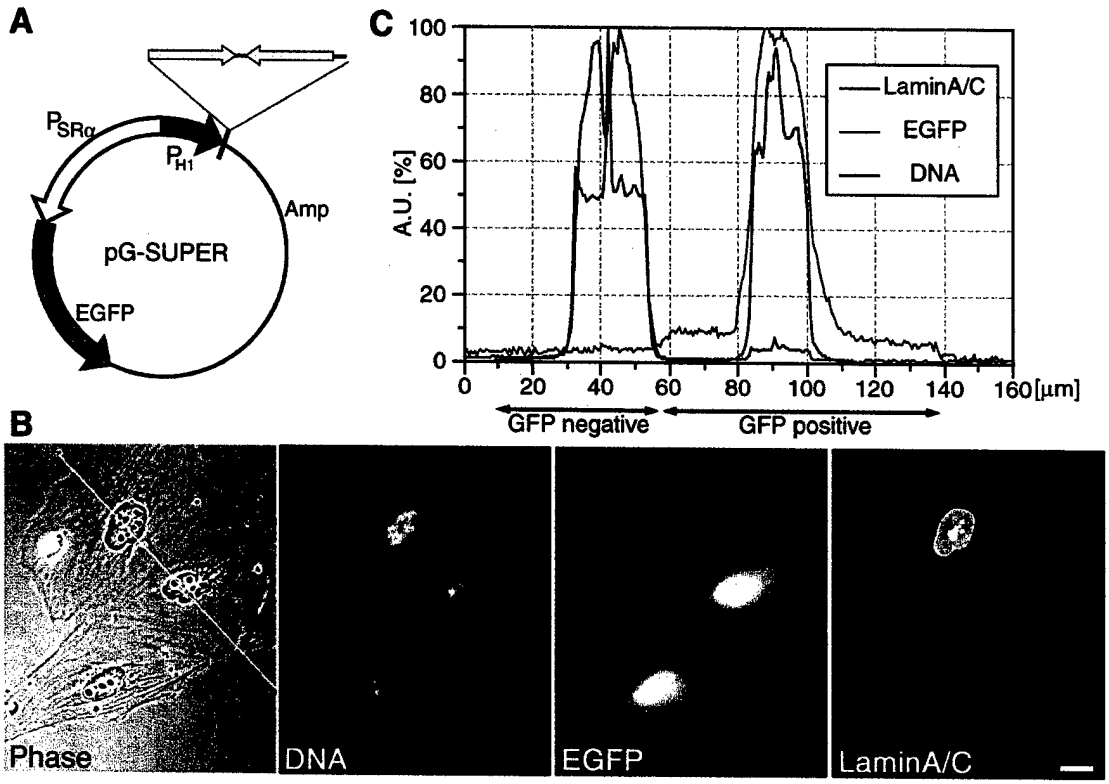
A
$P_{SR\alpha}$
P_{H1}
Amp
pG-SUPER
EGFP
C
100
80
60
40
20
0
A.U. [%]
0
20
40
60
80
100
120
140
160[μm]
LaminA/C
EGFP
DNA
GFP negative
GFP positive
B
Phase
DNA
EGFP
LaminA/C

Fig.1

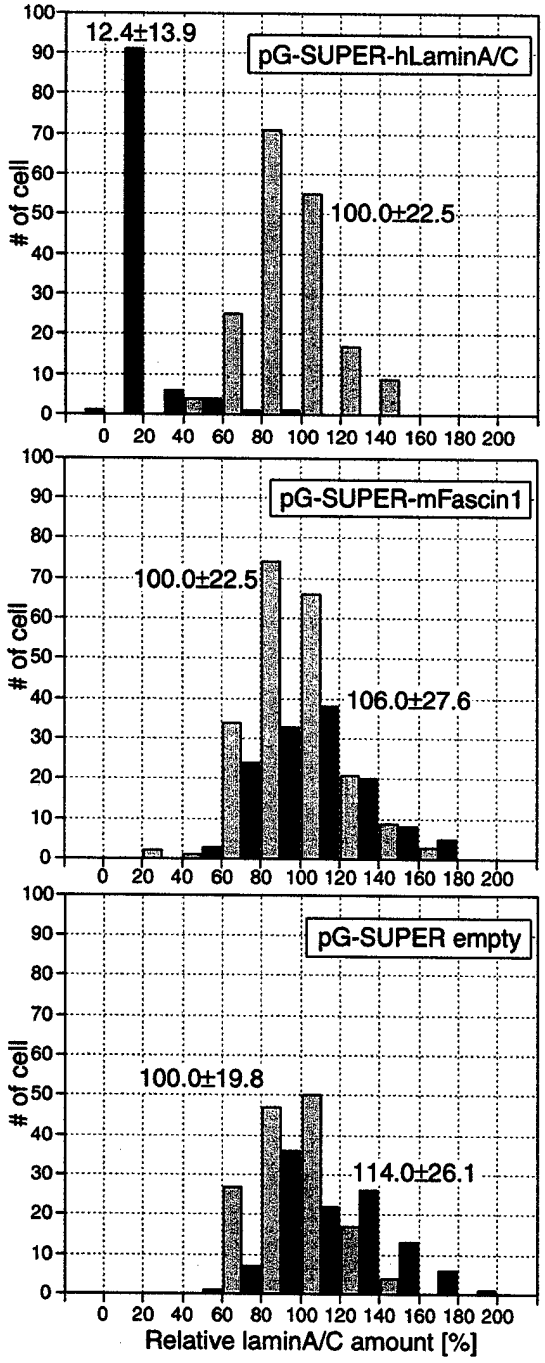
12.4±13.9
pG-SUPER-hLaminA/C
100.0±22.5
# of cell
pG-SUPER-mFascin1
100.0±22.5
106.0±27.6
pG-SUPER empty
100.0±19.8
114.0±26.1
Relative laminA/C amount [%]

Fig.2

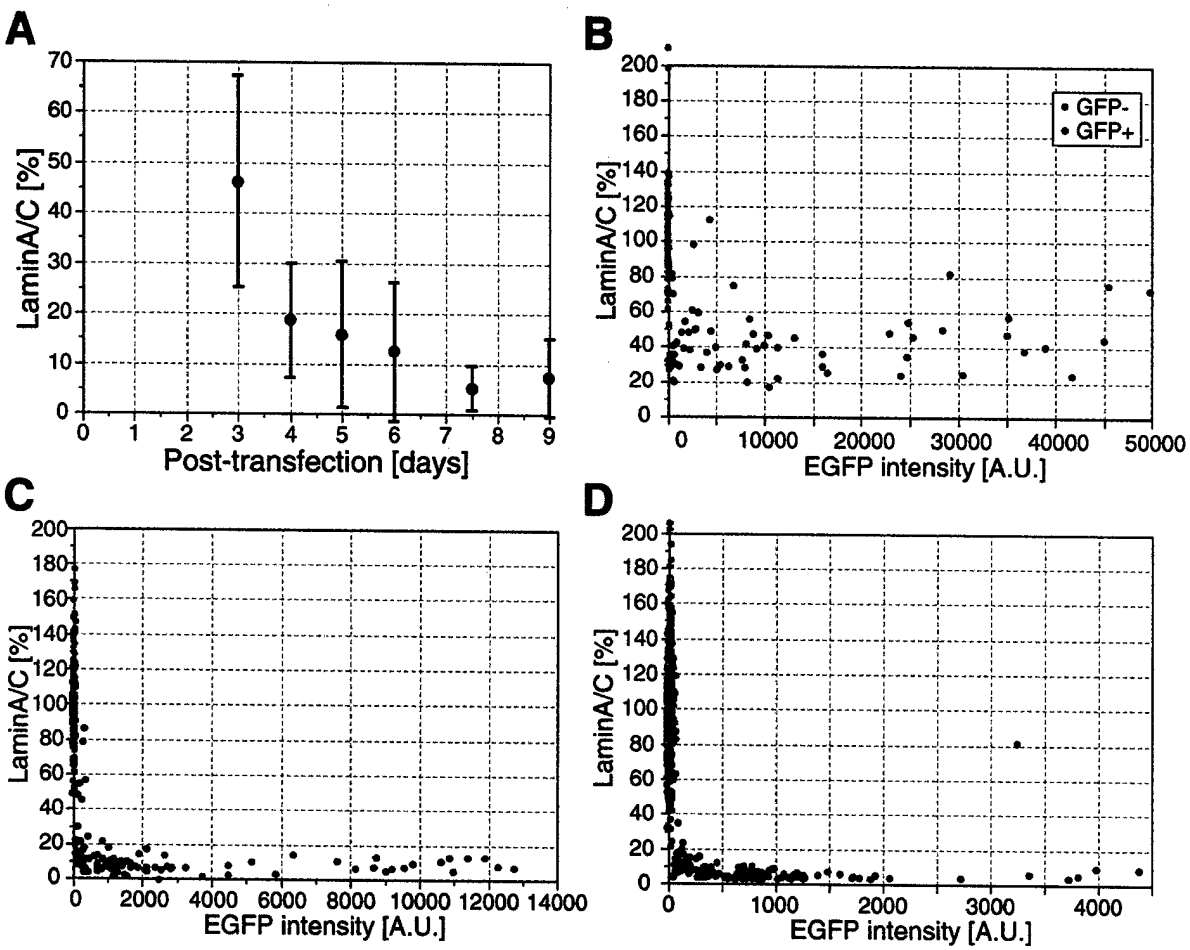
A
LaminA/C [%]
Post-transfection [days]
B
LaminA/C [%]
EGFP intensity [A.U.]
GFP-
GFP+
C
LaminA/C [%]
EGFP intensity [A.U.]
D
LaminA/C [%]
EGFP intensity [A.U.]

Fig.3

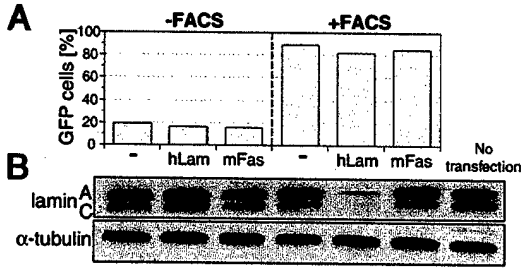
A
-FACS
+FACS
GFP cells [%]
100
80
60
40
20
0
-
hLam
mFas
-
hLam
mFas
No transfection
B
lamin A C
α-tubulin

Fig.4

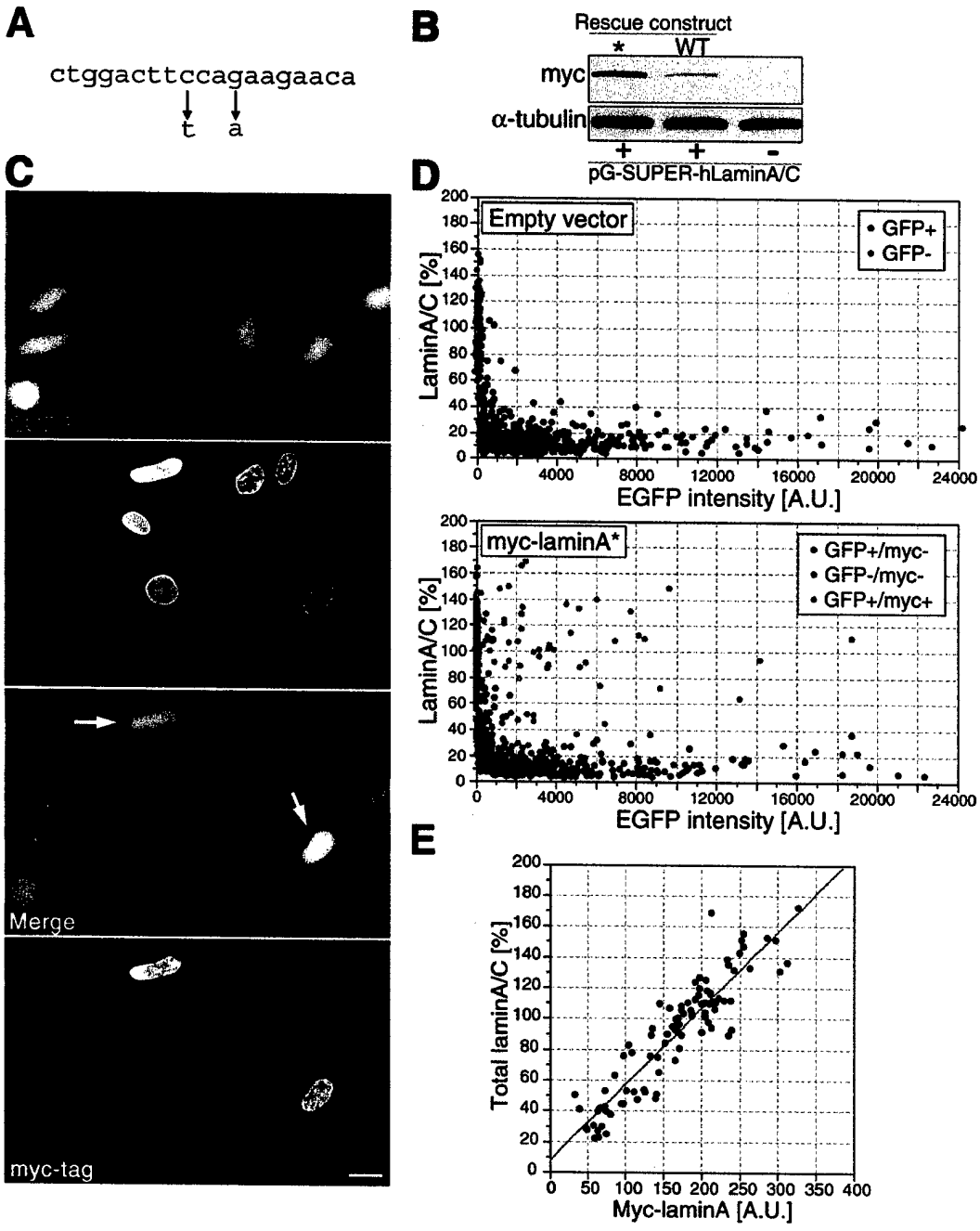
A
ctggacttccagaagaaca
t a
B
Rescue construct
*
WT
myc
α-tubulin
+ + -
pG-SUPER-hLaminA/C
C
Merge
myc-tag
D
Empty vector
• GFP+
• GFP-
LaminA/C [%]
EGFP intensity [A.U.]
myc-laminA*
• GFP+/myc-
• GFP-/myc-
• GFP+/myc+
LaminA/C [%]
EGFP intensity [A.U.]
E
Total laminA/C [%]
Myc-laminA [A.U.]

Fig.5